HIGH FREQUENCY SCATTERING FROM CANONICAL IMPEDANCE STRUCTURES

Martin I. Herman
John L. Volakis

May 1987

389271-2-T

High Frequency Scattering from Canonical Impedance Structures*

by

Martin I. Herman and John L. Volakis

Radiation Laboratory
Department of Electrical Engineering and Computer Science
The University of Michigan
1301 Beal
Ann Arbor, Michigan 48109-2122

*This work was also submitted as a dissertation by the first author in partial fulfillment of the requirements for the degree of Doctor of Philosophy in The University of Michigan.

ABSTRACT

HIGH FREQUENCY SCATTERING FROM CANONICAL IMPEDANCE STRUCTURES

High frequency uniform diffraction coefficients for impedance half planes and wedges are presented which rigorously account for surface wave effects. Similar coefficients for the resistive and conductive half planes are also presented. A primary concern in this dissertation is the evaluation of the diffraction associated with multi-edge structures. This is accomplished by employing the Extended Spectral Ray Method (ESRM) which remains applicable even in regions where the fields are non ray-optical and where conventional GTD techniques fail. The resulting integrals are evaluated via the modified Pauli-Clemmow steepest descent method to yield the diffraction coefficients. Uniform diffraction coefficients are obtained for impedance, resistive and conductive strips. These include second and third order interactions in addition to contributions due to possible surface waves in a rigorous and uniform manner. The diffraction by double wedge structures is then considered. In this case key identities are introduced which enable the integrals to be evaluated as stated above. Without them, derivatives of extremely complex functions must be performed. Also highly accurate approximations for the Maliuzhinets function of the wedge formulation are derived, applicable to any external wedge angle. Examples of double wedge structures are thick half planes, inserts in a full plane and convex polygonal cylinders, where the strip is a special case. Bistatic as well as backscatter patterns are presented for all of the aforementioned structures. Several comparisons of our results with corresponding moment method data or other data available in the literature are included with excellent correlation in all cases.

TABLE OF CONTENTS

LIST OF FIGURES

Figure

LIST OF SYMBOLS

Symbols

C^+	reflection coefficient
C^-	transmission coefficient
D	total diffracted field
D_{21}	double diffraction coefficient
D^{dGO}	geometrical optics diffraction coefficient
D^{dNU}	non-uniform diffraction coefficient
D^{dSW}	surface wave diffraction coefficient
$\overline{E}$	electric field
E^{GO}	geometrical optics electric field
E^{SW}	surface wave electric field
E^S	scattered electric field from an edge
E_1	scattered electric field from an edge (Q_1)
E_2	scattered electric field from an edge (Q_2)
E_z^d	total diffracted electric field
E_z^i	incident electric field
E_z^{dGO}	geometrical optics diffracted electric field
E_z^{dNU}	non-uniform diffracted electric field
E_z^{dSW}	surface wave diffracted electric field
E_T^s	total scattered electric field
E_{21}^d	doubly diffracted electric field (resistive strip)
$E_{21_{pc}}^d$	doubly diffracted electric field (perfectly conducting strip)
E_{121}^d	triply diffracted electric field (resistive strip)
$E_{121_{pc}}^d$	triply diffracted electric field (perfectly conducting strip)
$E_{21_{conductive}}^d$	doubly diffracted electric field (conductive strip)
$E_{21_{impedance}}^d$	doubly diffracted electric field (impedance strip)
$E_{121_{conductive}}^d$	triply diffracted electric field (conductive strip)
$E_{121_{impedance}}^d$	triply diffracted electric field (impedance strip)
F	spectral function

F_C	Clemmow transition function
F_{KP}	UTD transition function
gd	Gudermann function
$\overline{H}$	magnetic field
H_z^i	incident magnetic field
j	$\sqrt{-1}$
k	wave number $(2\pi/\lambda)$
$K_\pm(\alpha)$	split function
$K_{\pm c}(\alpha)$	$K_\pm(\alpha)/\sin(\alpha/2)$
$K_{-u}(\alpha)$	$\{1-\sqrt{2}\cos((\frac{3\pi}{2}-\alpha-\theta)/2)\}K_-(\alpha)$
K_A	non-singular function
K_B	non-singular function
$\overline{K}_E$	electric current sheet
$\overline{K}_M$	magnetic current sheet
m	external wedge angle π
n	external wedge angle/π
$P_{2\pi}$	unit rect function with width 2π
p	external wedge angle/π
Q_1	edge where phase reference is taken
Q_2	edge where phase reference is not taken
r	phase factor
R	resistivity
R^*	conductivity
SDP	steepest descent path
u_o	unit step function
u_1^d	primary diffraction mechanism at Q_1
u_2^d	primary diffraction mechanism at Q_2
u_{21}^d	double diffraction mechanism
u_{121}^d	triple diffraction mechanism
u_{IV}^d	quadruple diffraction mechanism
w	width of strip or common wedge face
x	Cartesian coordinate
y	Cartesian coordinate
z	Cartesian coordinate when used as a subscript, otherwise a complex number
Z_o	free space impedance
$\beta^\pm$	$\phi \pm \phi_o$
ϵ_r	relative permittivity
η	normalized surface impedance

η_o	normalized impedance of common double wedge face
$\eta_{1,2}$	normalized impedances of outer double wedge faces
θ	for E-polarization it equals $\sin^{-1}(\frac{1}{\eta})$ whereas for H-polarization it equals $\sin^{-1}(\eta)$
λ	wavelength
ρ	observation distance
σ	echowidth per wavelength
τ	thickness parameter
ϕ	observation angle measured with respect to Q_1
ϕ_o	incidence angle measured with respect to Q_1
ϕ_2	observation angle measured with respect to Q_2
Φ	half the external wedge angle
Ψ	wedge function composed of Maliuzhinets functions
Ψ_π	Maliuzhinets function for a half plane
Ψ_Φ	Maliuzhinets function for a external wedge angle 2Φ

LIST OF APPENDICES

Appendix

CHAPTER I

INTRODUCTION

Interest in diffraction from dielectric and material coated structures has prompted investigations for deriving uniform diffraction coefficients for geometries composed of canonical shapes such as half planes and wedges (see figures 1.1 and 1.2) as well as strips, double wedges and polygonal cylinders in which multi-edge diffractions could be significant.

The non-uniform solution for a wedge with arbitrary face impedances and included angles was given by Maliuzhinets in 1951 (dissertation) and was published in the English literature in 1958 [1]. His solution was based upon function theoretic techniques, however, because of the difficulty in evaluating special functions (henceforth to be referred to as the Maliuzhinets functions) associated with the resulting expressions, its utility was limited except for a few wedge angles of which the half plane was not one. Only recently has a highly accurate analytic approximation been developed for the Maliuzhinets function associated with the half plane [2] and thus easing the calculation of diffraction patterns and encouraging the development of the complete analytic solution for the half plane.

In 1952, Senior [3] solved for the diffraction from an impedance half plane using a Wiener-Hopf approach involving the current spectra. His solution was uniform with respect to the geometrical optics fields but did not include surface wave contributions. Later, Senior showed the relationship between his split function and Maliuzhinets' special function [4] which is crucial in establishing the equivalence of the two formulations for the case of the impedance half plane. In any case, both approaches are based on the impedance boundary condition which is briefly reviewed in Appendix A. However, Senior's solution has the particular advantage of being able to decouple the contributions due to electric and magnetic currents and thus extending our capabilities to study resistive and conductive half planes

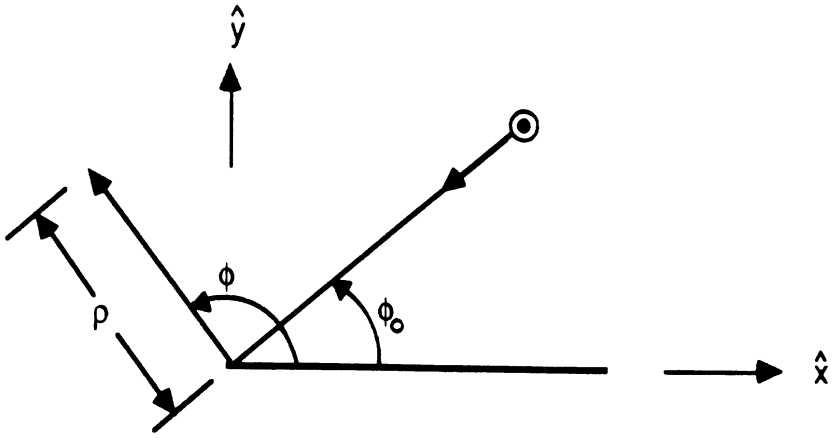

Figure 1.1 — Geometry of a half plane

ϕ_o is the incidence angle, ϕ is the observation angle and ρ is the observation distance

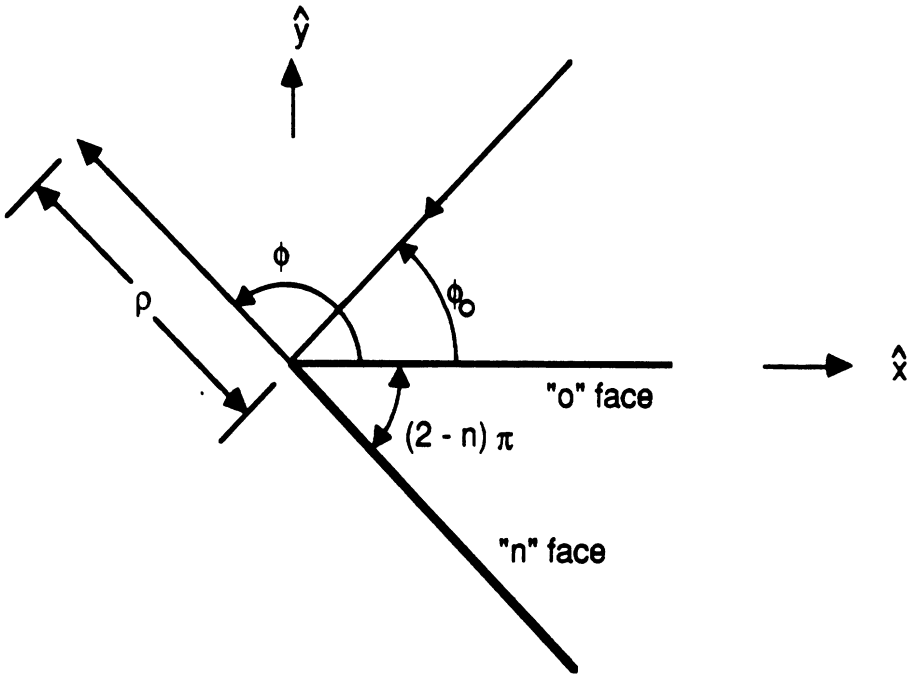

Figure 1.2 — Geometry of a wedge

ϕ_o is the incidence angle, ϕ is the observation angle, ρ is the observation distance and $n\pi$ is the external wedge angle

and strips. Thus, the diffraction from an impedance half plane may be thought of as the summation of the diffraction contributions from individual resistive and conductive half planes.

Senior's solution for the diffraction by an impedance half plane was uniform at the geometrical optics boundaries. It is therefore of interest to present a uniform formulation which includes the surface wave contributions as well as the geometrical optics ones. Bucci and Franceschetti [5] studied the conditions under which surface waves may exist for capacitive, resistive and inductive impedance half planes for both E and H polarizations. However, their solution did not uniformly account for surface wave contributions. Anderson [6], in 1979, presented an analysis of the diffraction by a thin dielectric (resistive) half plane which included the residue contribution of the surface wave pole but did not perform a uniform evaluation of the surface wave field. In view of this, chapter II contains the derivation of a uniform first order diffraction coefficient using a method introduced by Clemmow [7] (see also Senior [8]) and expounded upon by Volakis and Herman [9]. Backscatter patterns presented emphasize the importance of surface wave contributions.

The impedance, resistive or conductive strips can be modeled via a superposition of impedance, resistive and conductive half planes, respectively. Because the impedance strip is amenable to an analytic solution, Bowman [10], Senior [11, 12], and Tiberio et. al. [13] have investigated its scattering behavior. In all of these investigations the goal has been to obtain a high frequency solution for the multiply diffracted fields which can be added to the first order contribution [1, 3, 13] for predicting the total scattered field by the strip. However, a rigorous uniform evaluation of the multiply diffracted field in the context of the Geometrical Theory of Diffraction (GTD) and for all angles of incidence and diffraction is not yet available.

The difficulty in obtaining a valid solution for the multiply diffracted fields is primarily due to the non-ray optical behavior of the field which illuminates the second edge after diffraction from the first. This occurs for incidence angles near edge-on and can be quite dominant in the backscatter and forward directions. Because of the non-ray optical behavior of the interacting fields in these situations, the concept of slope diffraction [14, 15] is not applicable.

Senior [12] presented an approximate higher order solution for the diffraction by a resistive strip via the introduction of caustic matching functions drawn from the known uniform solution [16] for the perfectly conducting strip. However, his result did not include the effect of the surface wave pole which is significant in the case of strips simulating thin dielectric layers. Tiberio et. al. [13] developed a valid high frequency solution for the diffraction by an impedance strip which included the effect of the surface wave pole but was restricted to edge-on incidence. Their approach in treating the non-ray optical fields involved the use of the Extended Spectral Ray Method (ESRM) [13, 17] which has been found quite successful, and its principles will also be employed in our analysis whenever multi-edge diffraction is involved. The ESRM can be considered as an extension of the Uniform Geometrical Theory of Diffraction (UTD) [18] and is related to the Spectral Theory of Diffraction introduced by Rahmat-Samii and Mittra [19, 20, 21]. Chapter III presents an overview of the ESRM with particular emphasis on the geometrical interpretation of the spectral rays.

In Chapter IV, the ESRM is employed to find explicit simple expressions for the double and triple diffraction mechanisms for a resistive strip using the current spectra formulation given by Senior [3]. It is then shown that the solutions for the conductive and impedance cases are easily derived from the known resistive case. This is due to the fact that the electric and magnetic currents are decoupled for a planar topology [22]. Far field bistatic and backscatter patterns are also presented and compared to moment method data [23]. Example cases where the strip may or may not support surface waves are given.

The more general problem of uniform diffraction from an impedance wedge is developed in chapter V. Tiberio et. al.[24] presented a uniform solution for an impedance wedge which included only the geometrical optics fields using a modified Pauli-Clemmow steepest descent asymptotic approach. In chapter V, a diffraction coefficient which is uniform at the geometrical optics and surface wave boundaries is derived using the same technique described in chapter II for the impedance half plane. In this chapter some identities are also introduced which will be of particular importance when considering the evaluation of integrals representing the contributions of the multiply diffracted fields. Also, simple and highly accurate analytic expressions are presented for the special functions which arise in

the Maluizhinets formulation associated with any external wedge angle [25].

Uniform diffraction coefficients up to and including the triple diffraction mechanism associated with an impedance (isolated) double wedge structure whose, outer faces do not intersect. are presented in chapter VI using a combination of the ERSM and the Modified Pauli-Clemmow steepest descent asymptotic evaluation. The contribution of the surface waves are rigorously included in the solution. Prior work in this area has only been reported for a perfectly conducting double wedge structure where only the contributions of the primary and double diffraction mechanisms were included [26]. In this chapter we also demonstrate the versatility associated with the ESRM when evaluating higher order diffraction coefficients including that for the fourth order mechanism. Examples of bistatic and backscatter patterns from isolated double wedges such as thick impedance half planes and impedance inserts in a full plane are presented. Some calculations for the scattering by these structures have recently appeared in the literature [27, 28] and are therefore of interest for the purpose of verifying the present solution. Also in our presentation we include examples of isolated double wedge structures with varying external wedge angles. The solution is general enough such that each external angle and wedge face impedance may be defined independently.

In the case of isolated double wedges, all interactions are among two edges. However, when considering the scattering by a polygonal cylinder, the present solution is extended to include the contribution of triply diffracted mechanisms which may include up to three wedge vertices of the polygon. This development is accomplished in chapter VII, where bistatic and backscatter patterns are also given for triangular and square cylinders. The selected examples demonstrate the importance of the multiple interactions and as a check of the validity of the high frequency solution, the results are compared to moment method data.

A special case of the polygonal cylinder is the impedance strip. Complete uniform diffraction coefficients are presented up to and including the triple diffraction mechanism. The advantage of this strip solution to that presented in chapter IV is that the impedance values of the top and bottom of the strip can be independently assigned.

Chapter VIII of this dissertation is the conclusion along with some recommendations

for future work.

CHAPTER II

DIFFRACTION FROM RESISTIVE, CONDUCTIVE AND IMPEDANCE HALF PLANES

In this chapter the formulation of the diffraction coefficient from an impedance half plane is presented. It is based on Senior's integral formulation [3] for an impedance half plane in which both top and bottom face impedances are equal. A uniform evaluation of this integral equation is obtained using a method introduced by Clemmow [7] (also Senior [8]) and expounded upon by Volakis and Herman [9] (see Appendix B).

The scattering from an impedance half plane may be written in terms of the sum of electric and magnetic currents which are uncoupled [22]. As a consequence of this fact we can associate the field due to the electric current with a "resistive" half plane and the magnetic current[1] with that of a "conductive" half plane.

Formulation

Assuming an E-polarized plane wave normally incident [2] on an impedance half plane shown in figure 1.1,

$$E_z^i = e^{jk(x\cos\phi_o + y\sin\phi_o)} \tag{2.1}$$

we find from [3] that an integral representation of the scattered field is

$$E^s = -\frac{j}{2\pi}\int_C \frac{1}{\cos\alpha+\cos\phi_o}\left\{1 \mp \eta\sqrt{(1+\cos\alpha)(1+\cos\phi_o)}\right\} \cdot K_+(\alpha)K_+(\phi_o)e^{-jk\rho\cos(\alpha-\phi)}d\alpha; \qquad y \gtrless 0 \tag{2.2}$$

---

[1] Although a fictitious quantity, the concept of a magnetic current is a useful analytic tool .

[2] Throughout this dissertation an $e^{j\omega t}$ time convention is assumed and suppressed.

where C is depicted in figure 2.1, ϕ_o is the incident angle, ϕ is the observation angle, η [1] is the normalized impedance and $K_+(\alpha)$ is the split function, defined by

$$K_+(\alpha) = 2^{\frac{3}{2}}\sqrt{\frac{2}{\eta}}\sin\frac{\alpha}{2}\left\{\frac{\Psi_\pi(\frac{3\pi}{2}-\alpha-\theta)\Psi_\pi(\frac{\pi}{2}-\alpha+\theta)}{\Psi_\pi^2(\frac{\pi}{2})}\right\}^2 \Bigg/\left\{\left(1+\sqrt{2}\cos\left(\frac{\frac{\pi}{2}-\alpha+\theta}{2}\right)\right)\left(1+\sqrt{2}\cos\left(\frac{\frac{3\pi}{2}-\alpha-\theta}{2}\right)\right)\right\}, \tag{2.3}$$

$$\Psi_\pi(z) \approx \begin{cases} 1-0.0139z^2 & \mathrm{Im}(z) \le 4.2 \\ 1.05302\sqrt{\cos\frac{1}{4}(z-j(\ln 2)}\exp\left\{\frac{jz}{2\pi}e^{jz}\right\} & \mathrm{Im}(z) > 4.2 \end{cases} \tag{2.4}$$

provided $\mathrm{Re}(z) < \frac{\pi}{2}$; otherwise, the identities

$$\Psi_\pi(z) = \{\Psi_\pi(\frac{\pi}{2})\}^2\frac{\cos(\frac{z}{4}-\frac{\pi}{8})}{\Psi_\pi(z-\pi)},$$

$$\Psi_\pi(-z) = \Psi_\pi(z),$$

$$\Psi_\pi(z^*) = \Psi_\pi^*(z),$$

where the asterisk denotes the complex conjugate, must be employed as many times as necessary until the argument is in suitable form for use in (2.4). The above is a highly accurate approximation of the Maliuzhinets function [1] $\Psi_\pi(z)$ given by Volakis and Senior[2]. Finally, the variable θ is related to the normalized impedance by the relation $\sin\theta = \frac{1}{\eta}$ for E-polarization and $\sin\theta = \eta$ for H-polarization .

In order to perform a uniform asymptotic evaluation of (2.2) it is necessary to consider the effect of the geometrical optics and surface wave poles as they approach the saddle point at $\alpha = \phi$. Clearly the geometrical optics (g.o.) poles are located at $\alpha = \pi - \phi_o$ and $\pi + \phi_o$, while the surface wave pole at $\alpha = -\theta$ corresponds to the zero of the term $1+\sqrt{2}\cos[(\frac{3\pi}{2}-\alpha-\theta)/2]$ appearing in the expression for $K_+(\alpha)$. The object of the uniform evaluation is to maintain total field continuity for all pattern angles ϕ. For the perfectly conducting case (all poles lie on the real axis) a uniform evaluation referred in the context of UTD(Uniform Theory of Diffraction) [18] involved a modified Pauli-Clemmow [29] evaluation of the integral by retaining the first non-zero term of the pertinent Maclaurin series expansion of the integrand. Thus, it is restricted to cases where the pole crosses the

[1] It is assumed throughout this dissertation that the real part of η is positive. This corresponds to a passive material.

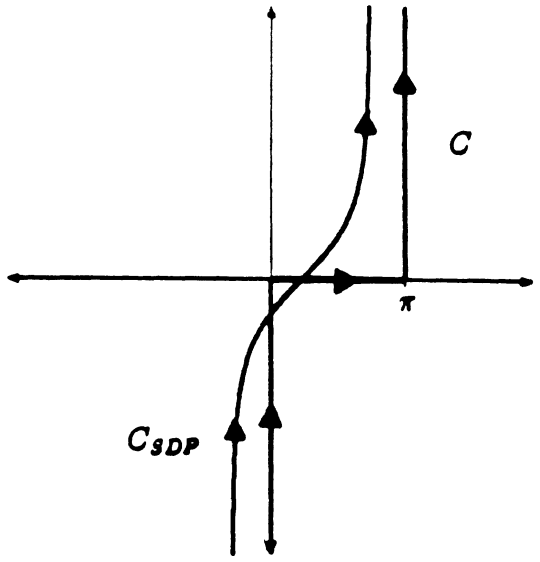

Figure 2.1 — Topology of the integral representation of the edge diffracted field

saddle point as ϕ is varied and therefore not applicable to the present situation where a pole having a complex value may appear.

The approach for evaluating (2.2) follows the one described by Volakis and Herman [9](see Appendix B). It involves first the subtraction and addition (to the integral) of certain auxiliary functions, each containing one of the singularities of the integrand. The auxiliary functions can be usually integrated exactly and the residue of the pertinent singularity is equal to that obtained with the original integrand. Thus, the new expression can be subdivided into singular and non-singular parts. The non-singular parts are evaluated asymptotically in a non-uniform manner while the singular ones correspond to the added auxiliary functions which are integrated exactly and will therefore be uniform.

Appropriate auxiliary functions for the integral at hand are

$$G_{pi}(\alpha,\phi) = \sec\left(\frac{\alpha - \alpha_{pi} \mp \pi}{2}\right); \qquad i = 1,2,3 \tag{2.5}$$

which are clearly singular at $\alpha = \alpha_{pi}$, where $\alpha_{p1} = \pi - \phi_o$, $\alpha_{p2} = \pi + \phi_o$, and $\alpha_{p3} = -\theta$ correspond to the poles of the integrand in (2.2). Proceeding as discussed above, we can express the uniform diffracted field by an impedance half plane as

$$E_z^d(\phi,\phi_o;\eta) = E_z^{dNU}(\phi,\phi_o;\eta) + E_z^{dGO}(\phi,\phi_o;\eta) + E_z^{dSW}(\phi,\phi_o;\eta) \tag{2.6}$$

In the above, E_z^{dNU} denotes the non-uniform diffracted field by the impedance half plane, E_z^{dGO} represents the contribution of the g.o. poles to the diffracted field and E_z^{dSW} denotes a similar contribution caused by the existence of the surface wave pole. They are given by

$$\begin{aligned} E_z^{dNU} =& j\sqrt{\frac{2\pi}{k\rho}}\left\{t_o(\phi)\sec\frac{\beta^+}{2} + t_1(\phi)\sec\frac{\beta^-}{2}\right\} \\ & \cdot K_+(\phi)e^{-j\frac{\pi}{4}}e^{-jk\rho}, \end{aligned} \tag{2.7}$$

$$\begin{aligned} E_z^{dGO} = \Bigg[& j\sqrt{\frac{2\pi}{k\rho}}\left\{-t_o(\alpha_{p1})K_+(\alpha_{p1})\sec\frac{\beta^+}{2}\right. \\ & \left.-t_1(\alpha_{p2})K_+(\alpha_{p2})\sec\frac{\beta^-}{2}\right\} \\ & \mp t_o(\alpha_{p1})K_+(\alpha_{p1})4\sqrt{\pi}F_c[\pm\sqrt{2k\rho}\cos\frac{\beta^+}{2}] \\ & \mp t_1(\alpha_{p2})K_+(\alpha_{p2})4\sqrt{\pi}F_c[\pm\sqrt{2k\rho}\cos\frac{\beta^-}{2}]\Bigg] e^{-j\frac{\pi}{4}}e^{-jk\rho}, \end{aligned} \tag{2.8}$$

$$E_z^{dSW} = - K_{+u}(\alpha_{p3}) \left\{ t_{\frac{0}{2}}(\alpha_{p3}) \sec(\frac{-\theta+\phi_o}{2}) + t_{\frac{1}{3}}(\alpha_{p3}) \sec(\frac{-\theta-\phi_o}{2}) \right\}$$
$$\cdot \left[j\sqrt{\frac{2\pi}{k\rho}} \sec(\frac{\mp\pi \pm \phi + \theta}{2}) \right.$$
$$\left. \mp 4\sqrt{\pi} F_c[\pm\sqrt{2k\rho}\cos(\frac{\pm\phi \mp \pi + \theta}{2})] \right] e^{-j\frac{\pi}{4}} e^{-jk\rho}; \qquad y \gtrless 0, \qquad (2.9)$$

where

$$\beta^{\pm} = \phi \pm \phi_o, \qquad (2.10)$$

$$t_0(\alpha) = \frac{-j}{2\pi}\left[\frac{1}{4\sin\frac{\alpha}{2}\sin\frac{\phi_o}{2}} - \frac{\eta}{2}\right] K_+(\phi_o), \qquad (2.11)$$

$$t_1(\alpha) = \frac{-j}{2\pi}\left[-\frac{1}{4\sin\frac{\alpha}{2}\sin\frac{\phi_o}{2}} - \frac{\eta}{2}\right] K_+(\phi_o), \qquad (2.12)$$

$$t_2(\alpha) = \frac{-j}{2\pi}\left[\frac{1}{4\sin\frac{\alpha}{2}\sin\frac{\phi_o}{2}} + \frac{\eta}{2}\right] K_+(\phi_o), \qquad (2.13)$$

$$t_3(\alpha) = \frac{-j}{2\pi}\left[-\frac{1}{4\sin\frac{\alpha}{2}\sin\frac{\phi_o}{2}} + \frac{\eta}{2}\right] K_+(\phi_o), \qquad (2.14)$$

$$K_{+c}(\pm\alpha) = \frac{K_+(\pm\alpha)}{\sin(\frac{\pm\alpha}{2})}, \qquad (2.15)$$

$$K_{+u}(\alpha) = \left\{1 + \sqrt{2}\cos[(\frac{3\pi}{2} - \alpha - \theta)/2]\right\} K_+(\alpha), \qquad (2.16)$$

and

$$F_c(\pm z) = e^{jz^2} \int_{\pm z}^{\infty} e^{-j\tau^2} d\tau \qquad (2.17)$$

is the Clemmow [7] transition function satisfying the identity

$$F_c(-z) = \sqrt{z} e^{-j\frac{\pi}{4}} e^{jz^2} - F_c(z), \qquad (2.18)$$

essential for maintaining total field continuity. In (2.17), the minus sign is chosen when $\frac{\pi}{4} < \arg(z) < \frac{5\pi}{4}$, otherwise the positive sign is used. To illustrate how continuity is maintained, figure 2.2 shows the position of the surface wave pole in relation to the closed contour and the corresponding argument of F_C. Contour C is detoured to close the path of integration in the steepest descents method of integration. This path (steepest descent path) is described by the Gudermann function and the location where it crosses the real α axis is determined by the observation angle ϕ. When the closed contour C and curve 1 (the

SDP) captures the surface wave pole, we find in (2.17) that arg(z)> $\frac{\pi}{4}$ and therefore the negative sign is chosen. Thus, (2.18) must be invoked to recover the residue contribution of the surface wave pole. When the pole lies directly on the steepest descent path (contour 2) the corresponding phase of the argument of F_c is exactly $\frac{\pi}{4}$. Finally when the surface wave pole is not captured by the closed contour (curve 3) the phase of the argument of F_c is less than $\frac{\pi}{4}$ requiring the choice of the positive sign in (2.17).

As mentioned above, when the $\pm$ sign within the transition function changes, we can apply the identity given by equation (2.18) to recover the residue contributions of the poles. Such a result is, of course, easily checked by calculating this residue contribution directly from the integral. Applying (2.18) to the transition functions appearing in (2.8), we find that the residue contributions of the geometrical poles are

$$-4\pi j t_o(\alpha_{p1}) K_+(\alpha_{p1}) e^{jk\rho\cos\beta^+} \tag{2.19}$$

$$-4\pi j t_1(\alpha_{p2}) K_+(\alpha_{p2}) e^{jk\rho\cos\beta^-}. \tag{2.20}$$

In addition, from (2.9) we obtain the surface wave pole residue contribution to be

$$4\pi j t_o(\alpha_{p3}) K_{+u}(\alpha_{p3}) \sec\left(\frac{-\theta+\phi_o}{2}\right) e^{-jk\rho\cos(\theta+\phi)} \qquad y>0 \tag{2.21}$$

$$4\pi j t_2(\alpha_{p3}) K_{+u}(\alpha_{p3}) \sec\left(\frac{-\theta-\phi_o}{2}\right) e^{-jk\rho\cos(\theta-\phi)} \qquad y<0. \tag{2.22}$$

Clearly (2.21) and (2.22) represent (attenuating) plane waves traveling on the upper or lower face of the half plane, respectively.

When considering the general class of surface waves, it is important to distinguish between the contributions due to the residue of the surface wave pole and that due to surface wave diffraction. The first is generally referred to as the surface wave field. However, even if the surface wave field is absent (the surface wave pole is not captured by the closed contour), the diffracted field (termed surface ray field) given by (2.9), must still be included for a complete uniform representation of the total field.

Equations (2.6)-(2.9) give the uniform diffracted field from an impedance half plane in terms of the Clemmow transition function. We can easily rewrite the result using the transition function introduced by Kouyoumjian and Pathak [18] in the context of UTD by

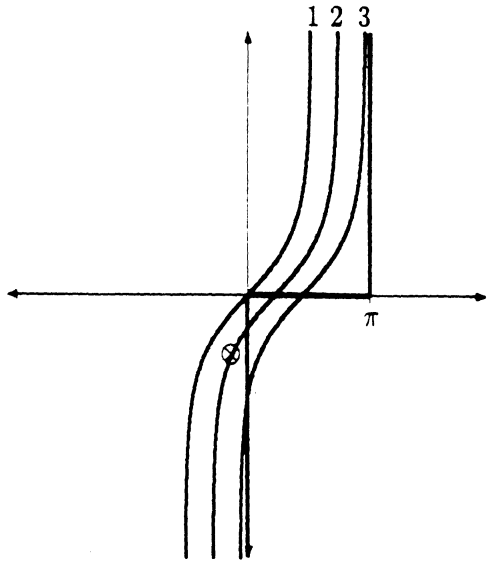

α plane

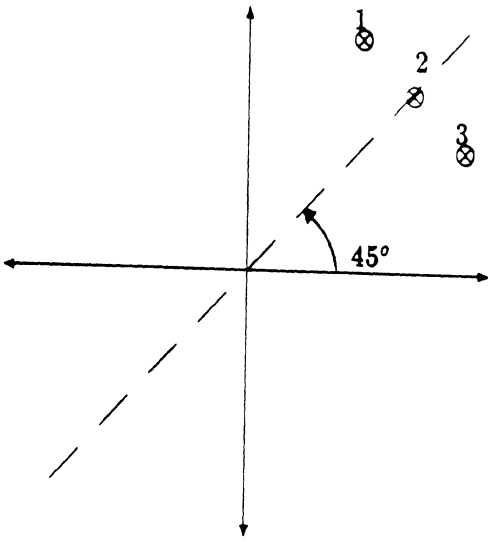

Surface Wave Continuity
(phase of the argument of F_c)

Figure 2.2 — Continuity of the surface wave field and the corresponding argument in the Clemmow transition function

employing the relation,

$$F_{KP}(z^2) = \pm 2jzF_C(\pm z). \tag{2.23}$$

The diffracted field can now be expressed as

$$E^s = D(\phi, \phi_o; \eta)\frac{e^{-jk\rho}}{\sqrt{\rho}} \tag{2.24}$$

with

$$D(\phi, \phi_o; \eta) = D^{dNU}(\phi, \phi_o; \eta) + D^{dGO}(\phi, \phi_o; \eta) + D^{dSW}(\phi, \phi_o; \eta) \tag{2.25}$$

being the uniform diffraction coefficient. From (2.7)-(2.9) and (2.23) we find that

$$D^{dNU} = j\sqrt{\frac{2\pi}{k}}K_+(\phi)\left\{t_o(\phi)\sec\frac{\beta^+}{2} + t_1(\phi)\sec\frac{\beta^-}{2}\right\}e^{-j\frac{\pi}{4}} \tag{2.26}$$

$$\begin{aligned} D^{dGO} = &-j\sqrt{\frac{2\pi}{k}}\left\{t_o(\alpha_{p1})K_+(\alpha_{p1})\sec\frac{\beta^+}{2}\left(1 - F_{KP}[2k\rho\cos^2\left(\frac{\beta^+}{2}\right)]\right)\right. \\ &\left. + t_1(\alpha_{p2})K_+(\alpha_{p2})\sec\frac{\beta^-}{2}\left(1 - F_{KP}[2k\rho\cos^2\left(\frac{\beta^-}{2}\right)]\right)\right\}e^{-j\frac{\pi}{4}} \end{aligned} \tag{2.27}$$

$$\begin{aligned} D^{dSW} = &-j\sqrt{\frac{2\pi}{k}}K_{+u}(\alpha_{p3})\sec\left(\frac{\mp\pi \pm \phi + \theta}{2}\right) \\ &\left\{\left(t_{\underset{2}{0}}(\alpha_{p3})\sec\left(\frac{-\theta + \phi_o}{2}\right) + t_{\underset{3}{1}}(\alpha_{p3})\ \sec\left(\frac{-\theta - \phi_o}{2}\right)\right)\right. \\ &\left.\cdot\left(1 - F_{KP}[2k\rho\cos^2\left(\frac{\pm\phi \mp \pi + \theta}{2}\right)]\right)\right\}e^{-j\frac{\pi}{4}} \qquad y \underset{<}{>} 0 \end{aligned} \tag{2.28}$$

The above diffraction coefficient for the impedance half plane includes the contribution of both electric and magnetic currents. In order to obtain a corresponding diffraction coefficient for a resistive half plane, one needs to only keep those terms associated with the electric currents. This is easily done by retaining the first term of $t_n(\alpha)$ in (2.11)-(2.14). If the second term of $t_n(\alpha)$ in (2.11)-(2.14) is retained, we will obtain the diffraction coefficient corresponding to a conductive half plane which supports magnetic currents only.

For the case of E-polarization a capacitive material will support a surface wave [5]. This corresponds to a negative reactance in the impedance value. In terms of half planes the impedance and resistive structures can support a surface wave if the following criteria is met

$$0 < Re(\theta) < |gd(Im(\theta))|, \qquad -Im(\theta) < 0 \tag{2.29}$$

where $gd(x) = \cos^{-1}(\frac{1}{\cosh(x)})sgn(x)$ is the Gudermann function. Conductive and impedance half plane may support surface waves if the impedance is inductive and the incident field is

H-polarized. As expected an inductive impedance has a positive reactance. The criteria in which surface waves do exist is still given by (2.29). Finally, for the special case in which the impedance is purely resistive (reactance is zero) the surface wave pole is real and can never satisfy (2.29). Naturally, this material cannot support a surface wave but the surface ray field may still be important. This is true for the case of a high resistivity and E-polarization. When the surface wave pole is real an ambiguity can exist between the surface wave and geometrical optics poles which could indicate that a double pole exits. In order to avoid this situation we can use another auxilary function in the present formulation to eliminate this possibility.

Numerical Results

Six sets of bistatic patterns of echowidth (σ) (per wavelength) versus angle of observation are presented in figures 2.3 - 2.14 . The echowidth is defined as

$$\sigma = 10\log\left[\lim_{\rho\to\infty} 2\pi\rho\frac{|E_T^s|^2}{|E_z^i|^2}\right]$$

where E_T^s is the total scattered field. Each data set consists of an impedance, resistive and conductive half plane patterns for the normalized impedances $\eta = 0.5 \pm j5$, $0.5 \pm j1$ and $0.5 \pm j0.5$. In every case an E-polarized wave is normally incident upon the half plane and observed at a distance of 1.6λ from the edge. In the cases when an inductive material was used ($\eta = 0.5 + j5$, $0.5 + j1$ and $0.5 + j0.5$) no surface waves existed [5] but surface ray fields were present, although usually small. This is easily seen by observing that the total field tends to zero as the observation angle approached the shadowed side of the half plane. However, when the half plane consisted of a capacitive material ($\eta = 0.5 - j5$, $0.5 - j1$ and $0.5 - j0.5$) it may (and did in these examples) support surface waves. The total field on the shadowed side of the half plane is now quite significant due to the surface wave field. It is clear from the prior examples that the most significant effects of the surface wave, when it exists, occur near grazing observations. This is especially important when accounting for the sources of higher order diffraction mechanisms as will be encountered in the chapter 4.

The magnetic current contribution dominated when the reactance was large as shown in figures 2.3 and 2.4. As the reactance decreased the electric current became dominant.

At the same time the strength of the surface wave contribution decreased. This effect is easily explained by the surface wave pole position in the complex plane moving away from the SDP and the saddle point.

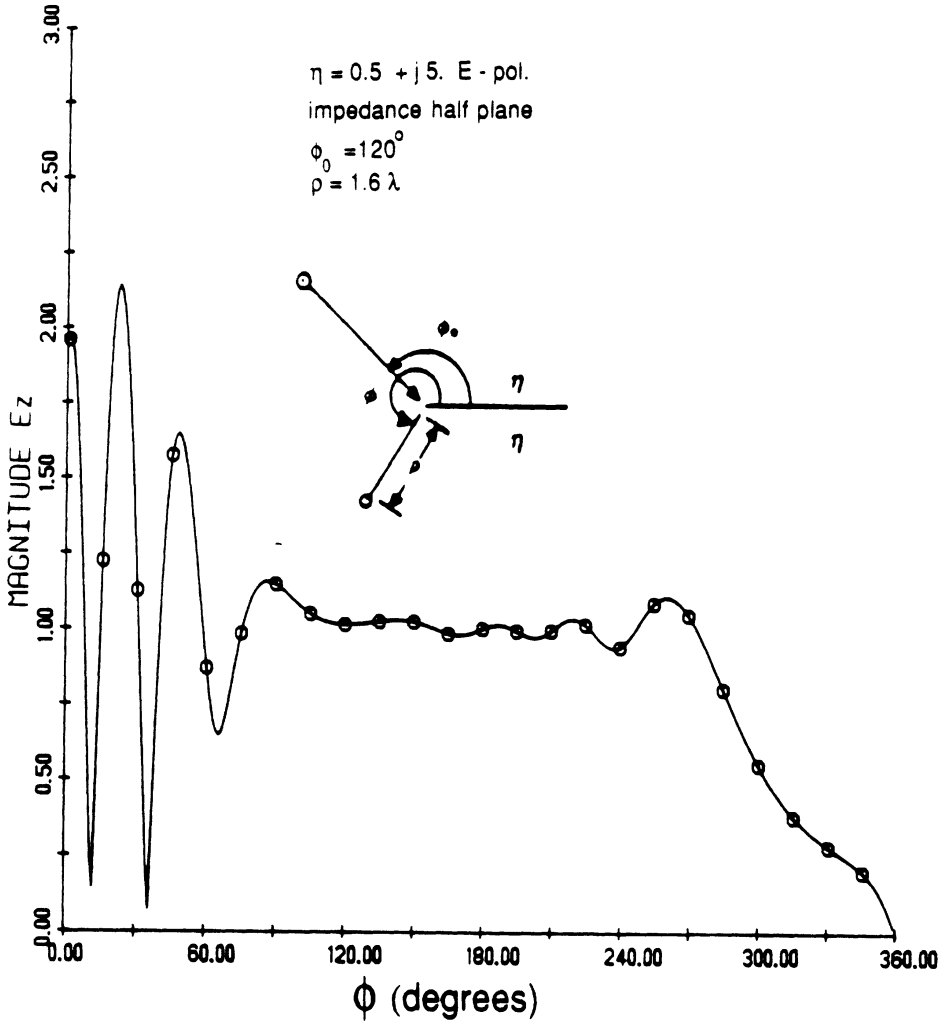

Figure 2.3 — Bistatic scattering from an impedance half plane ($\eta = 0.5 + j5$), E-polarization

Pattern of the total electric field due to a plane wave source.

Angle of incidence equals 120^o, and observation distance 1.6λ.

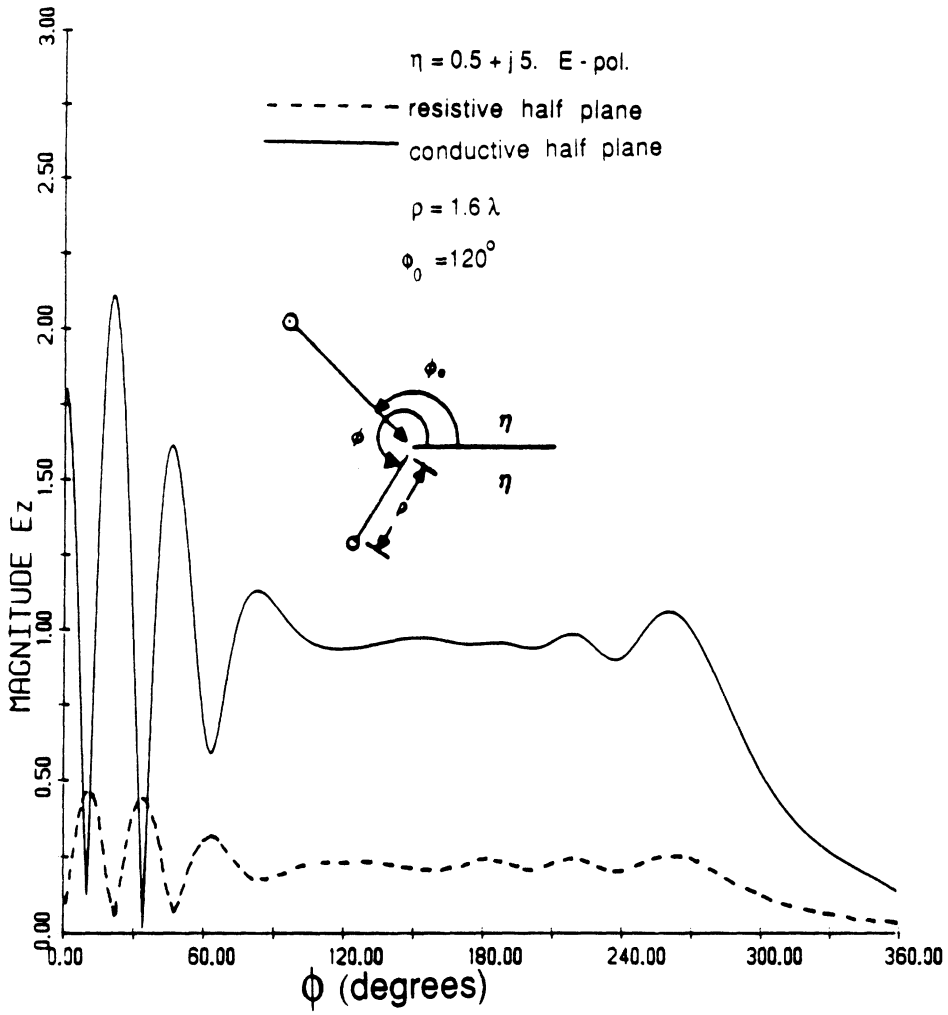

Figure 2.4 — Bistatic scattering from a resistive and conductive half planes ($\eta = 0.5 + j5$), E-polarization

Pattern of the total electric field due to a plane wave source.

Angle of incidence equals 120^o, and observation distance 1.6λ.

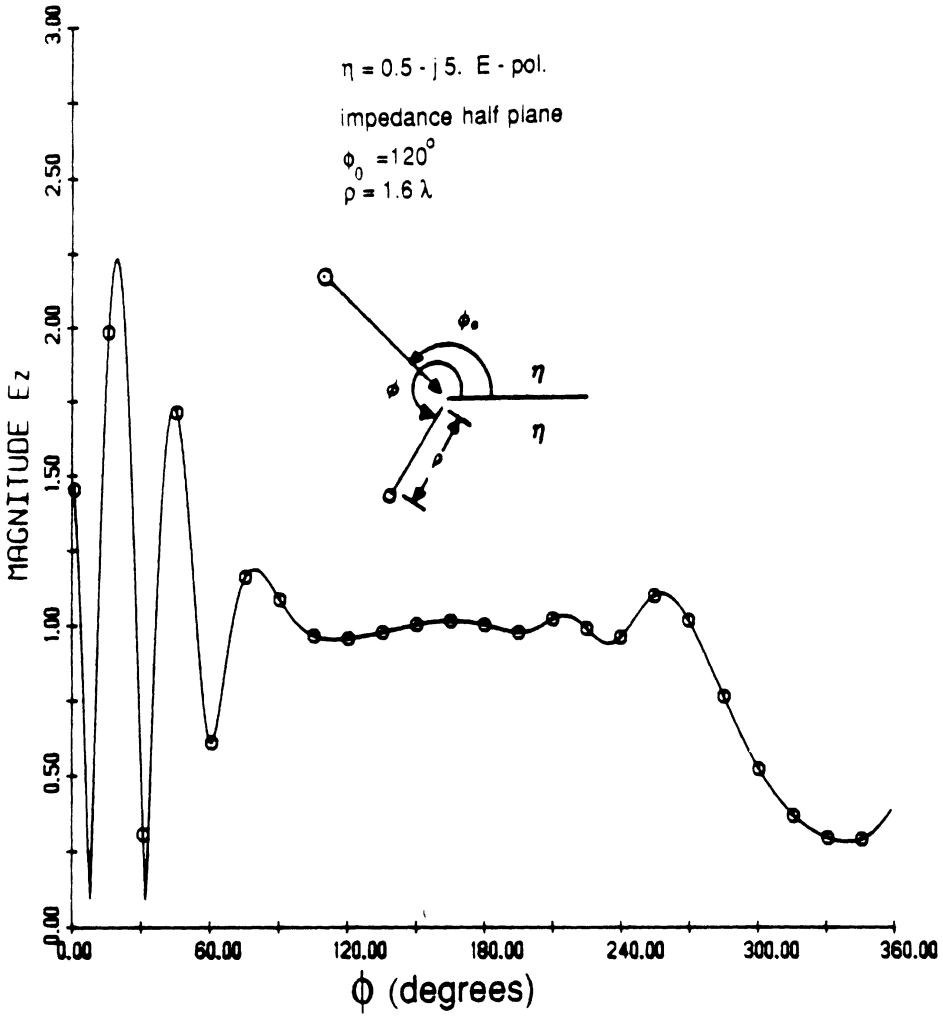

Figure 2.5 — Bistatic scattering from an impedance half plane ($\eta = 0.5 - j5$), E-polarization

Angle of incidence equals 120°, and observation distance 1.6λ.

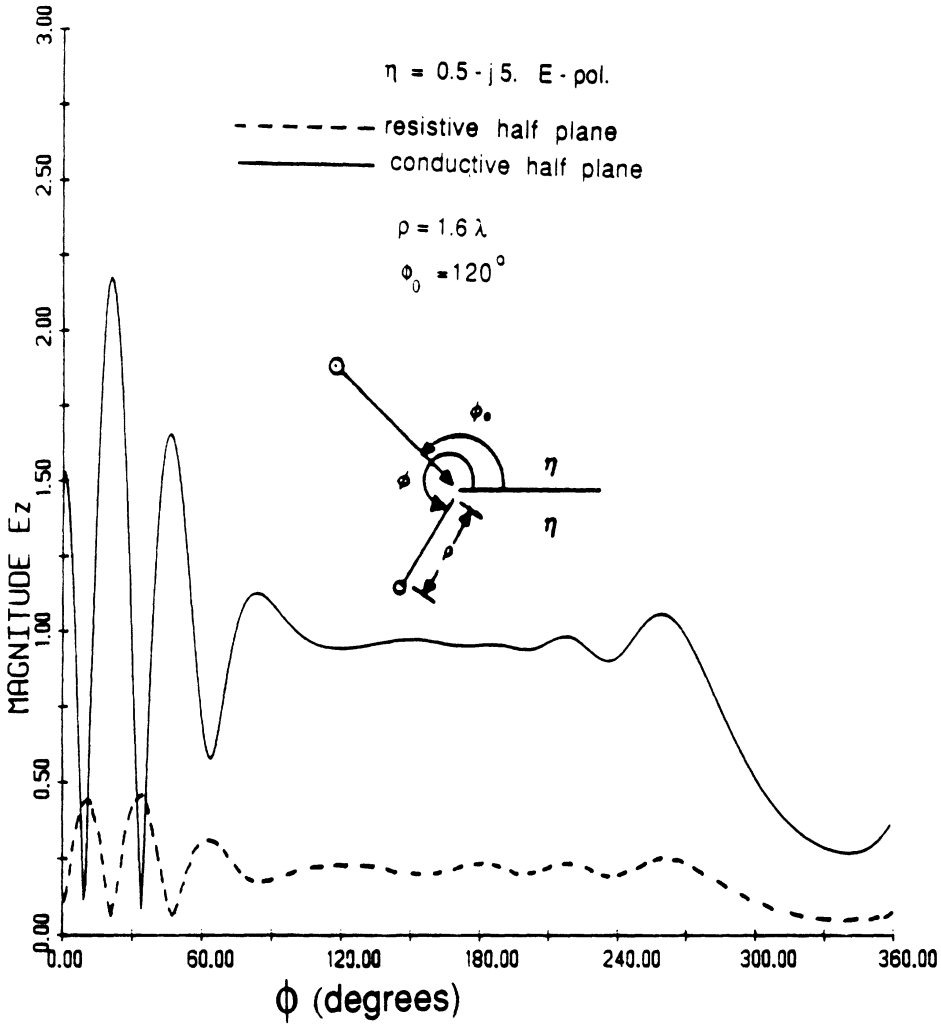

Figure 2.6 — Bistatic scattering from a resistive and conductive half planes ($\eta = 0.5 - j5$), E-polarization

Pattern of the total electric field due to a plane wave source.

Angle of incidence equals 120°, and observation distance 1.6λ.

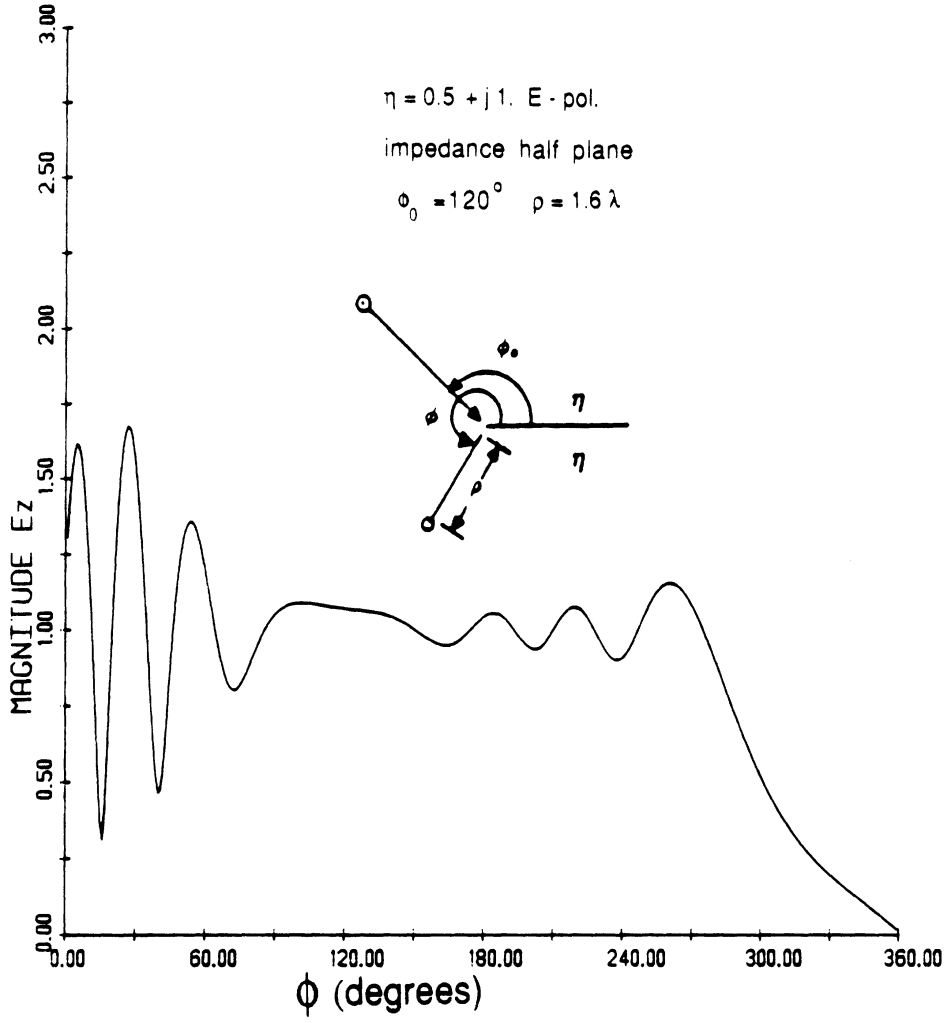

Figure 2.7 — Bistatic scattering from an impedance half plane ($\eta = 0.5 + j1$), E-polarization

Pattern of the total electric field due to a plane wave source.

Angle of incidence equals 120°, and observation distance 1.6λ.

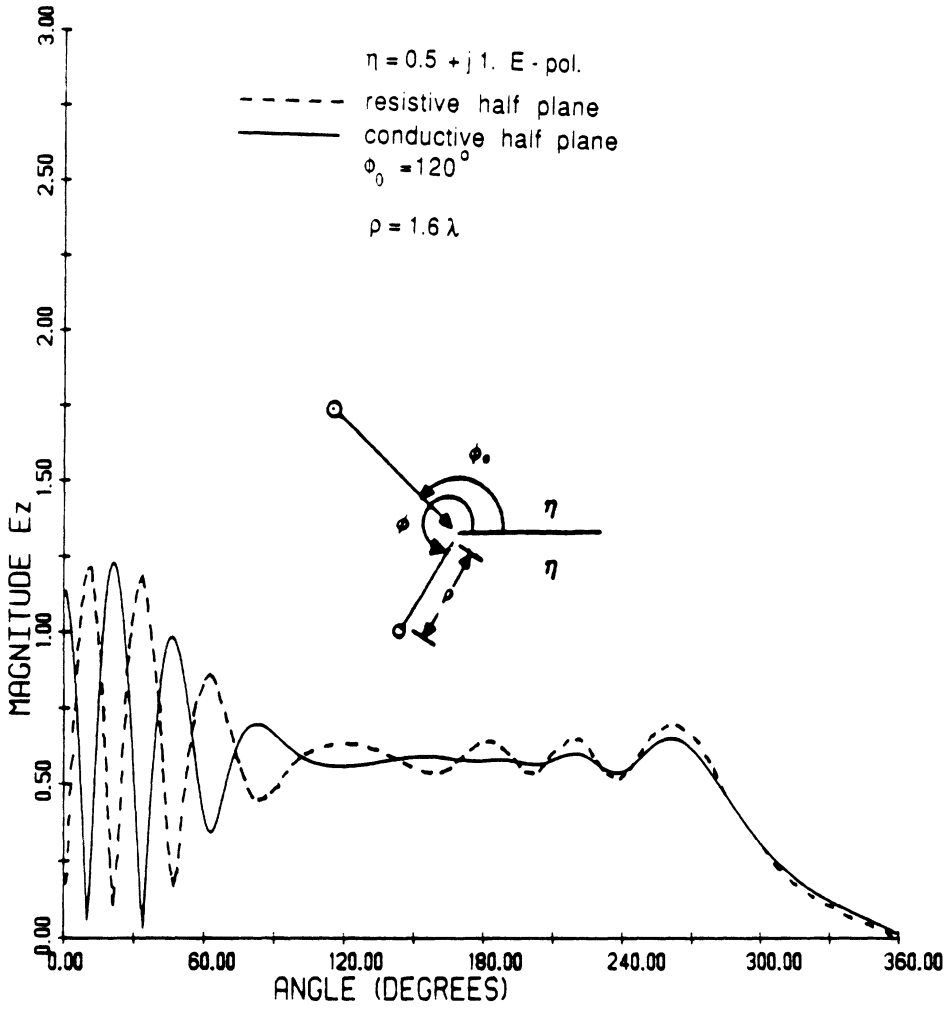

Figure 2.8 — Bistatic scattering from a resistive and conductive half planes ($\eta = 0.5 + j1$), E-polarization

Pattern of the total electric field due to a plane wave source.

Angle of incidence equals 120°, and observation distance 1.6λ.

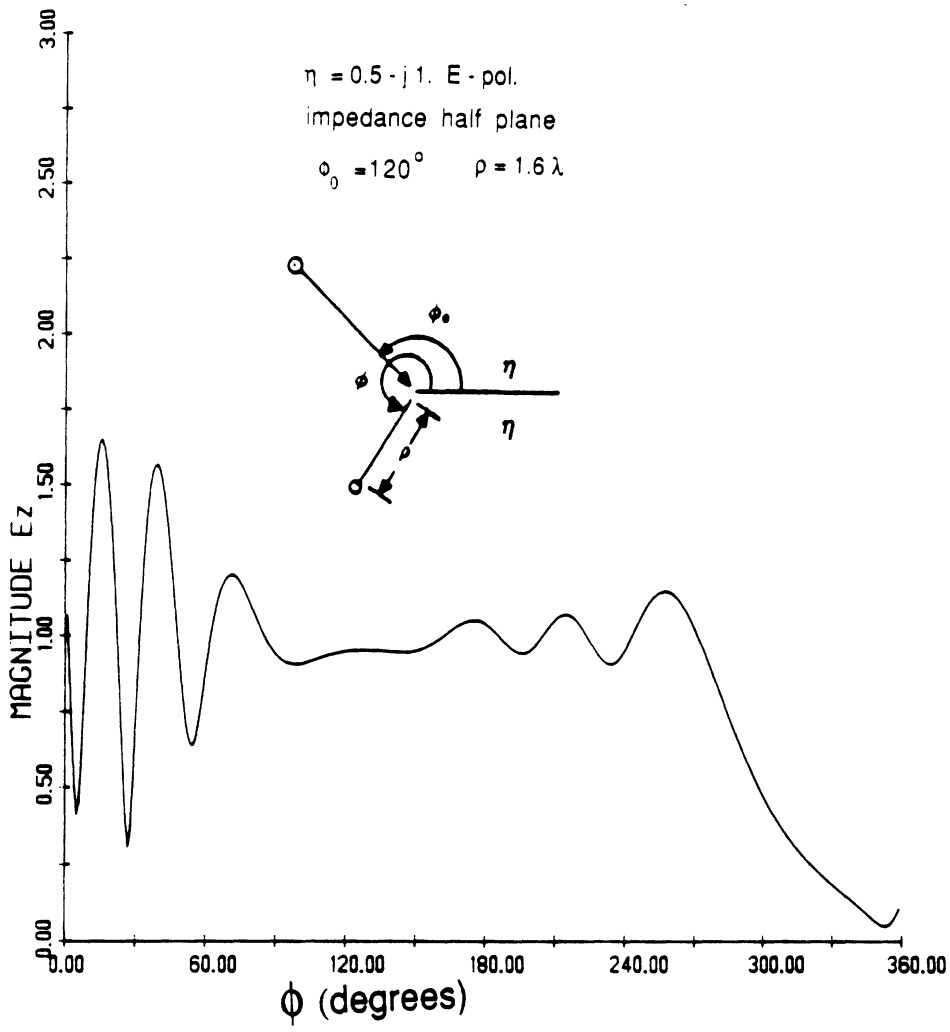

Figure 2.9 — Bistatic scattering from an impedance half plane ($\eta = 0.5 - j1$), E-polarization

Pattern of the total electric field due to a plane wave source.

Angle of incidence equals 120°, and observation distance 1.6λ.

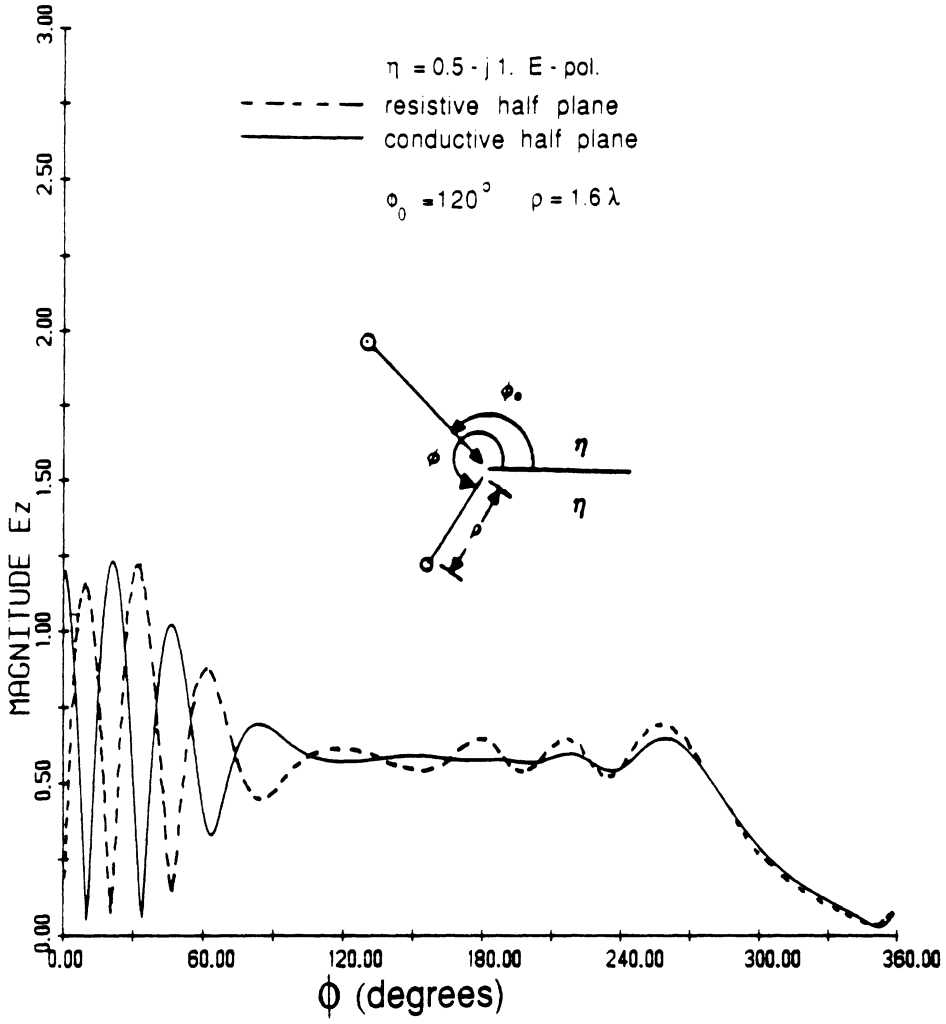

Figure 2.10 — **Bistatic scattering from a resistive and conductive half planes** ($\eta = 0.5 - j1$), **E-polarization**

Pattern of the total electric field due to a plane wave source.

Angle of incidence equals 120°, and observation distance 1.6λ.

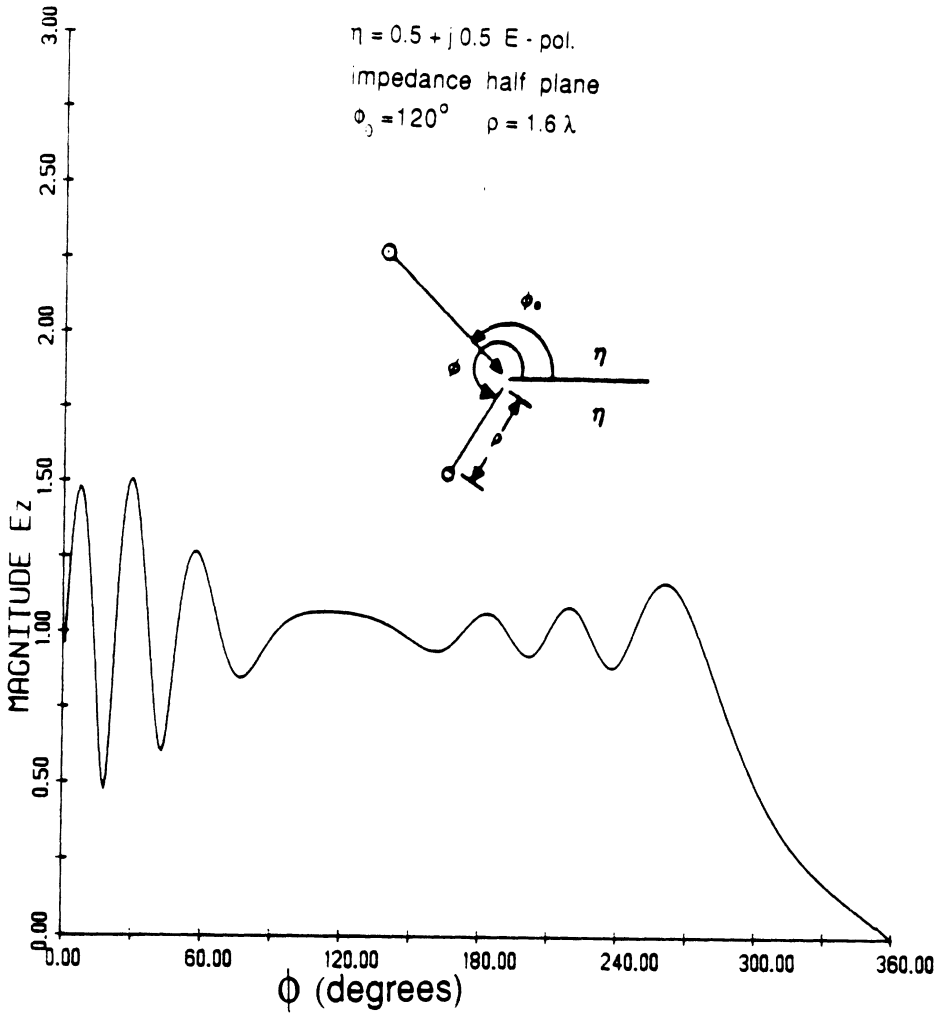

Figure 2.11 — Bistatic scattering from an impedance half plane ($\eta = 0.5 + j0.5$), E-polarization

Pattern of the total electric field due to a plane wave source.

Angle of incidence equals 120^o, and observation distance 1.6λ.

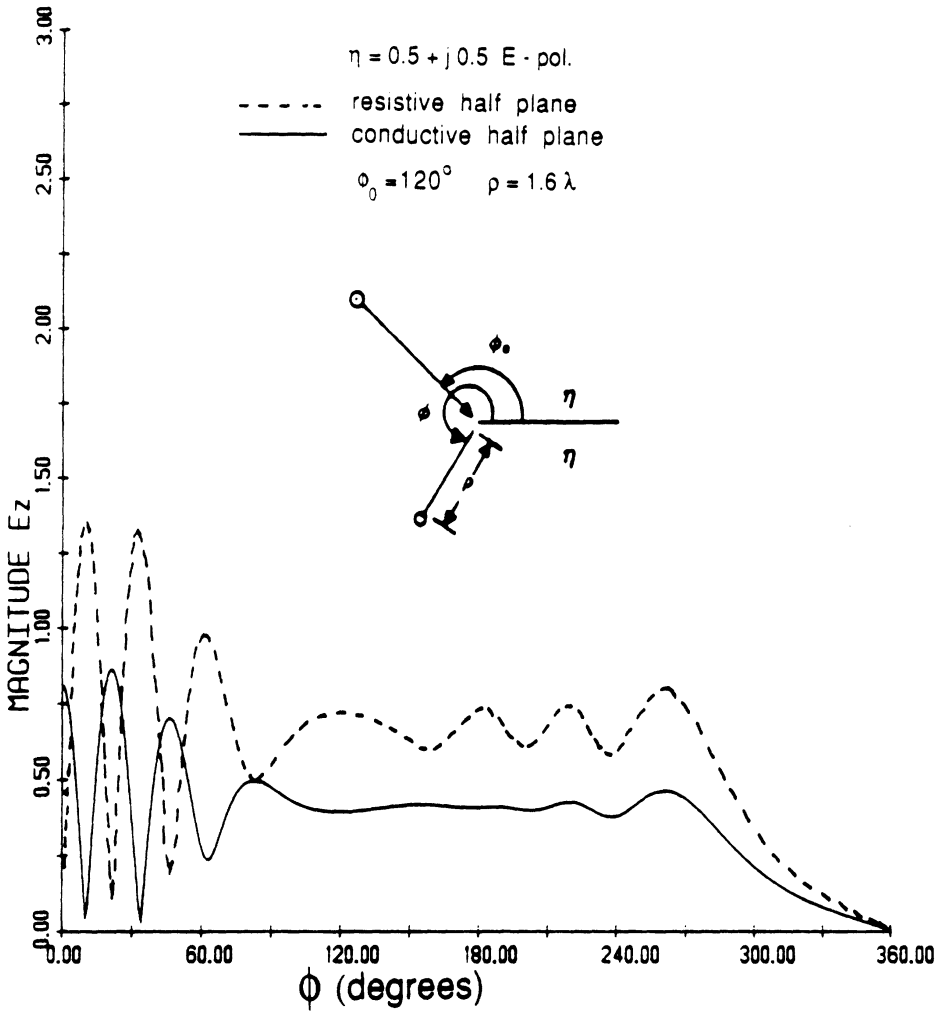

Figure 2.12 — Bistatic scattering from a resistive and conductive half planes ($\eta = 0.5 + j0.5$), E-polarization

Pattern of the total electric field due to a plane wave source.

Angle of incidence equals 120°, and observation distance 1.6λ.

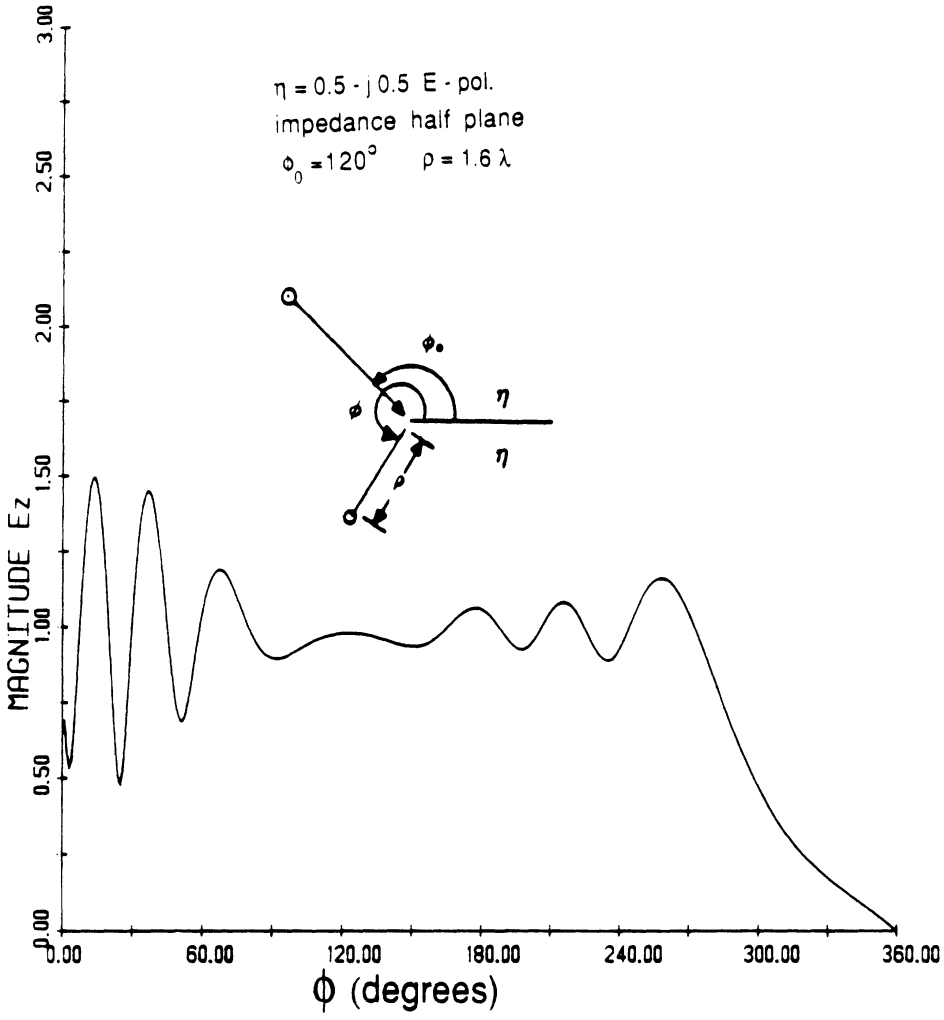

Figure 2.13 — Bistatic scattering from an impedance half plane ($\eta = 0.5 - j0.5$), E-polarization

Pattern of the total electric field due to a plane wave source.

Angle of incidence equals 120°, and observation distance 1.6λ.

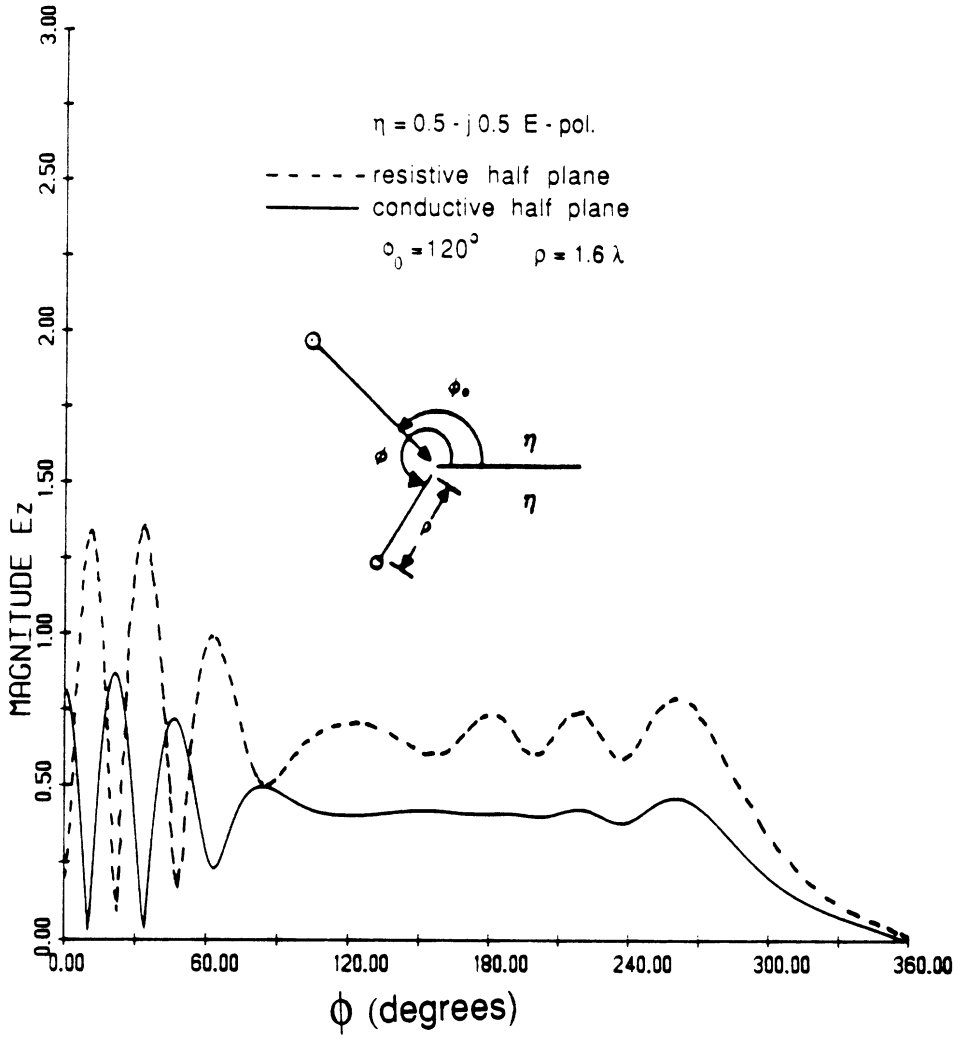

Figure 2.14 — Bistatic scattering from a resistive and conductive half planes ($\eta = 0.5 - j0.5$), E-polarization

Pattern of the total electric field due to a plane wave source.

Angle of incidence equals 120°, and observation distance 1.6λ.

CHAPTER III

THE EXTENDED SPECTRAL RAY METHOD

When one considers multiple edge diffraction the usual methods of self-consistent GTD [30] or slope diffraction [14, 15] fail if one edge lies in the transition region of the other. In this case the field impinging on the latter edge is non-ray optical. The approach employed to overcome this major problem is in the use of the Extended Spectral Ray Method (ESRM). The ESRM is a generalization of the Spectral Theory of Diffraction (STD) introduced by Rahmat-Samii and Mittra [19, 20, 21]. In accordance with the STD a field can be represented as an integral or "sum" of spectral plane waves, a formulation discussed by Clemmow [31]. Tiberio et. al. [13, 17] noted that the integral of the field diffracted by an edge is of the same form and can be thus interpreted as an infinite sum of inhomogeneous plane waves which clearly have a ray representation. This interpretation is the basis of the ESRM and allows the treatment of each of the inhomogeneous plane waves independently via known procedures.

As an example, when considering double diffractions, the field incident on the second edge is first written as an integral of inhomogeneous plane waves. Assuming these plane waves have a slowly varying spatial pattern, the diffraction of each of them at the second edge amounts to multiplying the integrand by the known plane wave diffraction coefficient after its analytic continuation in the complex plane. The resulting integral can be subsequently evaluated via standard asymptotic means. By invoking reciprocity, it will be seen that a similar procedure can be applied to the computation of higher order diffraction fields.

In order to gain a geometrical interpretation of the ESRM as it relates to our problem, let us assume a plane wave is incident upon the configuration in figure 3.1. The integral for

the singly diffracted field by the impedance wedge at Q_1 can then be written as

$$u_1^d(\phi,\phi_o) = \int_C F(\alpha,\phi_o) e^{-jk\rho\cos(\alpha-\phi)}\, d\alpha \tag{3.1}$$

whose asymptotic evaluation for large $k\rho$ gives

$$u_1^d(\phi,\phi_o) \sim D(\phi,\phi_o)\frac{e^{-jk\rho}}{\sqrt{\rho}} \tag{3.2}$$

In the above ϕ_o and ϕ are the incidence and observation angles, respectively. Both are measured with respect to the common wedge face as shown in figure 3.2. In addition, F is a known spectral function, D is the wedge diffraction coefficient and C denotes the steepest descent path of the integrand. When the field in (3.1) is incident onto Q_2 then $\phi = 0$ and the integral in (3.1) can now be thought as an infinite sum of inhomogeneous plane waves propagating towards Q_2. These plane waves form as angle of $-\alpha$ with respect to the common face at Q_1 and from geometrical considerations we find that they must be incident at Q_2 with a local angle of α when measured with respect to the common face at Q_2. Through analytic continuation it is clear that the diffracted field at Q_2 due to each inhomogeneous plane waves is $D(\phi_2,\alpha)\frac{e^{-jk\rho_2}}{\sqrt{\rho_2}}$, where ρ_2 is the far zone observation distance measured with respect to Q_2 and ϕ_2 is the observation angle measured with respect to the common wedge face at Q_2. Incorporating this into the diffraction integral in (3.1) gives the double diffracted field from Q_1 to Q_2 as

$$u_{21}^d(\phi,\phi_o) = \frac{e^{-jk\rho}\, e^{-jkw\cos\phi_2}}{\sqrt{\rho}} \int_C F(\alpha,\phi_o) D(\phi_2,\alpha) e^{-jkw\cos\alpha}\, d\alpha \tag{3.3}$$

where we have used the relation $\rho_2 = \rho + w\cos\phi_2$ so that the phase of u_{21}^d is referenced to Q_1. Note also that the factor $e^{-jkw\cos\alpha}$ in the integral simply accounts for the propagation delay of each of the spectral plane waves incident at Q_2.

As will be discussed later, the integral in (3.3) is amenable to a uniform asymptotic evaluation with considers all integrand poles that may be near the integration path. Furthermore, we note that although the ESRM was discussed above in relation to the double diffraction mechanism, it will be seen that its application is easily extended to higher order mechanisms.

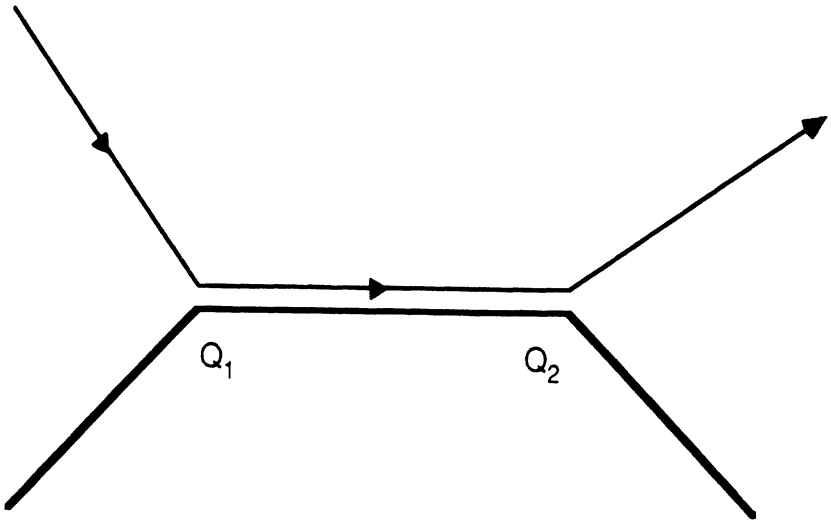

Figure 3.1 — Multi-edge ray path on a double wedge.

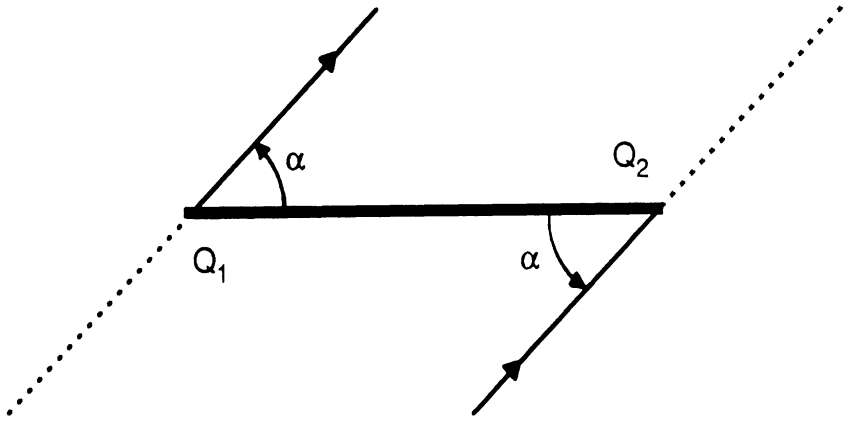

Figure 3.2 — Local angle notation of a doubly diffracted ray

The diffraction coefficient $D(\phi_2, \alpha)$ mentioned above can be in a uniform or non-uniform form. Clearly for far zone diffraction, the simple non-uniform form of $D(\phi_2, \alpha)$ is sufficient and applicable to our case. However, for near zone field calculations, the uniform diffraction coefficient must be employed. This will inevitably require the introduction of Fresnel integrals within the integral of (3.3). As a result the integrand term $F(\alpha, \phi_o)D(\phi_2, \alpha)$ may not be slowly varying and thus requiring a more careful evaluation of the expression for u_{21}^d than that considered in this work. It should further be noted that the accuracy of expression (3.3) for the double diffracted field is directly dependent on the accuracy of $D(\phi_2, \alpha)$ and its derivatives near the saddle point(s) through the steepest descent path C. Clearly, if the exact integral representation of $D(\phi_2, \alpha)$, as derived from (3.1) and (3.2), is substituted in (3.3), the resulting expression for u_{21}^d will be exact.

CHAPTER IV

SCATTERING FROM RESISTIVE, CONDUCTIVE AND IMPEDANCE STRIPS

The coefficients for the double and triple diffraction mechanisms are derived in this chapter for a resistive strip using the Extended Spectral Ray Method described in chapter III. These terms rigorously account for surface wave interactions which may in some cases be dominant for various materials. It is of particular interest to try to model a thin dielectric strip using a resistive strip. Due to the nature of the formulation, once the coefficients for the resistive strip are known it is easy to solve for the conductive strip since the currents are uncoupled[22]. As mentioned in chapter II, the resistive (conductive) strip, like the half plane, is associated with the electric (magnetic) current. As a consequence of this fact the impedance strip is just the summation of the prior results for the resistive and conductive cases.

The geometry of a strip is shown in figure 4.1. The incident field is normal to the plane of the plane of the strip and the impedances on both the top and bottom surfaces are equal. Throughout this chapter the phase reference is assumed to be at the left edge (Q_1).

Numerical results for all three types of strips are presented and compared with moment method solutions.

Primary Edge Diffraction

Chapter II presented the uniform edge diffraction coefficients for resistive, conductive, and impedance half planes. However, when one is concerned with plane wave incidence and far zone observations, the non-uniform solution is sufficient. Evaluating (2.2) non-uniformly

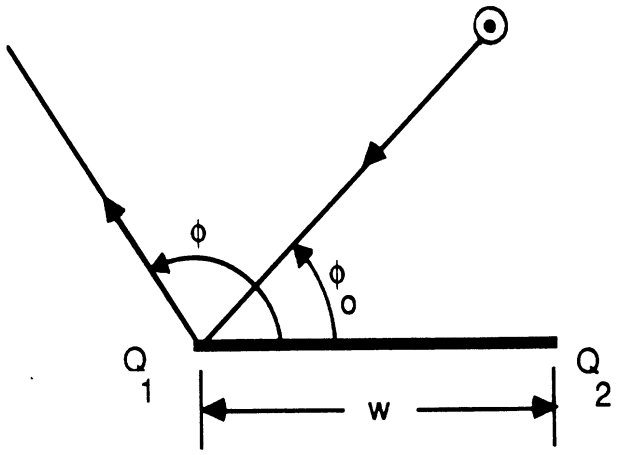

Figure 4.1 — Geometry of a strip

gives

$$E^s(\phi,\phi_0) = -\frac{j}{2\pi}\sqrt{\frac{2\pi}{k\rho}}e^{j\frac{\pi}{4}}e^{-jk\rho\cos\phi}\frac{1}{\cos\phi+\cos\phi_o}\left\{1\mp\eta\sqrt{(1+\cos\phi)(1+\cos\phi_o)}\right\} \cdot K_+(\phi)K_+(\phi_o)e^{-jkr}; \qquad y\gtrless 0. \tag{4.1}$$

The only new variable introduced in (4.1) was the phase factor r which equals zero for primary diffraction from Q_1 and $-w(\cos\phi_o+\cos\phi)$ from Q_2. Note that (4.1) is equivalent to (2.7).

Equation (4.1) is applicable to impedance strips. Within the braces, the terms not multiplied by η are associated with a resistive strip while the rest are associated with a conductive one.

Double Diffraction Mechanism For a Resistive Strip

The second order diffracted field is that which is diffracted from edge $Q_2(Q_1)$ after diffraction from $Q_1(Q_2)$. As shown in figure 4.2 there are four mechanisms associated with this phenomenon. In evaluating their contribution we must also consider the existence of possible surface waves in addition to the ray field components. A traditional approach would have been to repeatedly employ the uniform edge diffraction coefficient in (2.7)-(2.9) or in (2.25)-(2.28) with the incident field being the one diffracted from the previous edge. However, such a procedure requires that all incident fields be ray-optical , a condition which is obviously not satisfied when the argument of the transition function is small. For the second order mechanisms this occurs for near grazing incidence (ϕ_o near 180^o). In that case the second edge will be in the transition region of the first and thus one must resort to an alternative procedure for evaluating the second order fields.

As discussed earlier, the evaluation of the second order fields will be based on the principles of the ESRM (Extended Spectral Ray Method). The procedure to be followed is similar to that employed by Tiberio et. al.[26] for evaluating the second order diffraction by a perfectly conducting wedge. In short, the incident field to the second edge (4.2) is interpreted as a sum (integral) of inhomogeneous plane waves. Each one of these plane waves can then be treated individually. This implies that its far zone contribution to double

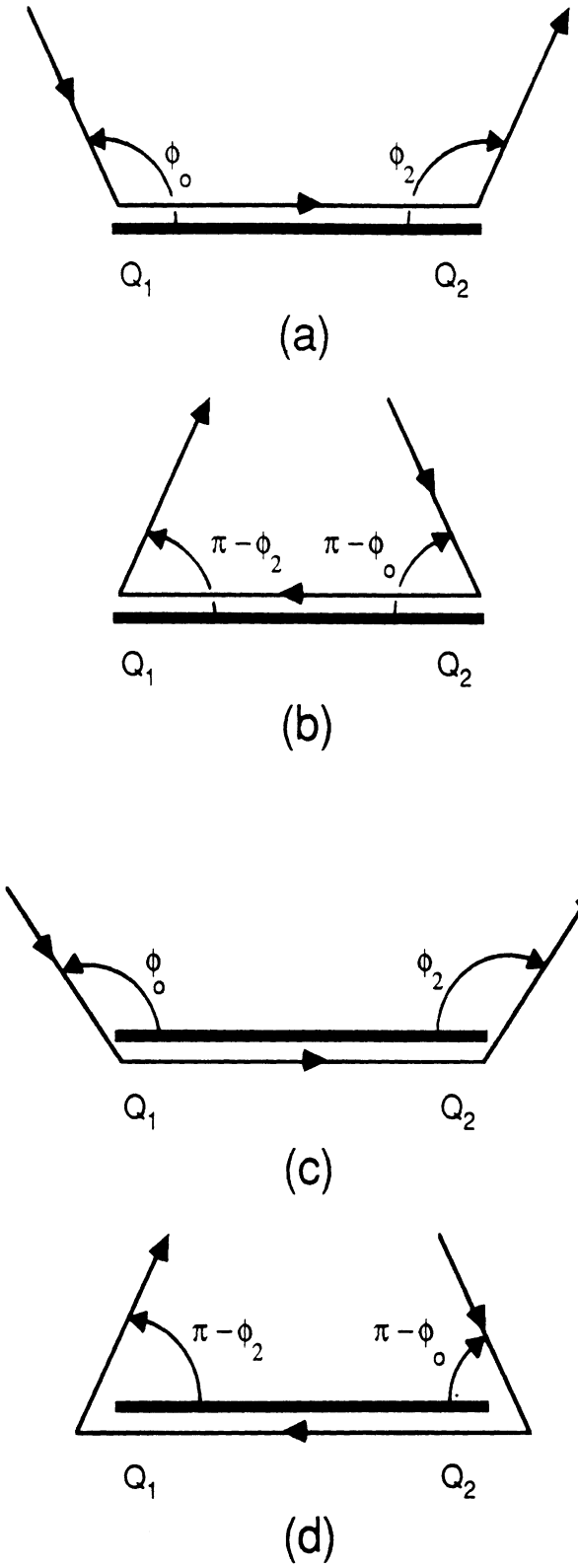

Figure 4.2 — Double diffraction ray mechanisms of a strip.

diffraction can be accounted for by simply multiplying its spectral strength with the non-uniform diffraction coefficient using complex angles of incidence. The total doubly diffracted field is subsequently found by summing (integrating) the contributions of all inhomogeneous plane waves. However, in the case of the resistive strip, when performing the integration it is necessary to also consider the effect of the surface wave pole which adds substantially to the complexity of the problem.

The exact integral representation of the field incident to edge Q_2 after diffraction from Q_1 is given by

$$E_1 = \frac{-j}{2\pi} \int_{S(0)} \frac{\sin\frac{\alpha}{2}}{\cos\alpha + \cos\phi_o} K_{+c}(\alpha) K_+(\phi_o) e^{-jk\rho\cos(\alpha)}\, d\alpha \tag{4.2}$$

From (4.2) we have a complex plane wave diffracting from Q_1 at an angle α. Therefore, in accordance with the ESRM we must have a plane wave incidence at Q_2 at an angle $-\alpha$. At the second edge we may invoke reciprocity and have a plane wave incident at an angle ϕ_2 (see figure 4.3) and diffracted at a complex angle $-\alpha$. By following the ESRM procedure we automatically prevent the false occurrence of a double surface wave pole in the double diffraction integrand. Equation (4.2) is evaluated non-uniformly to yield

$$E_2 = \frac{j}{2\pi}\sqrt{\frac{2\pi}{k\rho}} e^{j\frac{\pi}{4}} e^{-jk\rho} \frac{\sin(\alpha/2)}{\cos\alpha + \cos\phi_2} K_{+c}(-\alpha) K_+(\phi_2). \tag{4.3}$$

The integrand of (4.2) can now be multiplied by (4.3) to give the doubly diffracted field from edge Q_1 to Q_2 and then to the observer. We obtain

$$\begin{aligned} E_{21}^d(\phi_2, \phi_0) = -\frac{\sqrt{2\pi}}{4\pi^2} \frac{e^{j\pi/4} e^{-jk\rho}}{\sqrt{k\rho}} \int_{S(0)} & \frac{-\sin^2(\frac{\alpha}{2}) K_{+c}(\alpha) K_{+c}(-\alpha)}{[\cos\alpha + \cos\phi_o][\cos\alpha + \cos\phi_2]} \\ & \cdot K_+(\phi_o) K_+(\phi_2) e^{-jkw\cos\alpha}\, d\alpha, \end{aligned} \tag{4.4}$$

where the integral can be evaluated asymptotically via the steepest descents method (SDP). Before proceeding to do so, it is convenient to subdivide the integrand to a sum of simpler

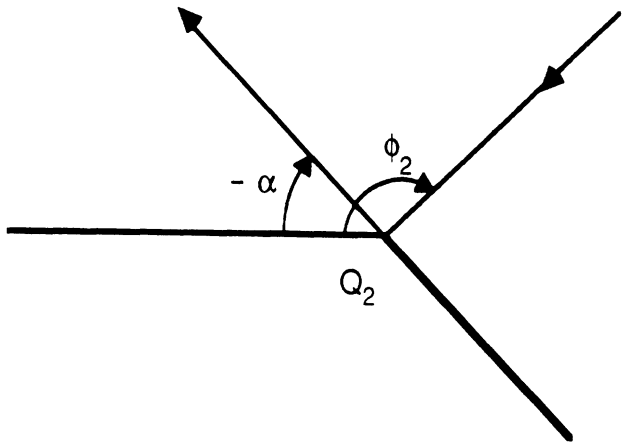

Figure 4.3 — Plane wave field incidence and diffraction at a complex angle $-\alpha$ on edge Q_2

components. Straightforward use of trigonometric identities gives

$$
\begin{aligned}
E_{21}^{d}(\phi_2,\phi_0) = & \frac{\sqrt{2\pi}}{64\pi^2}\frac{K_+(\phi_o)K_+(\phi_2)}{\cos\frac{\phi_o}{2}\cos\frac{\phi_2}{2}}\frac{e^{j\frac{\pi}{4}}e^{-jk\rho}}{\sqrt{k\rho}}\int_{S(0)}\frac{1}{\cos^2\frac{\alpha}{2}} \\
& \cdot\Big[\sec(\frac{\alpha-\phi_o}{2})\sec(\frac{\alpha+\phi_2}{2})K_{+c}(\alpha)K_{-c}(-\alpha)\sin^2\frac{\alpha}{2} \\
& +\sec(\frac{\alpha+\phi_o}{2})\sec(\frac{\alpha-\phi_2}{2})K_{+c}(\alpha)K_{+c}(-\alpha)\sin^2\frac{\alpha}{2} \\
& -\sec(\frac{\alpha-\phi_o}{2})\sec(\frac{\alpha+\phi_2}{2})K_{+c}(\alpha)K_{+c}(-\alpha)\sin^2\frac{\alpha}{2} \\
& -\sec(\frac{\alpha-\phi_o}{2})\sec(\frac{\alpha-\phi_2}{2})K_{-c}(\alpha)K_{+c}(-\alpha)\sin^2\frac{\alpha}{2}\Big] \\
& \cdot e^{-jkw\cos\alpha}\,d\alpha
\end{aligned}
\tag{4.5}
$$

Each one of the four terms composing the integrand in (4.5) is clearly associated with three poles located at $\alpha_{p1} = \pi \pm \phi_o$, $\alpha_{p2} = \pi \pm \phi_2$, and $\alpha_{p3} = -\theta$ (surface wave pole). Furthermore, we recognize that the first non-vanishing term associated with the SDP evaluation of (4.5) is the same for all integrand terms. Thus one needs only to evaluate the integral for one of the integrand terms and then multiply by 4. Using the results given in Appendix C we obtain that

$$
\begin{aligned}
E_{21}^{d}(\phi_2,\phi_0) \approx & +j\frac{K_+(\phi_o)K_+(\phi_2)}{4\pi k}K_{+c}^2(0)a_3 e^{-jkw}e^{-jk\rho}\sqrt{\frac{1}{\rho w}} \\
& \cdot[A\{1-F_{KP}(kwa_1)\}+B\{1-F_{KP}(kwa_2)\}+C\{1-F_{KP}(kwa_3)\}]
\end{aligned}
\tag{4.6}
$$

where

$$a_1 = 2\cos^2\frac{\phi_o}{2} \tag{4.7}$$

$$a_2 = 2\cos^2\frac{\phi_2}{2} \tag{4.8}$$

$$a_3 = 2\sin^2\frac{\theta}{2} \tag{4.9}$$

$$A = \frac{-1}{(a_2-a_1)(a_3-a_1)} \tag{4.10}$$

$$B = \frac{-1}{(a_1-a_2)(a_3-a_2)} \tag{4.11}$$

$$C = \frac{-1}{(a_1-a_3)(a_2-a_3)} \tag{4.12}$$

and

$$E^d_{21}(\phi_2,\phi) = D_{21}(\phi_2,\phi)e^{jkw\cos\phi_2}\frac{e^{-jk\rho}}{\sqrt{\rho}}.$$

Equation (4.6) is the second term and first non-zero one of the Maclaurin series expansion. The final result for the doubly diffracted field in (4.6) contains a factor of one-half to account for the grazing incidence at the second edge.

As a check of this bistatic solution for the double diffraction from a strip, we evaluate the case corresponding to a perfectly conducting strip ($\eta \to 0$). As η goes to zero we find that

$$a_3 \to \infty, \tag{4.13}$$

$$K_{-c}(\alpha = 0) \to \sqrt{2}, \tag{4.14}$$

and

$$K_{-}(\alpha) \to \sqrt{2}\sin(\alpha/2). \tag{4.15}$$

Substituting these values in (4.6) gives

$$E^d_{21pc}(\phi_2,\phi_0) \approx j\frac{4\sin\frac{\phi_o}{2}\sin\frac{\phi_2}{2}}{8\pi^{\frac{3}{2}}}\frac{e^{-jkw}e^{-jk\rho}}{\sqrt{k\rho}}\sqrt{\frac{\pi}{kw}}\left\{-\frac{1}{(a_2-a_1)}\{1-F_{KP}(kwa_1)\}\right.$$
$$\left.-\frac{1}{(a_1-a_2)}\{1-F_{KP}(kwa_2)\}-\frac{1}{\infty}\{1-F_{KP}(kwa_3)\}\right\} \tag{4.16}$$

$$\approx j\frac{\sin\frac{\phi_o}{2}\sin\frac{\phi 2}{2}}{2(a_2-a_1)\pi\sqrt{kw}}\frac{e^{-jkw}e^{-jk\rho}}{\sqrt{k\rho}}\{F_{KP}(kwa_1)-F_{KP}(kwa_2)\} \tag{4.17}$$

At edge-on incidence we have $\phi_o \to \pi, (a_1 \to 0)$ and $\phi_2 \to \pi - \phi$ (i.e. only two mechanisms exist), implying,

$$E^d_{21pc}(\pi-\phi,\pi) \approx \frac{-j\cos\frac{\phi}{2}}{2\pi\sin^2\frac{\phi}{2}\sqrt{kw}}e^{-jkw}\frac{e^{-jk\rho}}{\sqrt{k\rho}}F_{KP}(2kw\sin^2\frac{\phi}{2}) \tag{4.18}$$

This is the same second order result as derived by Tiberio et. al. [13] for the perfectly conducting strip.

Triple Diffraction Mechanisms For a Resistive Strip

As shown in figure 4.4 there are eight third order diffraction mechanisms to be considered. Four emanate from edge Q_1 and each gives an equal contribution to the diffracted

field. The other four emanate from edge Q_2 and likewise are of equal strength. Each mechanism involves first a diffraction from $Q_1(Q_2)$ to $Q_2(Q_1)$ and then a subsequent diffraction from $Q_2(Q_1)$ to $Q_1(Q_2)$ and back to the observer (not necessarily backscattering). In accordance with the ESRM, an integral representation for the triply diffracted field from Q_1 is

$$u^d_{121}(\phi,\phi_o) = \frac{-j}{2\pi}\frac{e^{-jk\rho}}{\sqrt{\rho}}\int_{S(0)} \frac{\sin\frac{\alpha}{2}}{\cos\alpha+\cos\phi} D_{21}(-\alpha,\varphi_o)K_{+c}(\alpha)K_+(\phi)e^{-jkw\cos(\alpha)}\,d\alpha \tag{4.19}$$

Equation (4.19) can again be considered as a sum of inhomogeneous plane waves incident on edge Q_2 at a complex angle -α. In the case of third order diffraction each one of these must first diffract from Q_2 to Q_1 before returning to the observer (because of reciprocity the incidence angle is now ϕ). Clearly, this scenario corresponds to that of a second order diffraction with plane wave incidence and far zone diffraction computed in the previous section. Using the result in (4.6), equation (4.19) becomes.

$$\begin{aligned} u^d_{121}(\phi,\phi_o) = \frac{1}{2\pi}\frac{e^{-jk\rho}}{\sqrt{\rho}}\int_{S(0)} & \\ \Bigg\{ & \frac{\sin\frac{\alpha}{2}}{4\cos\frac{\alpha}{2}\cos\frac{\phi}{2}}\left[\sec\left(\frac{\alpha+\phi_o}{2}\right)+\sec\left(\frac{\alpha-\phi_o}{2}\right)\right]K_{+c}(\alpha)K_+(\phi) \\ & \cdot K_+(\phi_o)K_+(-\alpha)K^2_{+c}(\alpha=0)a_3\frac{e^{-jkw-jkw\cos(\alpha)}}{4\pi k\sqrt{kw}} \\ & \cdot\Bigg[\frac{1}{(a_2-a_1)(a_3-a_1)}\{1-F_{KP}(kwa_1)\}+\frac{1}{(a_1-a_2)(a_3-a_2)}\{1-F_{KP}(kwa_2)\} \\ & +\frac{1}{(a_1-a_3)(a_2-a_3)}\{1-F_{KP}(kwa_3)\}\Bigg]\Bigg\}\,d\alpha \end{aligned} \tag{4.20}$$

This integral is evaluated via the modified Pauli-Clemmow steepest descents method

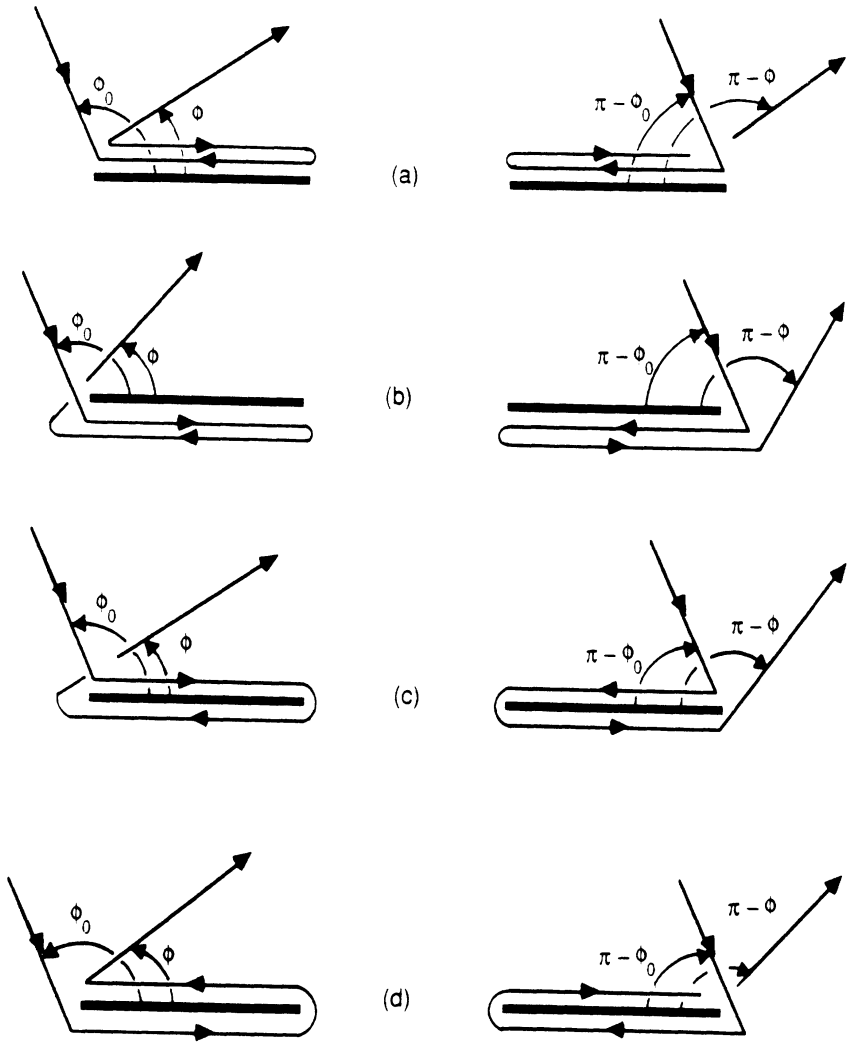

Figure 4.4 — Triple diffraction ray mechanisms of a strip.

to yield

$$E^d_{121}(\phi,\phi_o) = u^d_{121}(\phi,\phi_o) \sim j\frac{\sqrt{2}}{16(k\pi)^{\frac{3}{2}}w} e^{j3\pi/4}e^{-j2kw}K^4_{+c}(0)a_3^2K_+(\phi_o)K_+(\phi)$$
$$\cdot\left[\frac{1}{(2-a_1)(a_3-a_1)}\{1-F_{KP}(kwa_1)\}+\frac{1}{(a_1-2)(a_3-2)}\{1-F_{KP}(kw2)\}\right.$$
$$\left.+\frac{1}{(a_1-a_3)(2-a_3)}\{1-F_{KP}(kwa_3)\}\right]$$
$$\cdot\frac{1}{(a_3-a_4)}\{F_{KP}(kwa_3)-F_{KP}(kwa_4)\}\frac{e^{-jk\rho}}{\sqrt{\rho}} \tag{4.21}$$

where

$$a_4 = 2\cos^2\frac{\phi}{2}. \tag{4.22}$$

The details of the evaluation are given in Appendix D.

Equation 4.21 includes a multiplicative factor of 4 (for the four diffraction mechanism per edge) and one fourth to account for the double grazing effect.

As a check of this bistatic third order diffraction term we evaluate it for the perfectly conducting case as was done for the double diffraction term. Letting $\eta \to 0$ gives

$$E^d_{121_{pc}}(\phi,\phi_o) \approx j\sqrt{\frac{2\pi}{kw}}\frac{e^{j3\pi/4}e^{-j2kw}}{2\pi^2k\sqrt{w}}\sin\frac{\phi_o}{2}\sin\frac{\phi}{2}$$
$$\cdot\left[\frac{1}{(2-a_1)}\{1-F_{KP}(kwa_1)\}+\frac{1}{(a_1-2)}\{1-F_{KP}(2kw)\}\right]$$
$$\cdot\{F_{KP}(kwa_3)-F_{KP}(kwa_4)\}\frac{e^{-jk\rho}}{\sqrt{\rho}} \tag{4.23}$$
$$\approx\frac{je^{j3\pi/4}e^{-j2kw}\sin\frac{\phi_o}{2}\sin\frac{\phi}{2}}{\sqrt{2}(k\pi)^{3/2}w(2-a_1)}$$
$$\cdot(F_{KP}(2kw)-F_{KP}(kwa_1))(F_{KP}(kwa_3)-F_{KP}(kwa_4))\frac{e^{-jk\rho}}{\sqrt{\rho}} \tag{4.24}$$

If we further let $a_1 = 0, \phi_o = \pi$ (edge-on incidence)

$$E^d_{121_{pc}}(\phi,\pi) \approx\frac{je^{j3\pi/4}e^{-j2kw}\sin\frac{\phi}{2}}{2\sqrt{2}kw\pi^{3/2}}(1-F_{KP}(2kw\cos^2\frac{\phi}{2}))\frac{e^{-jk\rho}}{\sqrt{k\rho}} \tag{4.25}$$
$$\approx\frac{-je^{-j\pi/4}e^{-j2kw}\sin\frac{\phi}{2}}{2\sqrt{2}kw\pi^{3/2}}(1-F_{KP}(2kw\cos^2\frac{\phi}{2}))\frac{e^{-jk\rho}}{\sqrt{k\rho}}, \tag{4.26}$$

which is the same third order term derived by Tiberio et. al. [13] for the perfectly conducting strip.

Conductive and Impedance Strips

The double diffraction integral for a resistive strip was given in (4.5). To reformulate this for the case of an impedance strip we would multiply the integrand in (2.2) by $E^s(-\alpha, \phi_o)$ as defined in (4.1) giving

$$E_{21}^d(\phi_2, \phi_o) = \frac{-1}{(2\pi)^2}\sqrt{\frac{2\pi}{k}} K_+(\phi_o) K_+(\phi_2) e^{j\frac{\pi}{4}} \frac{e^{-jk\rho}}{\sqrt{k\rho}}$$
$$\cdot \int_{S(0)} \frac{1}{\cos\alpha + \cos\phi_o} \{1 \mp \eta\sqrt{(1+\cos\alpha)(1+\cos\phi_o)}\}$$
$$\cdot \frac{1}{\cos\alpha + \cos\phi_2} \{1(\mp)\eta\sqrt{(1+\cos\alpha)(1+\cos\phi_2)}\}$$
$$\cdot K_+(\alpha) K_+(-\alpha) e^{-jkw\cos\alpha}\, d\alpha$$

This parallels the ESRM procedure used for the case of the resistive strip including the implicit use of reciprocity in the formulation. The integrand is expanded using simple trigonometric identities to place it in a form amenable to evaluation via the modified Pauli-Clemmow method of steepest descent. The integral expression for the double diffraction from an impedance strip becomes

$$E_{21}^{d}(\phi_2,\phi_0)=\frac{\sqrt{2\pi}}{64\pi^2}\frac{K_+(\phi_o)K_+(\phi_2)}{\cos\frac{\phi_o}{2}\cos\frac{\phi_2}{2}}\frac{e^{j\frac{\pi}{4}}e^{-jk\rho}}{\sqrt{k\rho}}\int_{S(0)}\frac{1}{\cos^2\frac{\alpha}{2}}$$

$$\cdot\Bigg\{\Bigg[\sec\left(\frac{\alpha+\phi_o}{2}\right)\sec\left(\frac{\alpha+\phi_2}{2}\right)K_{+c}(\alpha)K_{+c}(-\alpha)\sin^2\frac{\alpha}{2}$$

$$+\sec\left(\frac{\alpha+\phi_o}{2}\right)\sec\left(\frac{\alpha-\phi_2}{2}\right)K_{+c}(\alpha)K_{+c}(-\alpha)\sin^2\frac{\alpha}{2}$$

$$+\sec\left(\frac{\alpha-\phi_o}{2}\right)\sec\left(\frac{\alpha+\phi_2}{2}\right)K_{+c}(\alpha)K_{-c}(-\alpha)\sin^2\frac{\alpha}{2}$$

$$+\sec\left(\frac{\alpha-\phi_o}{2}\right)\sec\left(\frac{\alpha-\phi_2}{2}\right)K_{+c}(\alpha)K_{-c}(-\alpha)\sin^2\frac{\alpha}{2}\Bigg]$$

$$+\eta\Bigg[(\mp)\sec\left(\frac{\alpha+\phi_o}{2}\right)\sec\left(\frac{\alpha+\phi_2}{2}\right)K_{+c}(\alpha)K_{+c}(-\alpha)\sin\frac{\alpha}{2}\sin\alpha\cos\frac{\phi_2}{2}$$

$$(\mp)\sec\left(\frac{\alpha+\phi_o}{2}\right)\sec\left(\frac{\alpha-\phi_2}{2}\right)K_{+c}(\alpha)K_{+c}(-\alpha)\sin\frac{\alpha}{2}\sin\alpha\cos\frac{\phi_2}{2}$$

$$(\mp)\sec\left(\frac{\alpha-\phi_o}{2}\right)\sec\left(\frac{\alpha+\phi_2}{2}\right)K_{+c}(\alpha)K_{+c}(-\alpha)\sin\frac{\alpha}{2}\sin\alpha\cos\frac{\phi_2}{2}$$

$$(\mp)\sec\left(\frac{\alpha-\phi_o}{2}\right)\sec\left(\frac{\alpha-\phi_2}{2}\right)K_{+c}(\alpha)K_{+c}(-\alpha)\sin\frac{\alpha}{2}\sin\alpha\cos\frac{\phi_2}{2}$$

$$\mp\sec\left(\frac{\alpha+\phi_o}{2}\right)\sec\left(\frac{\alpha+\phi_2}{2}\right)K_{+c}(\alpha)K_{+c}(-\alpha)\sin\frac{\alpha}{2}\sin\alpha\cos\frac{\phi_o}{2}$$

$$\mp\sec\left(\frac{\alpha+\phi_o}{2}\right)\sec\left(\frac{\alpha-\phi_2}{2}\right)K_{+c}(\alpha)K_{+c}(-\alpha)\sin\frac{\alpha}{2}\sin\alpha\cos\frac{\phi_o}{2}$$

$$\mp\sec\left(\frac{\alpha-\phi_o}{2}\right)\sec\left(\frac{\alpha+\phi_2}{2}\right)K_{+c}(\alpha)K_{+c}(-\alpha)\sin\frac{\alpha}{2}\sin\alpha\cos\frac{\phi_o}{2}$$

$$\mp\sec\left(\frac{\alpha-\phi_o}{2}\right)\sec\left(\frac{\alpha-\phi_2}{2}\right)K_{+c}(\alpha)K_{+c}(-\alpha)\sin\frac{\alpha}{2}\sin\alpha\cos\frac{\phi_o}{2}\Bigg]$$

$$+\eta^2\Bigg[\mp(\mp)\sec\left(\frac{\alpha+\phi_o}{2}\right)\sec\left(\frac{\alpha+\phi_2}{2}\right)K_{+c}(\alpha)K_{+c}(-\alpha)\sin^2\frac{\alpha}{2}\cos\frac{\phi_o}{2}\cos\frac{\phi_2}{2}$$

$$\mp(\mp)\sec\left(\frac{\alpha+\phi_o}{2}\right)\sec\left(\frac{\alpha-\phi_2}{2}\right)K_{+c}(\alpha)K_{+c}(-\alpha)\sin^2\frac{\alpha}{2}\cos\frac{\phi_o}{2}\cos\frac{\phi_2}{2}$$

$$\mp(\mp)\sec\left(\frac{\alpha-\phi_o}{2}\right)\sec\left(\frac{\alpha+\phi_2}{2}\right)K_{+c}(\alpha)K_{+c}(-\alpha)\sin^2\frac{\alpha}{2}\cos\frac{\phi_o}{2}\cos\frac{\phi_2}{2}$$

$$\mp(\mp)\sec\left(\frac{\alpha-\phi_o}{2}\right)\sec\left(\frac{\alpha-\phi_2}{2}\right)K_{+c}(\alpha)K_{+c}(-\alpha)\sin^2\frac{\alpha}{2}\cos\frac{\phi_o}{2}\cos\frac{\phi_2}{2}\Bigg]\Bigg\}$$

$$\cdot e^{-jkw\cos\alpha}\,d\alpha \qquad (4.27)$$

The terms associated with the electric currents are contained in the first set of brackets also the second set contains the terms associated with the coupling of the currents. While the third set of brackets contains the magnetic current contributions for a conductive strip. The $(\mp)$ is used to denote the independence of sign choice from the $\mp$ set depending on which double diffraction mechanism is analyzed.

One may rigorously show that after evaluation of all double ray mechanisms the coupled terms will cancel as expected [22], leaving us with the conclusion that the impedance strip is just the superposition of resistive and conductive strips.

The evaluations of the double and triple diffraction mechanism for a conductive strip do not have to be explicitly calculated as in the resistive case. In fact, since the integrand is written such that a small argument approximation for $\sin\alpha$ is invoked, it becomes apparent that we can obtain the conductive strip coefficient from the resistive case. We find that the double diffracted fields for the conductive and impedance strips can be written as

$$E^d_{21_{conductive}}(\phi_2,\phi_o) = 4\eta^2\cos(\frac{\phi_o}{2})\cos(\frac{\phi_2}{2})E^d_{21}(\phi_2,\phi_o) \tag{4.28}$$

$$E^d_{21_{impedance}}(\phi_2,\phi_o) = E^d_{21_{conductive}}(\phi_2,\phi_o) - E^d_{21}(\phi_2,\phi_o) \tag{4.29}$$

where $E^d_{21}(\phi_2,\phi_o)$ is that of the resistive strip given in (4.6).

The triply diffracted field for the conductive and impedance strips can be also related to that of the resistive strip. Particularly, it can be shown that

$$E^d_{121_{conductive}}(\phi,\phi_o) = -8\eta^3\cos(\frac{\phi_o}{2})\cos(\frac{\phi}{2})E^d_{121}(\phi,\phi_o) \tag{4.28}$$

$$E^d_{121_{impedance}}(\phi,\phi_o) = E^d_{121_{conductive}}(\phi,\phi_o) + E^d_{121}(\phi,\phi_o) \tag{4.29}$$

where $E^d_{121}(\phi,\phi_o)$ is defined in (4.21).

Numerical Results

The sum of the fields due to the first, second and third order diffraction mechanisms was found to yield a good approximation of the total (bistatic) diffracted field by the resistive strip. In a series of patterns to be presented, the far zone field will be compared with corresponding data via the moment method. The goal in these comparisons is not only to validate the accuracy of the high frequency solution, but to also examine its inherent

limitations as the strip width becomes small. Also of interest is the verification that the resistive strips are capable of simulating thin dielectric layers.

Figures 4.6 to 4.17 present a variety of backscattering patterns for resistive strip widths ranging from 2λ down to $\lambda/8$, with four figures corresponding to each strip width. Two of these four figures refer to the case where $|\theta| = 2$ and the other two to the case of $|\theta| = .25$ (see figure 4.5). Clearly, for the last choice of θ, the surface wave pole is near the saddle point and may also be near one of the geometrical optics poles. Therefore, this situation corresponds to a more severe testing of the solution. Finally, we recognize that of the two figures associated with a specific $|\theta|$ and resistive strip width, one contains curves with capacitive impedances and the other with inductive impedances. For the last case, no surface waves exist and thus all higher order fields are simply due to surface ray diffraction. However, when the impedance is capacitive, $\mathrm{Im}(\theta) > 0$, the surface wave pole $(-\theta)$ may be captured during the detouring of the C contour to the steepest descent path. When this occurs the higher order diffracted fields become dominant as can be verified by examining the corresponding patterns in the 0^o to 20^o region. We further verified the continuity of the solution when the surface wave pole is just crossing the SDP contour. In any case, it is clear that all backscatter patterns obtained via the high frequency solution are in complete agreement with the moment method results for all values of θ, and for (resistive) strip widths down to $\lambda/8$.

The above examples examined the resistive strip in comparison with moment method data for various widths and impedance values in great depth since the conductive and impedance strip solutions are based on the resistive strip evaluation. Being consistent in the checking of the coefficients, the η values are varied but only one set of strip widths (0.5λ) are presented for backscatter patterns of conductive and impedance strips in comparison to moment method data. Figures 4.18 and 4.19 show the backscatter patterns for $|\theta| \sim 2$ and $|\theta| \sim 0.25$, respectively. While figures 4.20 and 4.21 show the corresponding case for an impedance strip. In all of the above cases the high frequency solution was in close agreement with the numerical data.

Next we examine the capability of a resistive strip to accurately model a thin dielectric

slab. For such a model, the resistivity of the strip is chosen to be

$$R = \frac{-jZ_o}{(\epsilon_r - 1)k\tau} \tag{4.30}$$

where τ is the thickness of the slab and $k\tau$ must be maintained very small. We selected, $\epsilon_r = 4(1 - j\tan\delta), \tan\delta = .1$ (loss tangent), $\tau = \frac{\lambda}{40}$ and a strip width of 5λ to correspond to the strip used in [32] (moment method solution). It is shown in figure 4.22 that the high frequency solution compared exactly with that given by Richmond [32]. As expected, the resistive strip corresponding to the dielectric slab will always support a surface wave field which is seen to be quite dominant for backscatter angles less than 45^o .

To further examine the validity of the solution for the smaller strip widths, figure 4.23 presents the edge-on backscatter echo width as a function of the width of the strip(w). The comparison with the moment method data [32] is excellent.

We now turn our attention to the bistatic case for a resistive strip. Again a series of patterns are presented in figures 4.24 to 4.39 with ϕ_o (incidence angle) = 150^o or 175^o and strip widths ranging from 2λ down to $\lambda/4$. Furthermore, the curves on each figure correspond to various impedance (or θ) values which follows the same format discussed for the backscatter patterns (see figures 4.6 to 4.17). The high frequency solution again compares very well with the moment method data except near forward scattering when the strip width is below $\lambda/4$. This is probably due to the need for additional higher order terms in the solution and also to errors associated with single precision arithmetic when performing the subtraction of infinities.

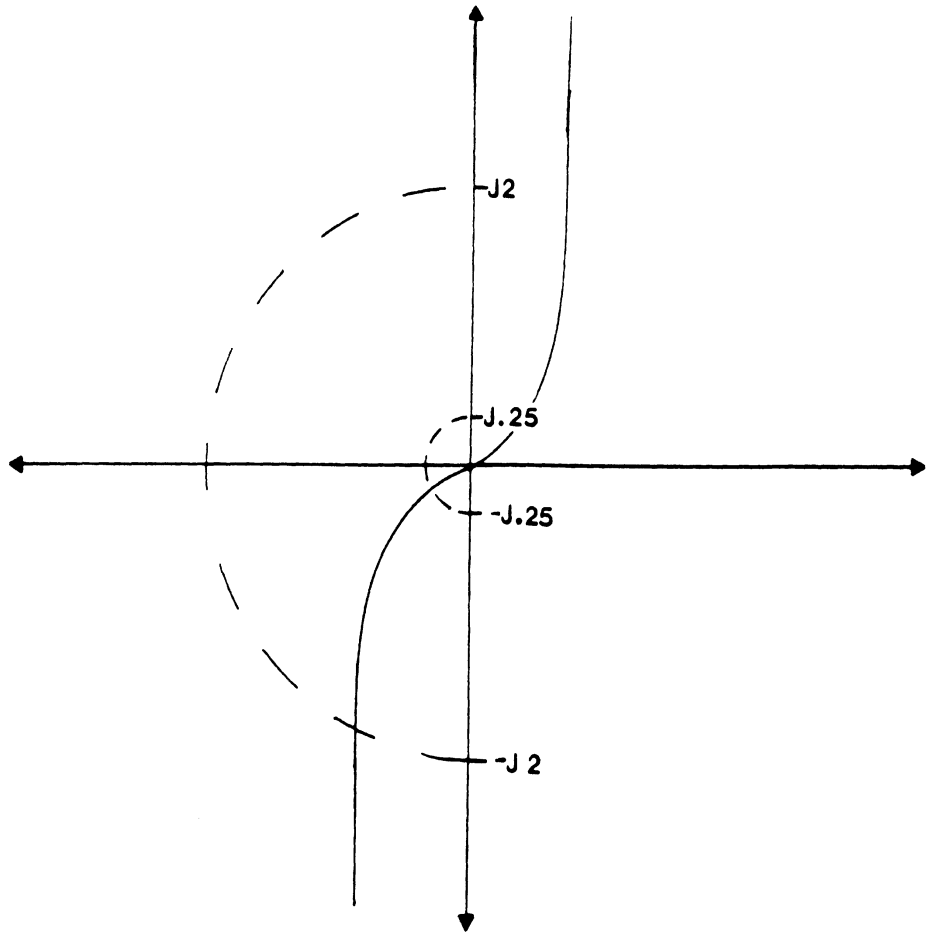

α plane

Figure 4.5 — Path of constant surface wave pole magnitudes (0.25 and 2) in relation to the steepest descent path (a Gudermann function)

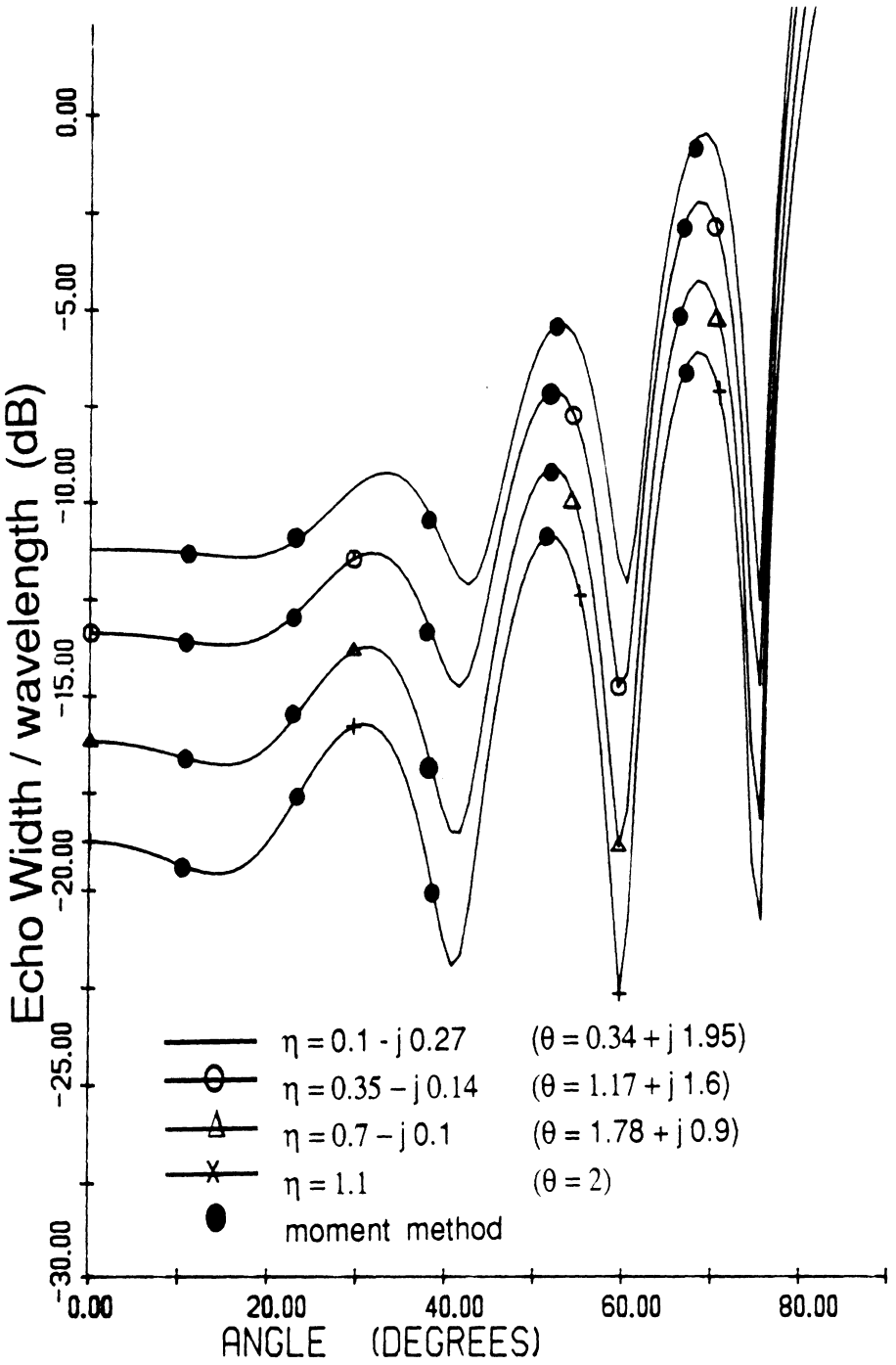

Figure 4.6 — Comparison of the solution for backscattering with moment method data from a 2λ wide resistive strip with $\eta = 0.1 - j0.27$, $0.35 - j0.14$, $0.7 - j0.1$ and 1.1 constant surface wave pole magnitude ~2, E-polarization

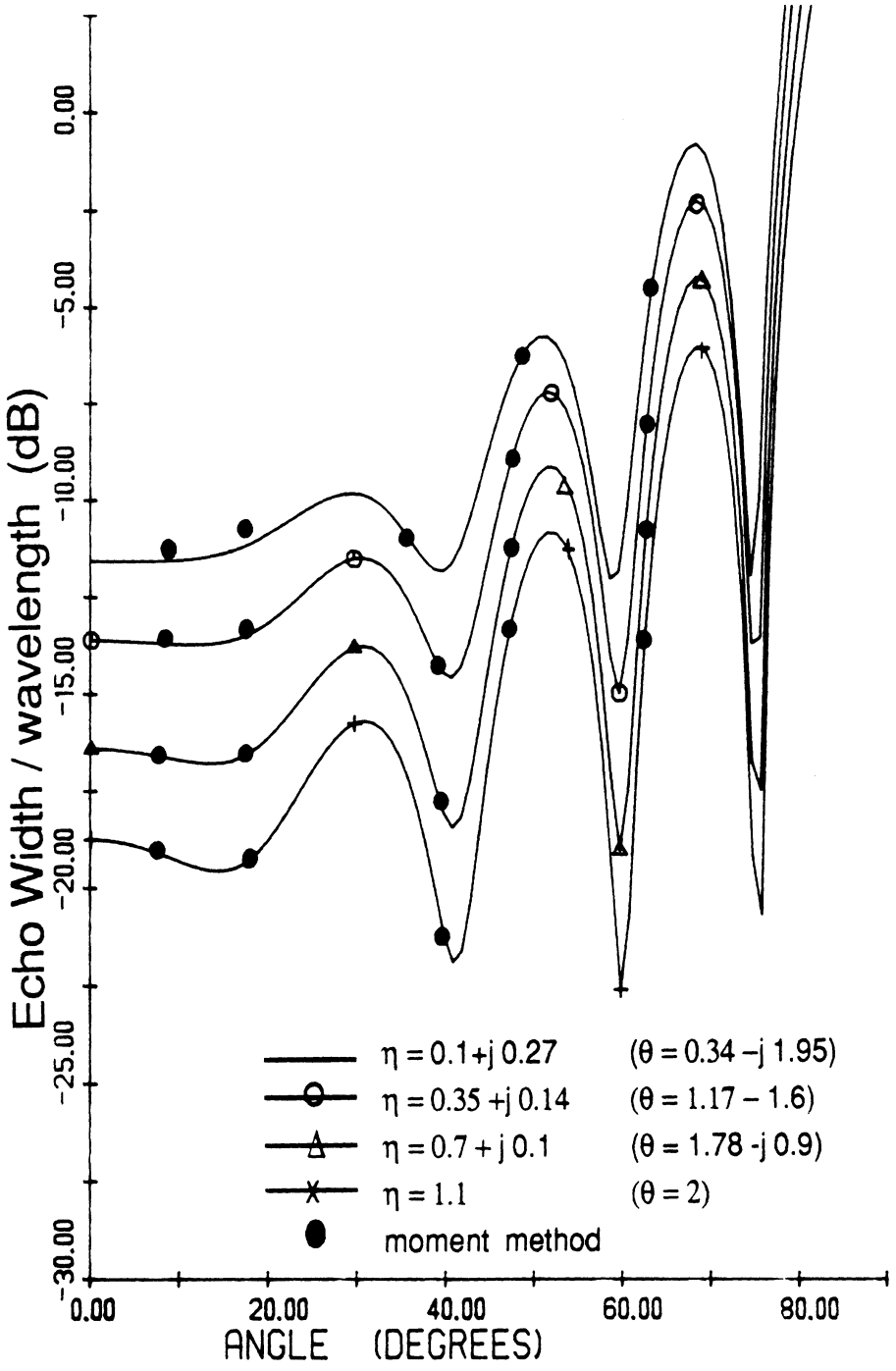

Figure 4.7 — Comparison of the solution for backscattering with moment method data from a 2λ wide resistive strip with $\eta = 0.1 - j0.27$, $0.35 - j0.14$, $0.7 + j0.1$ and 1.1 constant surface wave pole magnitude ~2. E-polarization

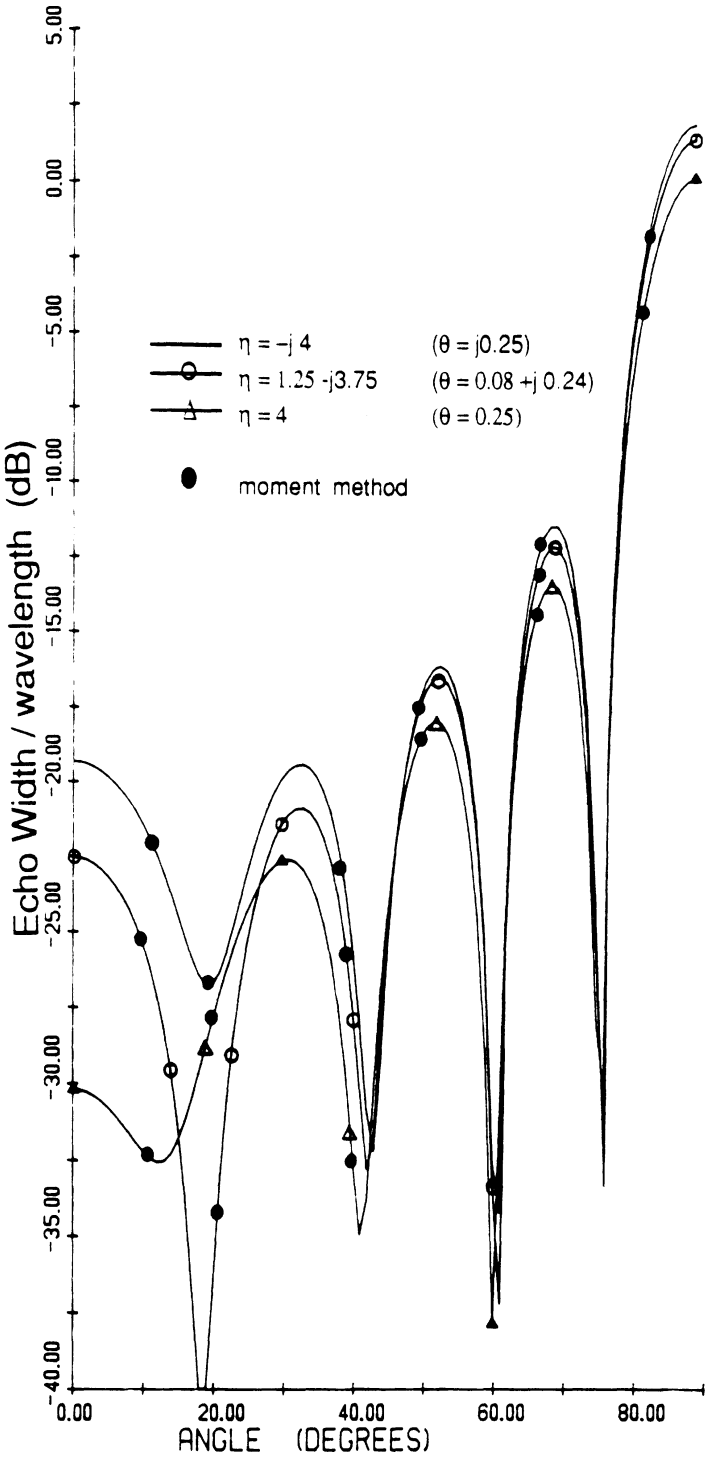

Figure 4.8 — Comparison of the solution for backscattering with moment method data from a 2λ wide resistive strip with $\eta = -j4$, $1.25 - j3.75$ and 4

constant surface wave pole magnitude ~0.25, E-polarization

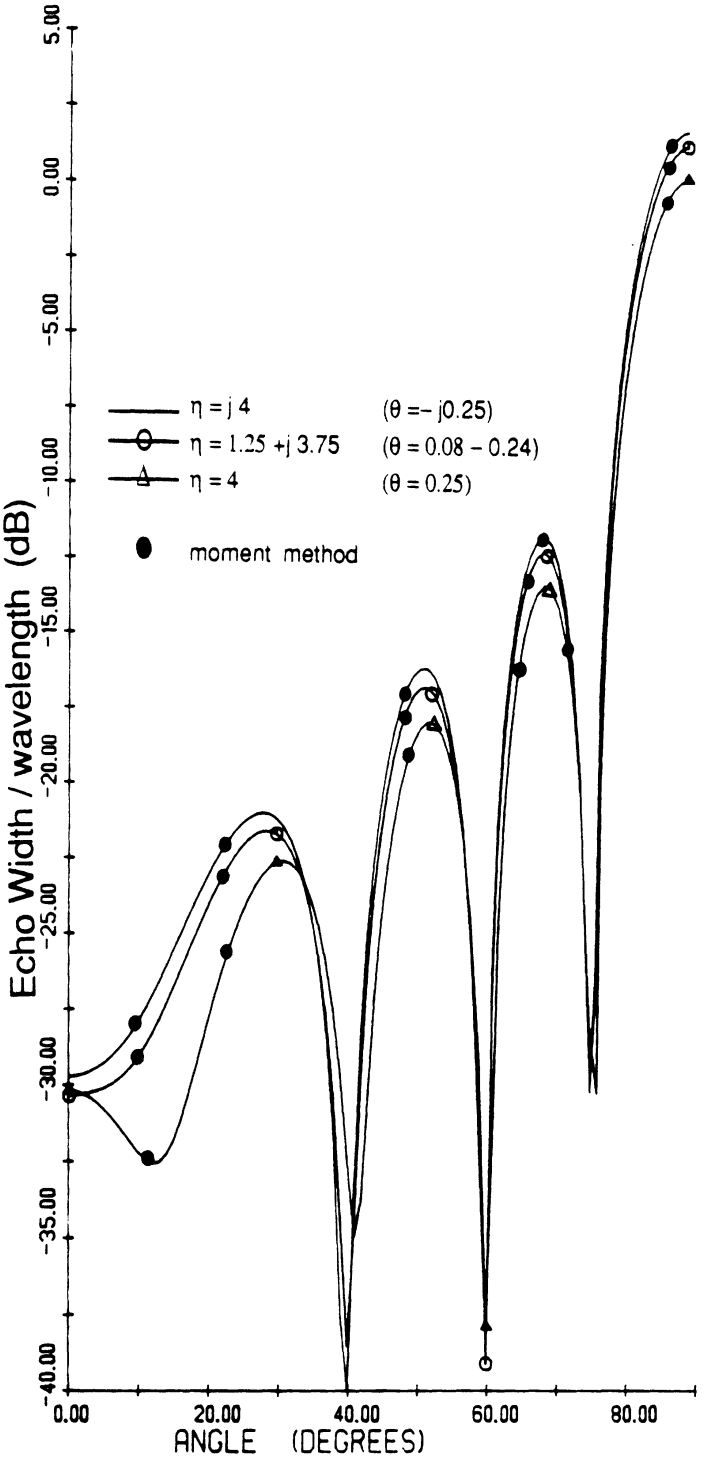

Figure 4.9 — Comparison of the solution for backscattering with moment method data from a 2λ wide resistive strip with $\eta = j4$, $1.25 + j3.75$ and 4

constant surface wave pole magnitude ~0.25, E-polarization

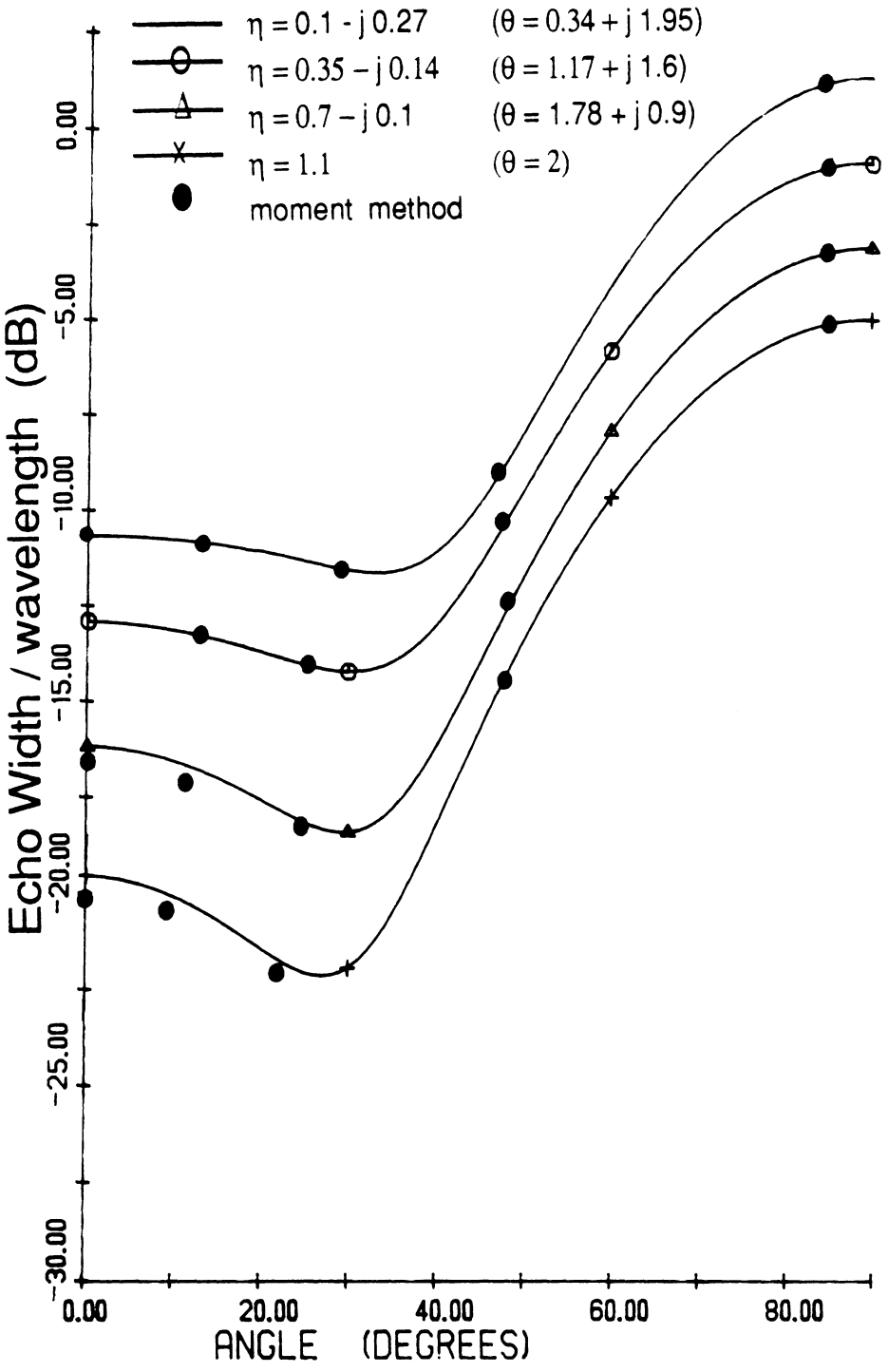

Figure 4.10 — Comparison of the solution for backscattering with moment method data from a 0.5λ wide resistive strip with $\eta = 0.1 - j0.27$, $0.35 - j0.14$, $0.7 - j0.1$ and 1.1

constant surface wave pole magnitude ~2, E-polarization

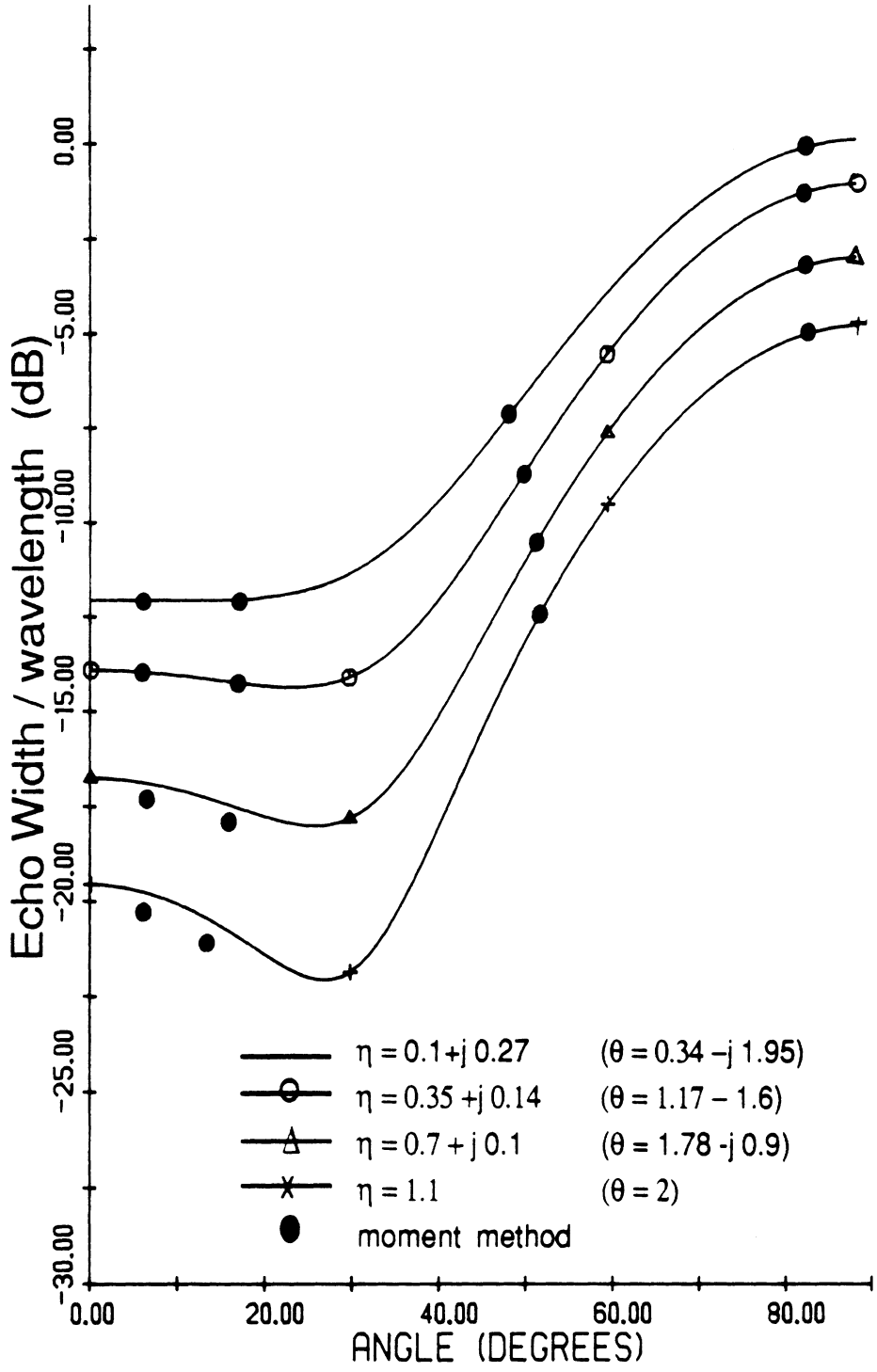

Figure 4.11 — Comparison of the solution for backscattering with moment method data from a 0.5λ wide resistive strip with $\eta = 0.1 - j0.27,\ 0.35 - j0.14,\ 0.7 - j0.1$ and 1.1 constant surface wave pole magnitude ~2. E-polarization

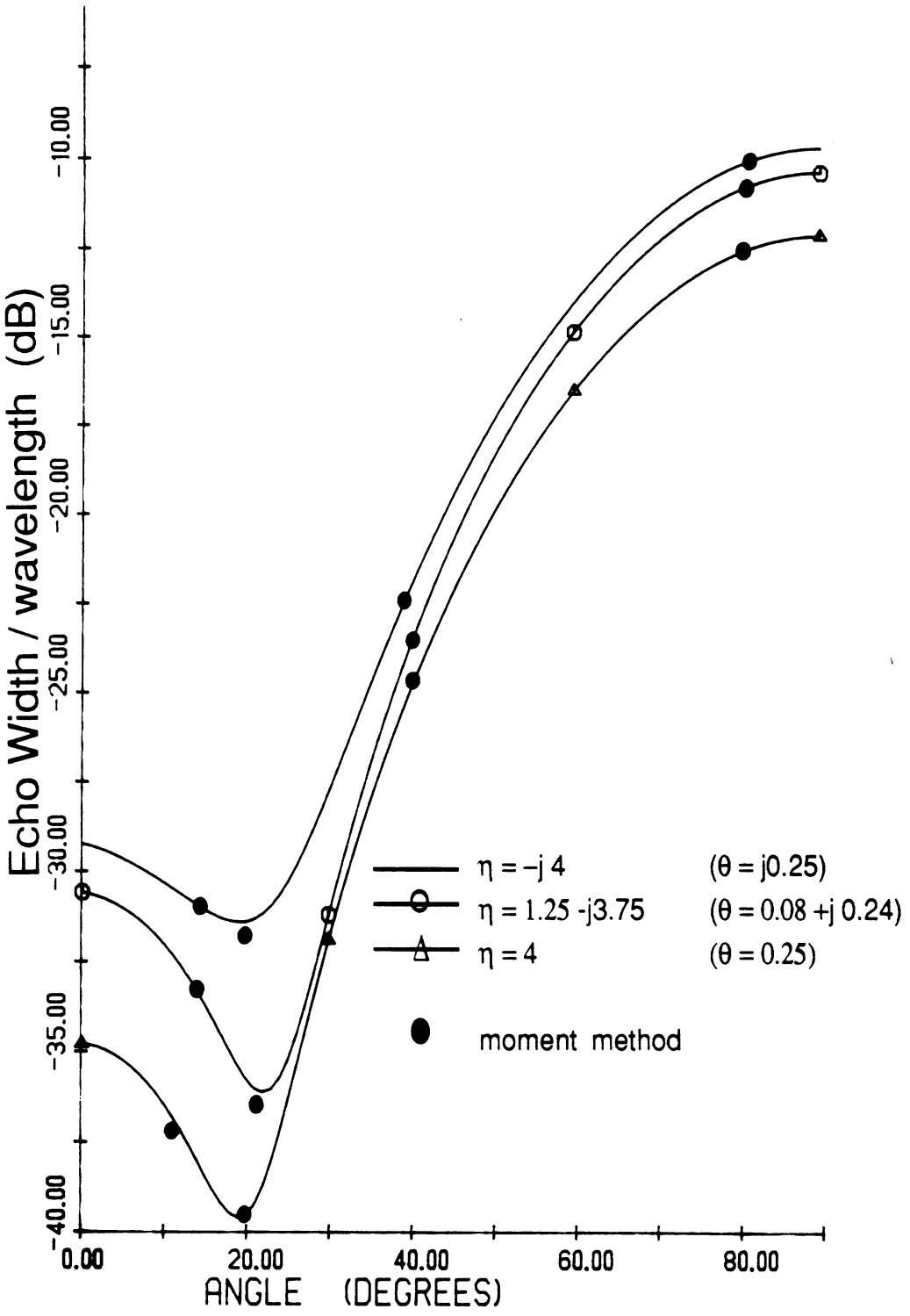

Figure 4.12 — Comparison of the solution for backscattering with moment method data from a 0.5λ wide resistive strip with $\eta = -j4,\ 1.25 - j3.75$ and 4

constant surface wave pole magnitude ~0.25. E-polarization

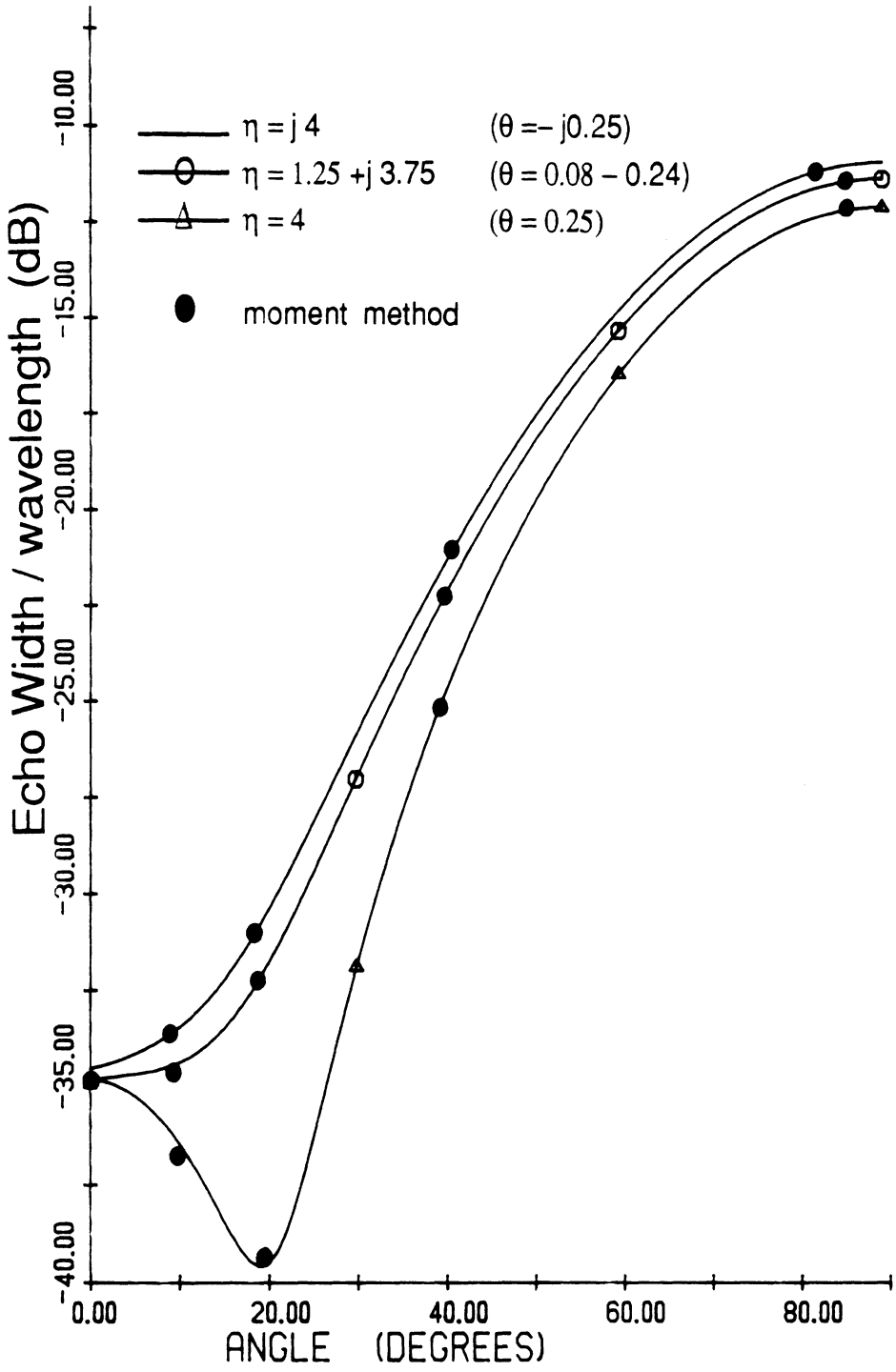

Figure 4.13 — Comparison of the solution for backscattering with moment method data from a 0.5λ wide resistive strip with $\eta = j4,\ 1.25 - j3.75$ and 4

constant surface wave pole magnitude ~0.25, E-polarization

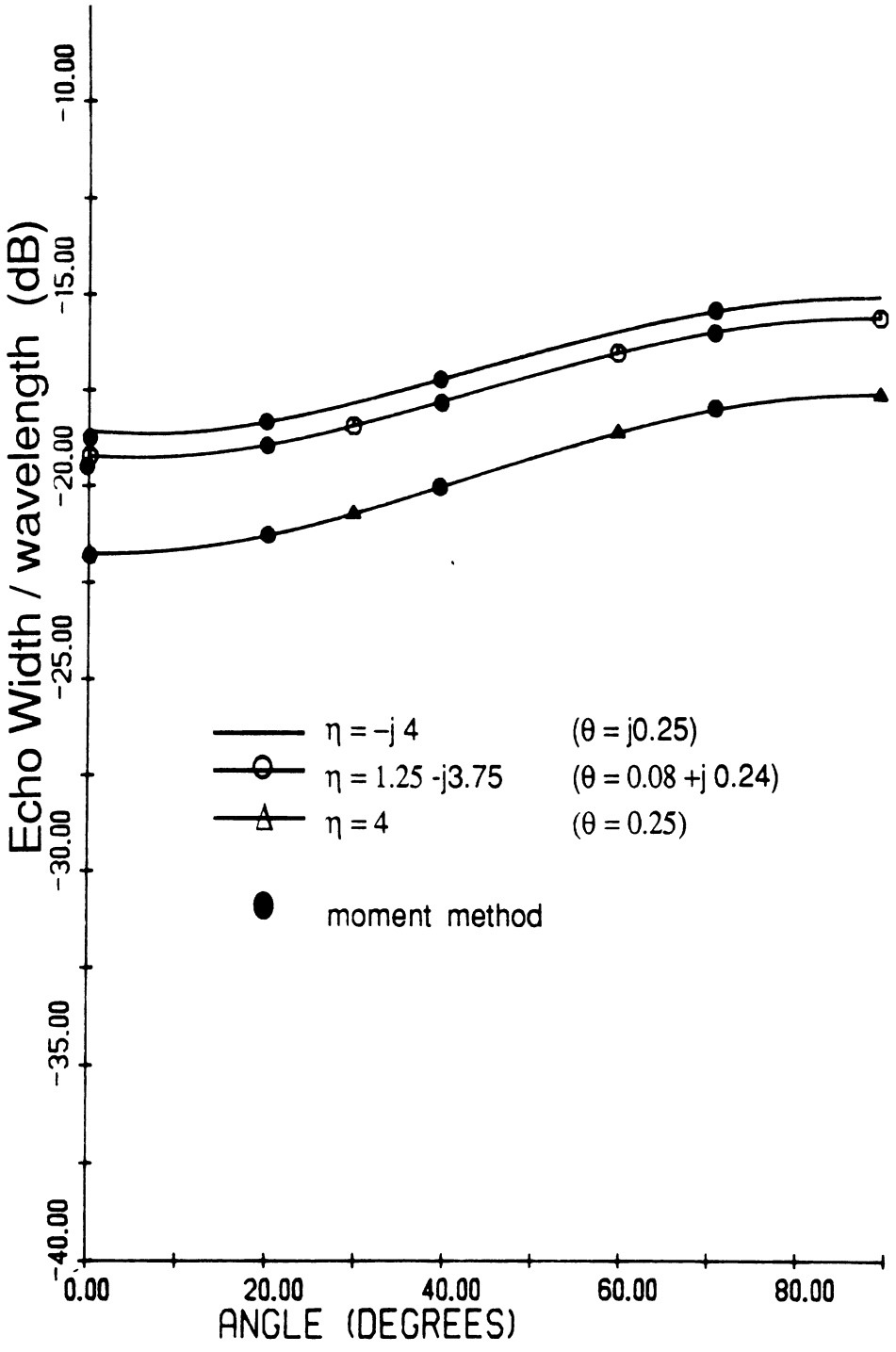

Figure 4.14 — Comparison of the solution for backscattering with moment method data from a 0.25λ wide resistive strip with $\eta = -j4$, $1.25 - j3.75$ and 4

constant surface wave pole magnitude ~0.25, E-polarization

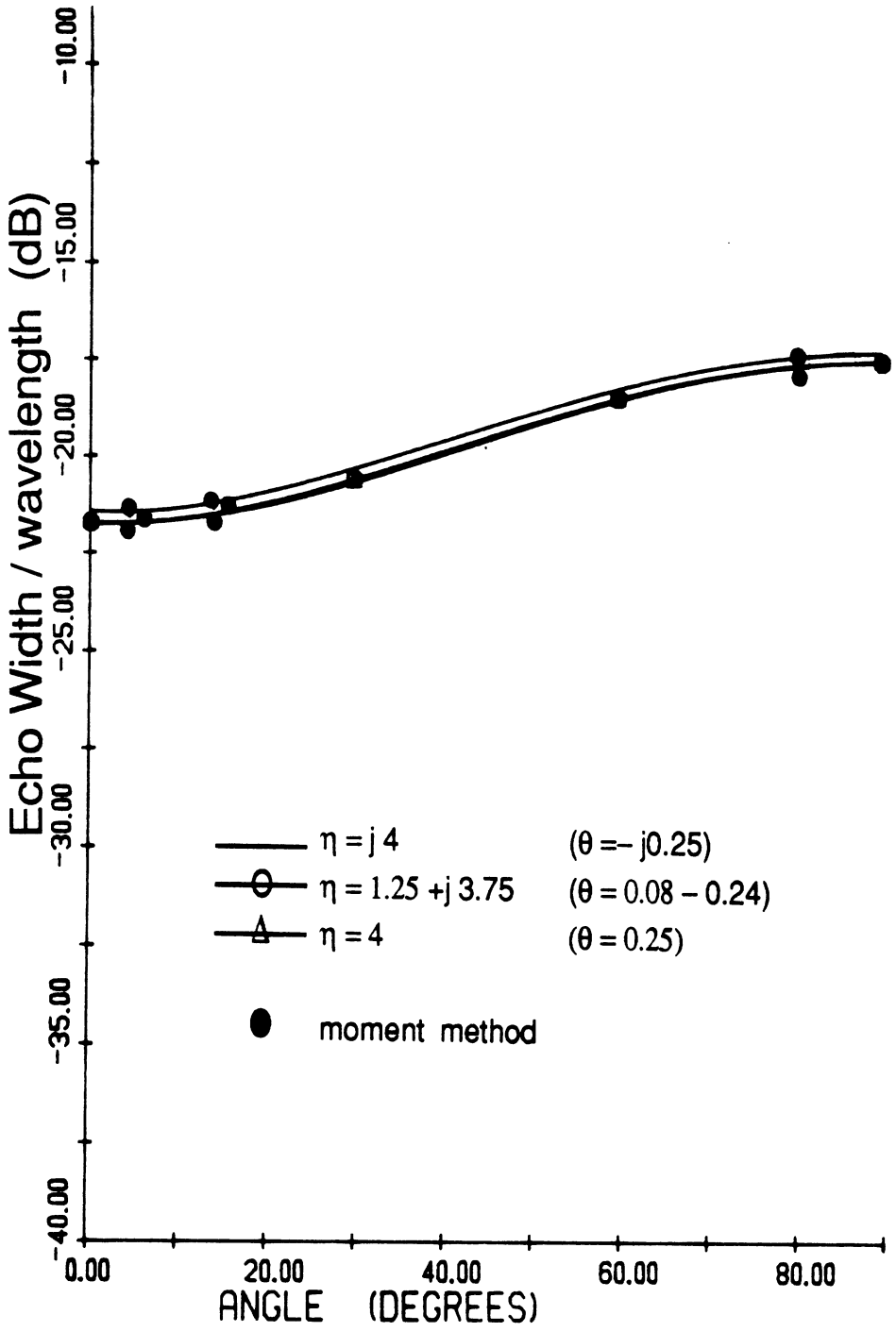

Figure 4.15 — Comparison of the solution for backscattering with moment method data from a 0.25λ wide resistive strip with $\eta = j4$, $1.25 + j3.75$ and 4

constant surface wave pole magnitude ~0.25, E-polarization

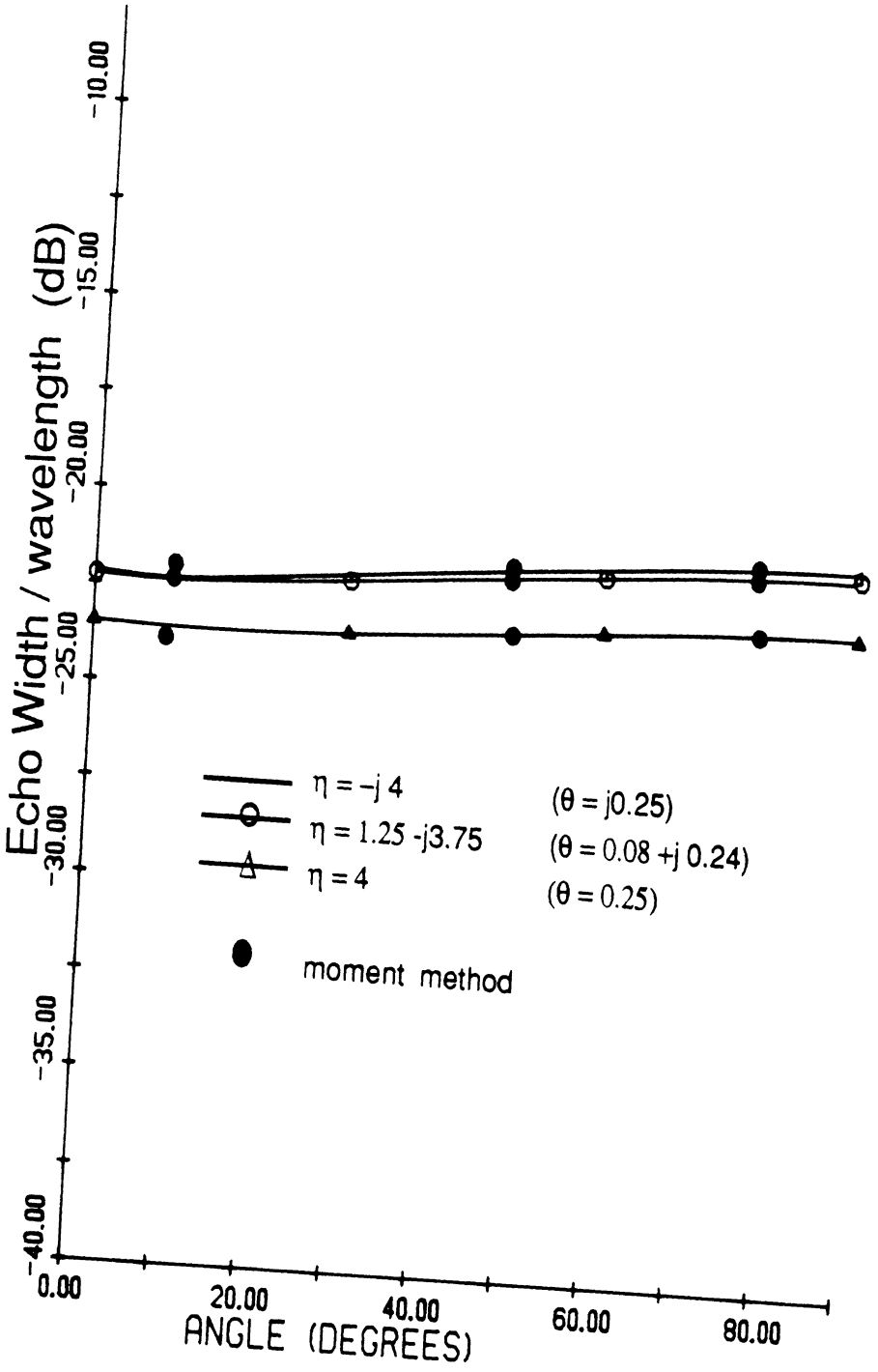

Figure 4.16 — Comparison of the solution for backscattering with moment method data from a 0.125λ wide resistive strip with $\eta = -j4,\ 1.25 - j3.75$ and 4 constant surface wave pole magnitude ~0.25. E-polarization

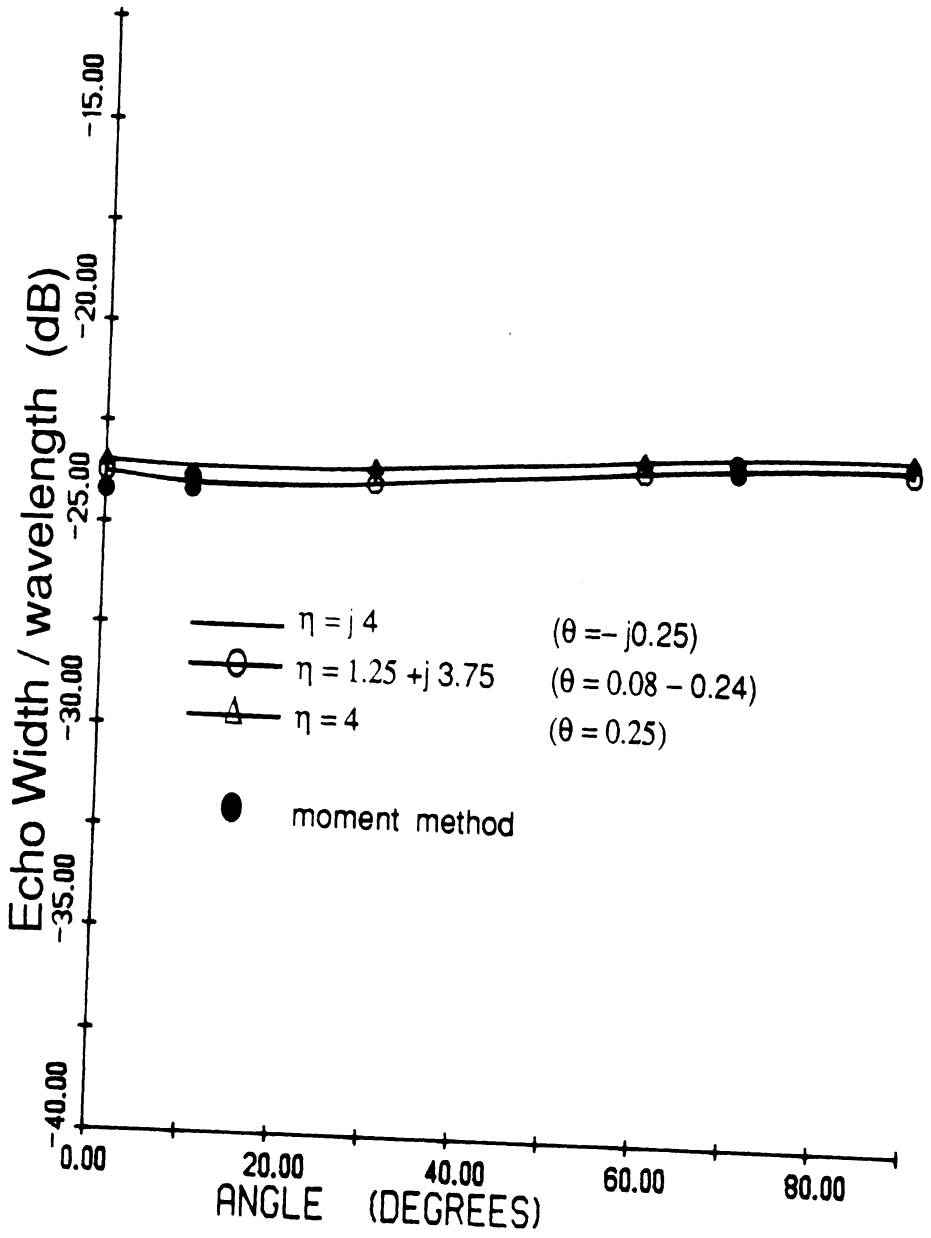

Figure 4.17 — Comparison of the solution for backscattering with moment method data from a 0.125λ wide resistive strip with $\eta = j4,\ 1.25 - j3.75$ and 4

constant surface wave pole magnitude ~0.25, E-polarization

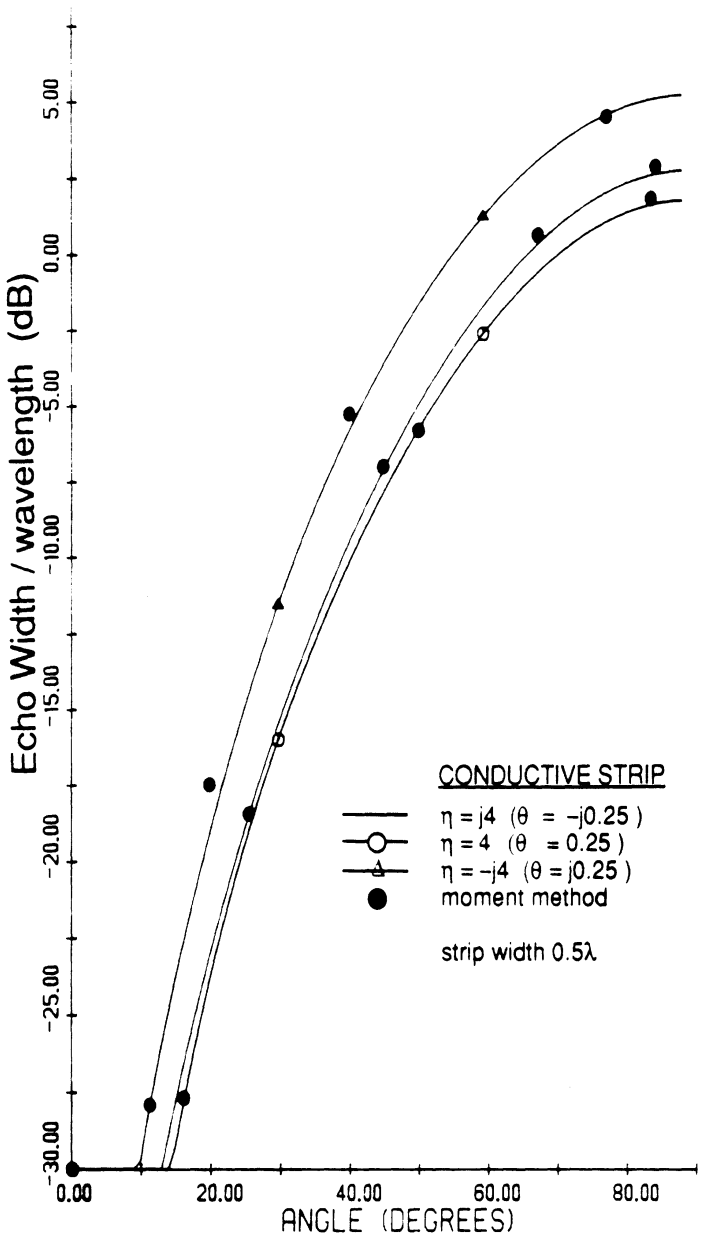

Figure 4.18 — Comparison of the solution for backscattering with moment method data from a 0.5λ wide conductive strip with $\eta = j4, 4$ and $-j4$

E-polarization

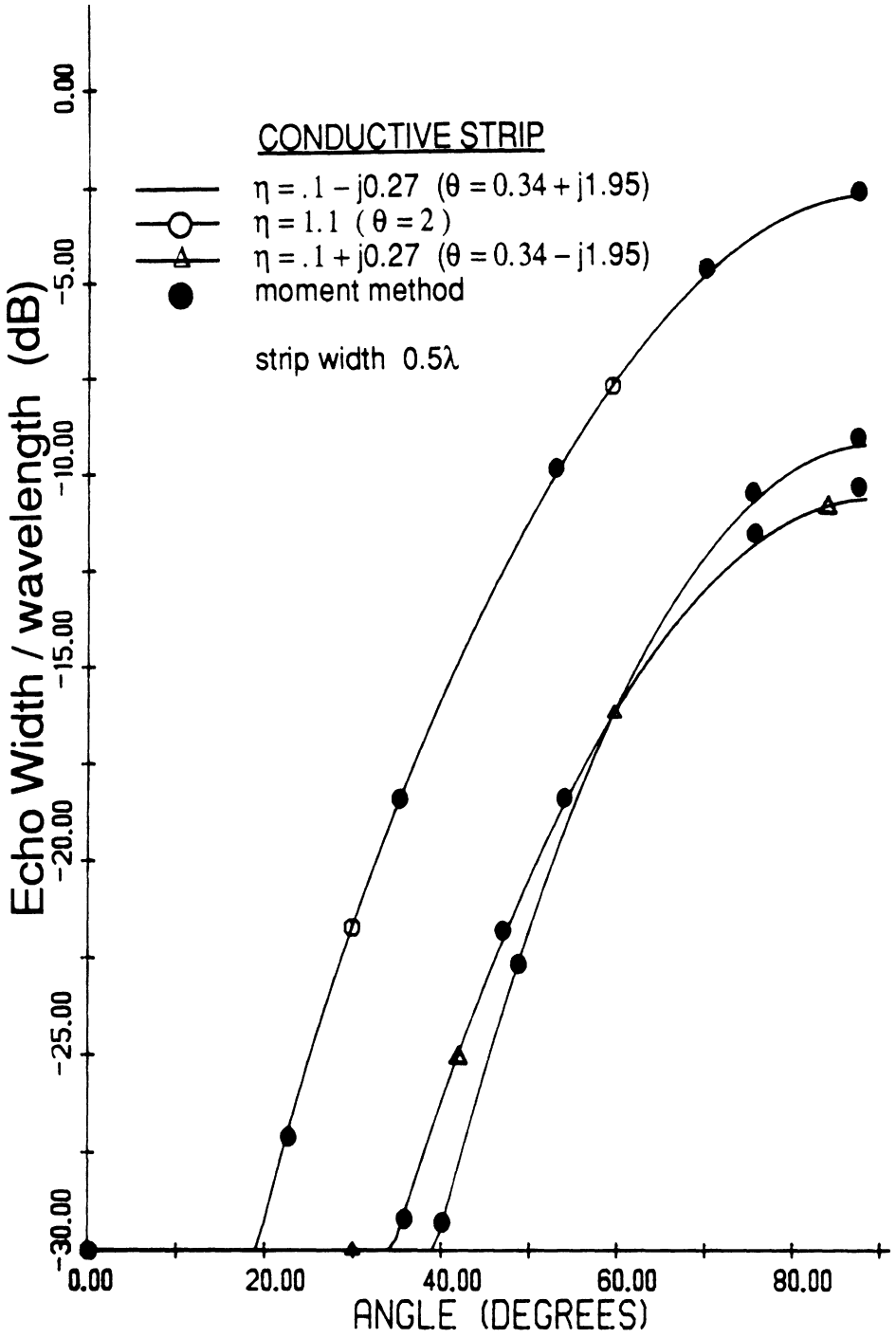

Figure 4.19 — Comparison of the solution for backscattering with moment method data from a 0.5λ wide conductive strip with $\eta = 0.1 - j0.27$, 1.1 and $0.1 - j0.27$

E-polarization

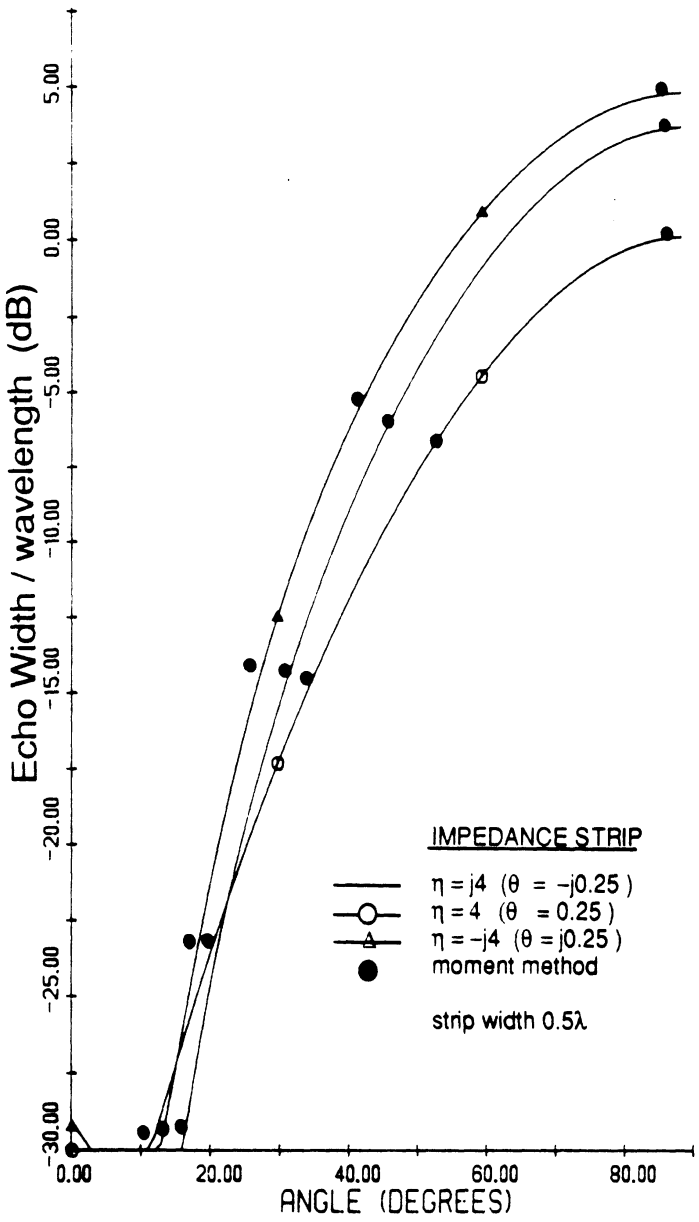

Figure 4.20 — Comparison of the solution for backscattering with moment method data from a 0.5λ wide impedance strip with $\eta = j4$, 4 and $-j4$

E-polarization

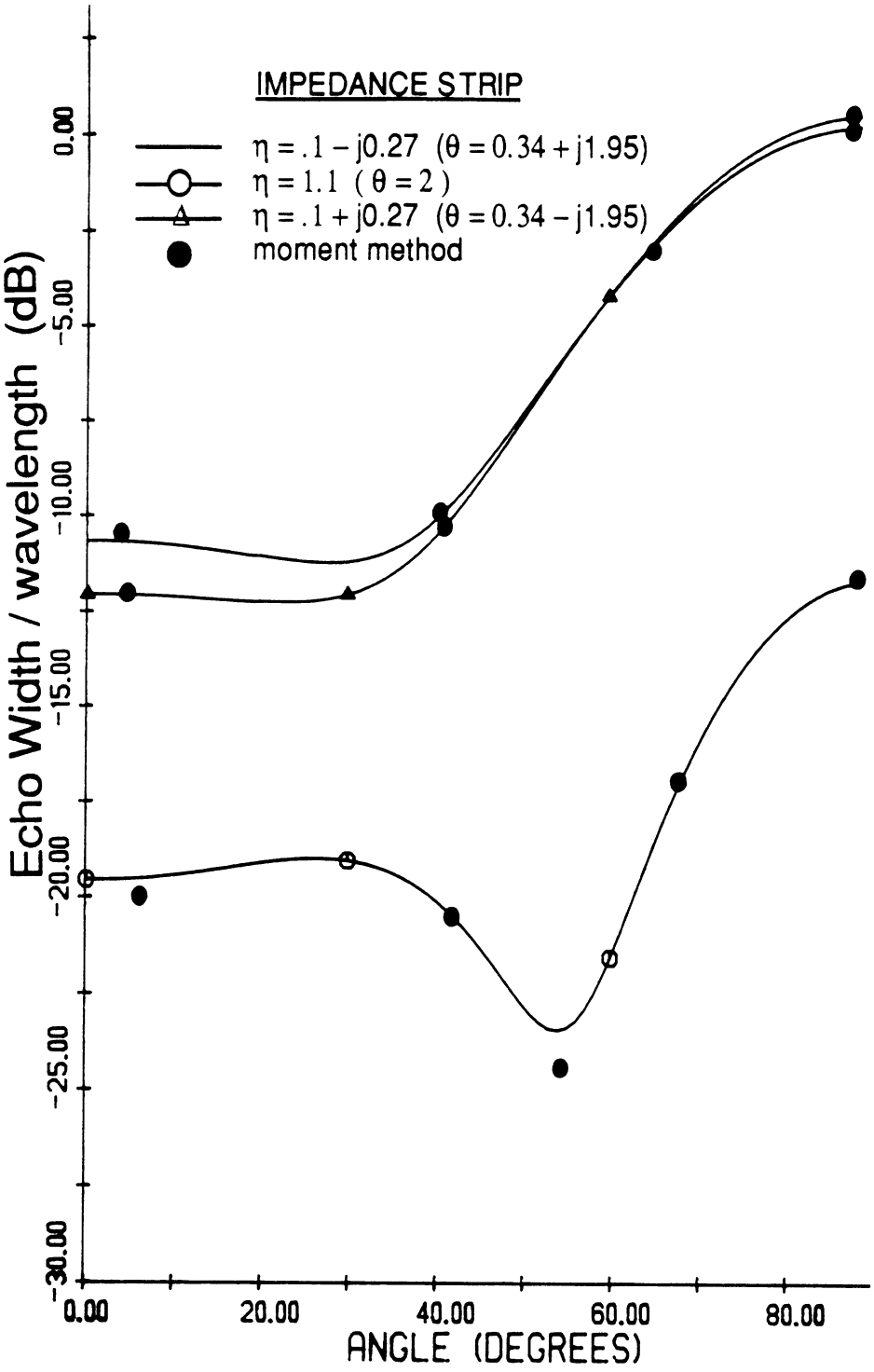

Figure 4.21 — Comparison of the solution for backscattering with moment method data from a 0.5λ wide impedance strip with $\eta = 0.1 - j0.27$, 1.1 and $0.1 + j0.27$

E-polarization

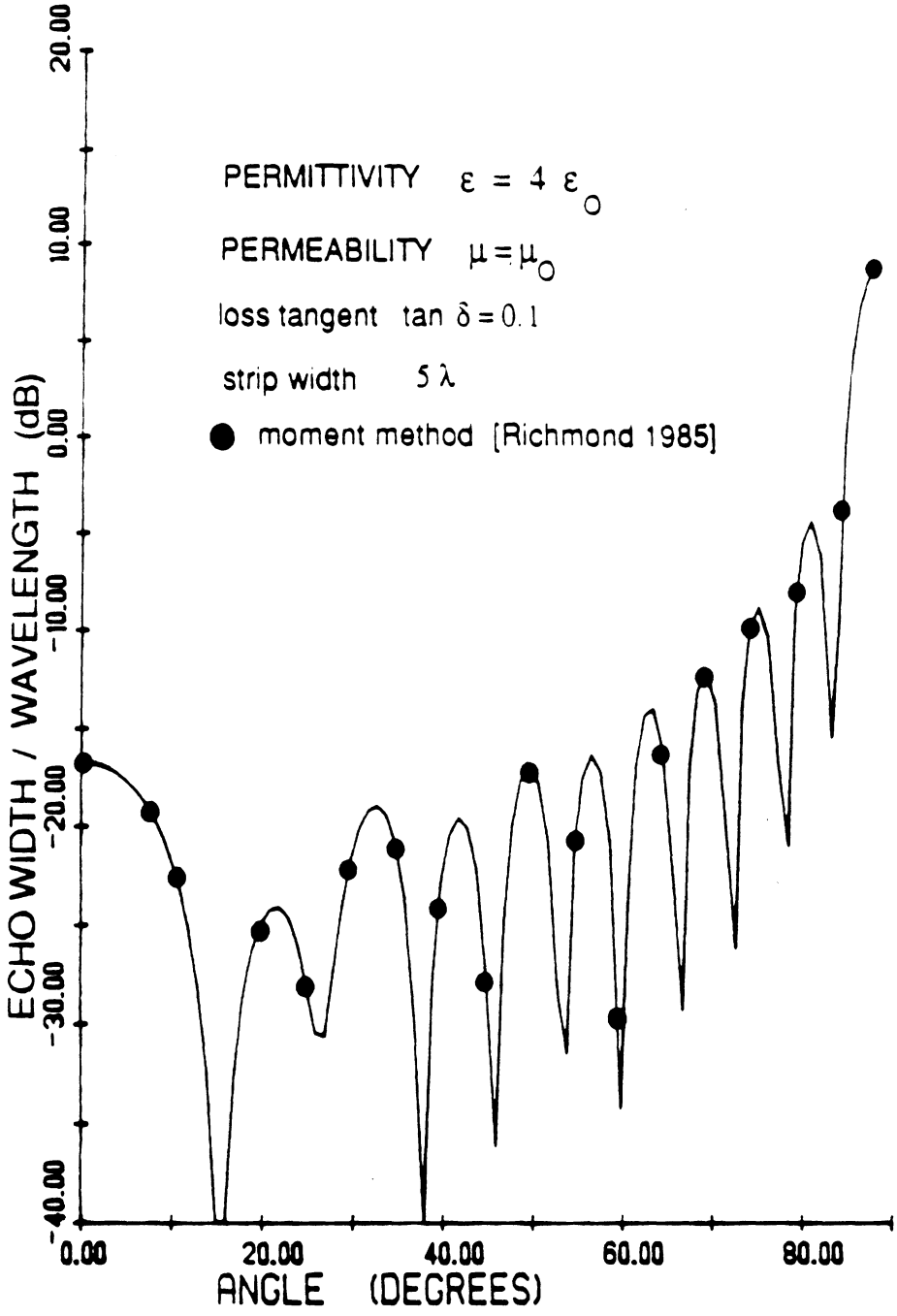

Figure 4.22 — Comparison of backscatter pattern with moment method for a resistive strip ($\eta = 0.55 - j4.2$) which models a thin dielectric slab with thickness $\frac{\lambda}{40}$ and $\epsilon_r = 4(1 - j0.1)$, E-polarization

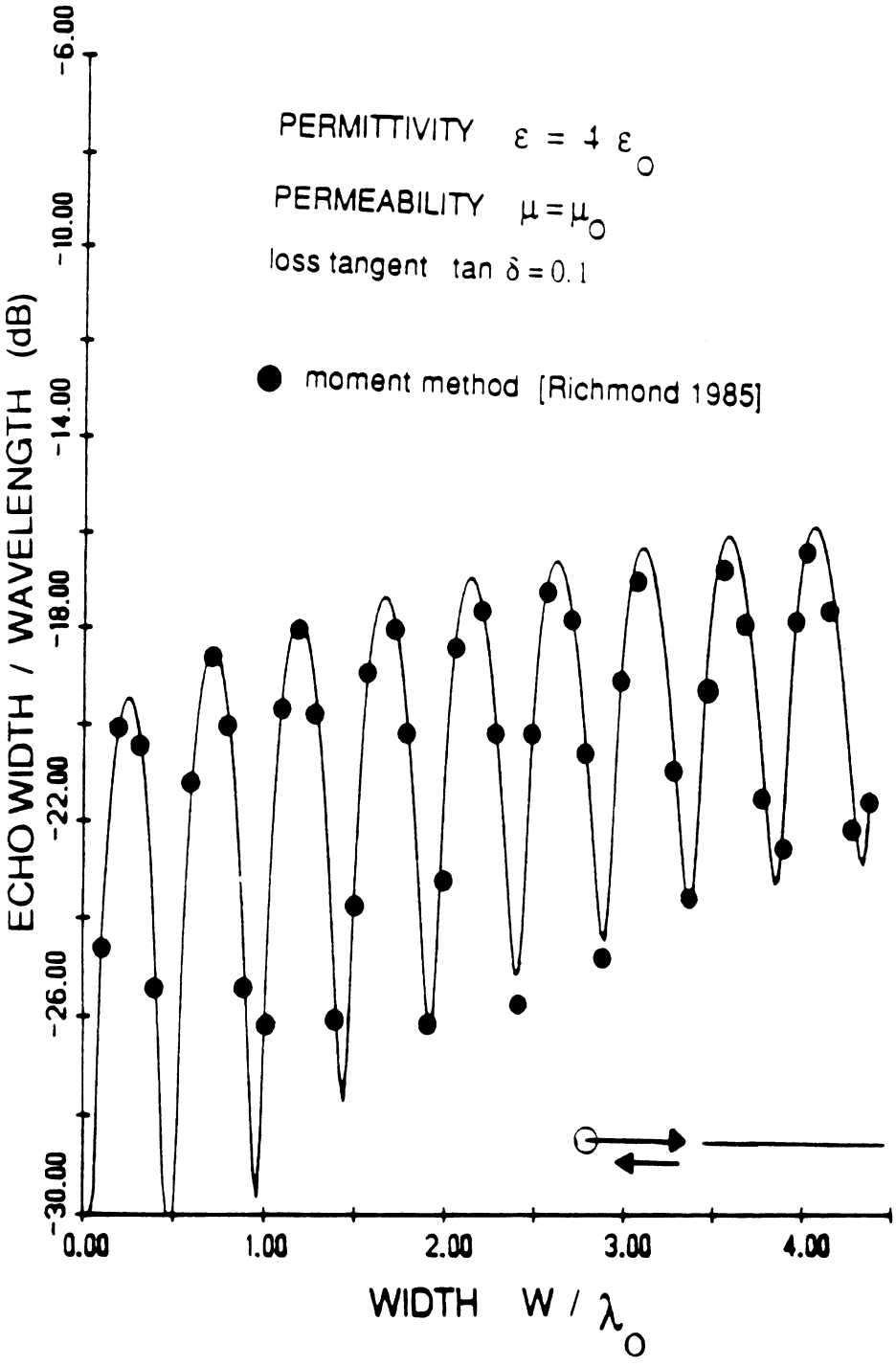

Figure 4.23 — Comparison of edge-on backscattering with width of a resistive strip. E-polarization

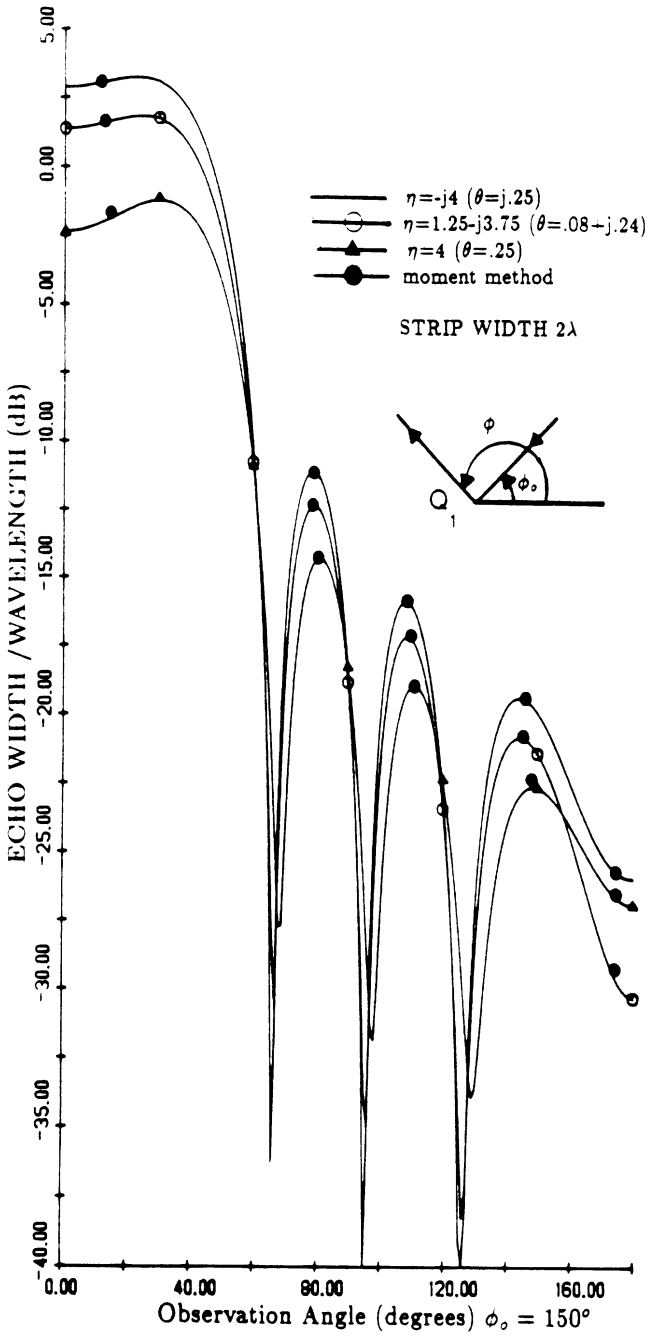

Figure 4.24 — Comparison of bistatic solution with moment method data for a 2λ wide resistive strip ($\eta = -j4.\ 1.25 - j3.75$ and $4.\ \phi_0 = 150°$)

constant surface wave pole magnitude ~0.25, E-polarization

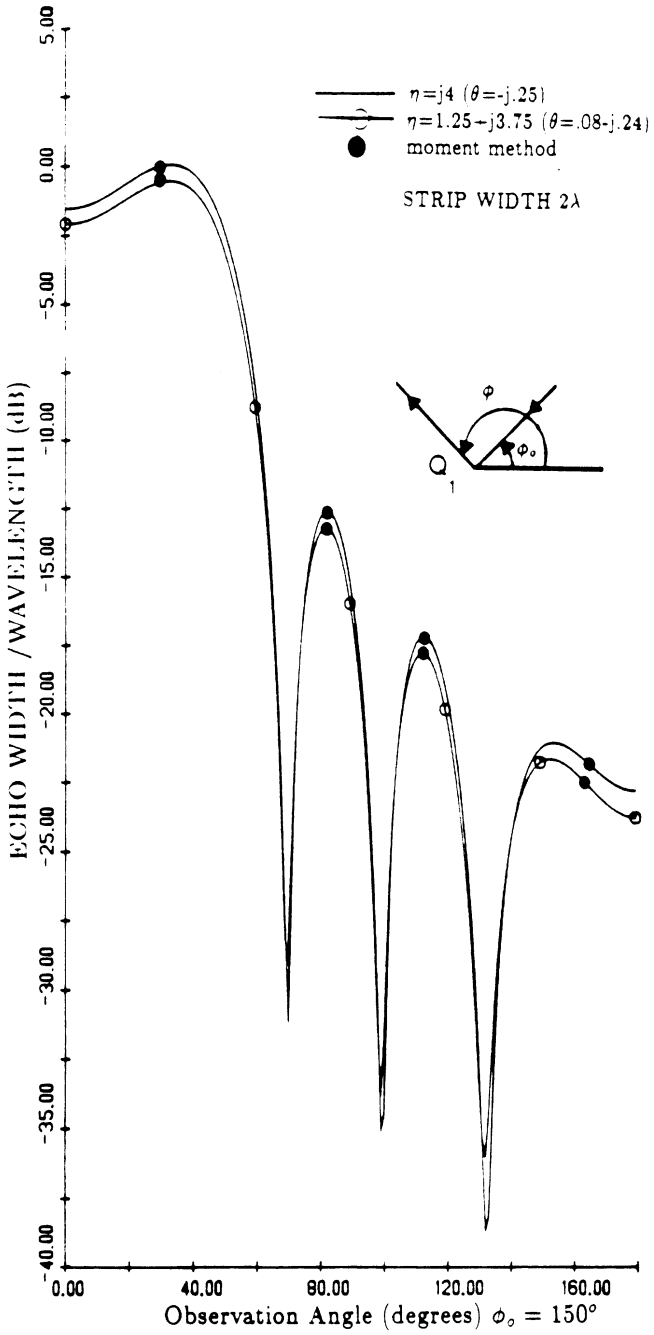

Figure 4.25 — Comparison of bistatic solution with moment method data for a 2λ wide resistive strip ($\eta = j4$ and $1.25 + j3.75$. $\phi_o = 150°$)

constant surface wave pole magnitude ~0.25, E-polarization

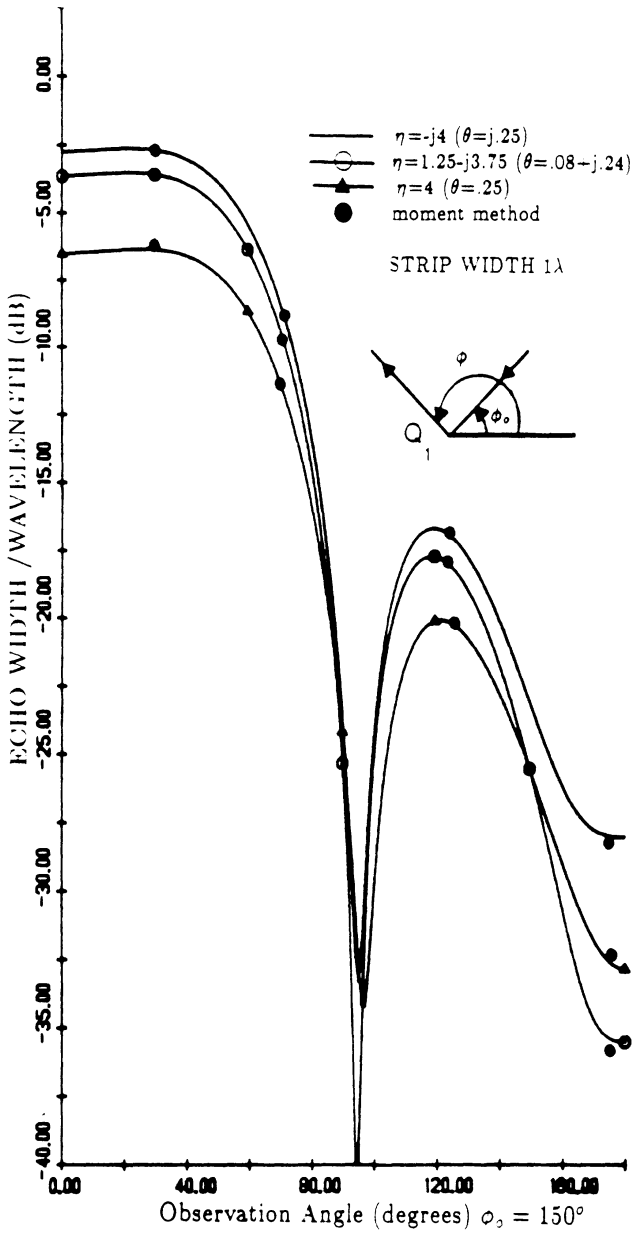

Figure 4.26 — Comparison of bistatic solution with moment method data for a 1λ wide resistive strip ($\eta = -j4,\ 1.25 - j3.75$ and $4.\ \phi_0 = 150°$)

constant surface wave pole magnitude ~0.25, E-polarization

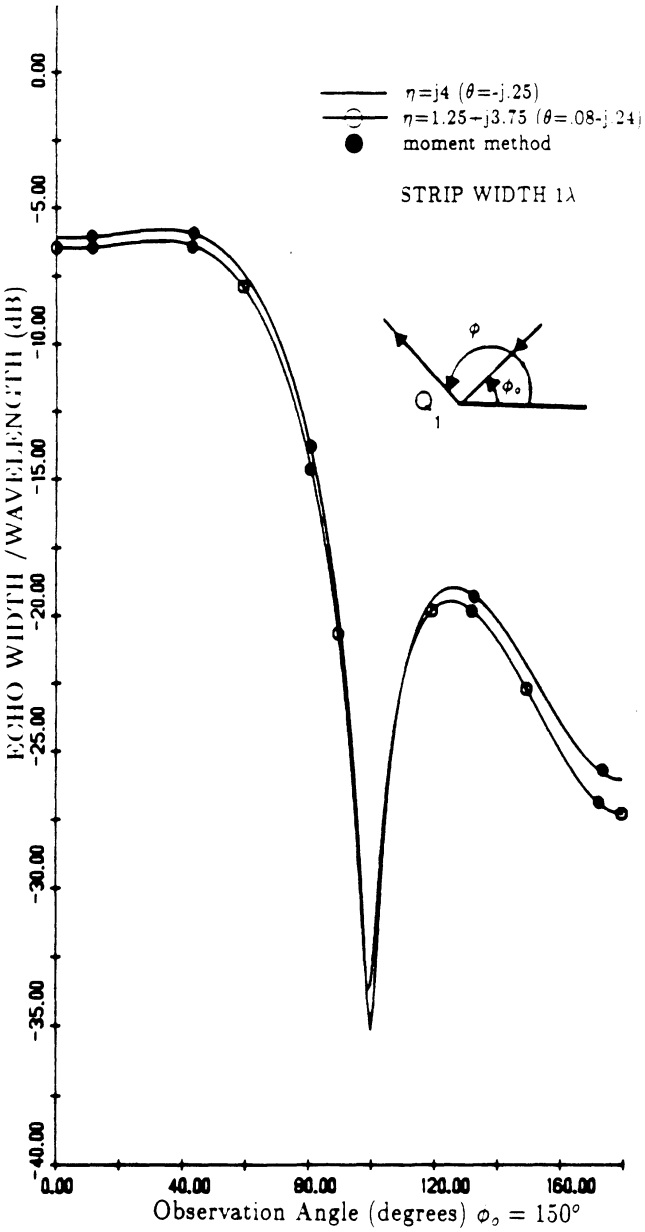

Figure 4.27 — Comparison of bistatic solution with moment method data for a 1λ wide resistive strip ($\eta = j4,\ 1.25 - j3.75$ and **4.** $\phi_0 = 150°$)

constant surface wave pole magnitude ~0.25, E-polarization

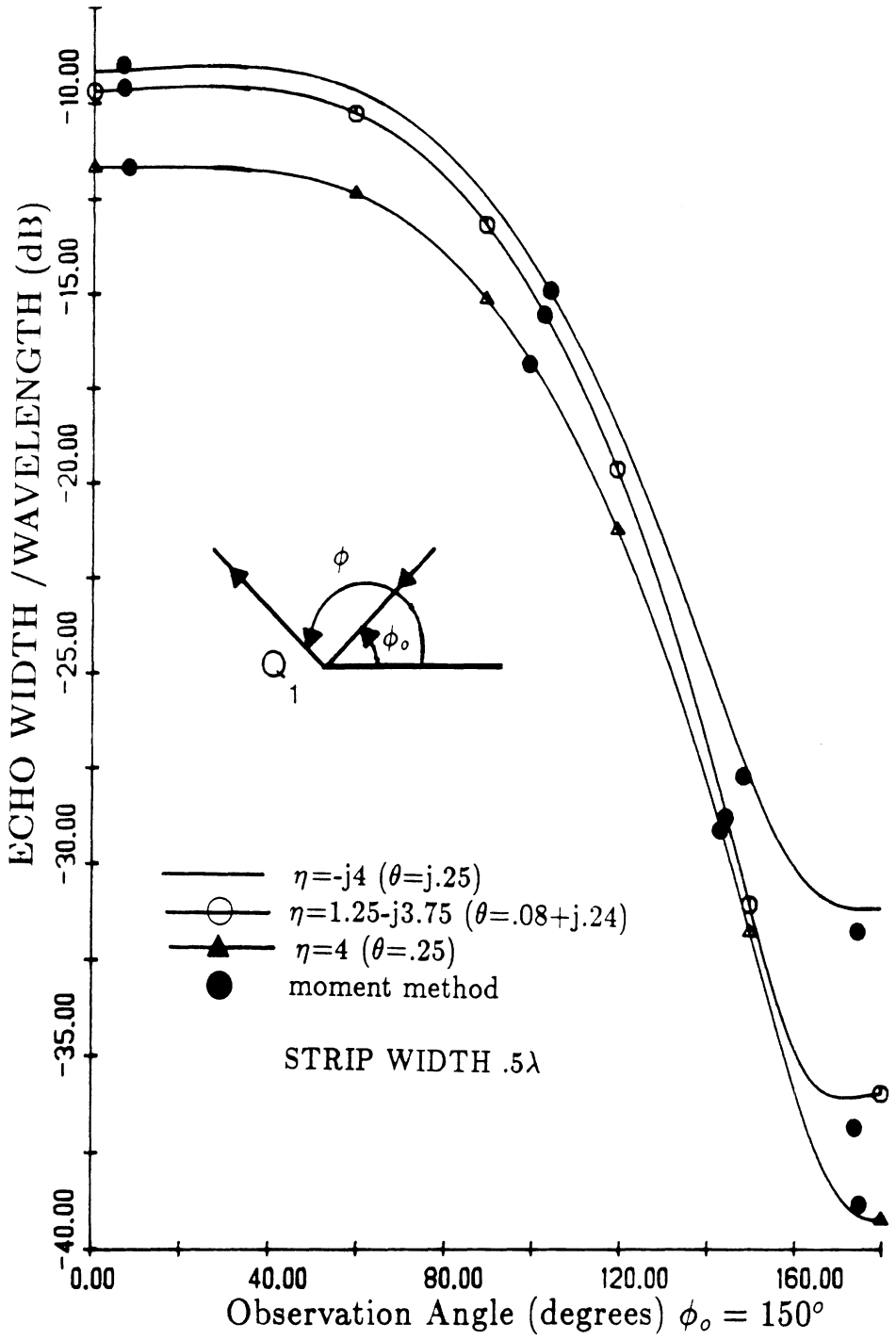

Figure 4.28 — Comparison of bistatic solution with moment method data for a 0.5λ **wide resistive strip** ($\eta = -j4$, $1.25 - j3.75$ **and 4.** $\phi_o = 150^o$)

constant surface wave pole magnitude ~0.25, E-polarization

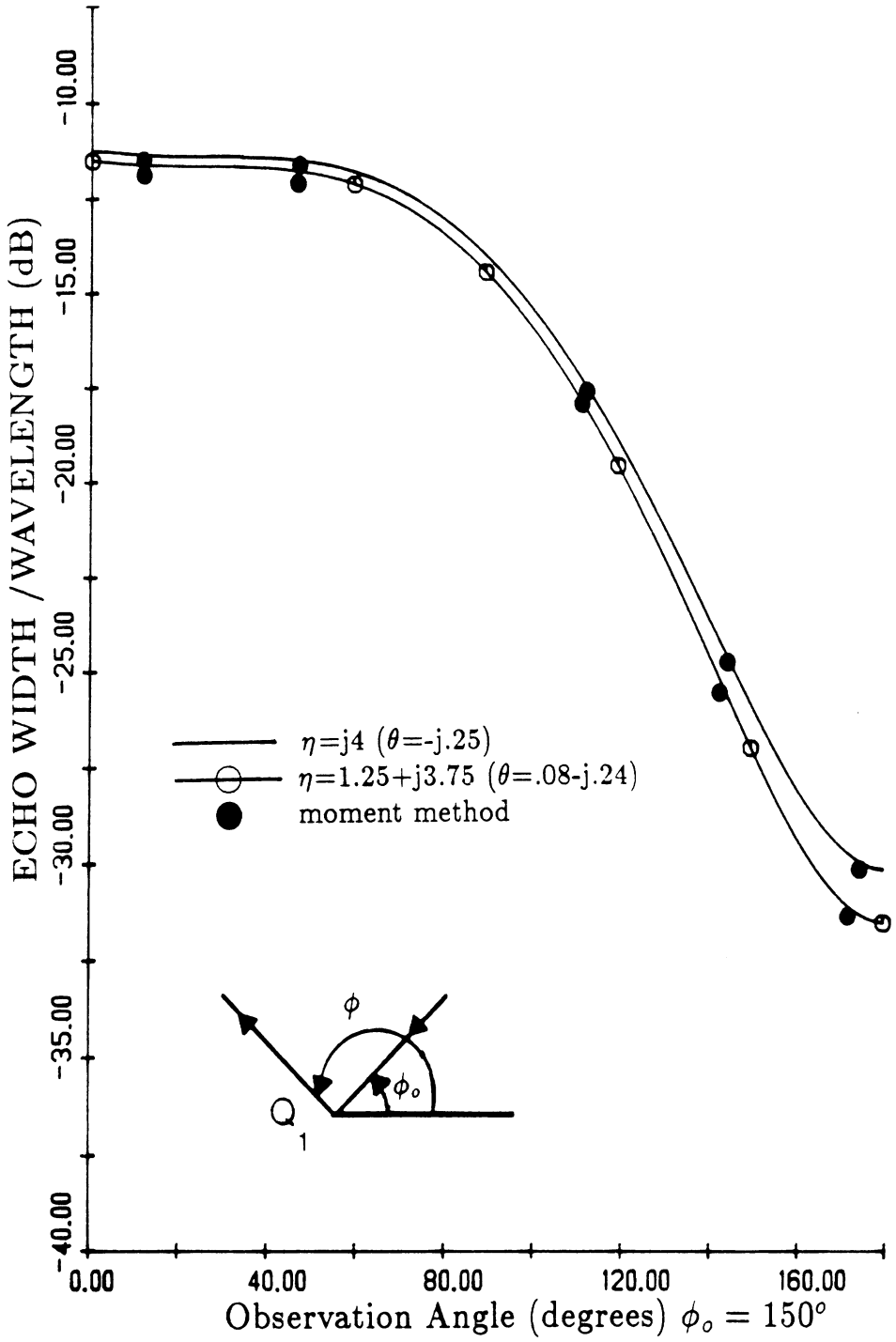

Figure 4.29 — Comparison of bistatic solution with moment method data for a 0.5λ wide resistive strip ($\eta = j4$ and $1.25 - j3.75$. $\phi_o = 150^o$)

constant surface wave pole magnitude ~0.25, E-polarization

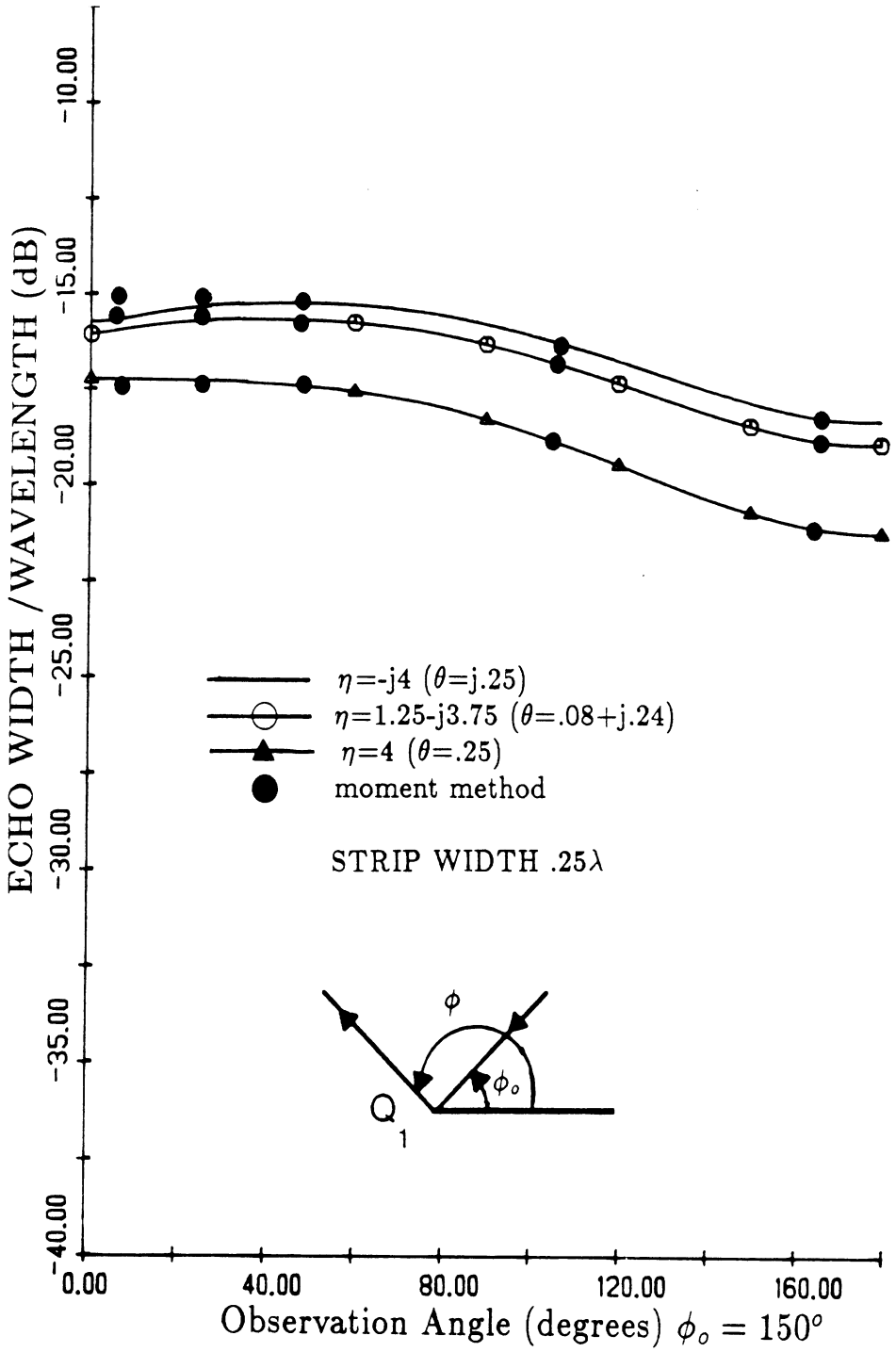

Figure 4.30 – Comparison of bistatic solution with moment method data for a 0.25λ wide resistive strip ($\eta = -j4$, $1.25 - j3.75$ and 4. $\phi_o = 150°$)

constant surface wave pole magnitude ~0.25. E-polarization

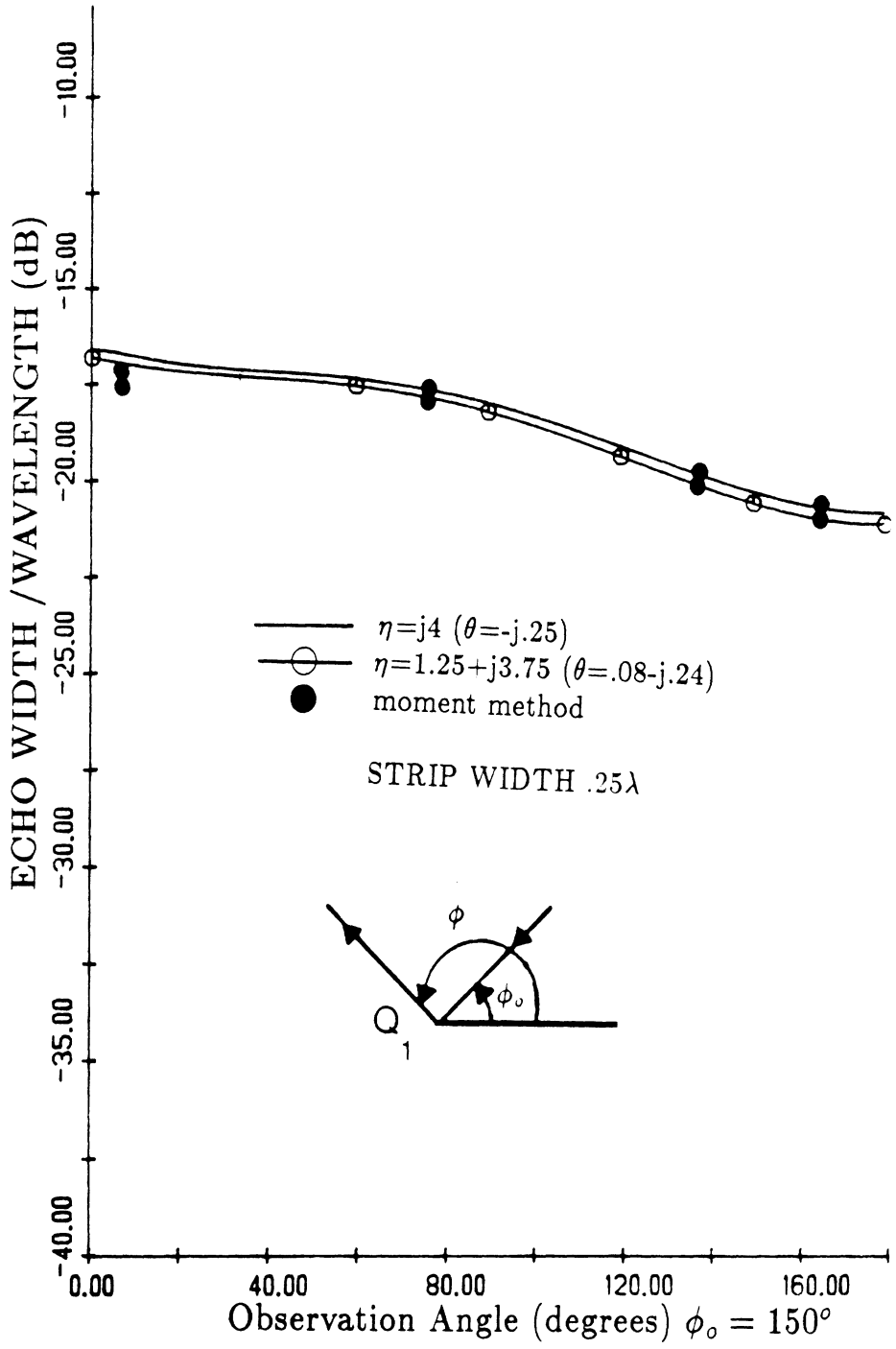

Figure 4.31 — Comparison of bistatic solution moment method data for a 0.25λ wide resistive strip with ($\eta = j4$ and $1.25 - j3.75$. $\phi_o = 150°$)

constant surface wave pole magnitude ~0.25. E-polarization

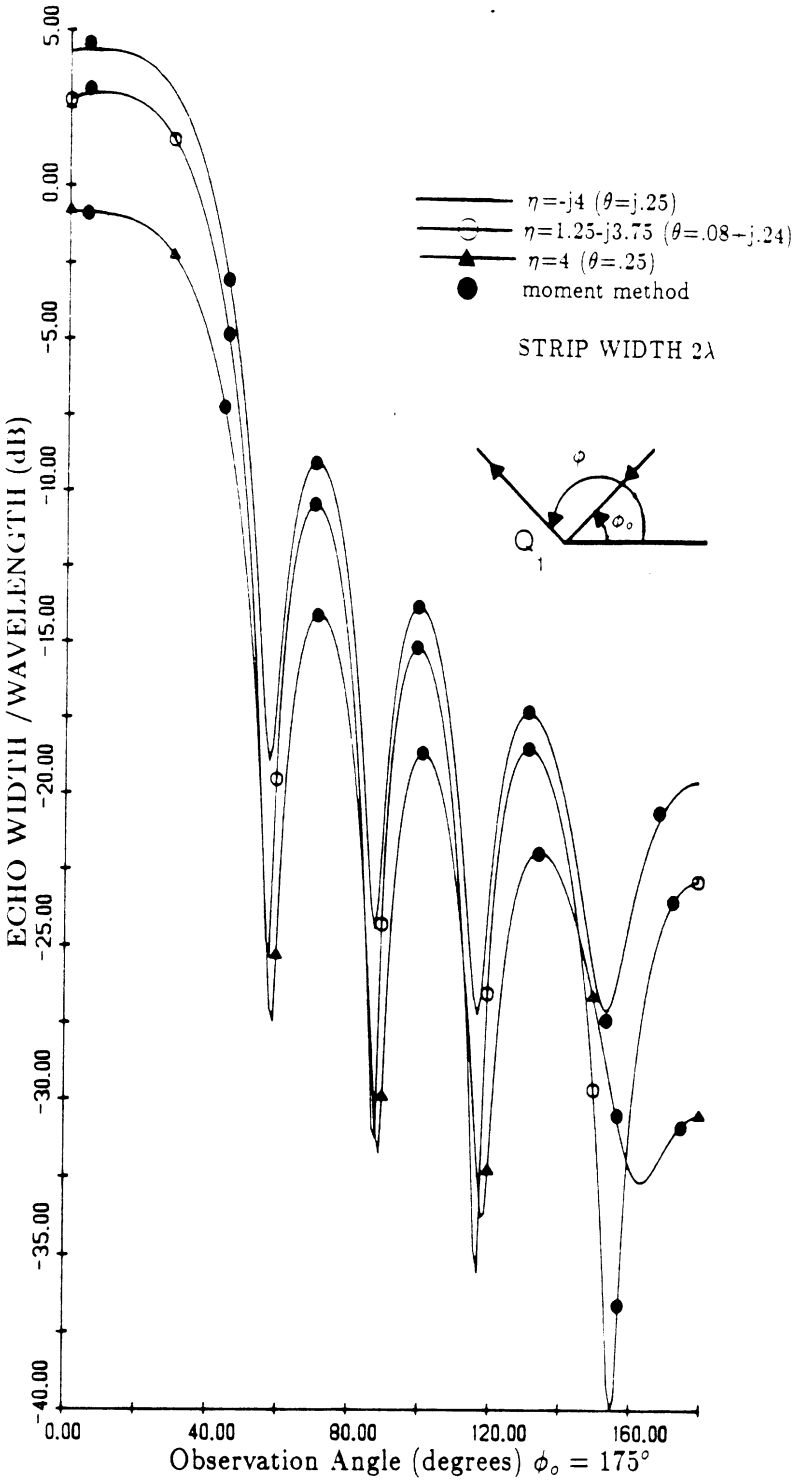

Figure 4.32 — Comparison of bistatic solution with moment method data for a 2λ wide resistive strip ($\eta = -j4$, $1.25 - j3.75$ and 4. $\phi_0 = 175°$)

constant surface wave pole magnitude ~0.25, E-polarization

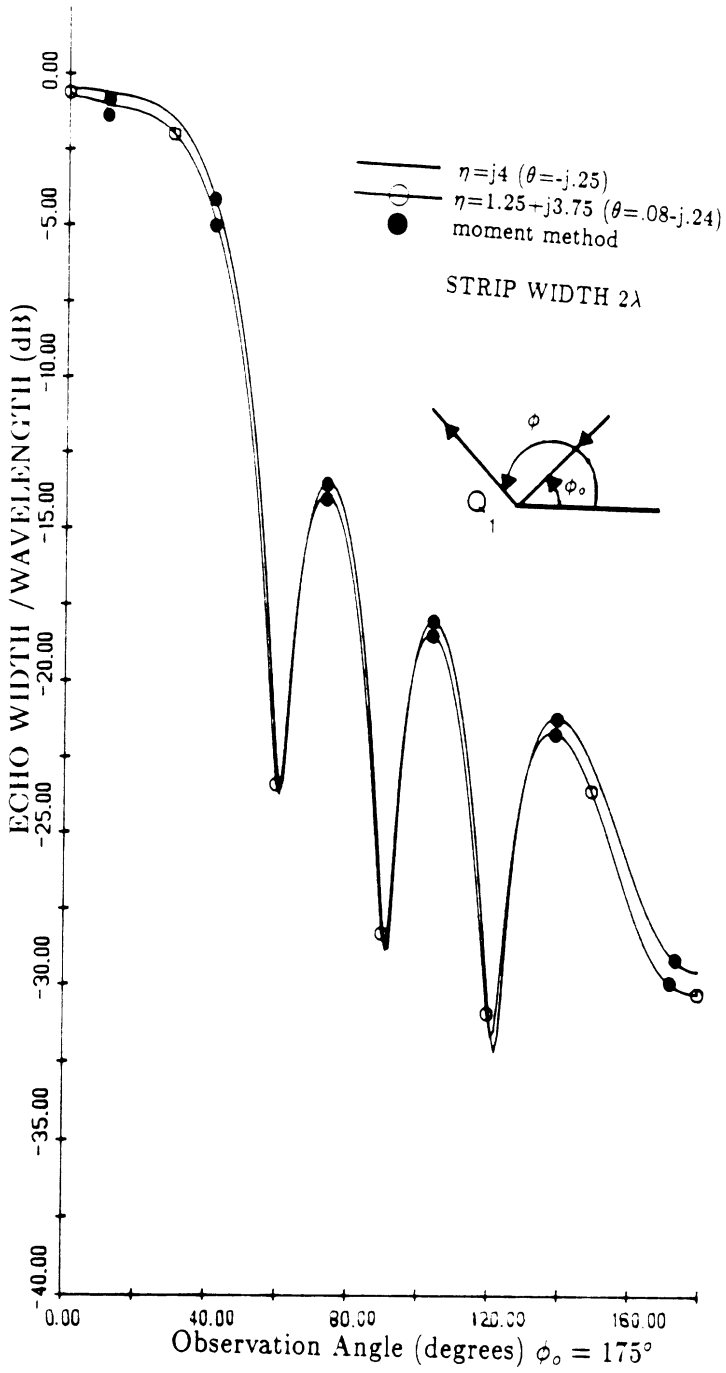

Figure 4.33 — Comparison of bistatic solution with moment method data for a 2λ wide resistive strip ($\eta = j4$ and $1.25 - j3.75$. $\phi_o = 175°$)

constant surface wave pole magnitude ~0.25, E-polarization

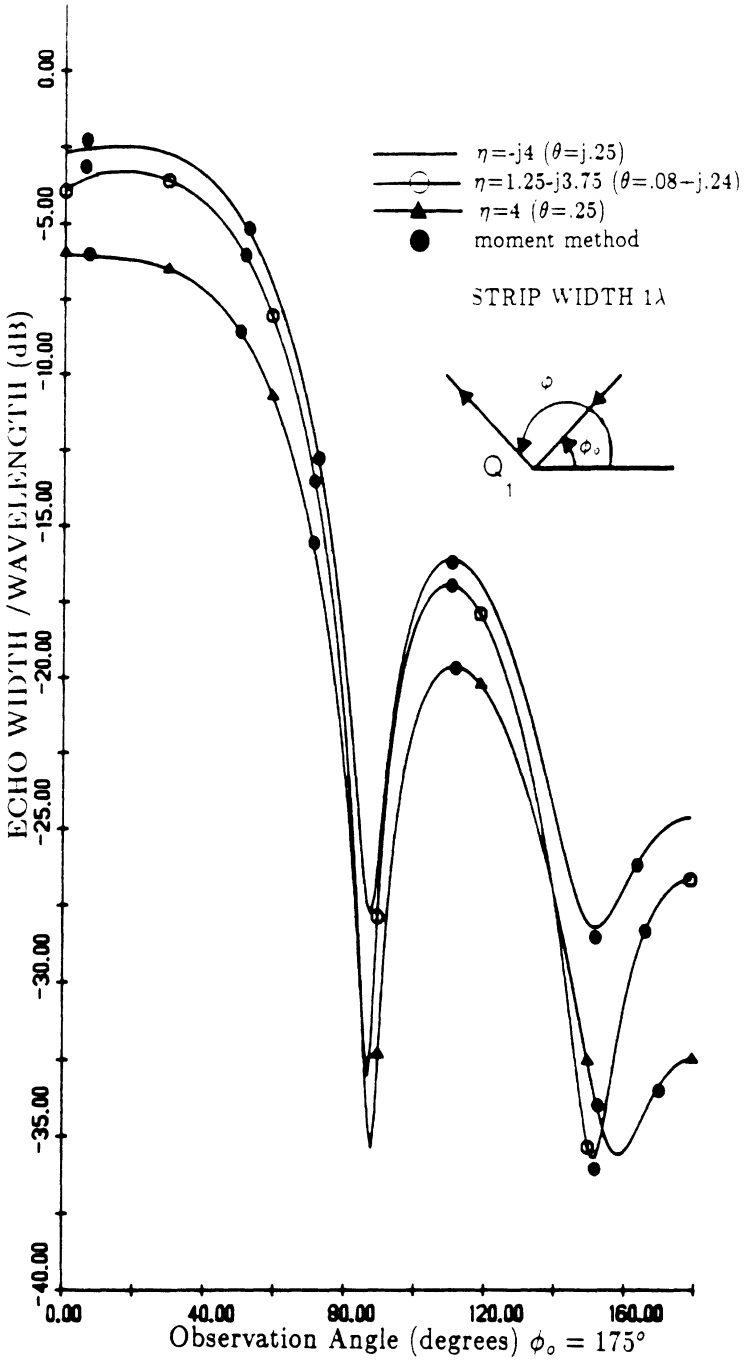

Figure 4.34 — Comparison of bistatic solution with moment method data for a 1λ wide resistive strip with ($\eta = -j4$, $1.25 - j3.75$ and 4. $\phi_o = 175^o$)

constant surface wave pole magnitude ~0.25, E-polarization

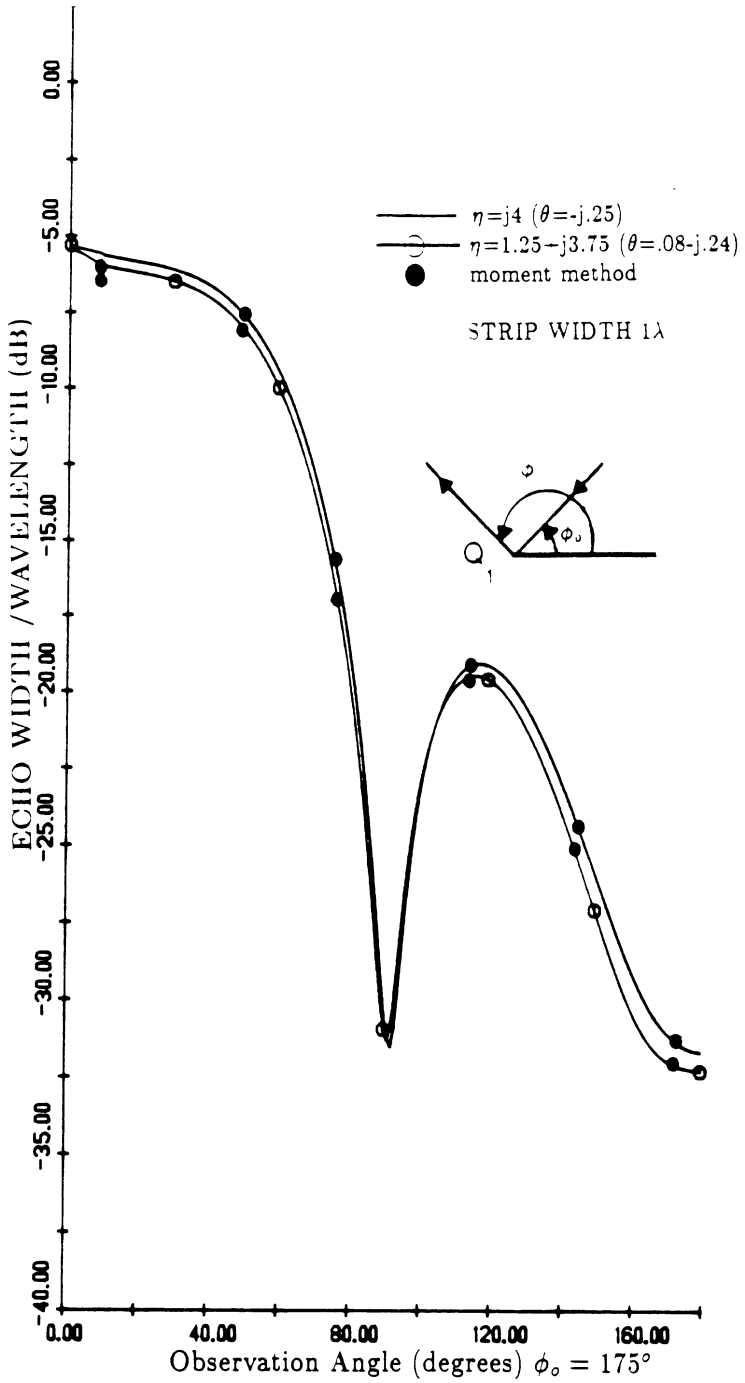

Figure 4.35 — Comparison of bistatic solution with moment method data for a 1λ wide resistive strip with ($\eta = j4$ and $1.25 + j3.75$. $\phi_o = 175°$)

constant surface wave pole magnitude ~0.25, E-polarization

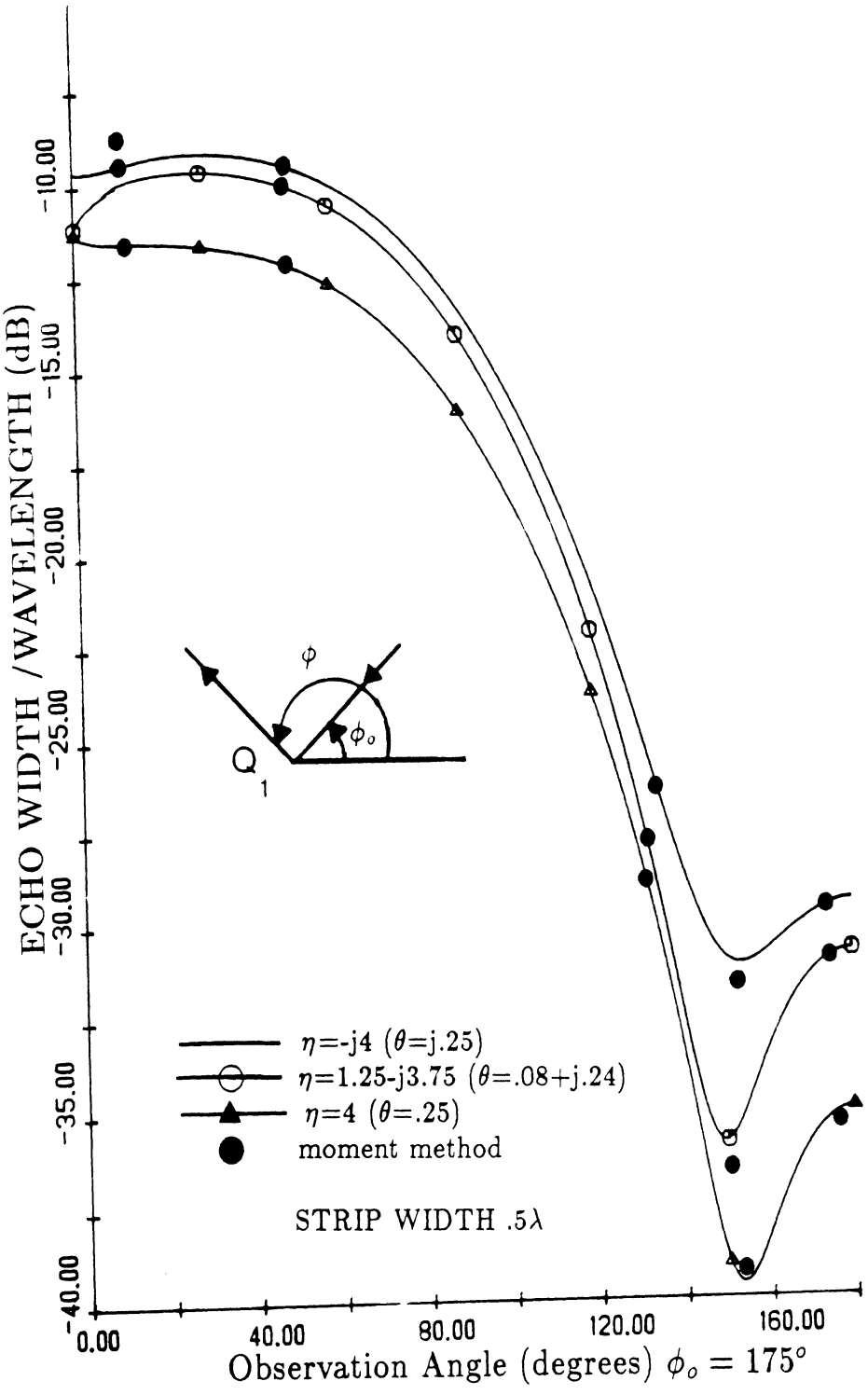

Figure 4.36 — Comparison of bistatic solution with moment method data for a 0.5λ wide resistive strip with (η = -j4, 1.25 - j3.75 and 4, ϕ_o = 175°)

constant surface wave pole magnitude ~0.25, E-polarization

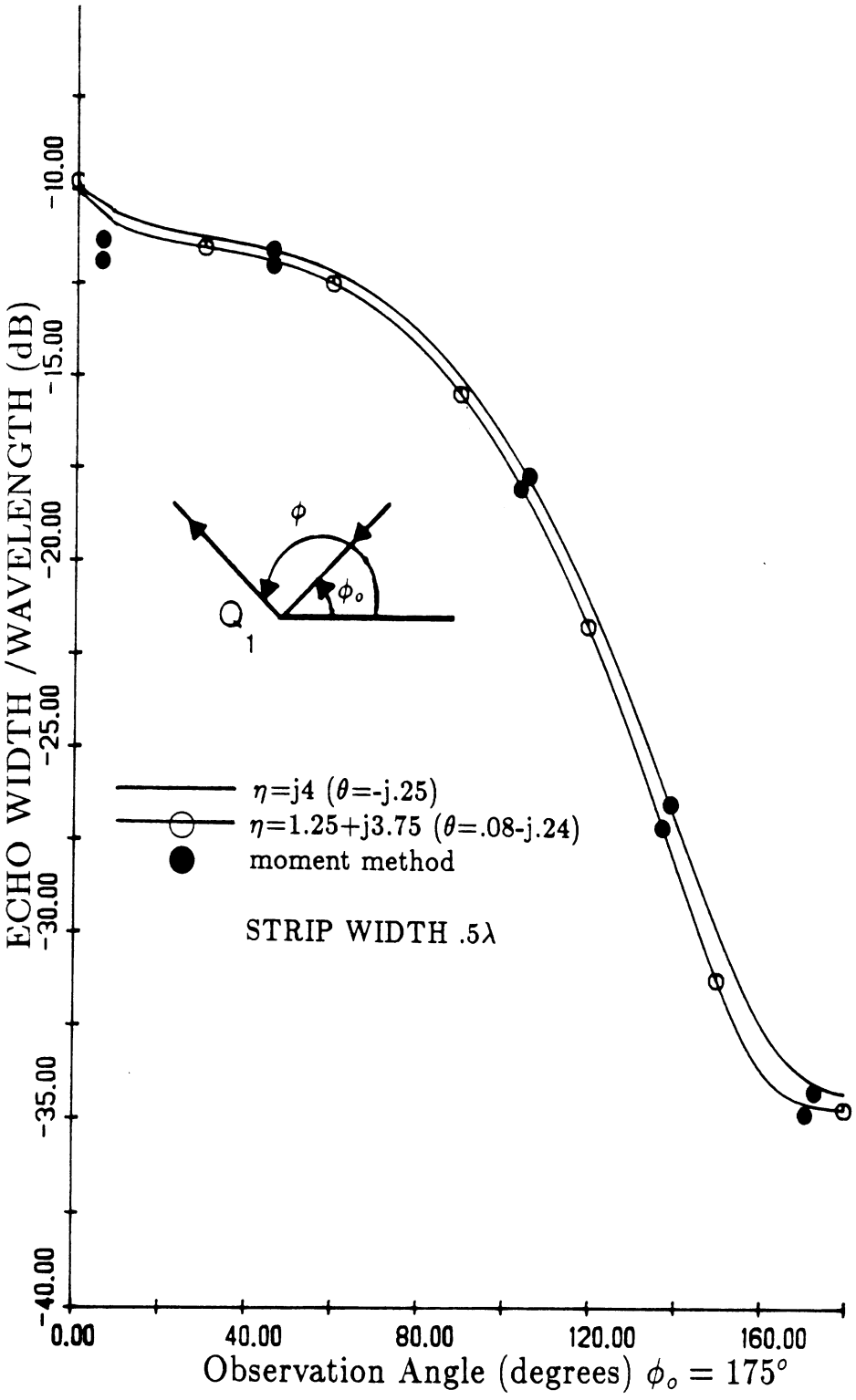

Figure 4.37 — **Comparison of bistatic solution with moment method data for a** 0.5λ **wide resistive strip with** ($\eta = j4$ **and** $1.25 + j3.75$. $\phi_o = 175°$)

constant surface wave pole magnitude ~0.25. E-polarization

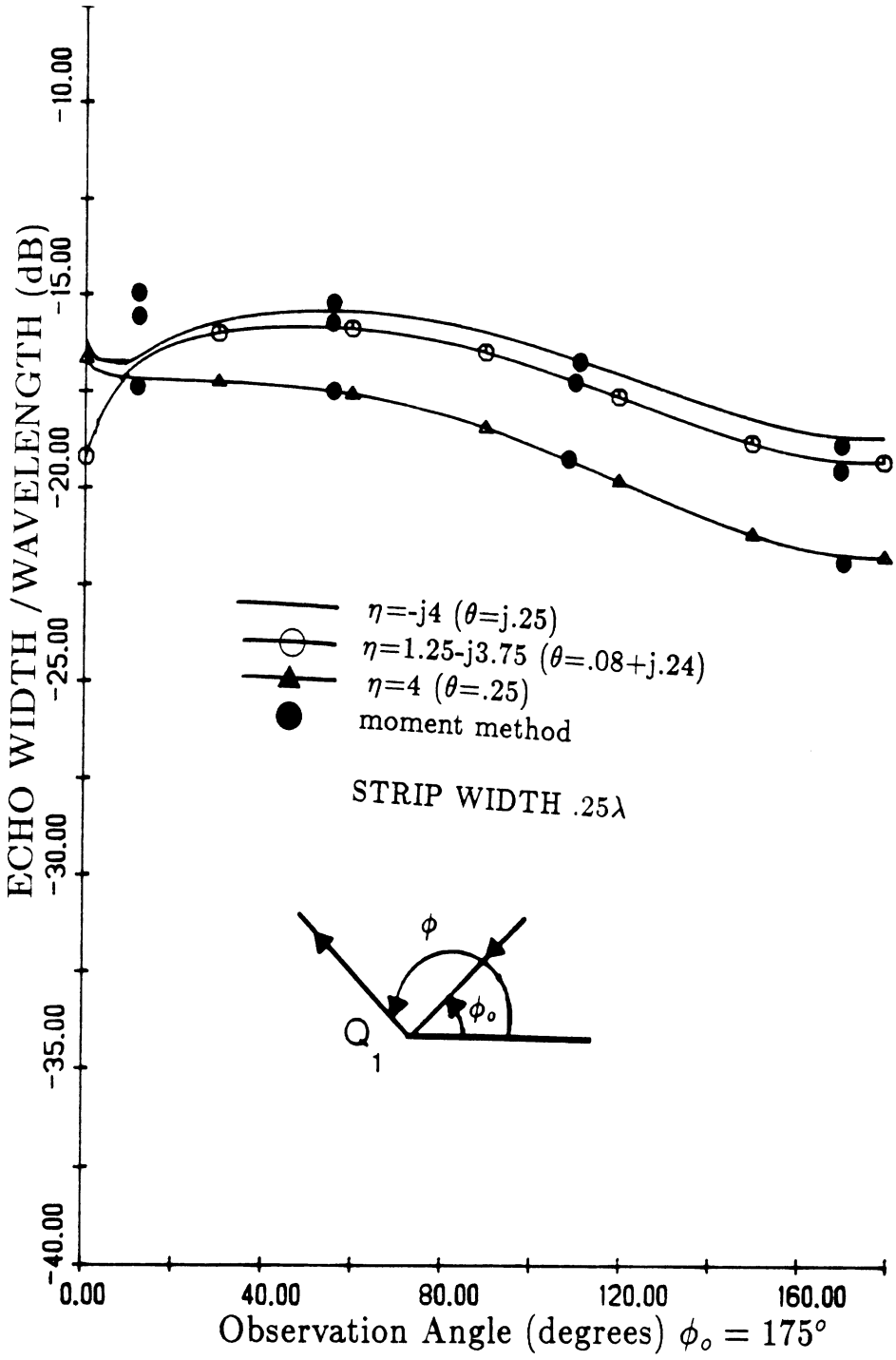

Figure 4.38 — Comparison of bistatic solution with moment method data for a 0.25λ wide resistive strip with (η = $-j4$, $1.25 - j3.75$ and 4. $\phi_o = 175°$)

constant surface wave pole magnitude ~0.25. E-polarization

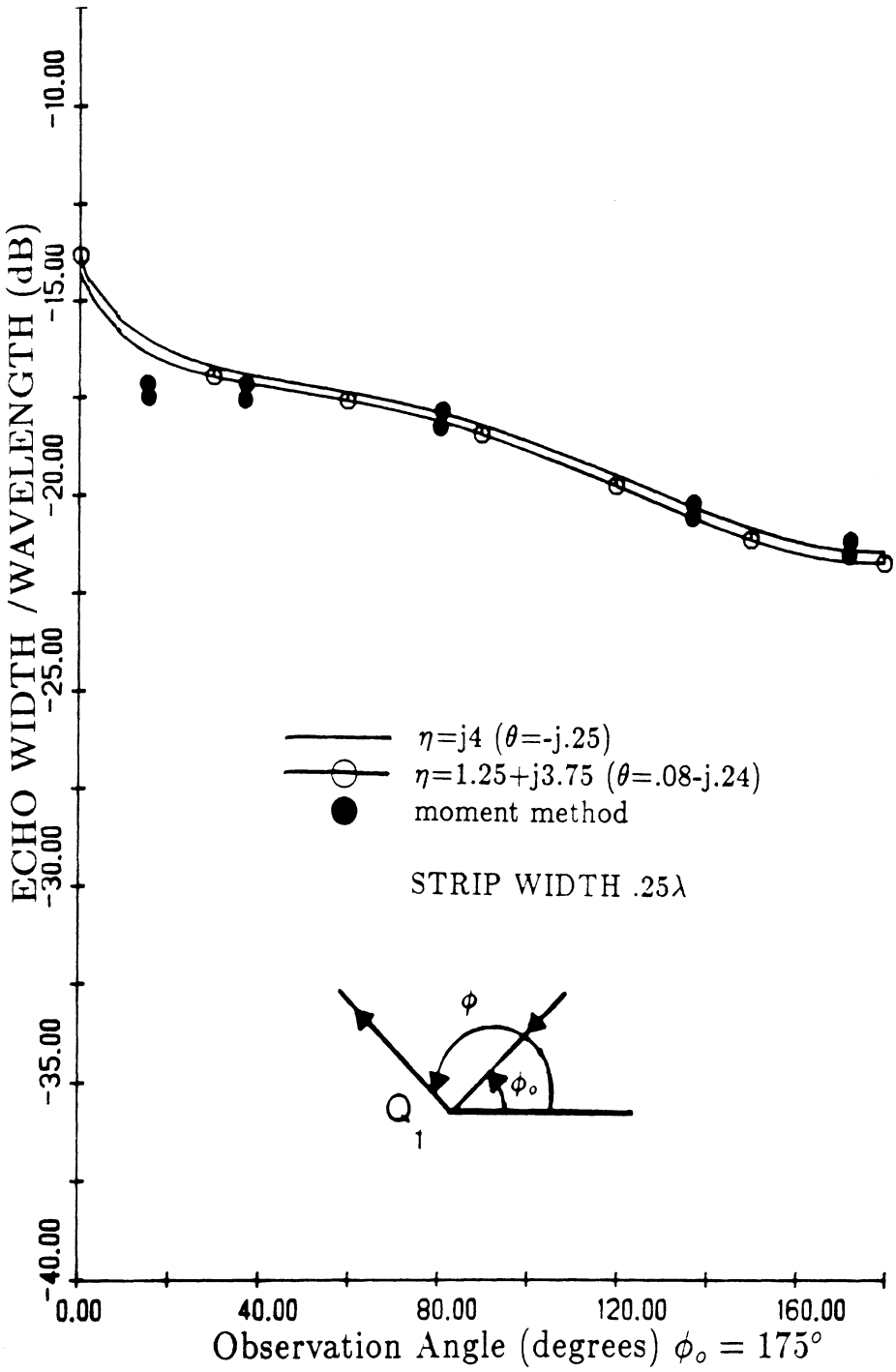

Figure 4.39 — Comparison of bistatic solution with moment method data for a 0.25λ wide resistive strip with ($\eta = j4$ and $1.25 - j3.75$, $\phi_o = 175°$)

constant surface wave pole magnitude ~0.25. E-polarization

Self-Consistent Formulation For a Resistive Strip

Although the surface wave field magnitude attenuates to zero in the far field the multi-diffracted surface rays do not. In fact, the sum of all the multi-diffracted surface ray fields can be a significant portion of the total field pattern and can dominate the geometrical optics multi-diffraction mechanisms. This section extends the "Self-Consistent GTD" technique introduced by R.C. Rudduck[33] and Nan Wang [30] to include surface ray fields. The original self-consistent approach accounts for the infinite number of multiple interactions for geometrical optics diffraction from polygonal cylinders. This concept is used here to account for the multiple interactions of the surface waves. The main assumptions to be made are that the surface waves do exist and dominate higher order diffraction. This approach will, of course, be more valid for wider strips.

We define four equivalent surface wave/ray fields impinging upon the edges of the strip (figure 4.40). The backscatter field is then defined as the superposition of the primary diffraction from the edges (figure 4.41) and that contributed by the surface waves/ray(s) evaluated via the self-consistent formulation. The equivalent surface waves are formed by using the reflection and transmission coefficients defined by Maliuzhinets [1] and are incident at the edges of the strip at the Brewster's angle (θ). By a simple matrix solution the equivalent surface waves are defined.

$$\begin{bmatrix} 1 & 0 & -C^+ & -C^- \\ 0 & 1 & -C^- & -C^+ \\ -C^+ & -C^- & 1 & 0 \\ -C^- & -C^+ & 0 & 1 \end{bmatrix} \begin{bmatrix} C_1 \\ C_2 \\ C_3 \\ C_4 \end{bmatrix} = \begin{bmatrix} D(0, \pi - \phi_o, \rho = w)e^{-jkr} \\ D(2\pi, \pi - \phi_o, \rho = w)e^{-jkr} \\ D(0, \phi_o, \rho = w) \\ D(2\pi, \phi_o, \rho = w) \end{bmatrix} \tag{4.33}$$

$$\text{S.W. Contribution} = \sum_{i=1}^{4} C_i D(\phi, \phi_o, \rho = \infty) e^{jkr_i}$$

where r_i is the phase factor referred to edge Q_1, $D(\phi, \phi_o, \rho)$ is the uniform edge diffraction coefficient, and C^+ and C^- are the reflection and transmission coefficients using the Brewster's angle, respectively.

This solution is used to analyze the same 5λ resistive strip which was used in the previous section (see figure 4.22) and is shown in figure 4.42. As expected, it matches the moment method results except near edge-on incidence. This is not surprising since this is a

this formulation we can infer from figure 4.42 that from 10° to 40° the pattern is dominated solely from multiple surface wave diffraction and not from geometrical optics multi-diffracted fields.

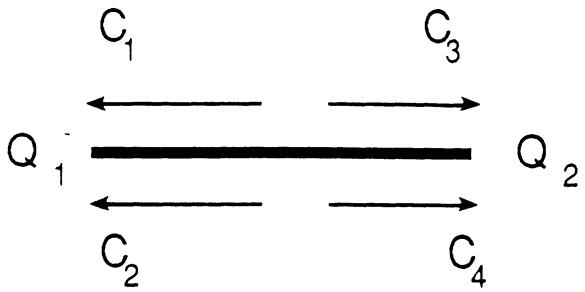

Figure 4.40 — Equivalent surface fields on a strip

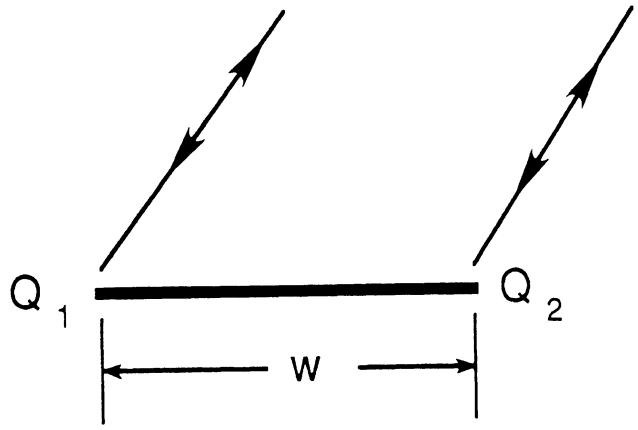

Figure 4.41 — Primary backscatter edge diffraction from a strip

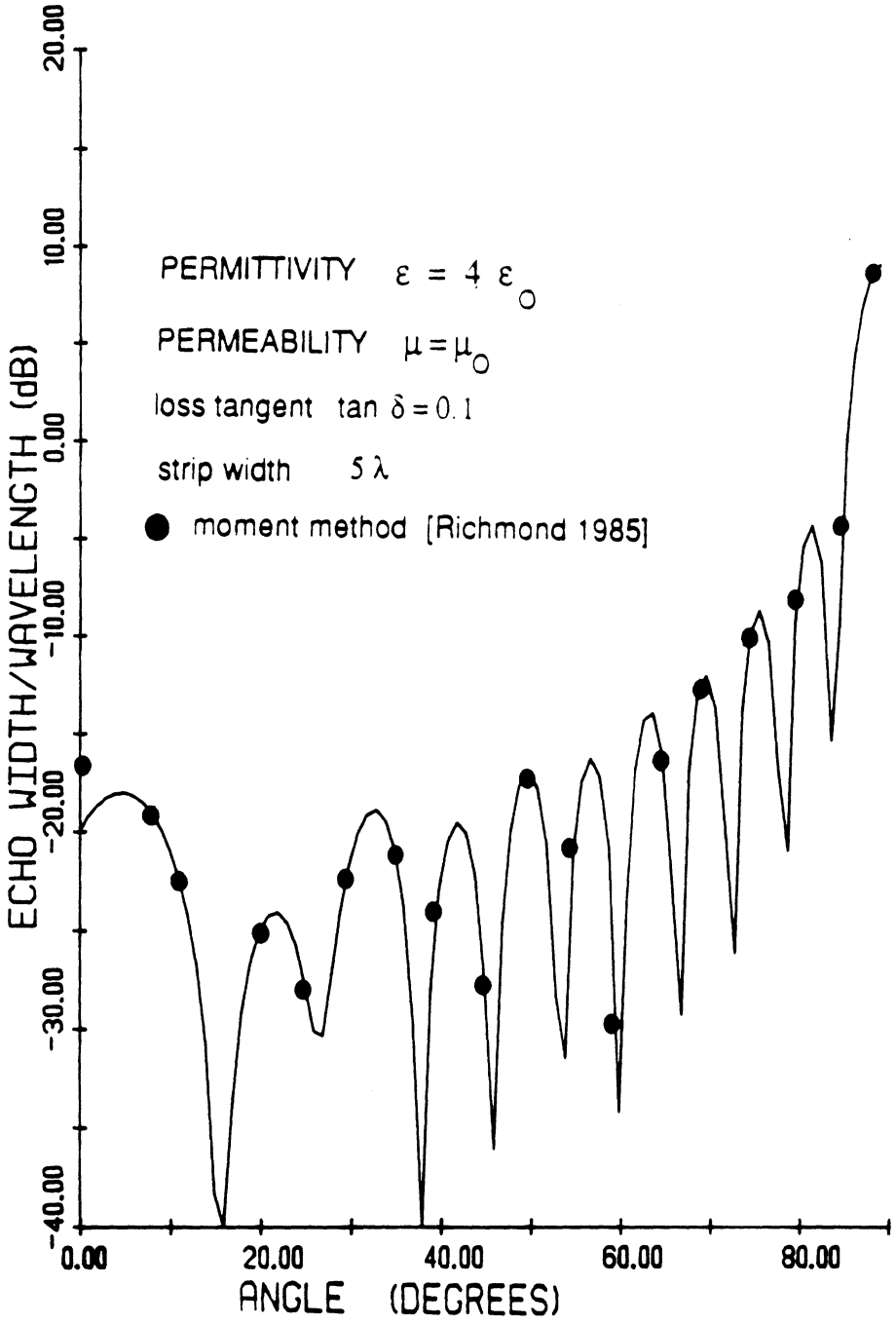

Figure 4.42 — Backscattering from a resistive strip using a self-consistent approach, and comparing the results to moment method results

Comments

Explicit high frequency expressions were given for the diffraction by a resistive strip. These included up to third order terms (primary, secondary and tertiary mechanisms) and compared very well with numerical data. Particularly, our solution was found remarkably accurate in the backscatter case down to strip widths of $\lambda/8$ and down to $\lambda/2$ near the forward scatter region.

The derivation of the second and third order diffracted fields was based on the principles of the Extended Spectral Ray Method (ESRM) and included the surface wave field effects in a uniform manner. A new uniform first order diffraction coefficient derived in chapter 2 which remains valid at the surface wave boundary was initially employed in a self-consistent manner (along with reciprocity) for the diffraction analysis of the strip. The (expected) failure of this approach then prompted us to consider a rigorous derivation of the higher order terms via the ERSM, again in conjunction with reciprocity. However, we have confirmed that when surface waves are supported multiple diffraction of surface rays may (and did in this case) contribute significantly to the total field pattern. In fact, for the case analyzed here the surface field contributions were dominate in comparison with multiply diffracted geometrical optics fields.

Finally, we used the results for the resistive strip combined with the knowledge that electric and magnetic current are uncoupled to give the diffraction coefficients for conductive and impedance strips.

CHAPTER V

DIFFRACTION FROM AN IMPEDANCE WEDGE

The first section of this chapter presents the uniform solution for the diffraction by an impedance wedge using the same approach employed in the analysis of the impedance half plane in chapter II. The second section discusses a number of identities which are required for casting the first order wedge diffraction coefficient in an alternate form. This form of the diffraction coefficient involves only a single ratio of Maliuzhinets functions and will be essential in the subsequent chapters for deriving the higher order diffraction terms.

Uniform Evaluation

A plane wave

$$\left.\begin{matrix} E_z^i \\ H_z^i \end{matrix}\right\} = e^{jk(x\cos\phi_o + y\sin\phi_o)} \tag{5.1}$$

is assumed to be normally incident upon the isolated wedge shown in figure 1.2. From Maliuzhinets[1] the integral representation of the diffracted field, repeated below, was (here and in all subsequent references u^d will represent E_z or H_z)

$$u_1^d = -\frac{\sin(\frac{\phi_o}{n})}{2n\pi j\Psi(\Phi-\phi_o)}\int_C\left[\frac{\Psi(\alpha+\Phi-\phi)}{\cos(\frac{\alpha-\phi}{n})-\cos(\frac{\phi_o}{n})}\right]e^{jk\rho\cos\alpha}\,d\alpha, \tag{5.2}$$

where C is the Sommerfeld contour as shown in figure 5.1, 2Φ is the external wedge angle ($\Phi = \frac{n\pi}{2}$), ϕ is the observation angle and ϕ_o is the incidence angle. Both ϕ and ϕ_o are referenced to the "o" face of the wedge. In addition $\Psi(\alpha)$ is the Maliuzhinets meromorphic function defined as

$$\Psi(\alpha) = \Psi_\Phi(\alpha+\Phi+\frac{\pi}{2}-\theta^+)\Psi_\Phi(\alpha-\Phi-\frac{\pi}{2}+\theta^-)\Psi_o(\alpha) \tag{5.3}$$

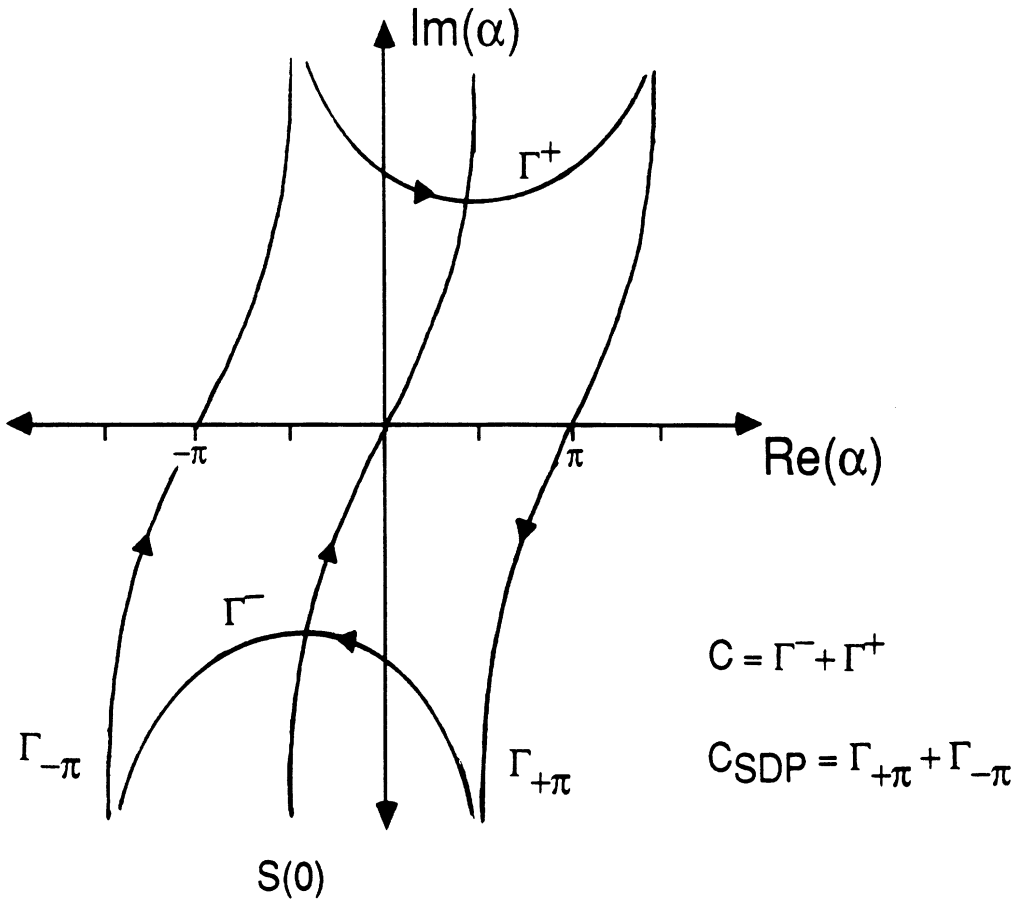

Figure 5.1 — Sommerfeld contour appearing in equation (5.2).

with

$$\Psi_o = \Psi_\Phi(\alpha + \Phi - \frac{\pi}{2} + \theta_+)\Psi_\Phi(\alpha - \Phi + \frac{\pi}{2} - \theta_-) \tag{5.4}$$

and again

$$\theta^\pm = \begin{cases} \sin^{-1}(\frac{1}{\eta}) & \text{E-pol.} \\ \sin^{-1}(\eta) & \text{H-pol.} \end{cases}, \tag{5.5}$$

where η is the normalized impedance and the $\pm$ corresponds to the common ("o") and outer ("n") faces of the wedge, respectively.

From [1] Ψ_Φ is defined as

$$\Psi_\Phi(z) = \exp\left[\frac{-j}{8\Phi}\int_0^z \int_{-j\infty}^{j\infty} \tan\frac{\pi\nu}{4\Phi}\frac{d\nu\, d\mu}{\cos(\nu-\mu)}\right]. \tag{5.6}$$

and until recently the evaluation of Ψ_Φ was not available for any arbitrary wedge angle (Φ). An alternate expression for the Maliuzhinets function (5.6) is [34]

$$\Psi_\Phi(z) = \exp\left\{-\frac{1}{2}\int_0^\infty \frac{\cosh(zs)-1}{s\cosh(\frac{\pi}{2}s)\sinh(2\Phi s)}ds\right\} \tag{5.7}$$

and is seen that $\Psi_\Phi(z)$ is an even function of z. Some additional properties of the function are

$$\Psi_\Phi(z) = \{\Psi_\Phi(\frac{\pi}{2})\}^2 \frac{\cos[\frac{\pi(z-\frac{\pi}{2})}{4\Phi}]}{\Psi_\Phi(z-\pi)}, \tag{5.8}$$

$$\Psi_\Phi(-z) = \Psi_\Phi(z), \tag{5.9}$$

$$\Psi_\Phi(z^*) = \Psi_\Phi^*(z), \tag{5.10}$$

where the asterisk denotes the complex conjugate. From (5.8)-(5.10) we now observe that the Maliuzhinets function can be determined throughout the entire complex plane from a knowledge of its behavior in the strip $0 < x < \frac{\pi}{2}$, $y \geq 0$. It is therefore sufficient to confine our attention to the strip shown in figure 5.2. We will further limit our interest to $\frac{\pi}{2} \leq \Phi \leq \pi$, corresponding to exterior wedge angles.

Due to the difficulty in evaluating the previous integral and the lack of accurate approximations for any arbitrary wedge angle the Maliuzhinets results was of limited use. Only recently have accurate approximations become available by Herman, Volakis and Senior [25]. For small arguments

$$\Psi_\Phi(z) \approx 1 - z^2(\frac{\delta}{\Phi^2}) \tag{5.11}$$

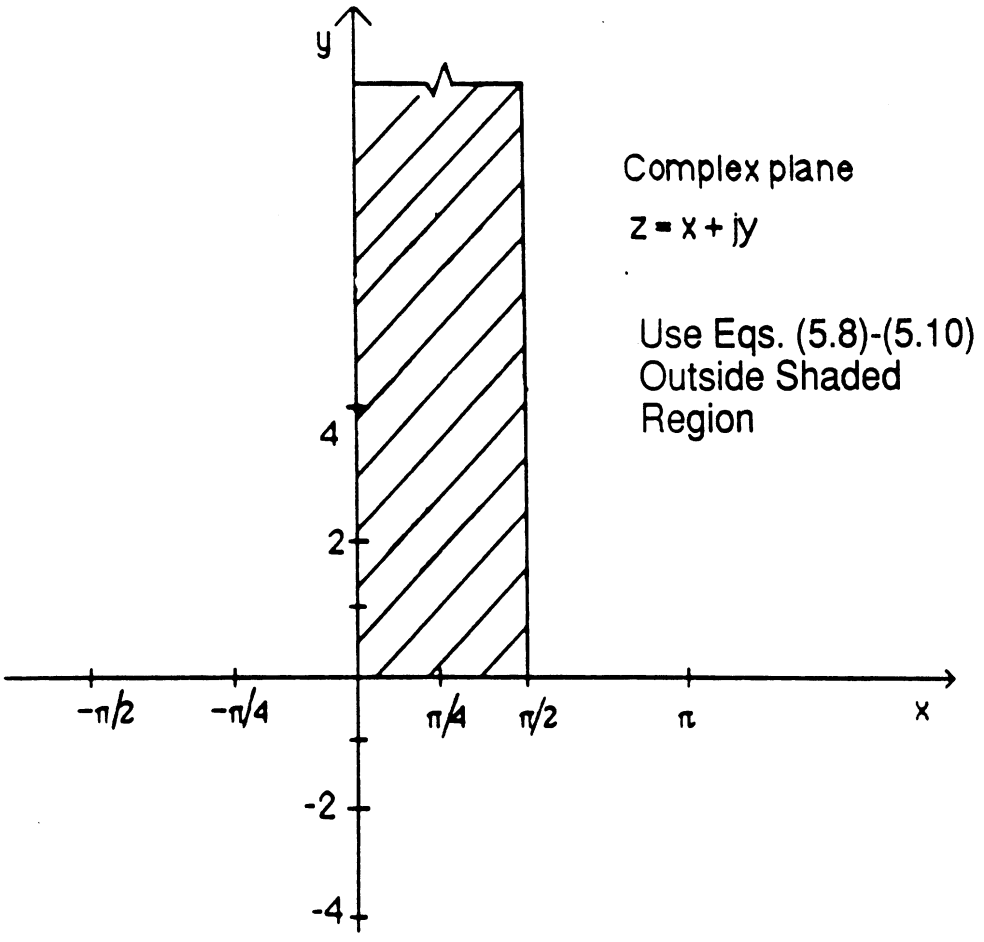

Figure 5.2 — Strip over which direct computation of $\Psi_4(z)$ is performed

with

$$\delta = 0.04626 + 0.054\Phi - 0.0078\Phi^2. \tag{5.12}$$

and for large arguments

$$\Psi_\Phi(z) \approx \sqrt{\cos\frac{\pi z}{4\Phi}}\exp\left(-\frac{\gamma}{\pi}\right) \tag{5.13}$$

where

$$\gamma = 2.556343\Phi - 3.259678\Phi^2 + 1.659306\Phi^3 - 0.3883548\Phi^4 + 0.03473964\Phi^5. \tag{5.14}$$

These approximations yield less than two percent error when the imaginary part of z is greater than 4 for the large argument and less than 4 for the small argument. If one desires less than 0.5 percent error the large argument approximation in (5.13) can be used for imaginary values greater than ten, however, for values less then ten a simple five point numerical integration will give the desired accuracy

$$\Psi_\Phi(z) \approx \exp\{-\frac{1}{2}(u + jv)\} \tag{5.15}$$

where

$$u = 0.3\sum_{n=1}^{5}\frac{\cosh[(0.3n-0.15)x]\cos[(0.3n-0.15)y] - 1}{(0.3n-0.15)\cosh[\pi(0.3n-0.15)/2]\sinh[2\Phi(0.3n-0.15)]}$$

$$v = 0.3\sum_{n=1}^{5}\frac{\sinh[(0.3n-0.15)x]\sin[(0.3n-0.15)y]}{(0.3n-0.15)\cosh[\pi(0.3n-0.15)/2]\sinh[2\Phi(0.3n-0.15)]}$$

The above are clearly Reimann sums of the real and imaginary parts of the integral in (5.7).

All the variables of the Maliuzhinets formulation have been defined and are amenable to evaluation. Now we are in a position to evaluate (5.2) in a uniform manner using the approach used previously in chapter II for the case of the impedance half plane (also see Appendix B).

Identification of the poles is the first task of the evaluation. The geometric poles are easily identified as the zeros of the trignometric terms in the denominator of (5.2). They are

$$\alpha_1 = \phi - \phi_o \tag{5.16}$$

$$\alpha_2 = \phi + \phi_o \tag{5.17}$$

$$\alpha_3 = -2n\pi + \phi + \phi_o \tag{5.18}$$

The surface wave poles are not as easily identified. Using the identity given by Maliuzhinets

$$\Psi_\Phi[z \pm (2\Phi + \frac{3\pi}{2})] = \pm \sin\frac{\pi(\pi \pm z)}{4\Phi} \csc\frac{\pi z}{4\Phi} \Psi_\Phi(2\Phi - \frac{\pi}{2} \pm z) \tag{5.19}$$

the surface wave pole is now put in a trigonometric form. For the present case there are two possible surface wave poles (one for each face) located at

$$\alpha_4 = \pi + \theta^+ + \phi \tag{5.20}$$

$$\alpha_5 = -n\pi - \pi - \theta^- + \phi \tag{5.21}$$

In evaluating (5.2) the C contour may be deformed to the steepest descent path $C_{SDP} = S(\pi) - S(-\pi)$. In so doing it is clear from (5.16)-(5.21) that the possible poles to be enclosed by $C + C_{SDP}$ are $\alpha_1, \alpha_2, \alpha_3, \alpha_4$ and α_5. The pole α_1 corresponds to the incident field while α_2 and α_3 refer to the reflected fields from the "o" and "n" faces of the wedge, respectively. Finally, the poles α_4 and α_5 are associated with the surface wave fields on the "o" and "n" faces, respectively. Clearly for $0 < \phi, \phi_o < n\pi$, the poles α_2 and α_4 can only cross $S(\pi)$, while α_3 and α_5 can only cross $S(-\pi)$. Meanwhile α_1 can cross either $S(\pi)$ or $S(-\pi)$. Furthermore since $\alpha_{1,2,3}$ are real, the crossing occurs through the saddle points whereas in the case of $\alpha_{4,5}$, which are usually complex, the crossing can occur anywhere along the length of $S(\pm\pi)$.

Based on the discussion in the above paragraph the total field can be expressed as

$$E_T^s = E^{GO} + E^{SW} + \frac{1}{2n\pi j}\frac{\sin(\frac{\phi_o}{n})}{\Psi(\Phi - \phi_o)} \int_{S(\pi)-S(-\pi)} \frac{\Psi(\alpha + \Phi - \phi)}{\cos(\frac{\alpha-\phi}{n}) - \cos(\frac{\phi_o}{n})} e^{jk\rho\cos\alpha}\, d\alpha. \tag{5.22}$$

E^{GO} is the geometrical optics field given by

$$\begin{aligned} E^{GO} = {} & e^{jk\rho\cos(\phi-\phi_o)} u_o(\pi - |\phi - \phi_o|) - \frac{\Psi(\Phi + \phi_o)}{\Psi(\Phi - \phi_o)} e^{jk\rho\cos(\phi+\phi_o)} u_o(\pi - \phi - \phi_o) \\ & - \frac{\Psi(-3\Phi + \phi_o)}{\Psi(\Phi - \phi_o)} e^{jk\rho\cos(-2n\pi+\phi+\phi_o)} u_o(\pi - 2n\pi + \phi + \phi_o) \end{aligned} \tag{5.23}$$

where $u(z)$ is the unit step function and E^{SW} is the surface wave field given by

$$\begin{aligned} E^{SW} = {} & 2\csc\left(\frac{\alpha_4 - \alpha_5}{2n}\right) \frac{\sin(\frac{\phi_o}{n})}{\Psi(\Phi - \phi_o)} \\ & \cdot \left[\frac{\Psi^+(\alpha_4 + \Phi - \phi)}{\cos(\frac{\alpha_4-\phi}{n}) - \cos\frac{\phi_o}{n}} e^{jk\rho\cos\alpha_4} u_o(\pi - \alpha_{R4} + gd(|\alpha_{I4}|)sgn(\alpha_{I4})) \right. \\ & \left. - \frac{\Psi^+(\alpha_5 + \Phi - \phi)}{\cos(\frac{\alpha_5-\phi}{n}) - \cos\frac{\phi_o}{n}} e^{jk\rho\cos\alpha_5} u_o(\pi + \alpha_{R5} - gd(|\alpha_{I5}|)sgn(\alpha_{I5})) \right] \end{aligned} \tag{5.24}$$

with $gd(x)$ is the Gudermann function and α_{Ri}, α_{Ii} the real and imaginary parts of the poles as defined above.

The SDP integral in (5.22) corresponds to the diffracted field by the impedance wedge whose uniform evaluation requires a consideration of all poles α_1 through α_5 which may be near the SDP path. In the next section we present an alternate uniform evaluation of the diffraction integral to account for the discontinuities of the surface wave boundaries associated with E^{SW} as well as those real boundaries associated with E^{GO}. The method described in Appendix B which was used for the impedance half plane is to be used here by considering each pole individually.

Formulation

In accordance with the formulation in Appendix B the diffracted field in (5.22) can be expressed as

$$\begin{aligned} E^s(\phi,\phi_o) = D(\phi,\phi_o)\frac{e^{-jk\rho}}{\sqrt{\rho}} = \frac{1}{2n\pi j}\frac{\sin\frac{\phi_o}{n}}{\Psi(\Phi-\phi_o)}\Bigg\{ & \int_{S(\pi)} K_A(\alpha,\phi)e^{-jk\rho\cos(\pi-\alpha)}\,d\alpha \\ & + \sum_{p=1,2,4} A_p \int_{S(\pi)} \sec\left(\frac{\alpha-\alpha_p-\pi}{2}\right) e^{-jk\rho\cos(\pi-\alpha)}\,d\alpha \\ & - \int_{S(-\pi)} K_B(\alpha,\phi)e^{-jk\rho\cos(\pi+\alpha)}\,d\alpha \\ & - \sum_{p=1,3,5} B_p \int_{S(-\pi)} \sec\left(\frac{\alpha-\alpha_p+\pi}{2}\right) e^{-jk\rho\cos(\pi+\alpha)}\,d\alpha \Bigg\} \end{aligned} \tag{5.25}$$

where $K_{A,B}(\alpha,\phi)$ are non-singular functions

$$K_A(\alpha,\phi) = \frac{\Psi(\alpha+\Phi-\phi)}{\cos(\frac{\alpha-\phi}{2})-\cos(\frac{\phi_o}{2})} - \sum_{p=1,2,4} A_p \sec(\frac{\alpha-\alpha_p-\pi}{2}) \tag{5.26}$$

$$K_B(\alpha,\phi) = \frac{\Psi(\alpha+\Phi-\phi)}{\cos(\frac{\alpha-\phi}{2})-\cos(\frac{\phi_o}{2})} - \sum_{p=1,3,5} B_p \sec(\frac{\alpha-\alpha_p+\pi}{2}) \tag{5.27}$$

Evaluating the integrals in (5.25) gives

$$
\begin{aligned}
D(\phi,\phi_o) \sim & \frac{1}{2n\pi j}\frac{\sin\frac{\phi_o}{n}}{\Psi(\Phi-\phi_o)}\sqrt{\frac{2\pi}{k}}e^{-j\frac{\pi}{4}} \\
& \cdot\Bigg\{(K_A(\pi,\phi)-K_B(-\pi,\phi)) \\
& +\Bigg[\sum_{p=1,2,4}A_p\frac{F_{KP}[\pm(\sqrt{2k\rho}\cos\frac{\alpha_p}{2})^2]}{\cos\frac{\alpha_p}{2}} \\
& -\sum_{p=1,3,5}B_p\frac{F_{KP}[\pm(\sqrt{2k\rho}\cos\frac{\alpha_p}{2})^2]}{\cos\frac{\alpha_p}{2}}\Bigg]\Bigg\}+O(\frac{1}{\kappa\rho})
\end{aligned}
\tag{5.28}
$$

where

$$A_1 = \frac{n}{2}\frac{\Psi(\Phi-\phi_o)}{\sin\frac{\phi_o}{n}}\cdot P_{2\pi}(\alpha_1-\pi) \tag{5.29}$$

$$A_2 = -\frac{n}{2}\frac{\Psi(\Phi+\phi_o)}{\sin\frac{\phi_o}{n}}\cdot P_{2\pi}(\alpha_2-\pi) \tag{5.30}$$

$$A_4 = n\frac{\csc(\frac{\alpha_4-\alpha_5}{2n})}{\cos(\frac{\alpha_4-\phi}{n})-\cos\frac{\phi_o}{n}}\Psi^+(\alpha_4+\Phi-\phi)\cdot P_{2\pi}(Re\{\alpha_4\}-\pi) \tag{5.31}$$

$$B_1 = -A_1\cdot\{1-P_{2\pi}(\alpha_1-\pi)\} \tag{5.32}$$

$$B_3 = \frac{n}{2}\frac{\Psi(-3\Phi+\phi_o)}{\sin\frac{\phi_o}{n}}\cdot P_{2\pi}(\alpha_3+\pi) \tag{5.33}$$

$$B_5 = n\frac{\csc(\frac{\alpha_4-\alpha_5}{2n})}{\cos(\frac{\alpha_5-\phi}{n})-\cos\frac{\phi_o}{n}}\Psi^+(\alpha_5+\Phi-\phi)\cdot P_{2\pi}(Re\{\alpha_5\}+\pi) \tag{5.34}$$

and $P_{2\pi}$ is the unit rect function (2π wide).

Numerical Results

Figures 5.3 to 5.6 show the bistatic patterns for a series of external wedge angles. The incidence angle is 30^o, observation distance is 1.6λ, and the impedance on both faces of the wedge are equal. In figures 5.3 and 5.5 the material is inductive ($\eta = 0.5+j5,\ 0.5+j1$) and does not support surface waves which is evident since the field tends toward zero on the "n" face. However, the material for figures 5.4 and 5.6 is capacitive ($\eta = 0.5-j5,\ 0.5-j1$) and does support surface waves. In this situation the surface wave contribution becomes stronger as the wedge approaches a full plane and as the reactance decreases the surface wave contribution decreases since the material is less capacitive.

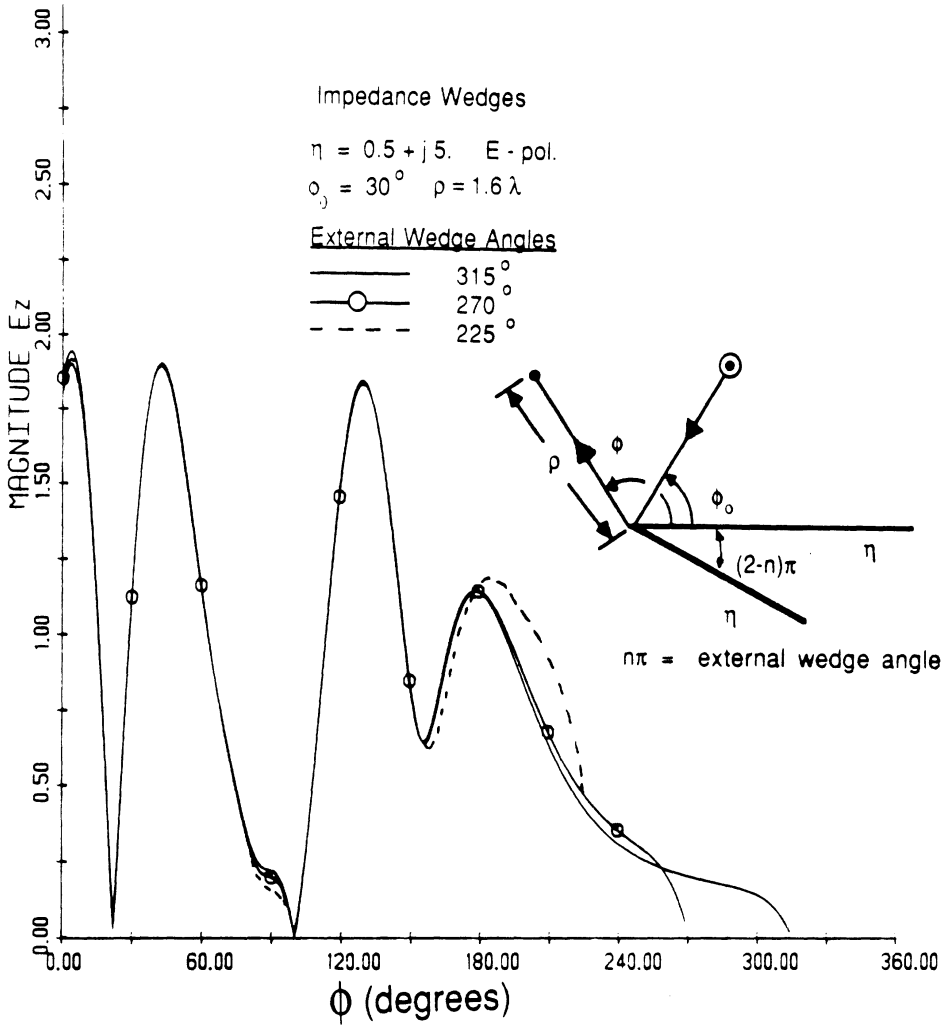

Figure 5.3 — Bistatic scattering from impedance wedges ($\eta = 0.5 - j5$). E-polarization

Pattern of the total electric field due to a plane wave source.

Angle of incidence equals 30°, and observation distance 1.6λ.

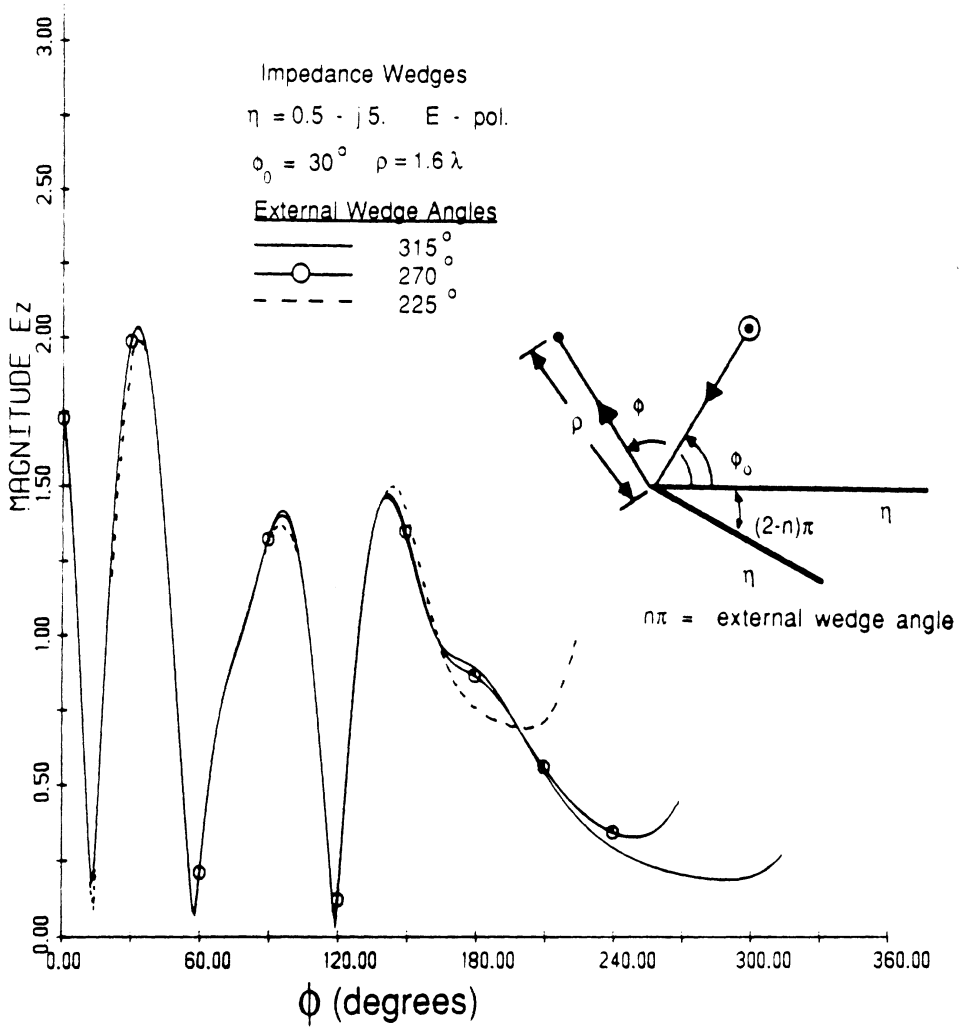

Figure 5.4 — Bistatic scattering from impedance wedges ($\eta = 0.5 - j5$). E-polarization

Pattern of the total electric field due to a plane wave source.

Angle of incidence equals 30°, and observation distance 1.6λ.

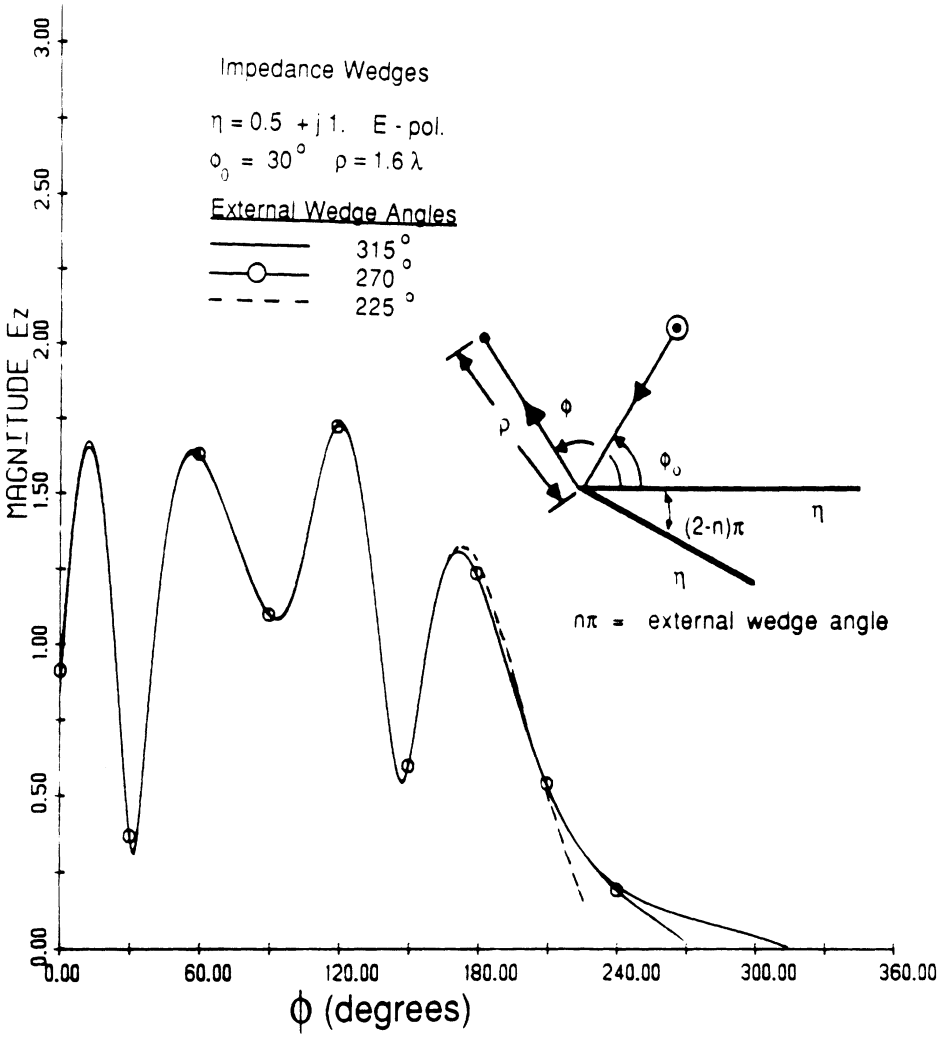

Figure 5.5 — Bistatic scattering from impedance wedges ($\eta = 0.5 + j1$), E-polarization

Pattern of the total electric field due to a plane wave source.

Angle of incidence equals 30°, and observation distance 1.6λ.

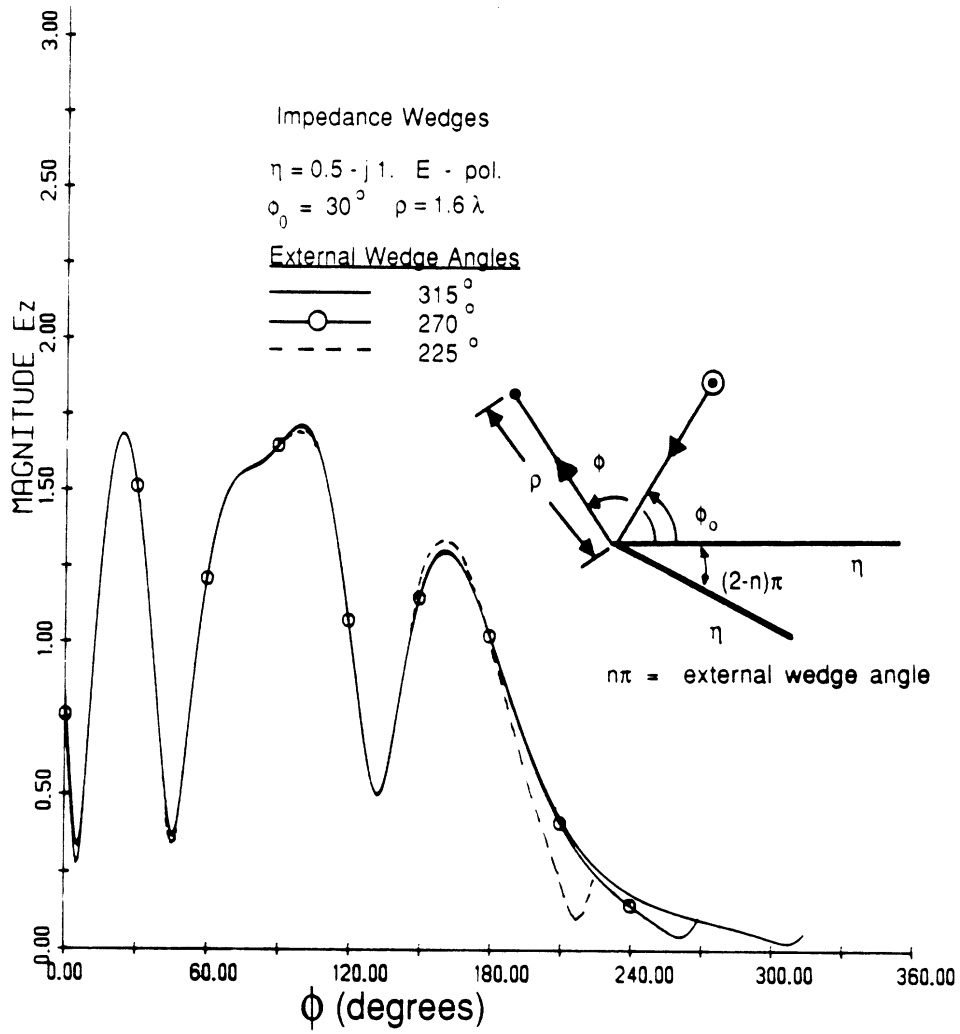

Figure 5.6 — Bistatic scattering from impedance wedges ($\eta = 0.5 - j1$), E-polarization

Pattern of the total electric field due to a plane wave source.

Angle of incidence equals 30°, and observation distance 1.6λ.

Non-Uniform Evaluation

In chapters VI and VII the ERSM will be used to compute multi-edge diffraction from impedance double wedge structures. Using this procedure a non-uniform first order coefficient is required in which a simple steepest descent approach can be utilized; however, the form of the result must be in the proper form to facilitate calculations for multi-diffraction mechanisms. The primary diffraction integral is

$$u_1^d(\phi,\phi_o) = \frac{j}{2\pi n}\int_{C_{SDP}} \frac{\sin\frac{\phi_c}{n}}{\Psi(\Phi-\phi_o)} e^{-jk\rho\cos\alpha} \cdot\left\{\frac{\Psi(\alpha+\pi+\Phi-\phi)}{\cos(\frac{\alpha+\pi-\phi}{n})-\cos(\frac{\phi_o}{n})} - \frac{\Psi(\alpha-\pi+\Phi-\phi)}{\cos(\frac{\alpha-\pi-\phi}{n})-\cos(\frac{\phi_o}{n})}\right\} d\alpha \tag{5.35}$$

where C_{SDP} is the steepest descent path (see figure 5.1) obtained after the deformation of the Sommerfeld contour.

Equation (5.35) can be rewritten in a form whose utility will be essential when considering the evaluation of the double diffraction integral having a vanishing integrand at the saddle point. Such a form is obtained by introducing the identity

$$\Psi(\alpha+\frac{n\pi}{2}-\pi) = C(\alpha,\theta^+,\theta^-,n)\Psi(\alpha+\frac{n\pi}{2}+\pi), \tag{5.36}$$

where

$$C = C(\alpha,\theta^+,\theta^-,n) = \frac{\sin(\frac{\alpha-\pi+\theta^+}{2n})\sin(\frac{\alpha-\theta^+}{2n})}{\sin(\frac{\alpha+\pi-\theta^+}{2n})\sin(\frac{\alpha+\theta^+}{2n})}\cdot\frac{\cos(\frac{\alpha-\pi+\theta^-}{2n})\cos(\frac{\alpha-\theta^-}{2n})}{\cos(\frac{\alpha+\pi-\theta^-}{2n})\cos(\frac{\alpha+\theta^-}{2n})}. \tag{5.37}$$

When (5.36) is substituted in (5.35) we obtain

$$u_1^d(\phi,\phi_o) = \frac{j}{2\pi n}\int_{S(0)} e^{-jk\rho\cos\alpha}\sin(\frac{\alpha-\phi}{n})\frac{\Psi(\alpha-\phi+\frac{n\pi}{2}+\pi)}{\Psi(\frac{n\pi}{2}-\phi_o)} \cdot\left\{\frac{1}{\cos(\frac{\pi+\phi_o}{n})-\cos(\frac{\alpha-\phi}{n})} - \frac{1}{\cos(\frac{\pi-\phi_o}{n})-\cos(\frac{\alpha-\phi}{n})} - \frac{\sin(\frac{\phi_o}{n})C_{on}(\alpha-\phi)}{\cos(\frac{\pi-\alpha+\phi}{n})-\cos(\frac{\phi_o}{n})}\right\} d\alpha. \tag{5.38}$$

In the above, we also made use of the relations

$$C = 1+(C-1), \tag{5.39}$$

$$C(\alpha,\theta^+,\theta^-,n)-1 = \sin(\frac{\alpha}{n})C_o(\alpha,\theta^+,\theta^-,n) = \sin(\frac{\alpha}{n})C_{on}(\alpha), \tag{5.40}$$

$$C_{on}(\alpha) = \frac{.25\{\sin(\frac{\theta^+}{n}) - \sin(\frac{\theta^-}{n}) - 2\sin(\frac{\pi}{n})\cos(\frac{\alpha}{n}) + \sin(\frac{\pi-\theta^+}{n}) + \sin(\frac{\theta^- - \pi}{n})\}}{\sin(\frac{\alpha+\pi-\theta^+}{2n})\sin(\frac{\alpha+\theta^+}{2n})\cos(\frac{\alpha+\pi-\theta^-}{2n})\cos(\frac{\alpha+\theta^-}{2n})} \tag{5.41}$$

and

$$\frac{\sin(\frac{\phi_o}{n})}{\cos(\frac{\alpha+\pi}{n}) - \cos(\frac{\phi_o}{n})} - \frac{\sin(\frac{\phi_o}{n})}{\cos(\frac{\alpha-\pi}{n}) - \cos(\frac{\phi_o}{n})} = \sin(\frac{\alpha}{n})\left\{\frac{1}{\cos(\frac{\pi+\phi_o}{n}) - \cos(\frac{\alpha}{n})} - \frac{1}{\cos(\frac{\pi-\phi_o}{n}) - \cos(\frac{\alpha}{n})}\right\}. \tag{5.42}$$

The first order asymptotic evaluation of (5.35) corresponds to the diffracted field from an isolated wedge whose non-uniform form (valid in the far zone) is

$$u_1^d(\phi,\phi_o) = \frac{j}{2\pi n}\sqrt{\frac{2\pi}{k\rho}}e^{-jk\rho}e^{j\frac{\pi}{4}}\frac{\sin\frac{\phi_o}{n}}{\Psi(\frac{n\pi}{2}-\phi_o)}\left[\frac{\Psi(\pi+\frac{n\pi}{2}-\phi)}{\cos(\frac{\pi-\phi}{n}) - \cos(\frac{\phi_o}{n})} - \frac{\Psi(-\pi+\frac{n\pi}{2}-\phi)}{\cos(\frac{\pi+\phi}{n}) - \cos(\frac{\phi_o}{n})}\right] \tag{5.43a}$$

or from (5.7)

$$u_1^d(\phi,\phi_o) = \frac{1}{2\pi n}\sqrt{\frac{2\pi}{k\rho}}e^{-jk\rho}e^{-j\frac{\pi}{4}}\sin(\frac{\phi}{n})\frac{\Psi(-\phi+\frac{n\pi}{2}+\pi)}{\Psi(\frac{n\pi}{2}-\phi_o)} \cdot \left\{\frac{1}{\cos(\frac{\pi+\phi_o}{n}) - \cos(\frac{\phi}{n})} - \frac{1}{\cos(\frac{\pi-\phi_o}{n}) - \cos(\frac{\phi}{n})} - \frac{\sin(\frac{\phi_o}{n})C_{on}(-\phi)}{\cos(\frac{\pi+\phi}{n}) - \cos(\frac{\phi_o}{n})}\right\} \tag{5.43b}$$

Since we are primarily concerned with far field patterns, a uniform primary diffraction coefficient is not required. If we were, however, interested in such a coefficient, then the approach discussed in the previous section of this chapter will be directly applicable for its derivation. Note that (5.43a) can be directly obtained from (5.28) by simply letting $\rho \to \infty$.

CHAPTER VI

ISOLATED IMPEDANCE DOUBLE WEDGE STRUCTURES

Interest in diffraction from material coated structures has prompted the investigation of geometries such as those of impedance strips, thick half planes, inserts in a full plane and convex polygonal cylinders. All of the above structures have a generic double wedge structure in which one face is common to both wedges.

The geometry of the isolated double wedge having external wedge angles of $n\pi$ at Q_1 and $m\pi$ at Q_2 is shown in figure 6.1. In this chapter only the interactions between the edges at Q_1 and Q_2 will be considered since the outer faces do not intersect. This restriction will be removed in chapter VII. The resulting solution will therefore be directly applicable to geometries such as the thick impedance half plane and impedance insert. Up to triple diffraction mechanisms will be included in the solution, and it will be seen that these are sufficient to accurately evaluate the scattering by double wedges having a common face of width as small as $\frac{\lambda}{8}$. The primary diffraction mechanism was presented in chapter V.

Throughout our analysis Q_1 will be our phase reference point and all local angles will be measured with respect to the common ("o") wedge face. In addition, η_0, η_1 and η_2 will denote the normalized impedances of the common face, the outer ("n") face at Q_1 and the outer ("n") face at Q_2 respectively.

Prior work in this area has been for the case of a perfectly conducting double wedge configuration which included only the primary and doubly diffracted mechanisms [26]. In this chapter we will present uniform diffraction coefficients up to and including third order mechanisms associated with the impedance double wedge and in which the contribution of the surface waves are rigorously included. The coefficients for the double and triple

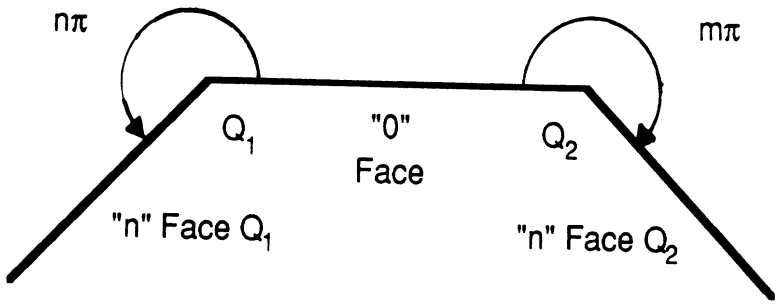

Figure 6.1 -- Isolated double wedge geometry

diffraction mechanisms are derived by using the Extended Spectral Ray Method and thus remain valid even when one edge lies in the transition region of another. This method was described in chapter III. Of particular importance in this derivation is the use of (5.43b) for the purpose of simplifying the Maclaurin series expansion associated with the modified Pauli-Clemmow steepest descent asymptotic evaluation of the integrals similar to the procedure in chapter IV. Without these, the evaluation of the derivatives of rather complex functions would be required.

Some calculations for the scattering by thick perfectly conducting and impedance half planes have recently appeared in the literature [27,28], and are therefore of interest for the purpose of verifying our solution.

Most other high frequency techniques become extremely unmanageable beyond the triple diffraction mechanism; therefore, we conclude this chapter with the derivation of the quadruple diffraction ray mechanism in order to demonstrate the versatility and relative ease to extend our high frequency solution via use of the ESRM.

Double Diffraction Mechanism

Starting with the geometry in figure 6.2, we will explicitly derive the bistatic second order mechanism from Q_1 to Q_2 via the ESRM. The integrand of (5.38) may be considered as an infinite sum of complex plane waves which are launched from Q_1 at an angle $-\alpha$. A simple geometrical argument now shows that plane waves forming a local angle $-\alpha$ at Q_1 will form a local angle α at Q_2 as demonstrated in figure 6.2. Thus, the complex plane wave launched from Q_1 at an angle $-\alpha$ will be incident at Q_2 at an angle α. Clearly, the diffracted field from Q_2 due to a plane wave incident at an angle α and diffracting at an angle ϕ_2 is (see (5.43b))

$$u_2^d(\alpha,\phi_2) = \frac{1}{2\pi m}\sqrt{\frac{2\pi}{k\rho}}e^{-jk\rho}e^{j\frac{3\pi}{4}}e^{-jkw\cos\alpha}\sin\frac{\alpha}{m}\frac{\Psi(-\alpha+\frac{m\pi}{2}+\pi)}{\Psi(\frac{m\pi}{2}-\phi_2)}$$
$$\cdot\left\{\frac{1}{\cos(\frac{\pi-\phi_2}{m})-\cos(\frac{\alpha}{m})}-\frac{1}{\cos(\frac{\pi+\phi_2}{m})-\cos(\frac{\alpha}{m})}+\frac{\sin(\frac{\phi_2}{m})C_{om}(-\alpha)}{\cos(\frac{\pi+\alpha}{m})-\cos(\frac{\phi_2}{m})}\right\} \tag{6.1}$$

after invoking reciprocity and when its phase is referenced to Q_1. In this case w is the width of the common wedge face.

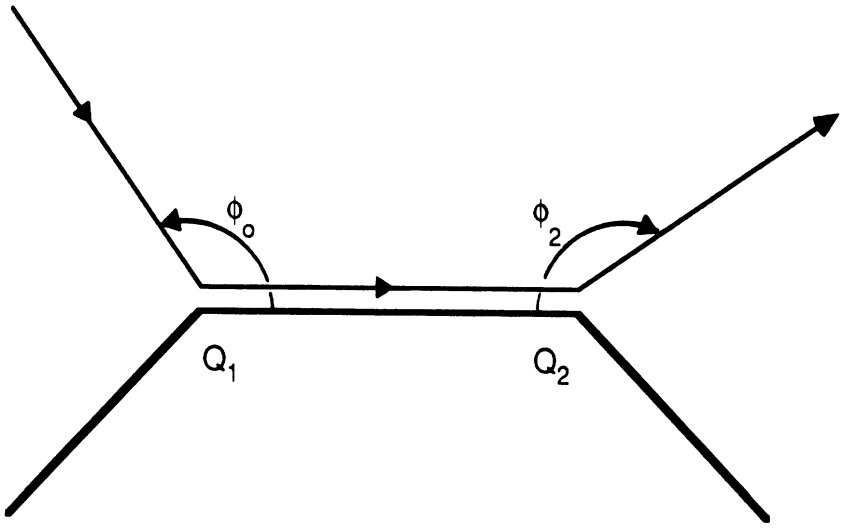

Figure 6.2 – Double diffraction mechanism from an isolated double wedge structure

In accordance with the above argument, the basic integral representing the far zone doubly diffracted field from Q_1 to Q_2 is obtained by multiplying the integrand of (5.38) by (6.1) to give

$$u_{21}^{d}(\phi_2,\phi_o) = \frac{-1}{4\pi^2 mn}\sqrt{\frac{2\pi}{k\rho}}\,e^{-jk\rho}e^{j\frac{\pi}{4}}\frac{1}{\Psi(\frac{n\pi}{2}-\phi_o)\Psi(\frac{m\pi}{2}-\phi_2)}$$
$$\cdot\int_{S(0)} e^{-jkw\cos\alpha}\sin(\frac{\alpha}{n})\sin(\frac{\alpha}{m})\Psi(\alpha+\frac{n\pi}{2}+\pi)\Psi(-\alpha+\frac{m\pi}{2}+\pi)$$
$$\cdot\left\{\frac{1}{\cos(\frac{\pi+\phi_o}{n})-\cos(\frac{\alpha}{n})}-\frac{1}{\cos(\frac{\pi-\phi_o}{n})-\cos(\frac{\alpha}{n})}-\frac{\sin(\frac{\phi_o}{n})C_{on}(\alpha)}{\cos(\frac{\pi-\alpha}{n})-\cos(\frac{\phi_o}{n})}\right\}$$
$$\cdot\left\{\frac{1}{\cos(\frac{\pi-\phi_2}{m})-\cos(\frac{\alpha}{m})}-\frac{1}{\cos(\frac{\pi+\phi_2}{m})-\cos(\frac{\alpha}{m})}+\frac{\sin(\frac{\phi_2}{m})C_{om}(-\alpha)}{\cos(\frac{\pi+\alpha}{m})-\cos(\frac{\phi_2}{m})}\right\}d\alpha. \tag{6.2}$$

The first term of the asymptotic expansion of this integral about the saddle point is zero. Therefore, we must employ a higher order expansion to obtain a non-zero approximation of the integral. As a result, higher order integrand derivatives must be computed. Such a computation is rather simple for the integrand in (6.2) because of the appearance of the product of sines. Clearly, this is the primary reason for preferring (5.38) and (5.43b) over (5.35) and (5.43a).

Equation (6.2) is in a form suitable for a uniform evaluation via the modified Pauli-Clemmow approach. It is further of importance to note that such an evaluation must account for the presence of the geometrical optics poles as well as the surface wave pole(s). Details of the evaluation are similar to those for the case of the resistive strip given in Appendix C. We find that the doubly diffracted field from Q_1 to Q_2 is

$$u_{21}^{d}(\phi_2,\phi_o) = \frac{-j}{\pi k(mn)^2}\frac{e^{-jkw}}{\sqrt{w}}\frac{e^{-jk\rho}}{\sqrt{\rho}}\frac{\Psi(\frac{n\pi}{2}+\pi)\Psi(\frac{m\pi}{2}+\pi)}{\Psi(\frac{n\pi}{2}-\phi_o)\Psi(\frac{m\pi}{2}-\phi_2)}$$
$$\cdot a_1a_2a_3[A\{1-F_{KP}(kwa_1)\}+B\{1-F_{KP}(kwa_2)\}+C\{1-F_{KP}(kwa_3)\}]$$
$$\cdot\left\{\frac{1}{1-\cos(\frac{\pi-\phi_o}{n})}-\frac{1}{1-\cos(\frac{\pi+\phi_o}{n})}-\frac{\sin(\frac{\phi_o}{n})C_{on}(0)}{\cos(\frac{\pi}{n})-\cos(\frac{\phi_o}{n})}\right\}$$
$$\cdot\left\{\frac{1}{1-\cos(\frac{\pi+\phi_2}{m})}-\frac{1}{1-\cos(\frac{\pi-\phi_2}{m})}+\frac{\sin(\frac{\phi_2}{m})C_{om}(0)}{\cos(\frac{\pi}{m})-\cos(\frac{\phi_2}{m})}\right\}\frac{e^{-jkr}}{2} \tag{6.3}$$

where

$$a_1 = 2\cos^2\frac{\phi_o}{2} \tag{6.4}$$

$$a_2 = 2\cos^2\frac{\phi_2}{2} \tag{6.5}$$

$$a_3 = 2\sin^2\frac{\theta}{2} \qquad (\theta \text{ of common face}) \tag{6.6}$$

$$A = \frac{-1}{(a_2 - a_1)(a_3 - a_1)} \tag{6.7}$$

$$B = \frac{-1}{(a_1 - a_2)(a_3 - a_2)} \tag{6.8}$$

$$C = \frac{-1}{(a_1 - a_3)(a_2 - a_3)} \tag{6.9}$$

where F_{KP} is the UTD transition function discussed in chapter II. By using the Clemmow identity (2.18) in u_{21}^d we can automatically account for the contribution of the surface wave fields in the formulation. Furthermore, in (6.3) $r = -w\cos\phi$ and a factor of one half was also included to account for grazing on the common wedge face.

Equation (6.3) represents the coefficient for the doubly diffracted field when the incident wave impinges first upon Q_1 and then diffracts to Q_2. If we were concerned with the reciprocal diffraction mechanism from Q_2 to Q_1, (6.3) is still valid provided the following substitutions are made : $r \rightarrow -w\cos\phi_o$, $\phi_o \rightarrow \pi - \phi_o$, $\phi_2 \rightarrow \pi - \phi_2$, $m \rightarrow n$, and $n \rightarrow m$.

Triple Diffraction Mechanism (two vertices)

The ray geometry of the triple diffraction mechanisms to be considered in this section is shown in figure 6.3.

In accordance with ESRM, an integral representation for the triply diffracted field from Q_1 to Q_2 and back to Q_1 is

$$u_{121}^d(\phi,\phi_o) = \frac{j}{2\pi n}\int_{S(0)} e^{-jkw\cos\alpha}\sin(\frac{\alpha}{n})u_{21}^d(\alpha,\phi_o)\frac{\Psi(\alpha+\frac{n\pi}{2}+\pi)}{\Psi(\frac{n\pi}{2}-\phi)}$$
$$\cdot\left\{\frac{1}{\cos(\frac{\pi+\phi}{n})-\cos(\frac{\alpha}{n})} - \frac{1}{\cos(\frac{\pi-\phi}{n})-\cos(\frac{\alpha}{n})} - \frac{\sin(\frac{\phi}{n})C_{on}(\alpha)}{\cos(\frac{\pi-\alpha}{n})-\cos(\frac{\phi}{n})}\right\}d\alpha \tag{6.10}$$

where $u_{21}^d(\alpha,\phi_o)$ is the doubly diffracted field incident at Q_1 and is given in (6.3) with $\rho = w$. We also note that in deriving (6.10), reciprocity was invoked for the final diffraction at Q_1 toward the far zone point. Therefore, the integrand of (6.10) can again be interpreted as

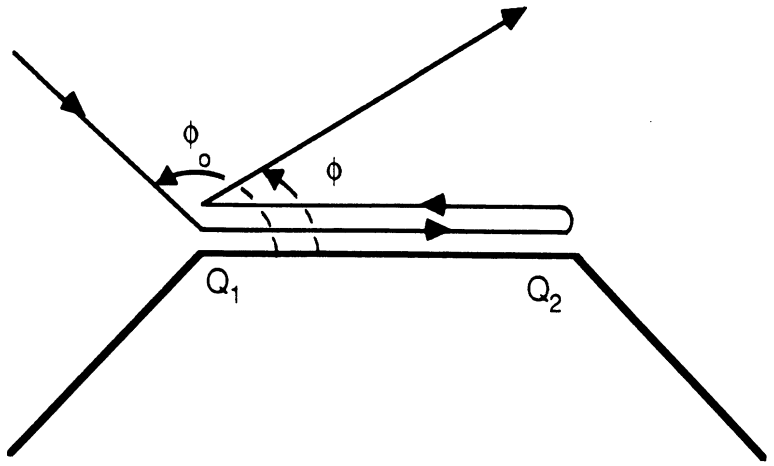

Figure 6.3 — Triple diffraction mechanism from an isolated double wedge structure at Q_1

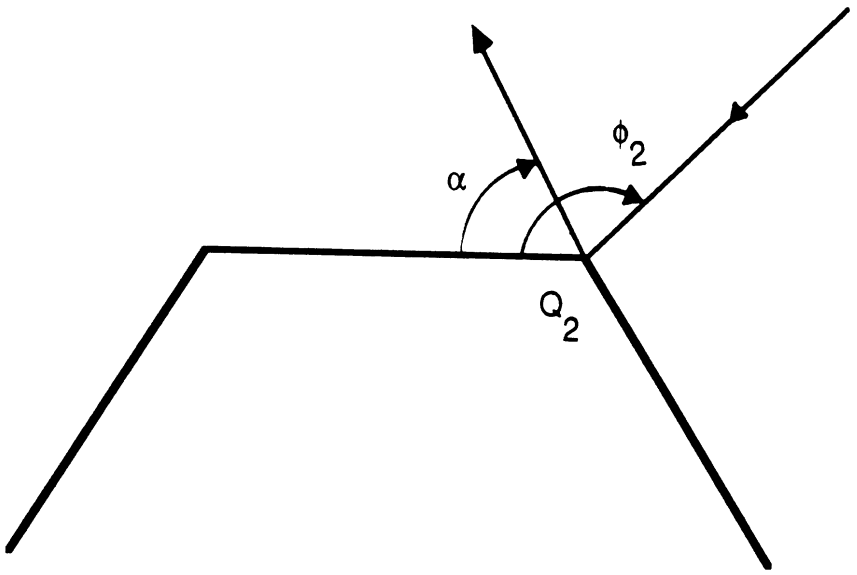

Figure 6.4 — Spectral plane wave with angle $-\alpha$ at Q_1 has an angle α at Q_2

an infinite sum of complex plane waves incident (diffracted) at Q_1 making a local angle of $-\alpha$ with the common face and diffracted (incident) at a local angle ϕ. We note that this choice of $\pm\alpha$ is consistent with our geometrical interpretation illustrated in figure 6.4.

Replacing u_{21}^d in (6.10) by (6.3) (without the 0.5 grazing factor) gives

$$\begin{aligned} u_{121}^d(\phi,\phi_o) =& \Delta \int_{S(0)} e^{-jkw\cos\alpha} \sin(\frac{\alpha}{n}) \sin(\frac{\alpha}{m}) \frac{\Psi(\alpha+\frac{n\pi}{2}+\pi)}{\Psi(\frac{m\pi}{2}-\alpha)} \\ & \cdot \left\{ \frac{-2\sin\frac{\pi}{m}}{[1-\cos(\frac{\pi+\alpha}{m})][1-\cos(\frac{\pi-\alpha}{m})]} + \frac{C_{om}(0)}{\cos(\frac{\pi}{m})-\cos(\frac{\alpha}{m})} \right\} \\ & \cdot \left\{ \frac{1}{\cos(\frac{\pi+\phi}{n})-\cos(\frac{\alpha}{n})} - \frac{1}{\cos(\frac{\pi-\phi}{n})-\cos(\frac{\alpha}{n})} - \frac{\sin(\frac{\phi}{n})C_{on}(\alpha)}{\cos(\frac{\pi-\alpha}{n})-\cos(\frac{\phi}{n})} \right\} \\ & \cdot a_2[A\{1-F_{KP}(kwa_1)\} + B\{1-F_{KP}(kwa_2)\} + C\{1-F_{KP}(kwa_3)\}]d\alpha \end{aligned} \tag{6.11}$$

where

$$\begin{aligned} \Delta =& \frac{e^{-jkw}e^{-jk\rho}}{2\pi^2 k(mn)^2 n\sqrt{w\rho}} \frac{\Psi(\frac{n\pi}{2}+\pi)\Psi(\frac{m\pi}{2}+\pi)}{\Psi(\frac{n\pi}{2}-\phi_o)\Psi(\frac{n\pi}{2}-\phi)} a_1 a_3 \\ & \cdot \left\{ \frac{1}{1-\cos(\frac{\pi-\phi_o}{n})} - \frac{1}{1-\cos(\frac{\pi+\phi_o}{n})} - \frac{\sin(\frac{\phi_o}{n})C_{on}(0)}{\cos(\frac{\pi}{n})-\cos(\frac{\phi_o}{n})} \right\}. \end{aligned} \tag{6.12}$$

Equation (6.11) must now be uniformly evaluated via the modified Pauli-Clemmow method of steepest descents while accounting for the presence of the surface wave and geometrical optics poles. The details of this procedure are similar to those of the resistive strip given in Appendix D and the result is

$$\begin{aligned} u_{121}^d(\phi,\phi_o) =& \frac{j2\sqrt{2}e^{-j2kw}e^{j\frac{3\pi}{4}}}{(k\pi)^{\frac{3}{2}}w(nm)^3 n} \frac{e^{-jk\rho}}{\sqrt{\rho}} \frac{\Psi^2(\frac{n\pi}{2}+\pi)\Psi(\frac{m\pi}{2}+\pi)}{\Psi(\frac{n\pi}{2}-\phi_o)\Psi(\frac{n\pi}{2}-\phi)\Psi(\frac{m\pi}{2})} \\ & \cdot \frac{a_1 a_3^2 a_4}{a_3-a_4}[A\{1-F_{KP}(kwa_1)\} + B\{1-F_{KP}(kwa_2)\} + C\{1-F_{KP}(kwa_3)\}] \\ & \cdot [F_{KP}(kwa_3) - F_{KP}(kwa_4)] \cdot \frac{e^{-jkr}}{4} \\ & \cdot \left\{ \frac{1}{1-\cos(\frac{\pi-\phi_o}{n})} - \frac{1}{1-\cos(\frac{\pi+\phi_o}{n})} - \frac{\sin(\frac{\phi_o}{n})C_{on}(0)}{\cos(\frac{\pi}{n})-\cos(\frac{\phi_o}{n})} \right\} \\ & \cdot \left\{ \frac{1}{1-\cos(\frac{\pi-\phi}{n})} - \frac{1}{1-\cos(\frac{\pi+\phi}{n})} - \frac{\sin(\frac{\phi}{n})C_{on}(0)}{\cos(\frac{\pi}{n})-\cos(\frac{\phi}{n})} \right\} \\ & \cdot \left\{ \frac{-2\sin\frac{\pi}{m}}{[1-\cos(\frac{\pi}{m})]^2} - \frac{C_{om}(0)}{1-\cos(\frac{\pi}{m})} \right\}, \end{aligned} \tag{6.13}$$

where a factor of $\frac{1}{4}$ was included to account for grazing on the common wedge face and

$$a_4 = 2\cos^2(\frac{\phi}{2}).$$

Also the value of r is zero when referring to the case of triple diffraction emanating from Q_1, as discussed above.

When considering the contribution of the triply diffracted field emanating from Q_2 as shown in figure 6.5 , (6.13) is still valid provided the transformations $\phi_o \rightarrow \pi - \phi_o$, $\phi \rightarrow \pi - \phi$, $m \rightarrow n$, and $n \rightarrow m$ are made in addition to setting $r = -w[\cos\phi + \cos\phi_o]$.

General Double Wedge Applications

The thick half plane and the impedance insert in a full plane, shown in figures 6.6 and 6.7, are two examples of double wedge structures whose outer wedge faces do not intersect.

The thick impedance half plane is composed of a double wedge structure in which both wedges have an external angle of 1.5π.

Figures 6.8 and 6.9 present backscatter patterns for the thick perfectly conducting half plane for both E and H incidences, respectively. The thickness of the half plane is varied from 0.95λ down to 0.01λ and in all cases we find that the patterns are nearly identical to those presented in [27] where the Angular Spectrum Method (ASM) along with the Generalized Scattering Matrix Formulation (GSMF) was employed. We note that even for a thickness of 0.01λ the two approaches give nearly identical results and particularly for the H-incidence where the contribution of the multiply diffracted fields is significant. Bistatic patterns for the perfectly conducting thick half plane are shown in figures 6.10 and 6.11, again for both polarizations and a similar set of thicknesses as before. The agreement with the ASM-GSMF still holds remarkably well.

Figures 6.12 to 6.15 presents backscatter patterns from a thick impedance half plane with E-incidence for $\eta(= \eta_o = \eta_1 = \eta_2) = .25,\ 4,\ 2 + j2$ and $2 - j2$, respectively and for various thicknesses ranging from 0.01λ to 0.4λ. Again, all patterns corresponding to the first three impedances are in agreement with those computed via the ASM-GSMF [28] except for some differences corresponding to the case of $\eta = 0.25$. We remark that this discrepancy is probably due to the inherent approximation associated with the solution given in [28].

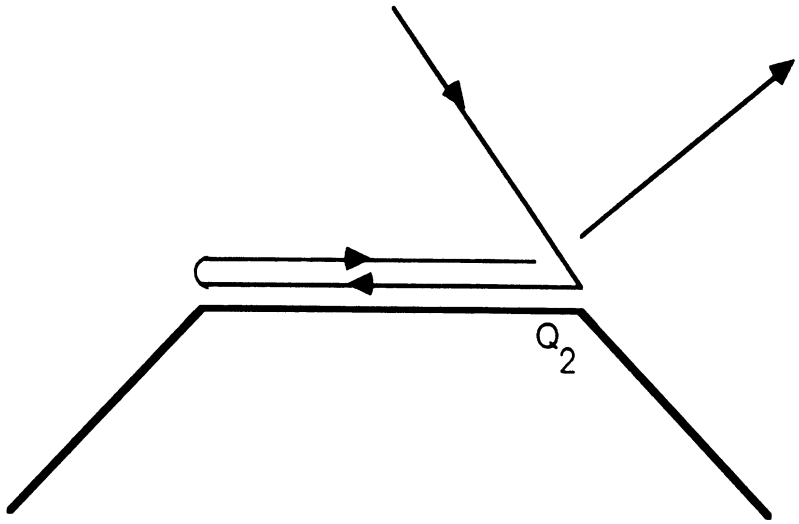

Figure 6.5 — Triple diffraction mechanism from an isolated double wedge structure at Q_2

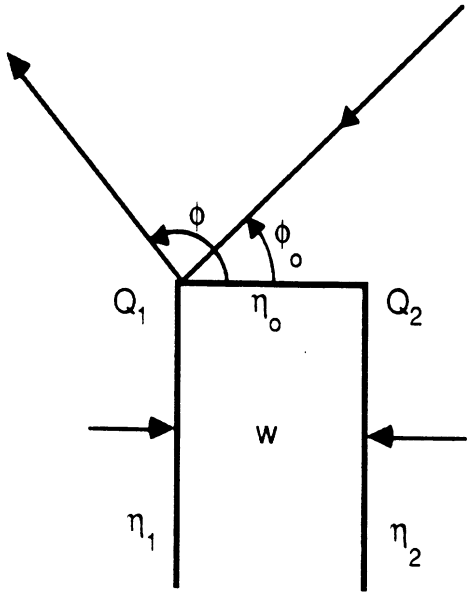

Figure 6.6 — Thick half plane geometry

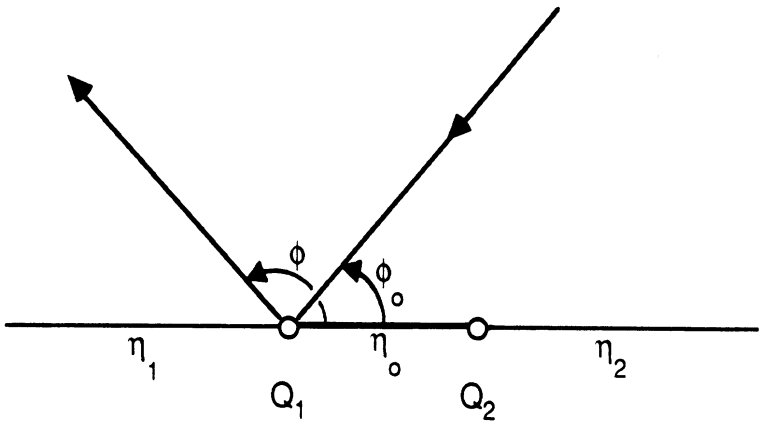

Figure 6.7 — Impedance insert in a full plane geometry

Finally, we note that although all face impedances in the above examples were kept the same, our formulation can certainly account for any arbitrary set of face impedances.

The impedance insert in a full plane is a special case of a double wedge configuration composed of two wedges each having external angles of $2\Phi = \pi$. Just like the thick half plane above, each face of the impedance insert configuration can be defined separately. However, for the examples to be presented, the outer sides of the insert will have equal impedance values. Figure 6.16 shows a bistatic pattern for an impedance insert in a ground plane with H-incidence. The impedance insert width was 1.6λ and the source was located just over the surface of the ground plane ($\phi_o = 1^o$). The normalized impedances of the insert were $-j.25, j.25$, and .25 and the results compare favorably with the moment method solution as well as a similar high frequency solution given in [35].

Figures 6.17 and 6.18 present the effects of varying the outer side impedances while holding the insert impedance constant ($\eta_o = 2 - j1$). In each case three E-incidence patterns are given corresponding to $\eta_1 = \eta_2 = 0.001$, 10, and 1000. We should note, of course, that the same patterns will correspond to H-incidence but with $\eta_1 = \eta_2 = 1000$, 0.1, and 0.001, respectively. The backscatter patterns shown for insert widths of 1λ and 0.5λ reveal that the surface wave interactions are noticeable at grazing aspects for the H-incidence particularly when the outer faces are perfectly conducting ($\eta_1 = \eta_2 = 0.001$). A similar observation also holds for the bistatic patterns given in figures 6.19 and 6.20 with incidence at 45^o.

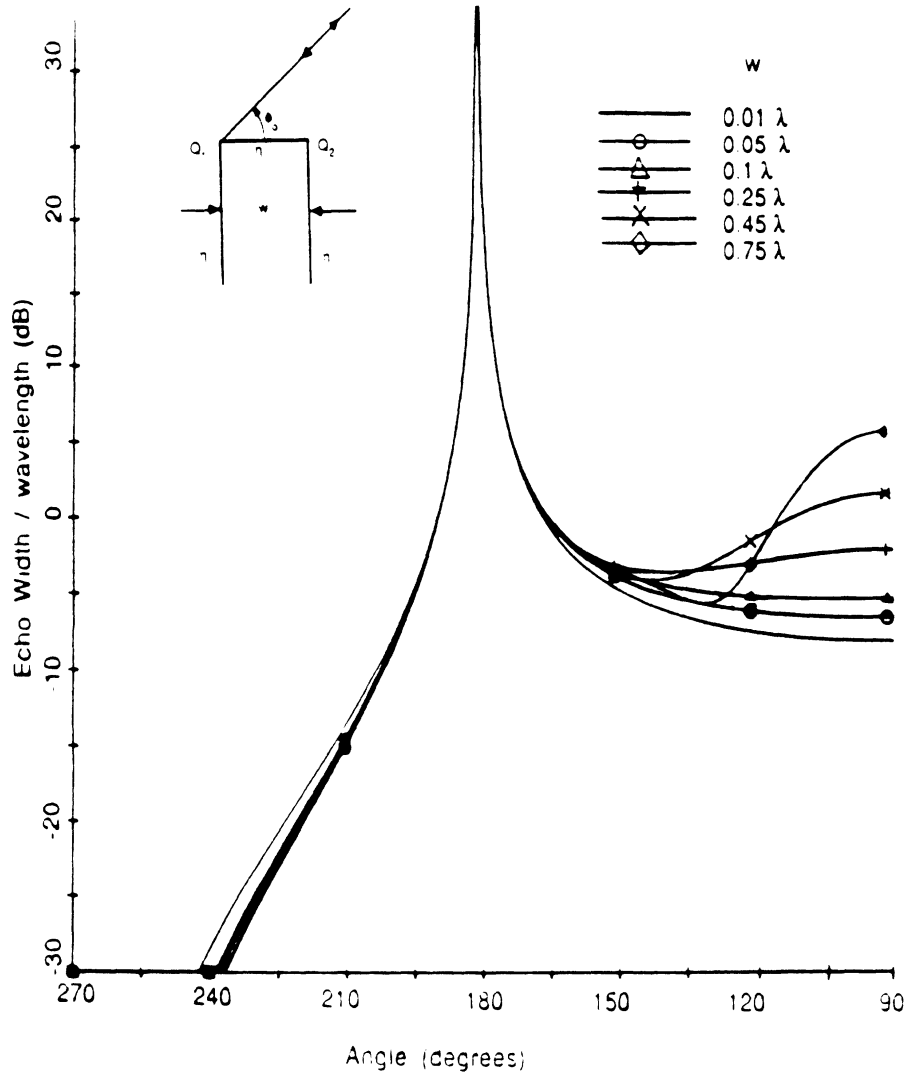

Figure 6.8 — Backscatter from a perfectly conducting thick half plane, E-polarization

Half plane widths are 0.01λ, 0.05λ 0.1λ, 0.25λ, 0.45λ and 0.75λ

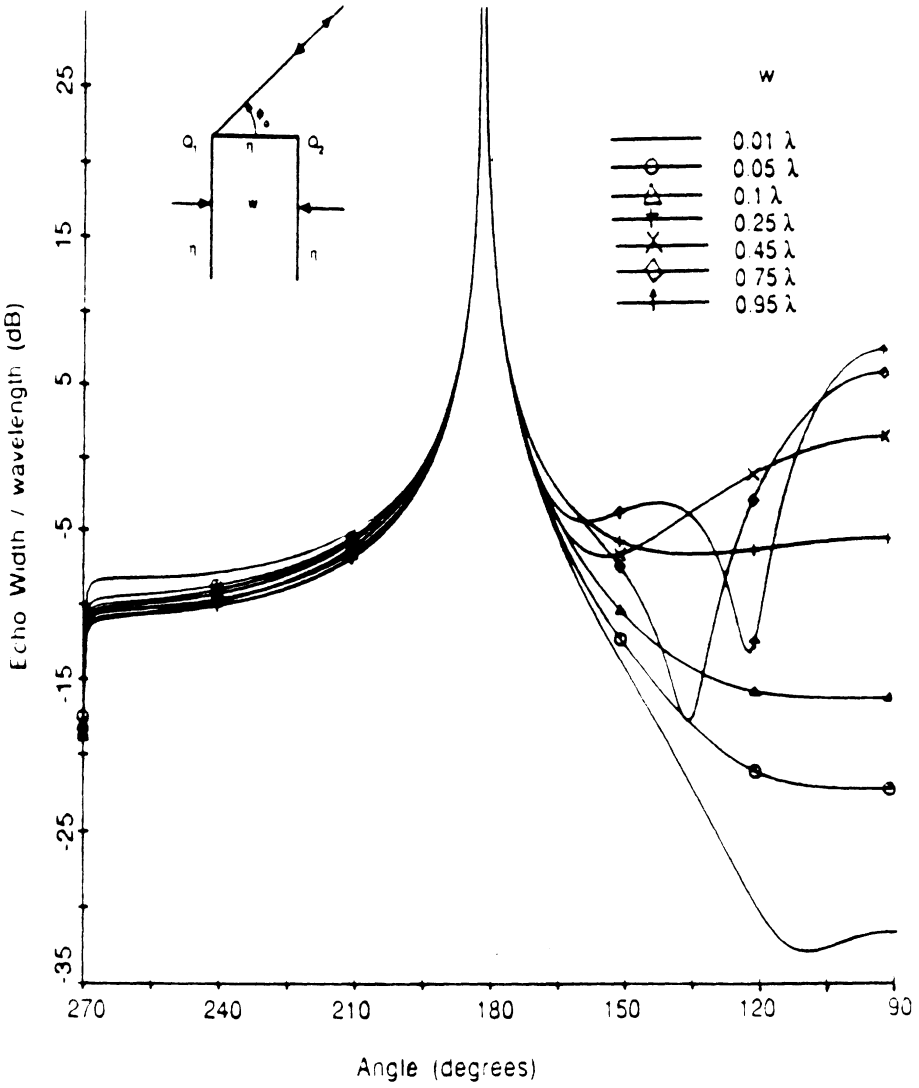

Figure 6.9 — Backscatter from a perfectly conducting thick half plane. H-polarization

Half plane widths are 0.01λ, 0.05λ 0.1λ, 0.25λ, 0.45λ, 0.75λ and 0.95λ

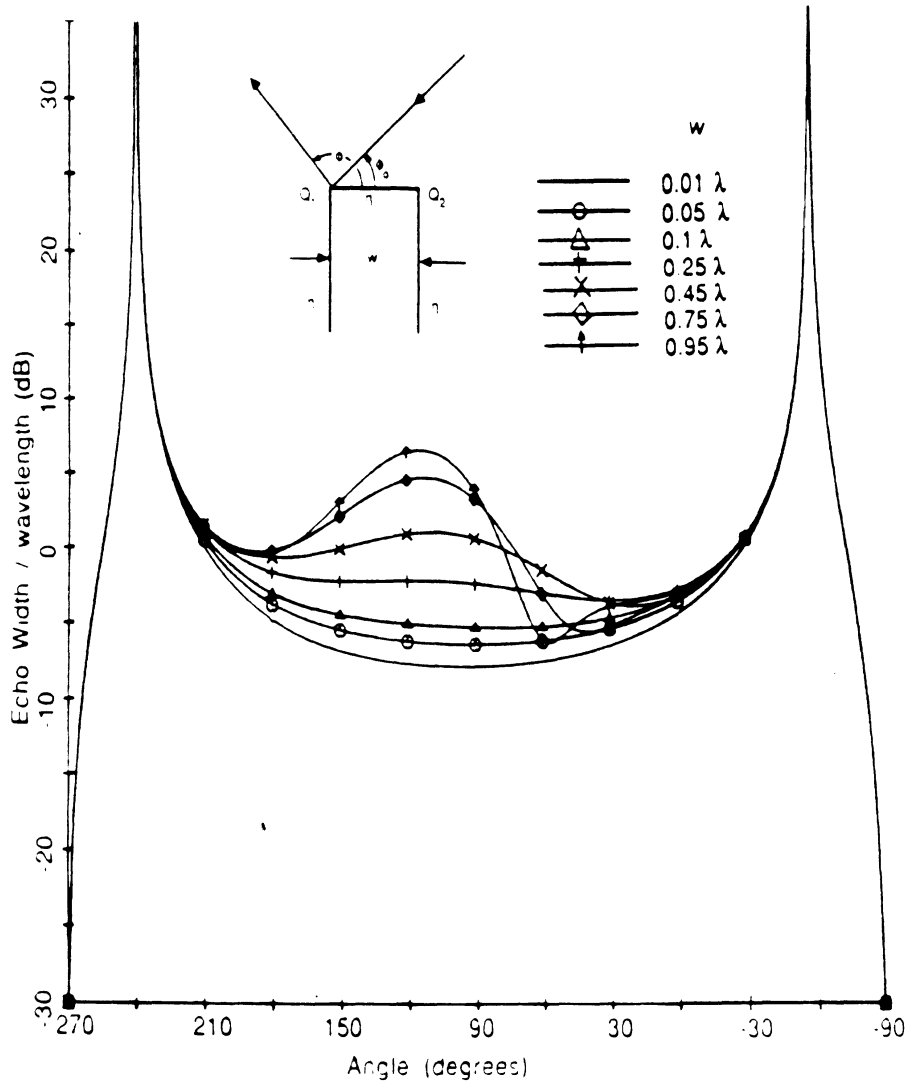

Figure 6.10 — Bistatic pattern from a perfectly conducting thick half plane. E-polarization. with an angle of incidence $\phi_0 = 60^\circ$

Half plane widths are 0.01λ, 0.05λ 0.25λ, 0.45λ, 0.75λ, and 0.95λ

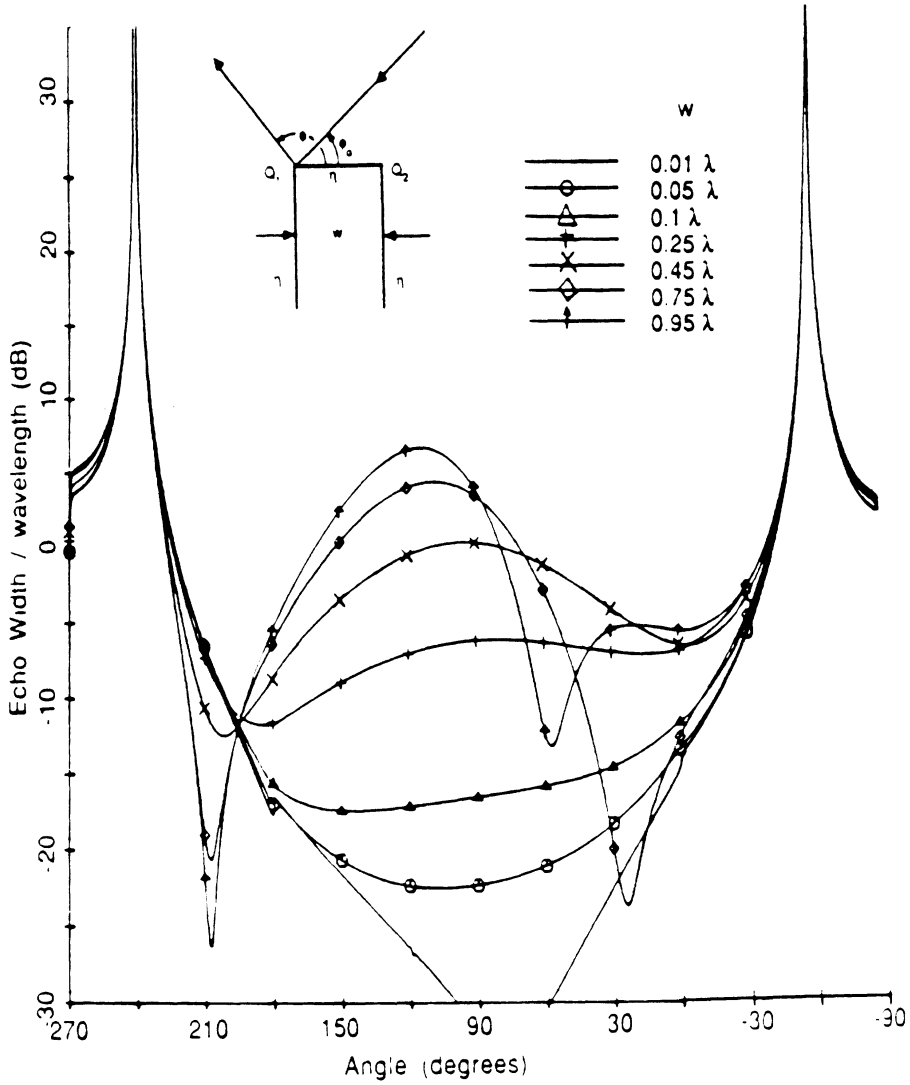

Figure 6.11 — Bistatic pattern from a perfectly conducting thick half plane. H-polarization, with an angle of incidence $\phi_i = 60°$

Half plane widths are 0.01λ, 0.05λ 0.25λ, 0.45λ, 0.75λ, and 0.95λ

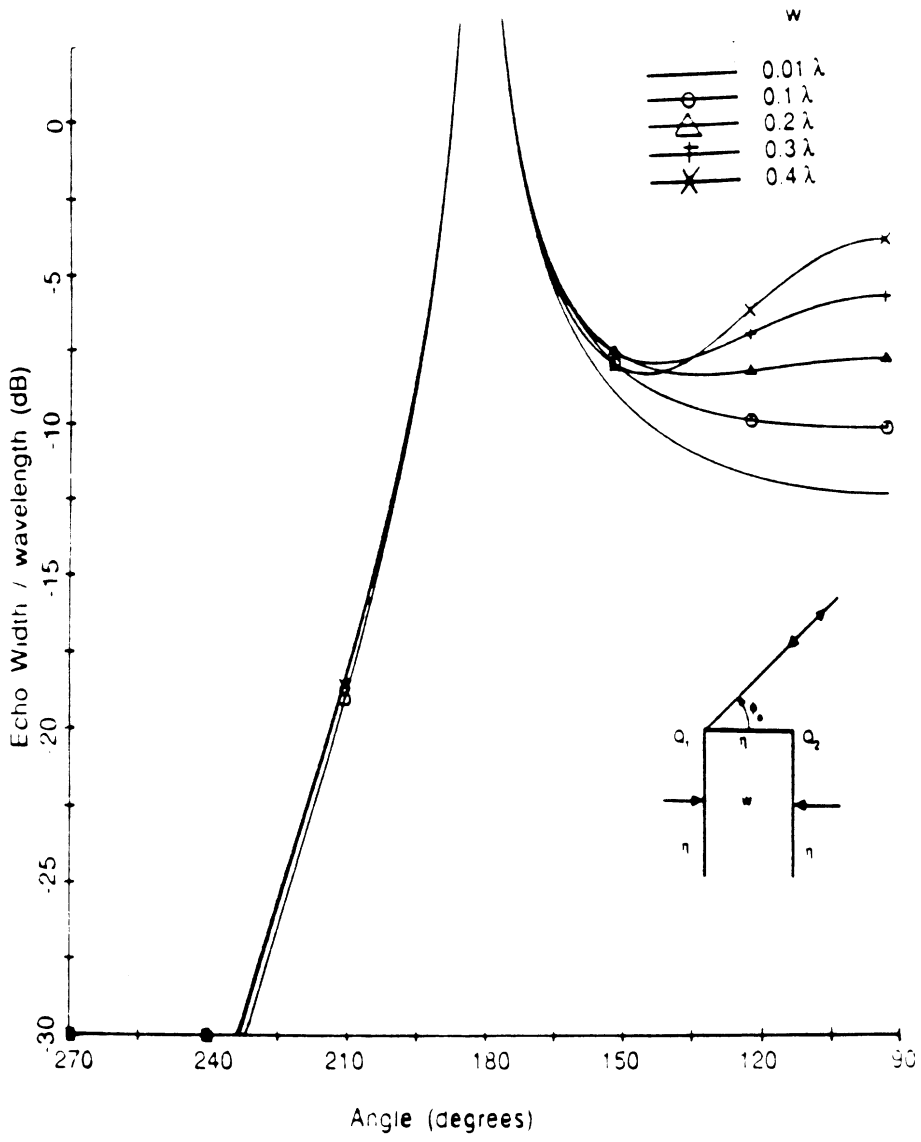

Figure 6.12 — Backscatter from a thick impedance half plane. E-polarization. with normalized impedance $\eta = 0.25$.

Half plane widths are 0.01λ, 0.1λ 0.2λ, 0.3λ, and 0.4λ

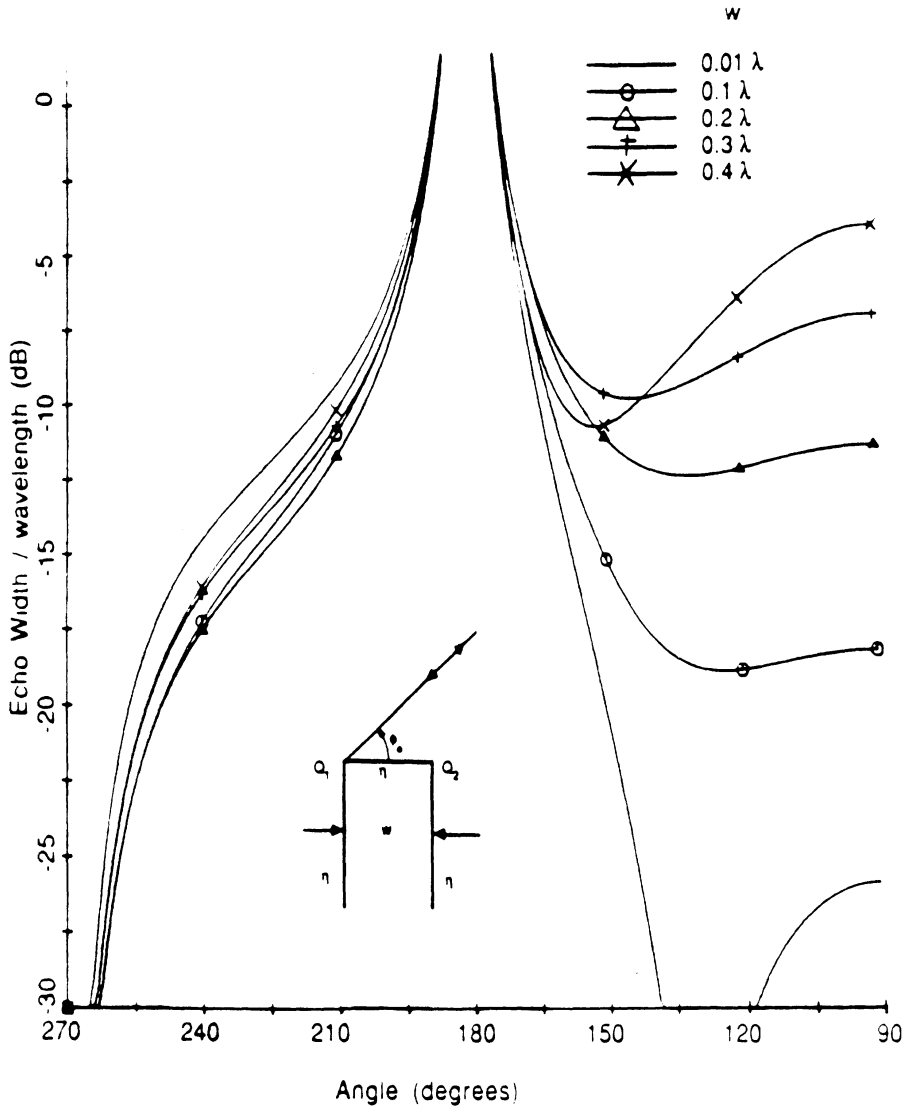

Figure 6.13 — Backscatter from a thick impedance half plane, E-polarization, with normalized impedance $\eta = 4$.

Half plane widths are 0.01λ, 0.1λ 0.2λ, 0.3λ, and 0.4λ

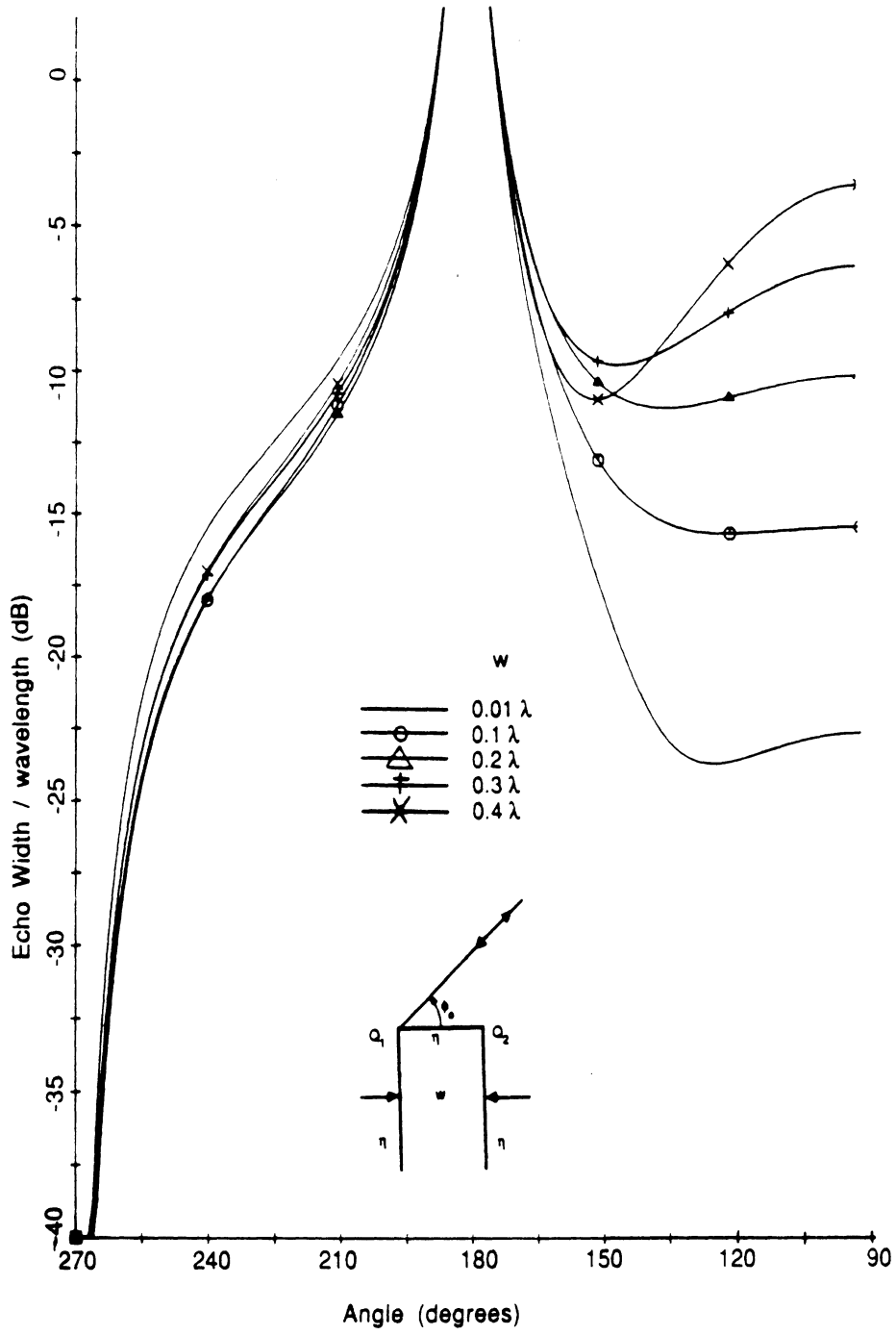

Figure 6.14 — Backscatter from a thick impedance half plane, E-polarization, with normalized impedance $\eta = 2 + j2$.

Half plane widths are 0.01λ, 0.1λ 0.2λ, 0.3λ, and 0.4λ

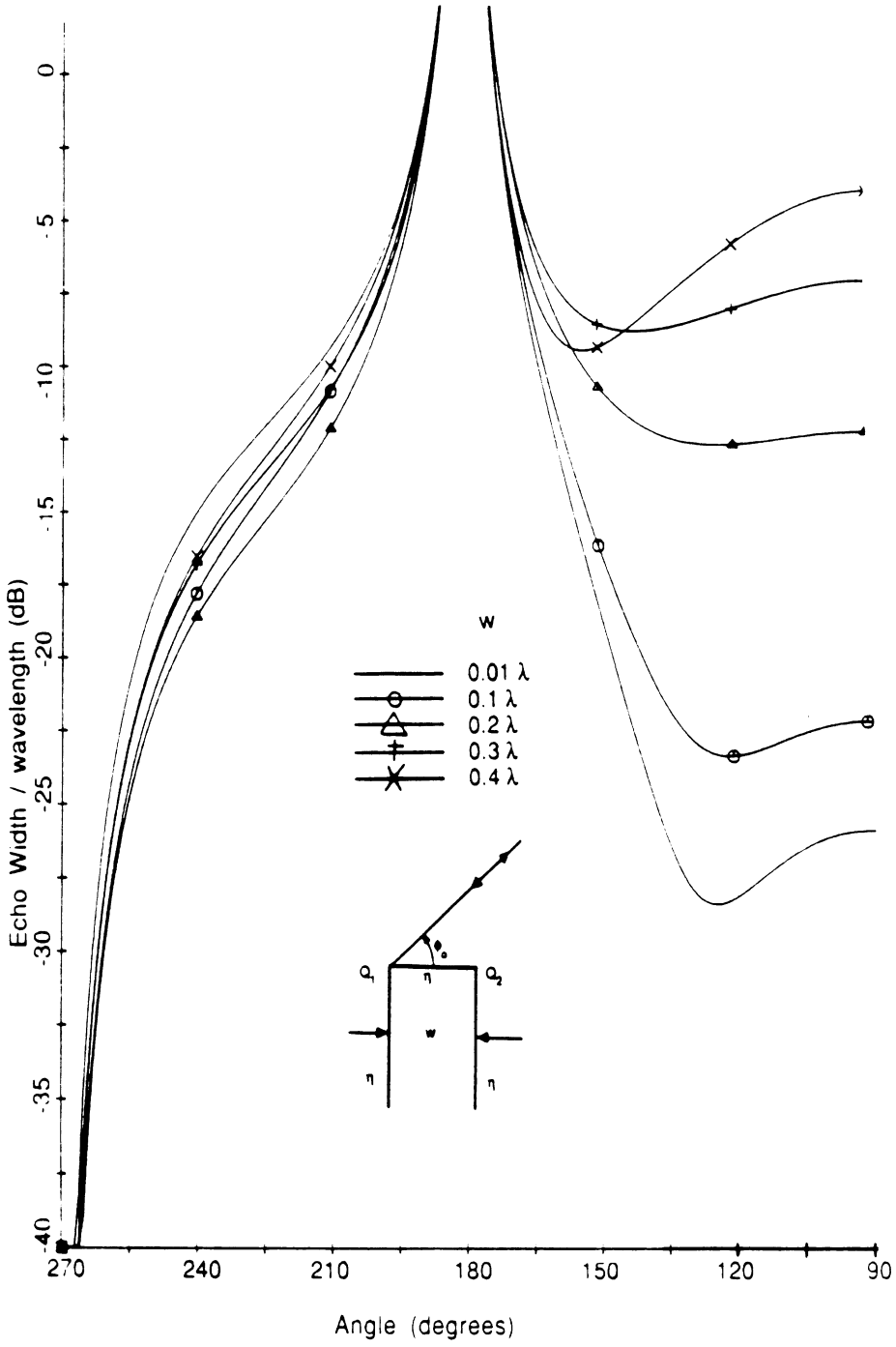

Figure 6.15 — Backscatter from a thick impedance half plane, E-polarization. with normalized impedance $\eta = 2 - j2$.

Half plane widths are 0.01λ, 0.1λ 0.2λ, 0.3λ, and 0.4λ

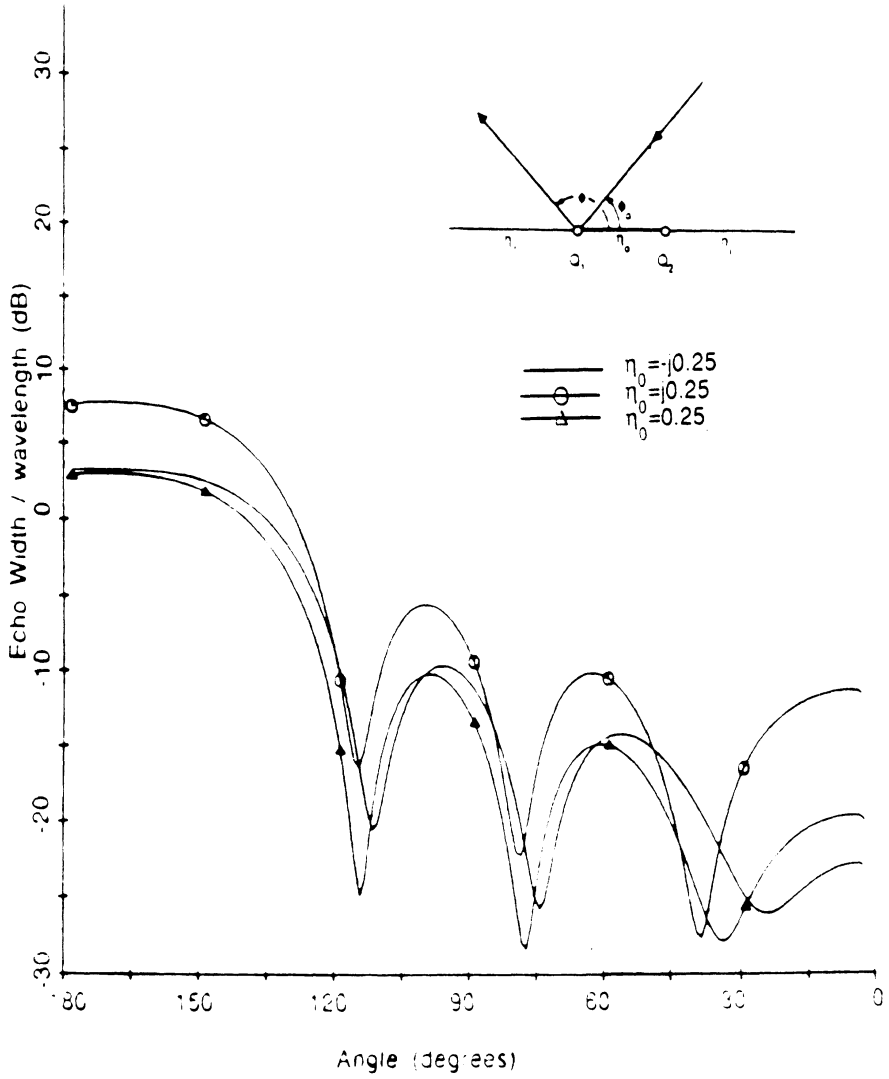

Figure 6.16 — Bistatic pattern from an impedance insert. H-polarization. with an angle of incidence $\theta_0 = 1°$.

The insert impedances are $\eta_0 = -j0.25$, $\eta_0 = j0.25$ and $\eta_0 = 0.25$.

The outer impedance is $\eta = 0$ and the width of the insert is 1.6λ

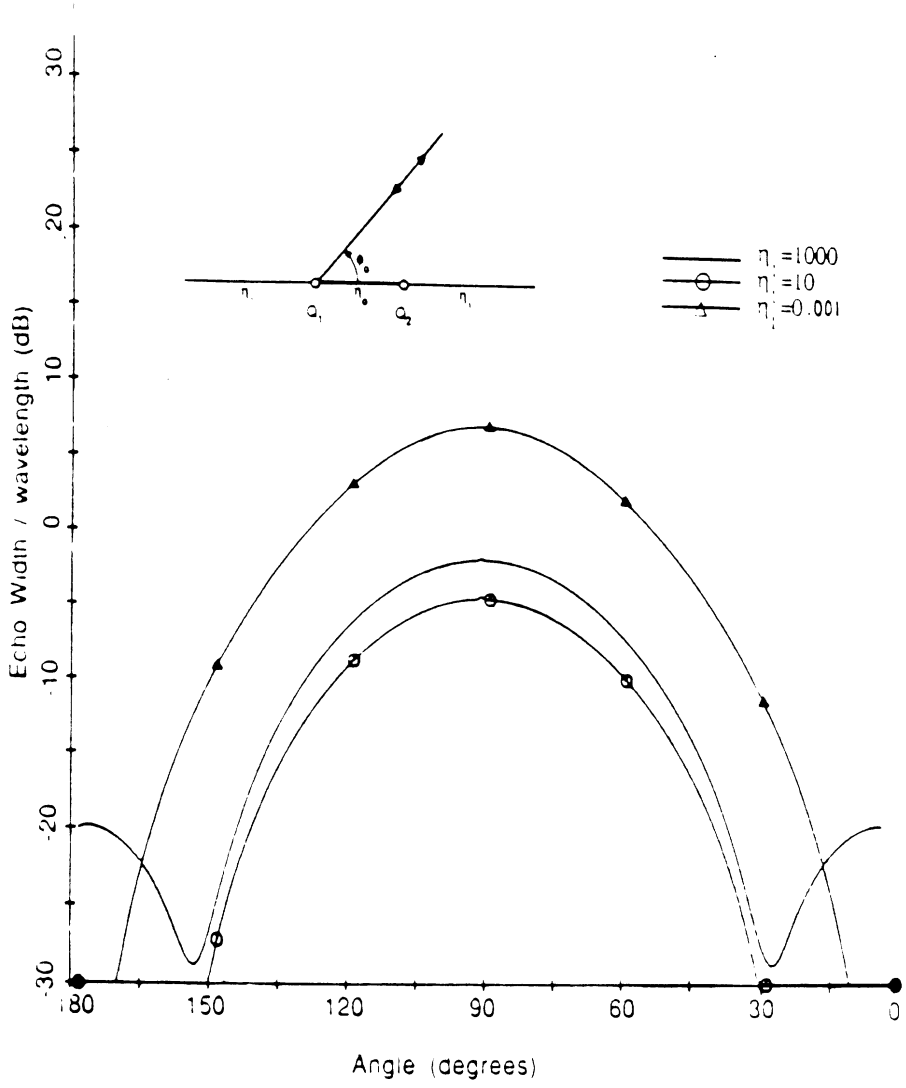

Figure 6.17 -- Backscatter from an impedance insert. E-pol. Insert Impedance is constant at $\eta_2 = 2 - j1$. Insert width is 0.5λ

The outer impedances are $\eta_1 = 1000$, $\eta_1 = 10$ and $\eta_1 = 0.001$.

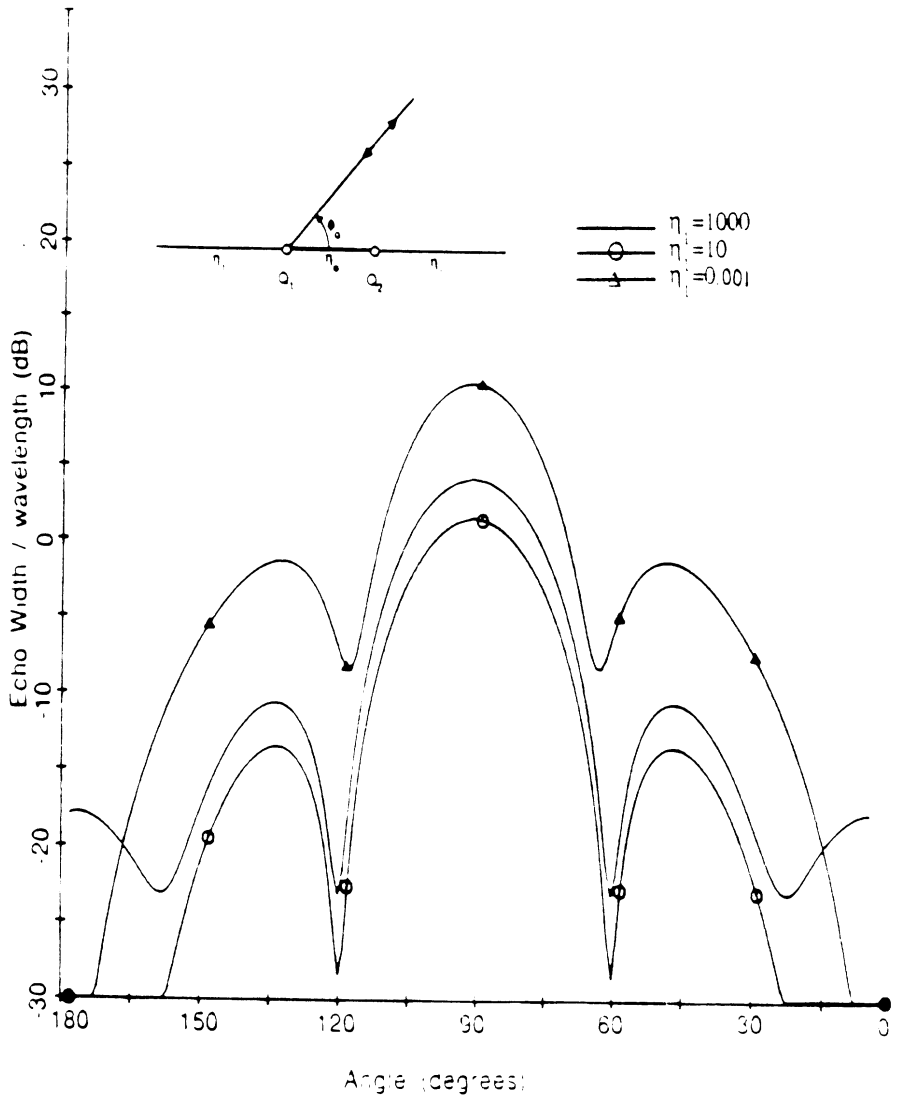

Figure 6.18 — Backscatter from an impedance insert. E-pol. Insert Impedance is constant at $\eta_2 = 2 - j1$. Insert width is 1λ

The outer impedances are $\eta_1 = 1000$, $\eta_1 = 10$ and $\eta_1 = 0.001$.

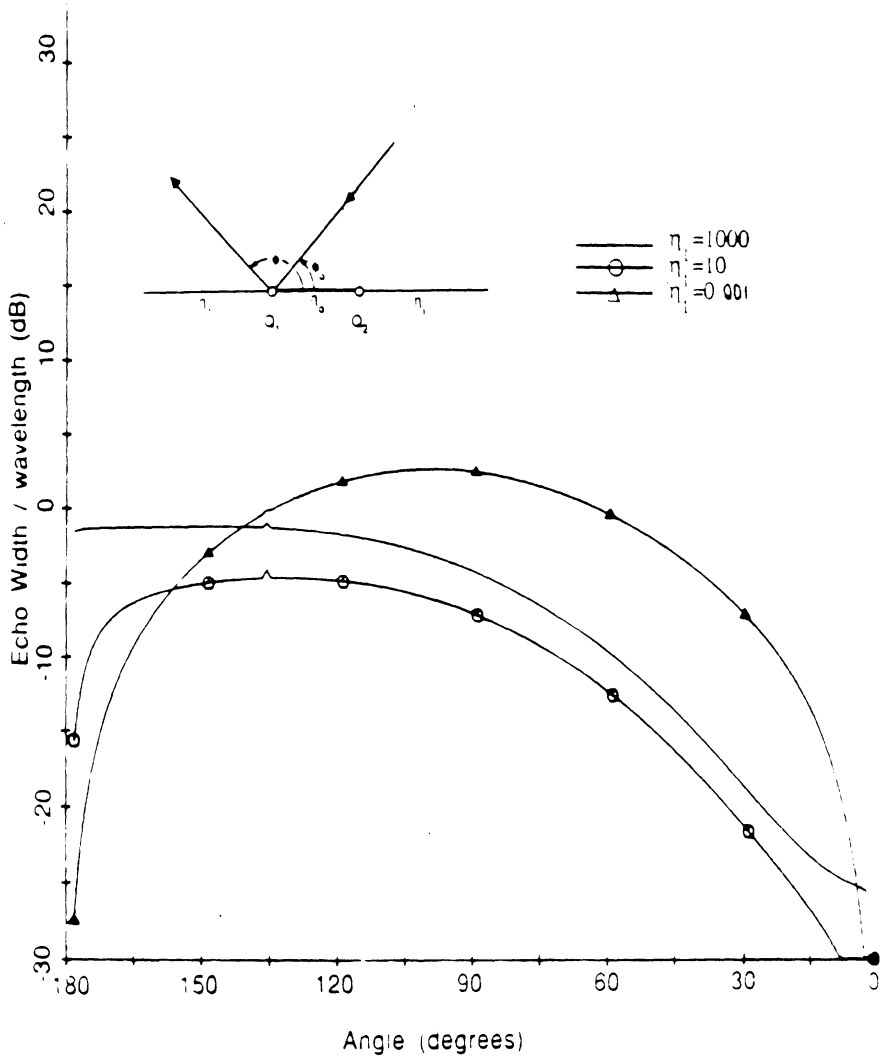

Figure 6.19 — Bistatic pattern from an impedance insert. E-pol. Insert Impedance is constant at $\eta_0 = 2 - j1$, $\phi_1 = 45°$. Insert width is 0.5λ.

The outer impedances are $\eta_1 = 1000$, $\eta_1 = 10$ and $\eta_1 = 0.001$.

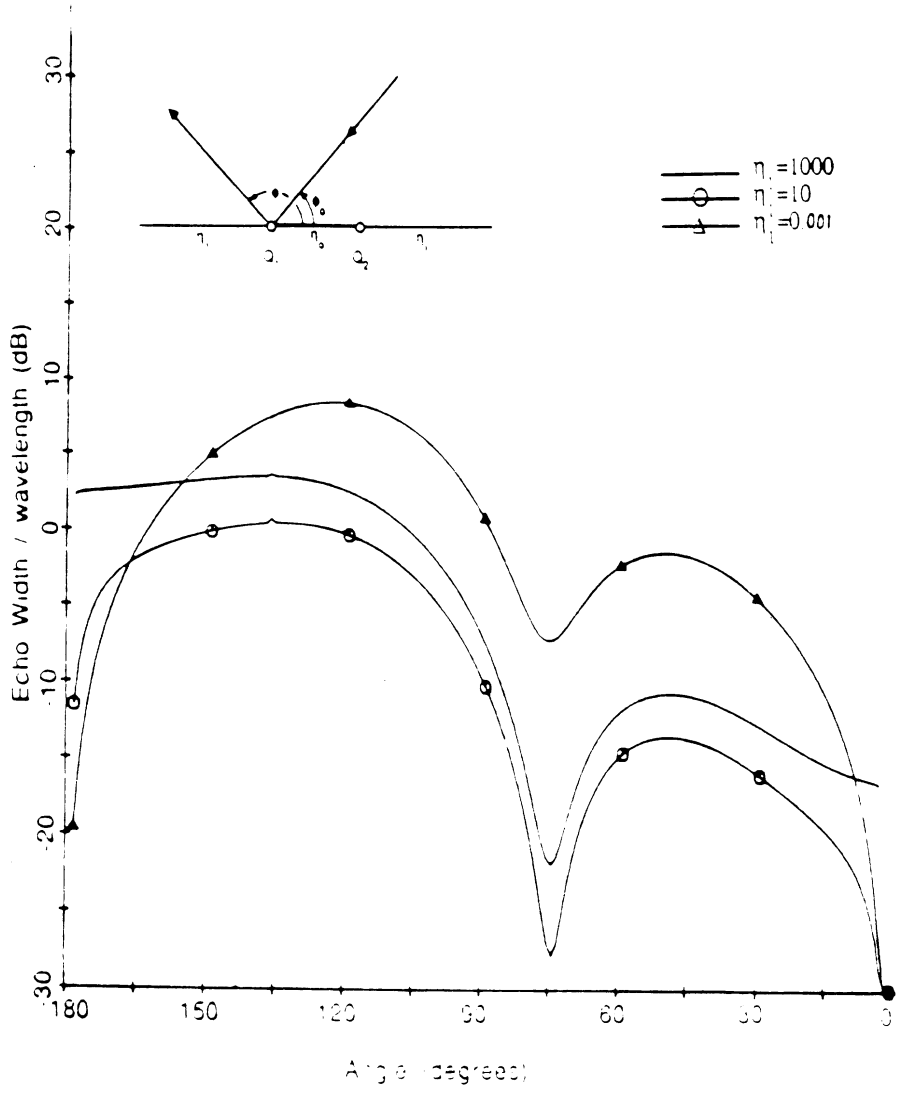

Figure 6.20 — Bistatic pattern from an impedance insert. E-pol. Insert Impedance is constant at $\eta_2 = 2 - j1$. $\alpha_2 = 45°$. Insert width is 1λ.

The outer impedances are $\eta_1 = 1000$, $\eta_1 = 10$ and $\eta_1 = 0.001$.

Using the approximate but simple formulas for the Maliuzhinets function given in chapter V, a final set of curves is presented next. These depict the scattering by the double wedge configuration in figure 6.1 as a function of the external wedge angles at Q_1 and Q_2. Particularly, figures 6.21 and 6.22 presents three backscatter curves corresponding to $n = m = 1.5$, 1.25 and 1. Results for both E and H (E incidence with inverse impedance) incidences are included where the common face impedance is $\eta_o = 0.5 - j0.25$ and the other outer face impedances are perfectly conducting. Bistatic curves for E and H incidences are given in figures 6.23 and 6.24 for a double wedge having a uniform impedance of $\eta = 0.25$. It is noted that the chosen incidence angle of $\phi_o = 1.3$ degrees is near grazing and therefore this situation corresponds to a more severe testing of the uniformity (and validity) of our results near the forward scattering region.

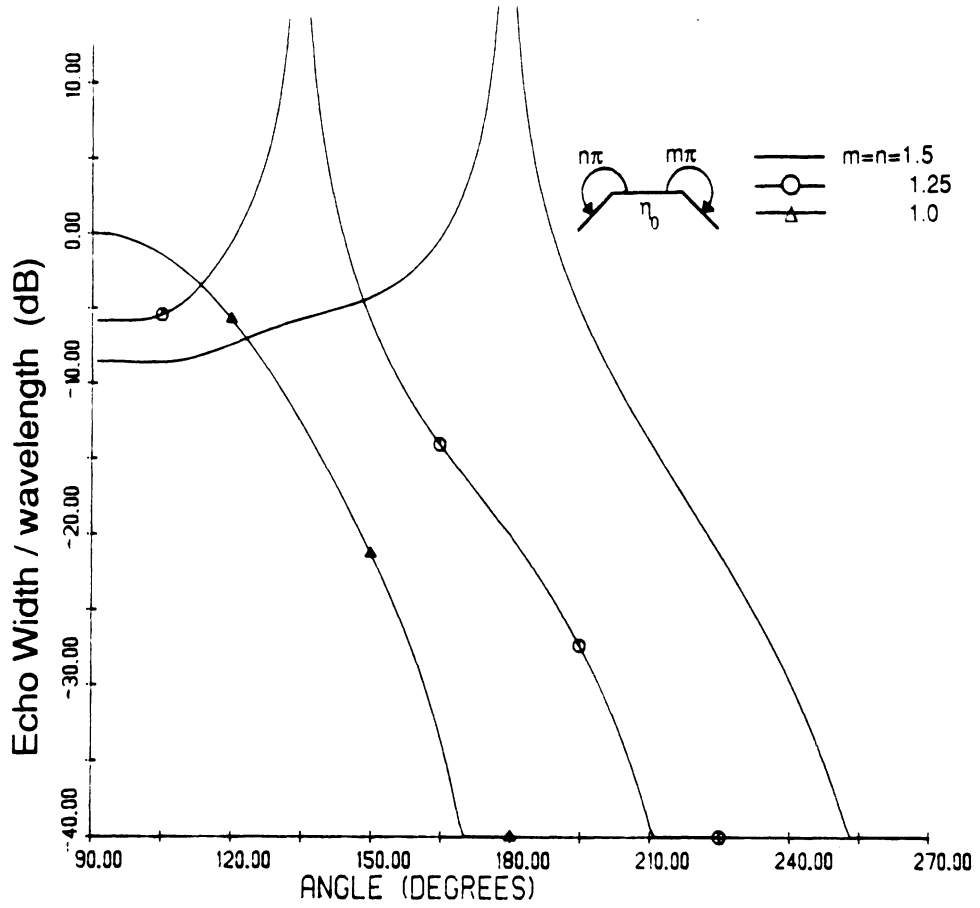

Figure 6.21 — Backscatter from an impedance double wedge with varying external angles ($m = n$). **E-polarization**

The common face has an impedance of $\eta_0 = 0.5 - j0.25$ and width of 0.5λ.

The outer face impedances are perfectly conducting.

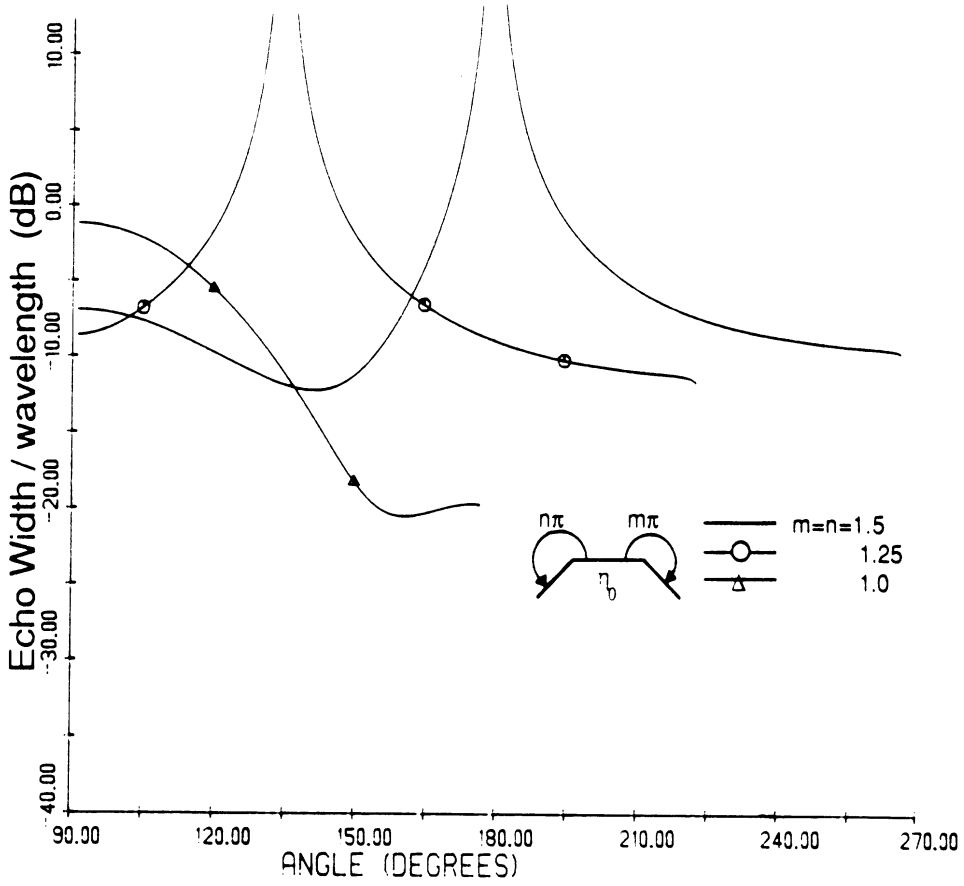

Figure 6.22 — Backscatter from an impedance double wedge with varying external angles ($m = n$). **H-polarization**

The common face has an impedance of $\eta_0 = 0.5 - j0.25$ and width of 0.5λ.

The outer face impedances are perfectly conducting.

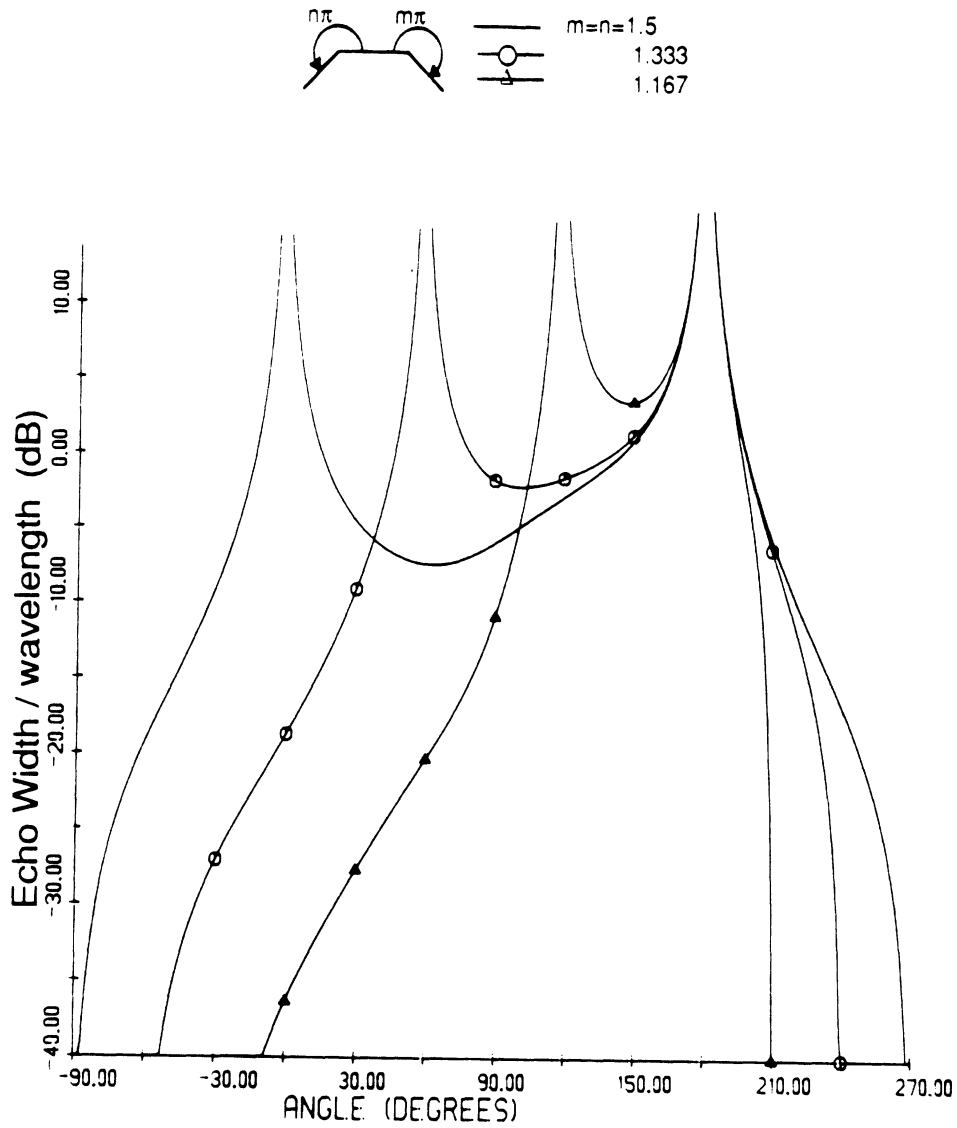

Figure 6.23 — Bistatic pattern from an impedance double wedge with varying external angles ($m = n$). **E-polarization.** $\sigma_e = 1.3$

All faces have an impedance of $\eta_e = 0.25$ and the common face has a width of 0.5λ.

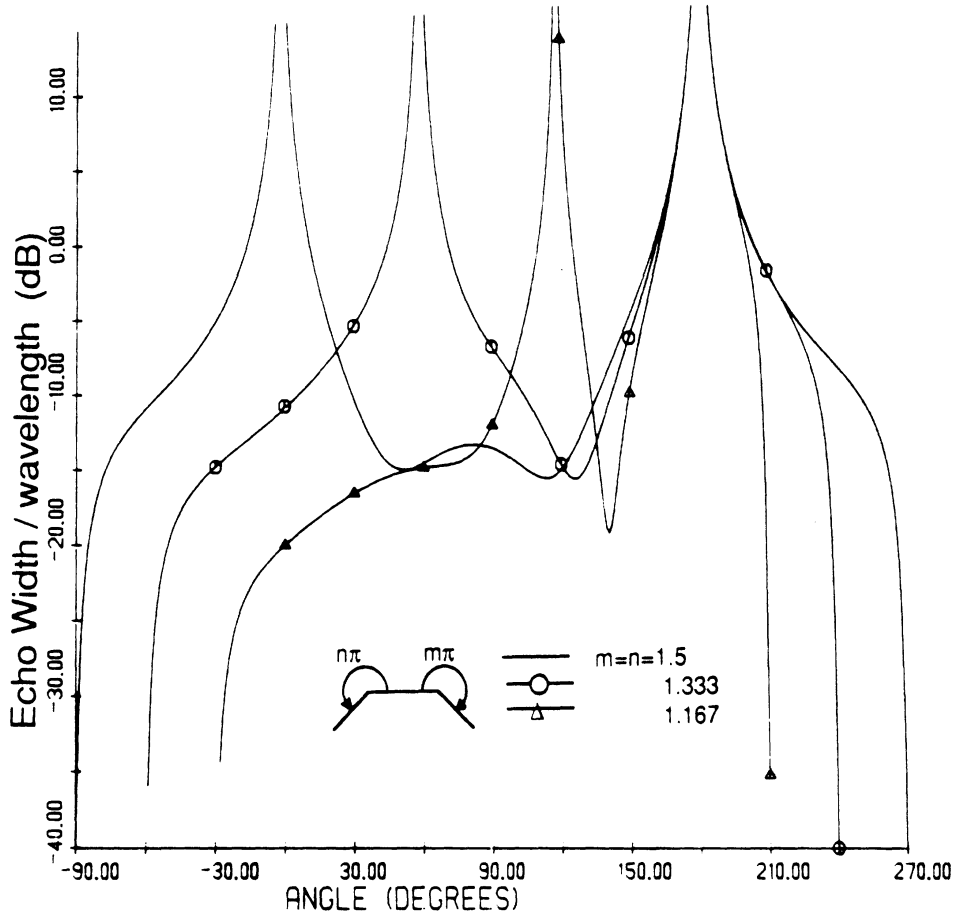

Figure 6.24 — Bistatic pattern from an impedance double wedge with varying external angles ($m = n$). H-polarization. $\rho_e = 1.3$

All faces have an impedance of $\eta_o = 0.25$ and the common face has a width of 0.5λ.

Higher Diffraction Mechanisms Using The ESRM

This section derives the quadruple diffraction mechanism for the isolated double wedge shown in figure 6.25. The purpose of going through this exercise is to show that it is easy to keep invoking the triple mechanism calculation described in Appendix D combined with the prior order coefficient to get the next higher order term. Most analytic approaches become unmanageable beyond the third order. The derived diffraction coefficients via the ESRM are easy to derive but long which is of no consequence with the use of computers.

The incident field impinges on Q_1 and the diffracted field emanates from Q_2 in this analysis. Using the same approach as the triple order ESRM evaluation we can write the quadruple integral equation as

$$u_{IV}^{d}(\phi_2,\phi_o) = \frac{j}{2\pi m}\int_{S(0)} e^{-jkw\cos\alpha}\sin\frac{\alpha}{m}\,u_{121}^{d}(\alpha,\phi_o)\,\frac{\Psi(\alpha+\frac{m\pi}{2}+\pi)}{\Psi(\frac{m\pi}{2}-\phi_2)} \cdot\left\{\frac{1}{\cos\left(\frac{\pi+\phi_2}{m}\right)-\cos\left(\frac{\alpha}{m}\right)}-\frac{1}{\cos\left(\frac{\pi-\phi_2}{m}\right)-\cos\left(\frac{\alpha}{m}\right)}-\frac{\sin\left(\frac{\phi_2}{m}\right)C_{cm}(\alpha)}{\cos\left(\frac{\pi-\alpha}{m}\right)-\cos\left(\frac{\phi_2}{m}\right)}\right\}d\alpha \tag{6.14}$$

where u_{121}^{d} was defined in (6.13). The evaluation of (6.14) using the modified Pauli-Clemmow steepest descent evaluation is similar to that described in Appendix D. For triple and higher order mechanisms, only the observation geometrical optics pole and the surface wave pole have to be accounted for.

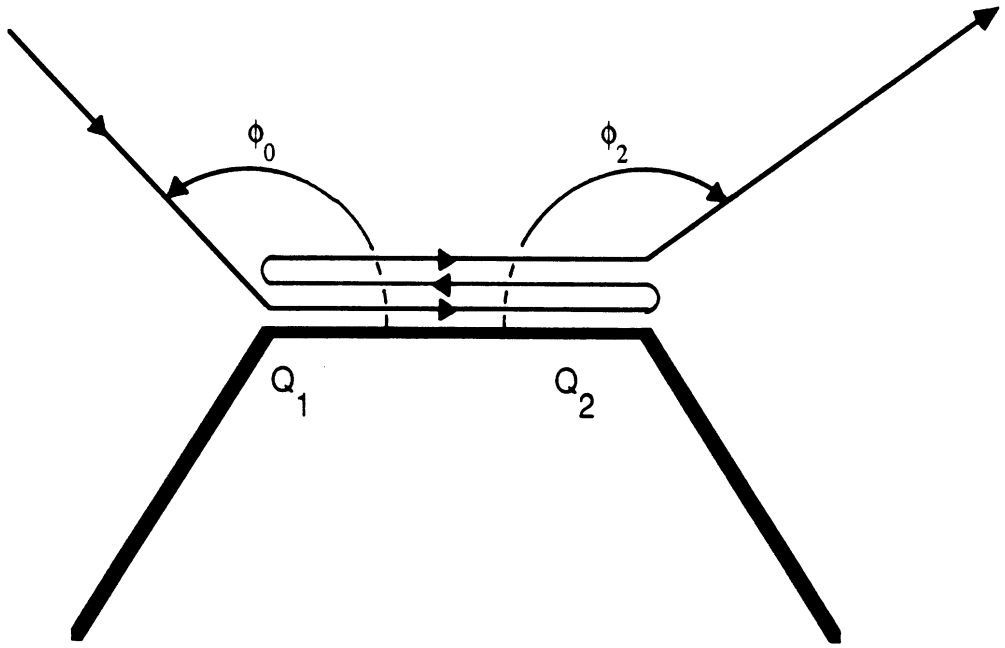

Figure 6.25 — Quadruple diffraction ray mechanism of an isolated double wedge

After repeating the ESRM process the quadruple mechanism is

$$
\begin{aligned}
u_{IV}^{d}(\phi_2,\phi_o) = {} & \frac{8e^{-j3kw}}{(k\pi)^2(w)^{1.5}(mn)^5}\frac{e^{-jk\rho}}{\sqrt{\rho}}\frac{\Psi^2(\frac{n\pi}{2}+\pi)\Psi^2(\frac{m\pi}{2}+\pi)}{\Psi(\frac{m\pi}{2})\Psi(\frac{n\pi}{2})\Psi(\frac{m\pi}{2}-\phi_2)\Psi(\frac{n\pi}{2}-\phi_o)} \\
& \cdot \frac{a_1 a_3^3 a_6}{(a_3-a_4)(a_3-a_6)}\frac{e^{-jkr}}{8} \\
& \cdot [A\{1-F_{KP}(kwa_1)\}+B\{1-F_{KP}(kwa_2)\}+C\{1-F_{KP}(kwa_3)\}] \\
& \cdot [F_{KP}(kwa_3)-F_{KP}(kwa_4)][F_{KP}(kwa_3)-F_{KP}(kwa_6)] \\
& \cdot \left\{\frac{1}{1-\cos\left(\frac{\pi-\phi_o}{n}\right)}-\frac{1}{1-\cos\left(\frac{\pi+\phi_o}{n}\right)}-\frac{\sin\frac{\phi_o}{n}C_{on}(0)}{\cos\frac{\pi}{n}-\cos\frac{\phi_o}{n}}\right\} \\
& \cdot \left\{\frac{1}{1-\cos\left(\frac{\pi-\phi_2}{m}\right)}-\frac{1}{1-\cos\left(\frac{\pi+\phi_2}{m}\right)}-\frac{\sin\frac{\phi_2}{m}C_{om}(0)}{\cos\frac{\pi}{m}-\cos\frac{\phi_2}{m}}\right\} \\
& \cdot \left\{\frac{2\sin\frac{\pi}{m}}{[1-\cos\frac{\pi}{m}]^2}+\frac{C_{om}(0)}{1-\cos\frac{\pi}{m}}\right\} \\
& \cdot \left\{\frac{2\sin\frac{\pi}{n}}{[1-\cos\frac{\pi}{n}]^2}+\frac{C_{on}(0)}{1-\cos\frac{\pi}{n}}\right\}
\end{aligned}
\tag{6.15}
$$

where

$$a_1 = 2\cos^2\frac{\phi_o}{2},$$

$$a_2 = a_4 = 2,$$

$$a_3 = 2\sin^2\frac{\theta^+}{2},$$

$$a_6 = 2\cos^2\frac{\phi_2}{2}$$

and r is the same phase factor as for the double diffraction case. All other variables have been defined in (6.13). The change in coefficient form from the double to triple diffraction is repeated (as expected) for the change in form from the triple to quadruple diffraction. This pattern is repeated for higher order mechanisms .

By including this coefficient in the isolated double wedge formulation one can easily check if the first three diffraction ray mechanisms are sufficient to account for all scattering effects.

CHAPTER VII

CONVEX CYLINDRICAL POLYGONS

In this chapter we remove the restriction requiring the outer sides of the double wedge not to intersect. Now the range of the external wedge angles (2Φ) can be such that $1 < m < 2$, $1 < n < 2$ and thus we can consider the scattering by any polygon whose adjacent sides form a convex shape. The strip is a special case of a polygon whose adjacent sides have zero included angles, and fits in the general framework of this analysis. Its scattered field is given later.

We will consider the far-zone scattered field by a polygon to include the contribution of all primary, double, and triple diffraction mechanisms. The primary and double diffraction mechanisms are the same as discussed in the previous chapter provided all parameters of the given expressions are applied to the local geometry of each wedge and double wedge forming the polygon. However, the contribution of the triply diffracted fields will include not only that caused by the interaction of two wedge vertices as discussed earlier, but also that due to interactions involving three wedge vertices as illustrated in figure 7.1. These last mechanisms have not yet been considered and thus expressions for their contribution are developed in the next section. The procedure used is, of course, parallel to that employed for the evaluation of the triply diffracted field associated with two wedge vertices.

Triple Diffraction Mechanism (three vertices)

This triple diffraction ray path is shown in figure 7.1. An incident wave on Q_n generates spectral waves diffracting at an angle $-\alpha$ and propagating toward Q_{n+1}. Using the same logic as in the double diffraction analysis we can invoke reciprocity and have an incident

wave impinge upon Q_{n+1} and diffracted at a local angle α. The field diffracted at Q_{n+1} is, of course, the doubly diffracted field given in (6.3) . After diffraction from Q_{n+1} a spectral wave may now propagate towards and diffract at Q_{n+2} before returning to the observer. Since we are concerned with the far field we can again invoke reciprocity and have an incident wave impinge upon Q_{n+2} at an angle ϕ, which will in sequence generate spectral waves diffracted at an angle $-\alpha$. Finally, the spectral waves will impinge at Q_{n+1} at a local angle α or $2\Phi-\alpha$ depending on the chosen face of reference. Thus an integral representation for the triply diffracted field is

$$u^d_{121}(\phi,\phi_o) = \frac{j}{2\pi p}\int_{S(0)} e^{-jkw_2\cos\alpha}\sin(\frac{\alpha}{p})u^d_{21}(2\Phi-\alpha,\phi_o)\frac{\Psi(\alpha+\frac{p\pi}{2}+\pi)}{\Psi(\frac{p\pi}{2}-\phi)} \cdot\left\{\frac{1}{\cos(\frac{\pi+\phi}{p})-\cos(\frac{\alpha}{p})}-\frac{1}{\cos(\frac{\pi-\phi}{p})-\cos(\frac{\alpha}{p})}-\frac{\sin(\frac{\phi}{p})C_{op}(\alpha)}{\cos(\frac{\pi-\alpha}{p})-\cos(\frac{\phi}{p})}\right\}d\alpha \tag{7.1}$$

where $p\pi$ is the external wedge angle at (Q_{n+2}) while, as before, $n\pi$ and $m\pi$ correspond to the external wedge angles at the first (Q_n) and second (Q_{n+1}) vertices, respectively. We further note that in the above, $u^d_{21}(\alpha,\phi_o)$ is given in (6.3).

Substituting for u^d_{21} gives

$$\begin{aligned} u^d_{121}(\phi,\phi_o) =& \Delta\int_{S(0)} e^{-jkw_2\cos\alpha}\sin(\frac{\alpha}{p})\sin(\frac{\alpha}{m})\frac{\Psi(\alpha+\frac{p\pi}{2}+\pi)}{\Psi(-\frac{m\pi}{2}+\alpha)} \\ &\cdot\left\{\frac{-2\sin\frac{\pi}{m}}{[1-\cos(\frac{\pi-\alpha+m\pi}{m})][1-\cos(\frac{\pi-m\pi+\alpha}{m})]}+\frac{C_{om}(0)}{\cos(\frac{\pi}{m})-\cos(\frac{m\pi-\alpha}{m})}\right\} \\ &\cdot\left\{\frac{1}{\cos(\frac{\pi+\phi}{p})-\cos(\frac{\alpha}{p})}-\frac{1}{\cos(\frac{\pi-\phi}{p})-\cos(\frac{\alpha}{p})}-\frac{\sin(\frac{\phi}{p})C_{op}(\alpha)}{\cos(\frac{\pi-\alpha}{p})-\cos(\frac{\phi}{p})}\right\} \\ &\cdot a_2[A\{1-F_{KP}(kw_1a_1)\}+B\{1-F_{KP}(kw_1a_2)\}+C\{1-F_{KP}(kw_1a_3)\}]d\alpha \end{aligned} \tag{7.2}$$

where

$$\begin{aligned} \Delta =& \frac{e^{-jkw_1}e^{-jk\rho}}{2\pi^2k(mn)^2p\sqrt{w_1\rho}}\frac{\Psi(\frac{n\pi}{2}+\pi)\Psi(\frac{m\pi}{2}+\pi)}{\Psi(\frac{n\pi}{2}-\phi_o)\Psi(\frac{p\pi}{2}-\phi)}a_1a_3 \\ &\cdot\left\{\frac{1}{1-\cos(\frac{\pi-\phi_o}{n})}-\frac{1}{1-\cos(\frac{\pi+\phi_o}{n})}-\frac{\sin(\frac{\phi_o}{n})C_{on}(0)}{\cos(\frac{\pi}{n})-\cos(\frac{\phi_o}{n})}\right\}. \end{aligned} \tag{7.3}$$

Equation (7.2) can now be uniformly evaluated using the modified Pauli-Clemmow method of steepest descent while accounting for the presence of the surface wave and geo-

metrical optics poles. The result is

$$
\begin{aligned}
u^d_{121} = & \frac{j\sqrt{2}e^{-jk(w_1+w_2)}e^{j\frac{3\pi}{4}}}{(k\pi)^{\frac{3}{2}}\sqrt{w_1 w_2}(nm)^2 p^2 m}\,\frac{e^{-jk\rho}}{\sqrt{\rho}}\,\frac{\Psi(\frac{n\pi}{2}+\pi)\Psi(\frac{m\pi}{2}+\pi)\Psi(\frac{p\pi}{2}+\pi)}{\Psi(\frac{n\pi}{2}-\phi_o)\Psi(\frac{p\pi}{2}-\phi)\Psi(-\frac{m\pi}{2})} \\
& \cdot \frac{a_1 a_2 a_3 a_4 a_5}{a_5 - a_4}\left[A\{1 - F_{KP}(kw_1 a_1)\} + B\{1 - F_{KP}(kw_1 a_2)\} + C\{1 - F_{KP}(kw_1 a_3)\}\right] \\
& \cdot \left[F_{KP}(kw_2 a_5) - F_{KP}(kw_2 a_4)\right] \cdot \frac{e^{-jkr}}{4} \\
& \cdot \left\{\frac{1}{1-\cos(\frac{\pi-\phi_o}{n})} - \frac{1}{1-\cos(\frac{\pi+\phi_o}{n})} - \frac{\sin(\frac{\phi_o}{n})C_{on}(0)}{\cos(\frac{\pi}{n})-\cos(\frac{\phi_o}{n})}\right\} \\
& \cdot \left\{\frac{1}{1-\cos(\frac{\pi-\phi}{p})} - \frac{1}{1-\cos(\frac{\pi+\phi}{p})} - \frac{\sin(\frac{\phi}{p})C_{op}(0)}{\cos(\frac{\pi}{p})-\cos(\frac{\phi}{p})}\right\} \\
& \cdot \left\{\frac{-2\sin\frac{\pi}{m}}{[1-\cos(\frac{\pi+m\pi}{m})][1-\cos(\frac{\pi-m\pi}{m})]} + \frac{C_{om}(0)}{1+\cos(\frac{\pi+m\pi}{m})}\right\}
\end{aligned}
\tag{7.4}
$$

where

$$
a_5 = 2\sin^2(\frac{\theta_{n+1}}{2}), \tag{7.5}
$$

in which θ_{n+1} is associated with the surface connecting Q_{n+1} and Q_{n+2}. In addition $r = -w'_2\cos(\phi) - w'_1\cos(\phi_o)$ with ϕ, ϕ_o, w'_1, and w'_2 as defined in figure 7.2.

Cylindrical Polygon Application

In this section we will explore the accuracy of the previously developed coefficients. Particularly, the sum of the contributions from all possible first, second, and triple order mechanisms will be used in predicting the scattered field by impedance polygons. The results will then be compared with corresponding moment method data. It is, of course, expected that as the sides of the polygon become smaller, the higher order mechanisms will become more significant and therefore the accuracy of our third order solution will decrease when fourth order mechanisms are of importance. The examples considered in this section are the triangular and square cylinders whose sides have equal length and impedances. Their geometries are shown in figure 7.3.

Backscatter patterns are presented in figures 7.4 to 7.9 for the triangular cylinder whose sides vary from 1λ down to 0.25λ. These pattern are with E-incidence and correspond to

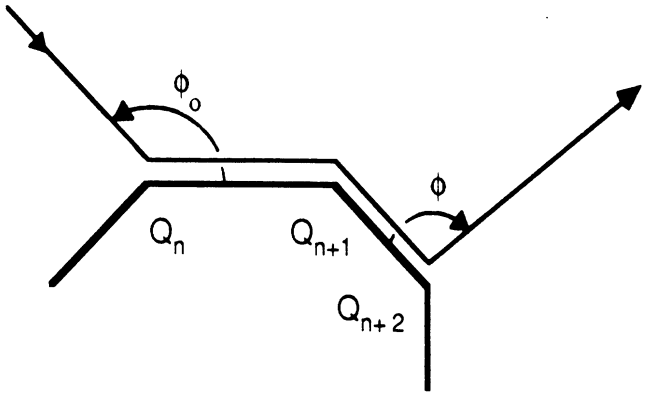

Figure 7.1 — Triple diffraction mechanism involving three vertices.

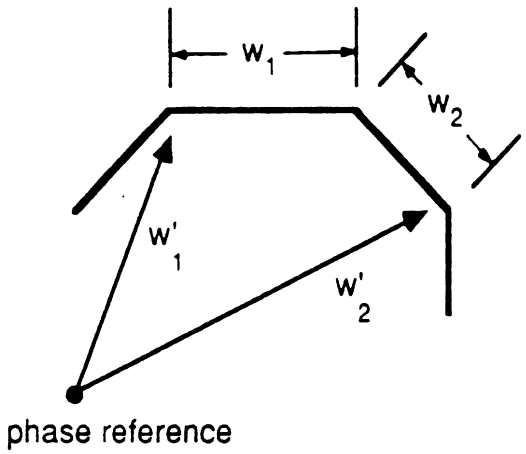

Figure 7.2 — Geometry of triple diffraction mechanism involving three vertices.

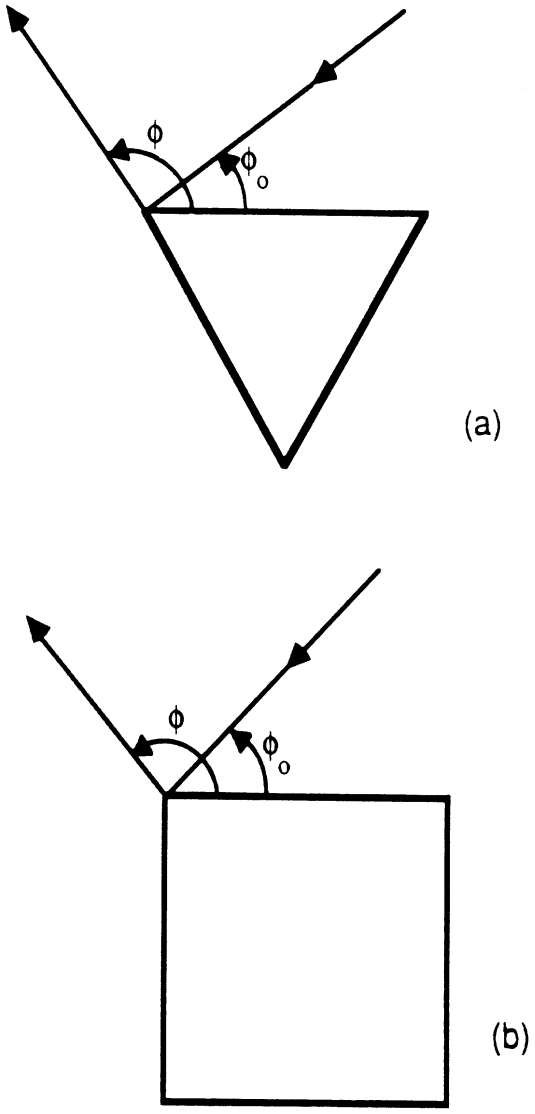

Figure 7.3 -- (a) Equilateral triangular and (b) square cylinders.

either $\eta = 2+j2$ (inductive) or $\eta = 2-j2$ (capacitive). As seen, our high frequency solution agrees remarkably well with the moment method for cylindrical sides as small as $\frac{\lambda}{4}$.

A set of bistatic patterns were also calculated and compared with moment method results. The conclusions are similar to those given for the backscatter case. It is also important to note that in these examples an edge of the cylinder may lie in the non-ray optical region of another edge. In such a situation the diffraction coefficients generated via the ESRM approach are still valid, where as those obtained via the self consistent GTD method [30] would not be applicable.

The backscatter patterns shown in figures 7.10 and 7.11 correspond to a square cylinder with a normalized impedance of $\eta = 4$, side length of 1λ and E-incidence. A mechanism to mechanism comparison reveals that the backscatter pattern is primarily a first order effect. However, for bistatic cases in which the direction of incidence is almost parallel with a face of the square, the higher order terms are significant. This is illustrated in figures 7.12 to 7.14 along with moment method results. The pattern due to primary diffraction matches the moment method data only near the backscatter direction. It is further seen to have several discontinuities most of which are compensated only after inclusion of the double diffraction effects. The rest of the discontinuities are associated with the triple diffraction mechanisms and particularly those involving three vertices. Thus, they are seen to vanish when the triply diffracted field is also included.

We conclude that overall, the agreement of our analytic solution with the moment method data is quite remarkable. Furthermore, although the considered polygons had equal impedances on all sides, it should be noted that our formulation is applicable for any convex polygon with arbitrary side impedances.

Impedance Strip

The impedance strip is a special case of the polygonal cylinder (both wedges have $2\Phi = 2\pi$) and is included here for completeness purposes. Prior work for an impedance strip with differing impedances on each face was developed for the special case of edge-on incidence only [36]. This limitation is overcome in the present formulation. The scattered field by an impedance strip was previously found in chapter IV via the ESRM. However, in that case the impedances on the top and bottom of the strip had to be equal.

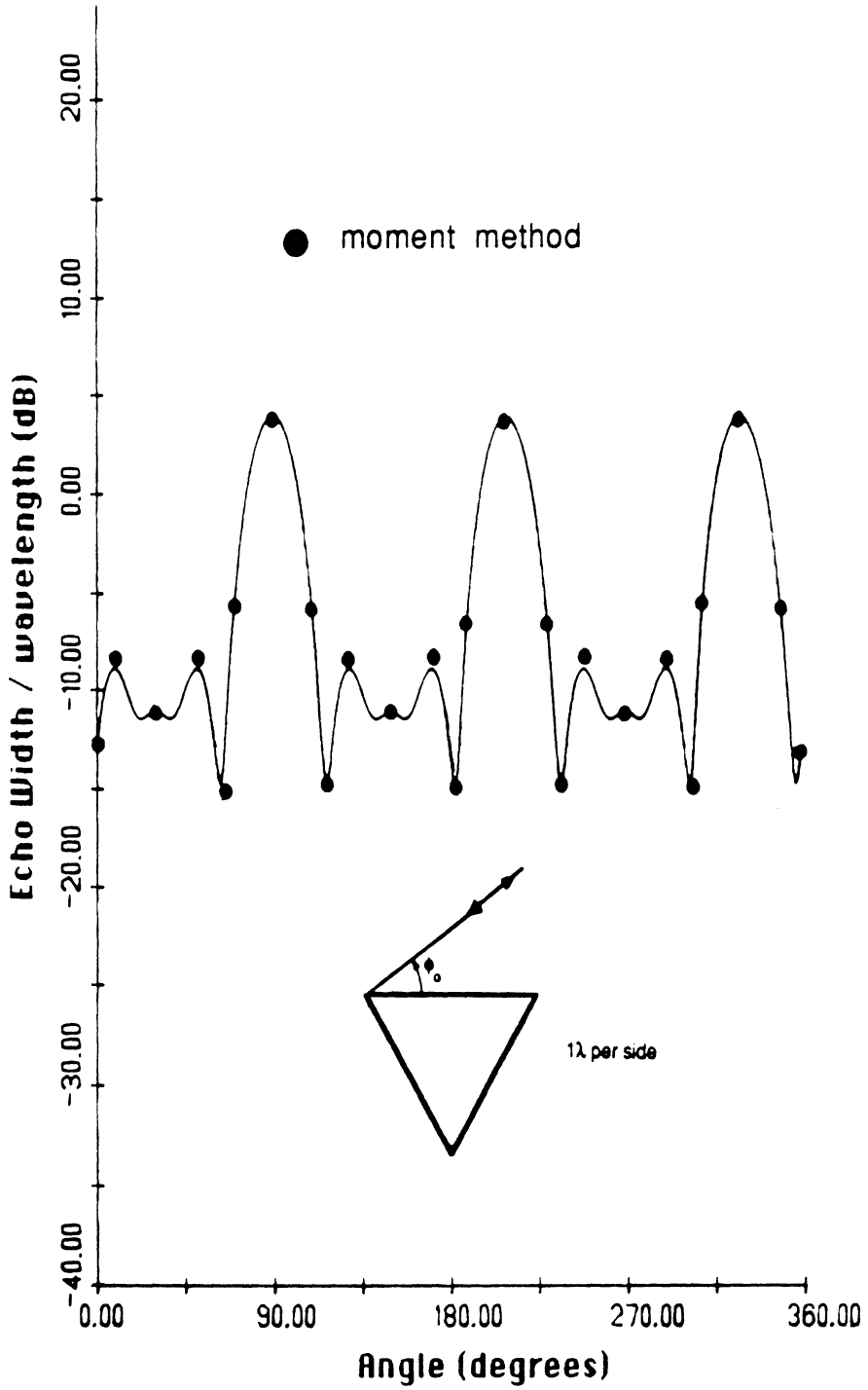

Figure 7.4 — Comparison of backscatter from an equilateral triangular cylinder (E-polarization) with moment method results. (1λ in length per side). $\eta = 2 - j2$

The impedances on all faces are equal

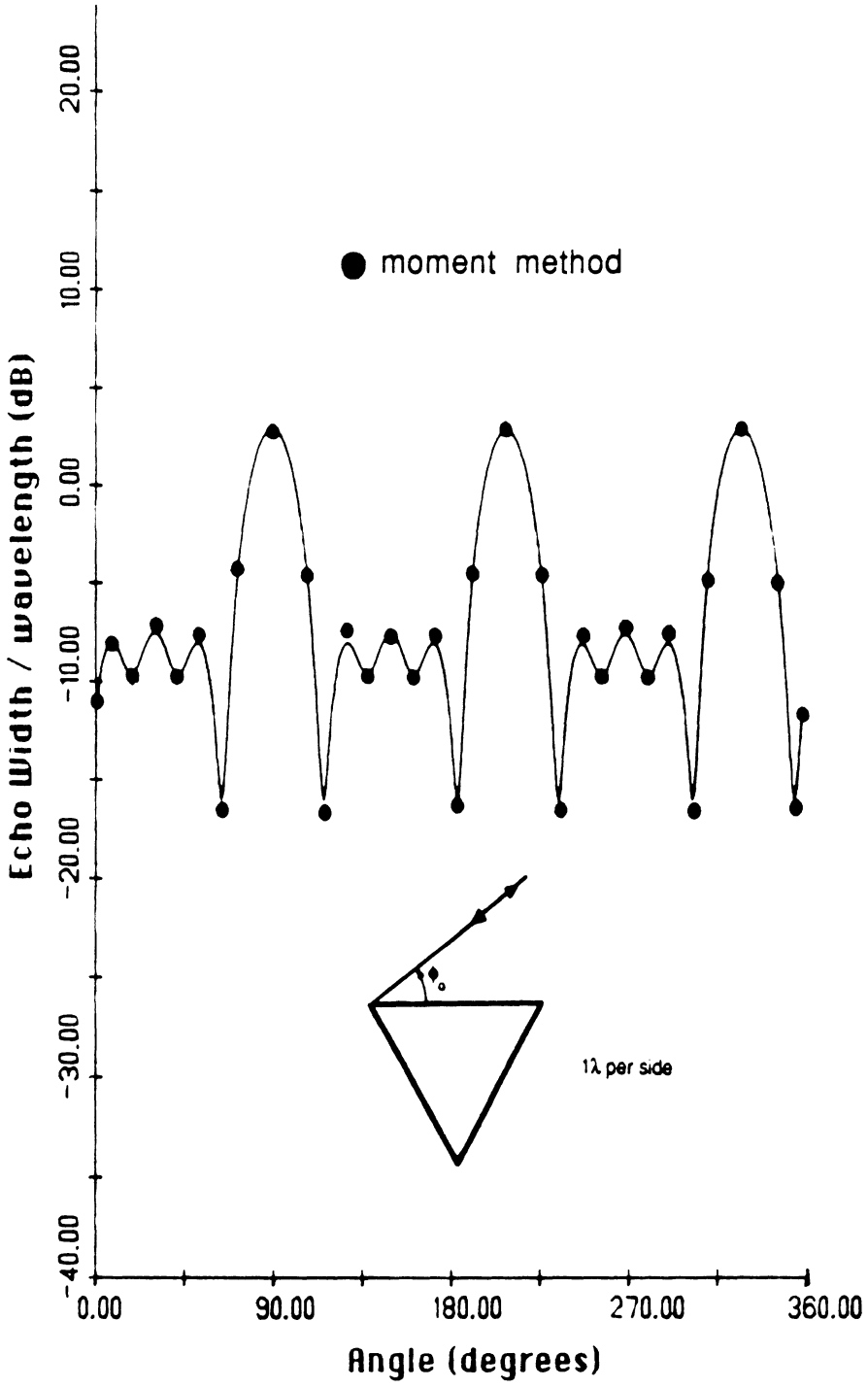

Figure 7.5 — Comparison of backscatter from an equilateral triangular cylinder (E-polarization) with moment method results. (1λ in length per side). $\eta = 2 - j2$

The impedances on all faces are equal.

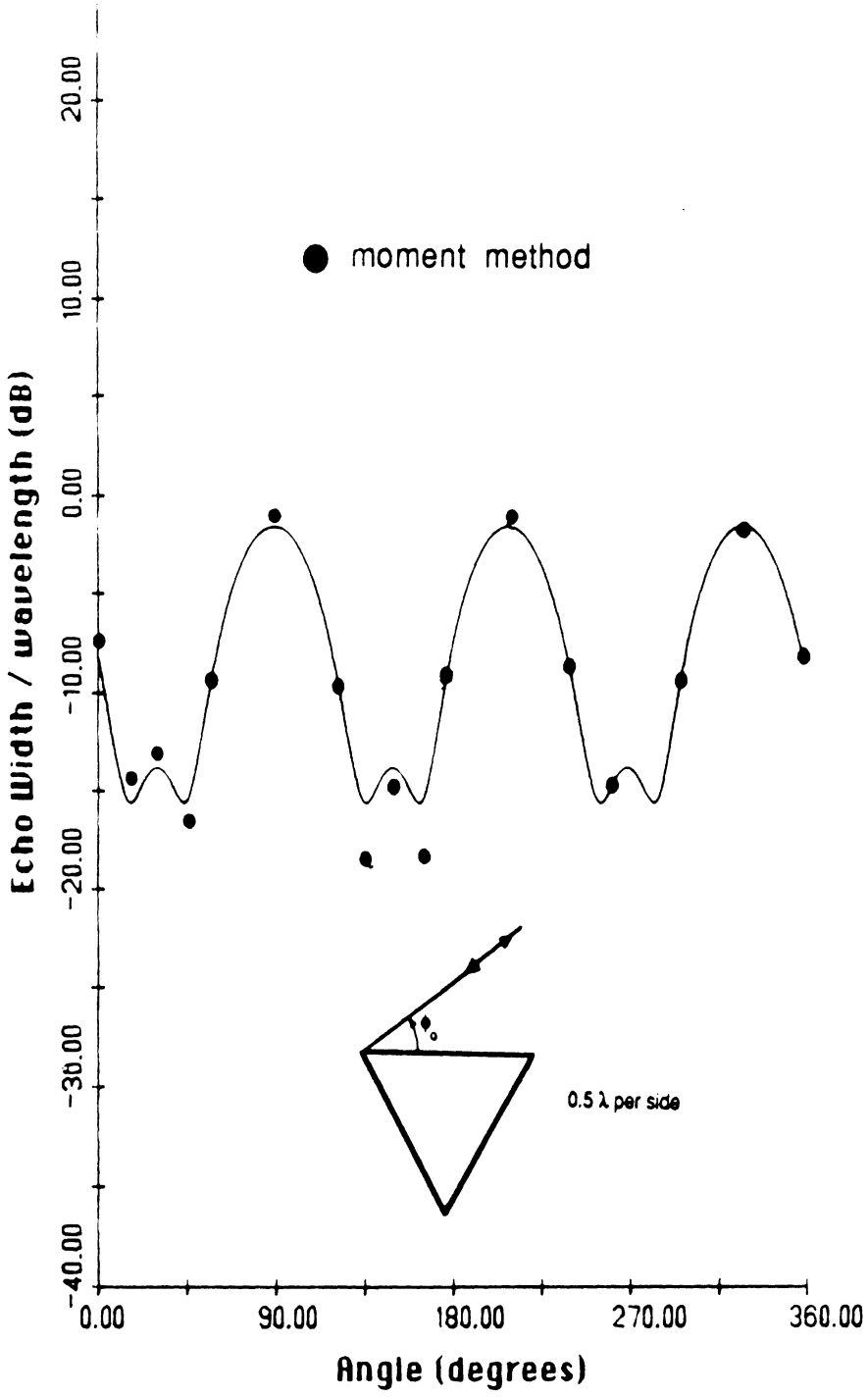

Figure 7.6 — Comparison of backscatter from an equilateral triangular cylinder (E-polarization) with moment method results. (0.5λ in length per side). $\eta = 2 - j2$

The impedances on all faces are equal.

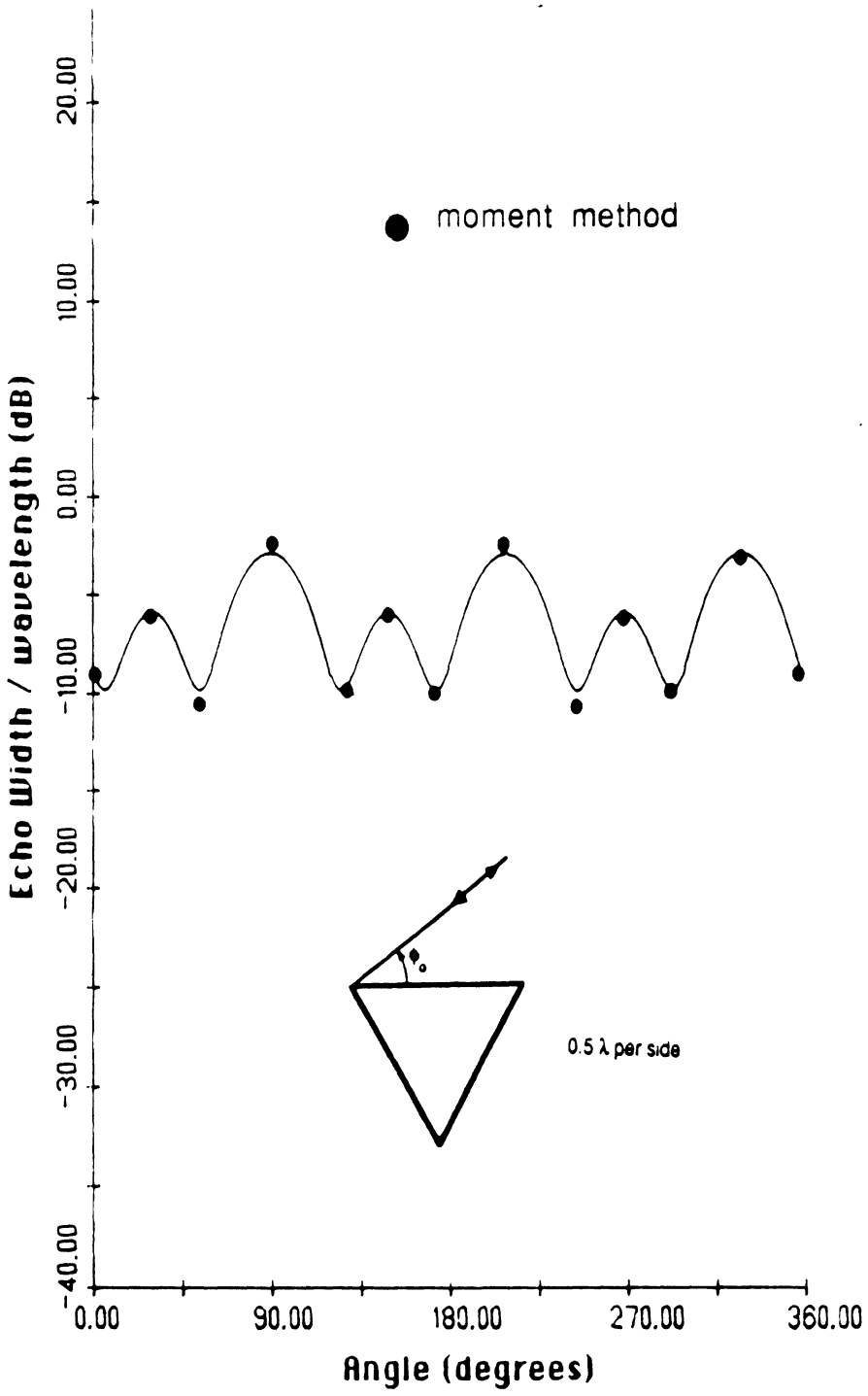

Figure 7.7 — Comparison of backscatter from an equilateral triangular cylinder (E-polarization) with moment method results. (0.5λ in length per side), $\eta = 2 - j2$

The impedances on all faces are equal.

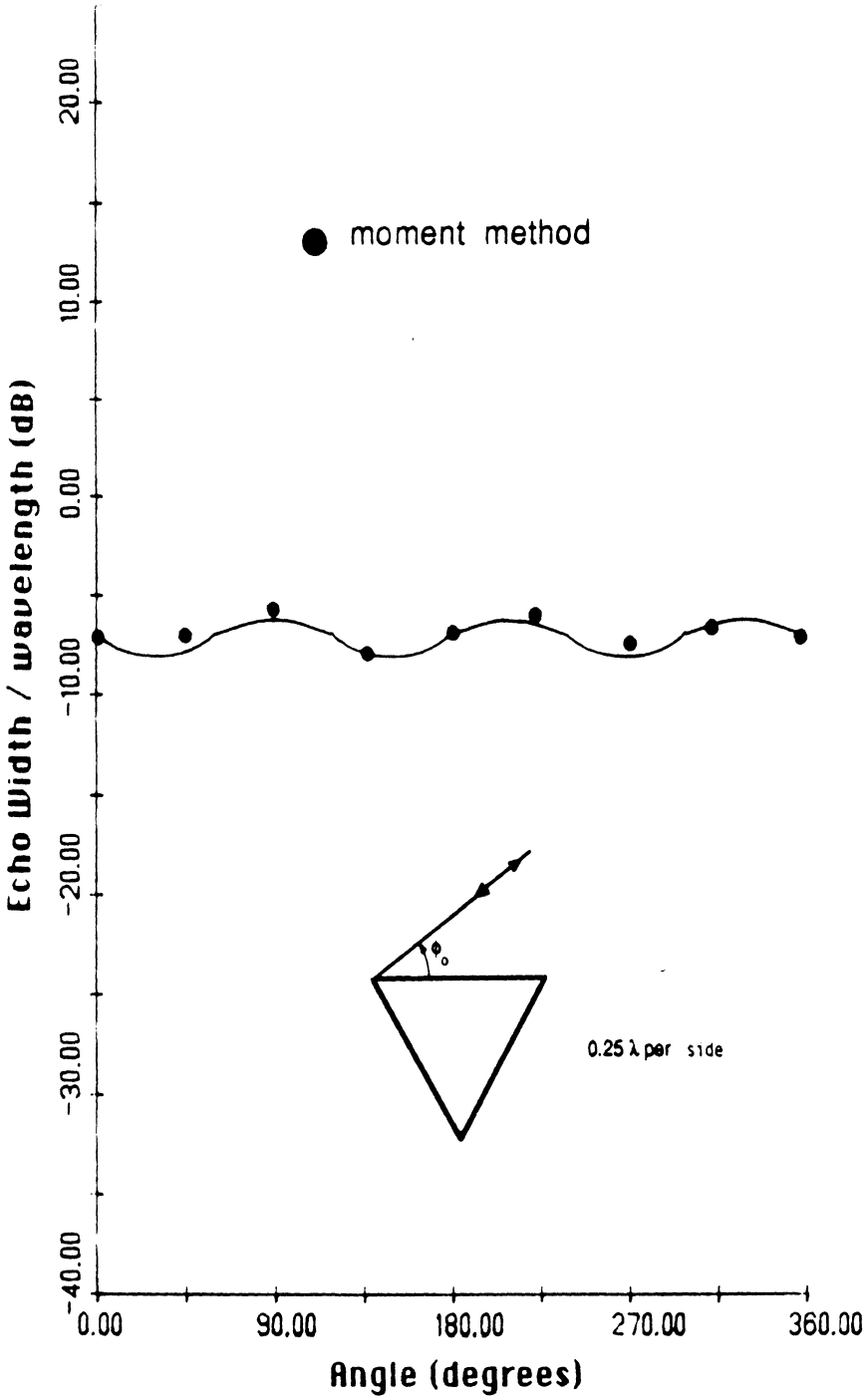

Figure 7.8 — Comparison of backscatter from an equilateral triangular cylinder (E-polarization) with moment method results. (0.25λ in length per side). $\eta = 2 - j2$

The impedances on all faces are equal.

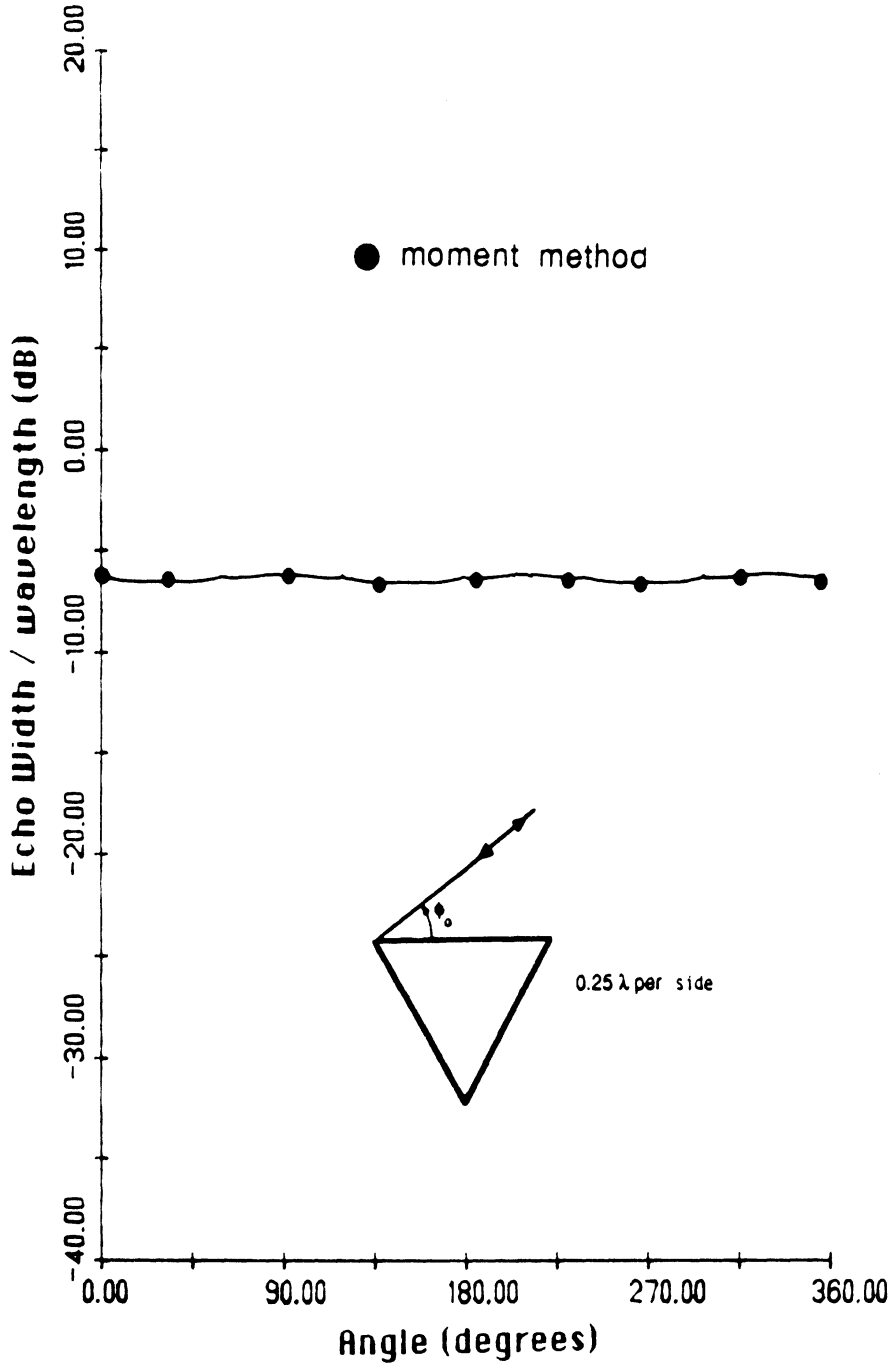

Figure 7.9 — Comparison of backscatter from an equilateral triangular cylinder (E-polarization) with moment method results. (0.25λ in length per side). $\eta = 2 - j2$

The impedances on all faces are equal.

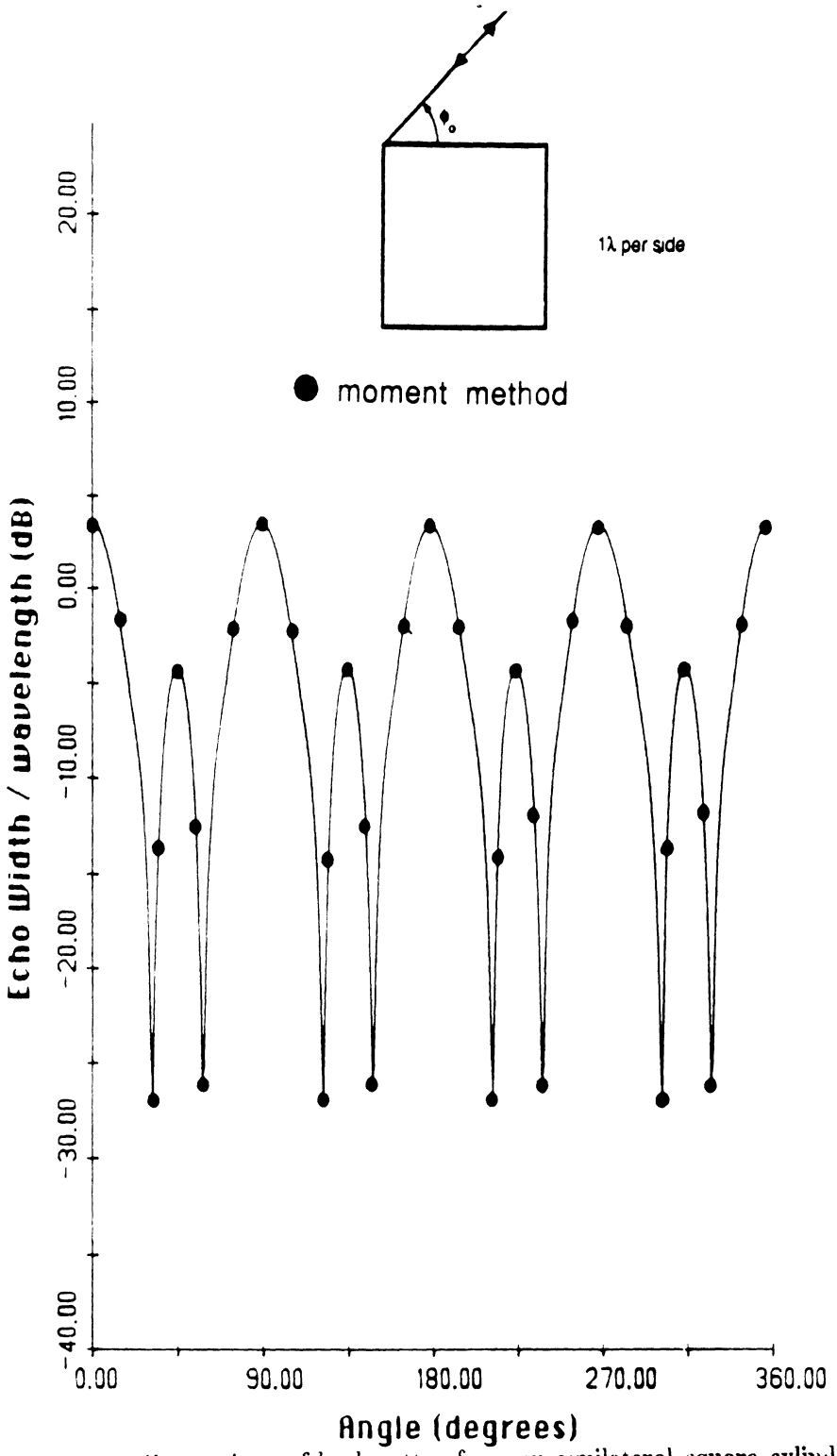

Figure 7.10 -- Comparison of backscatter from an equilateral square cylinder (E-polarization) with moment method results. (1λ in length per side). $\eta = 4$. Primary, double, and triple diffraction mechanisms.

The impedances on all faces are equal.

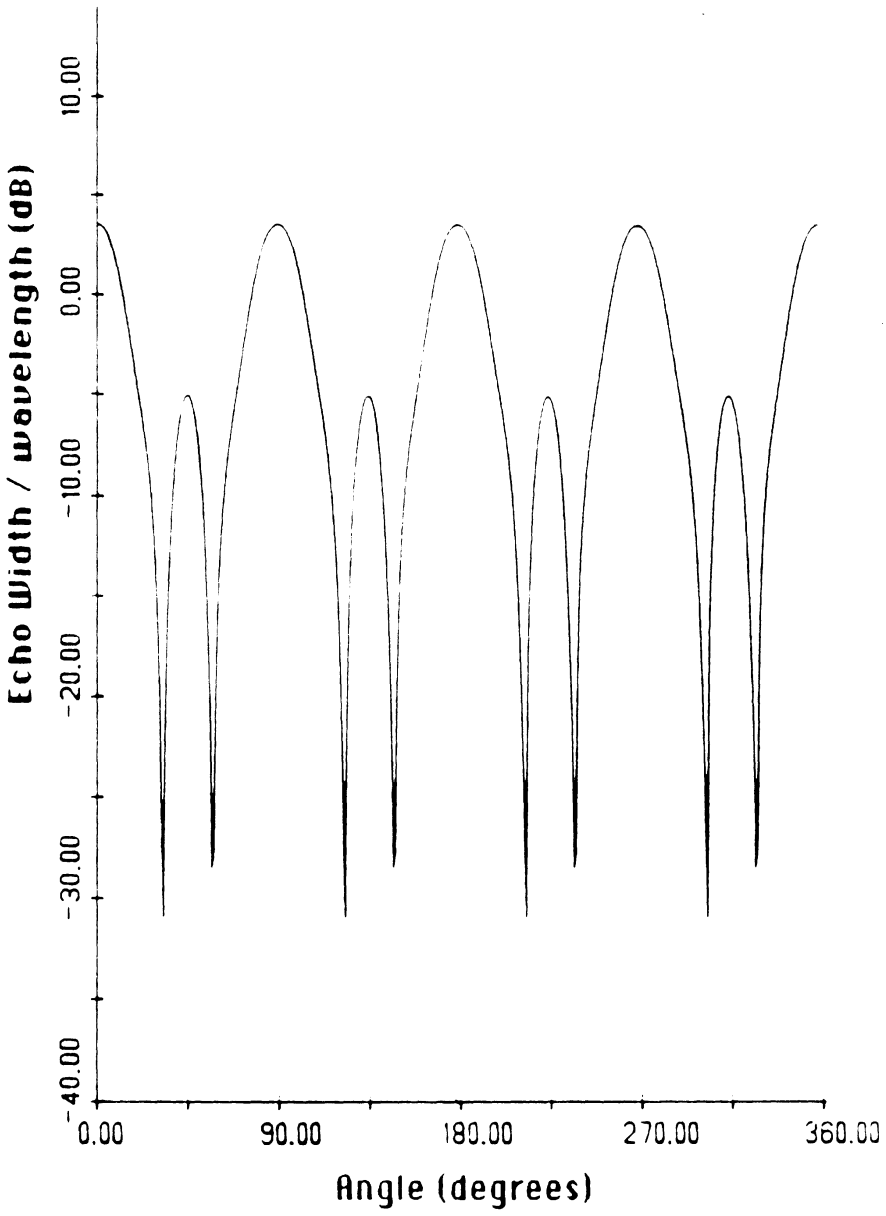

Figure 7.11 — Comparison of backscatter from an equilateral square cylinder (E-polarization) with moment method results. (1λ in length per side). $\eta = 4$. Primary diffraction contribution.

The impedances on all faces are equal.

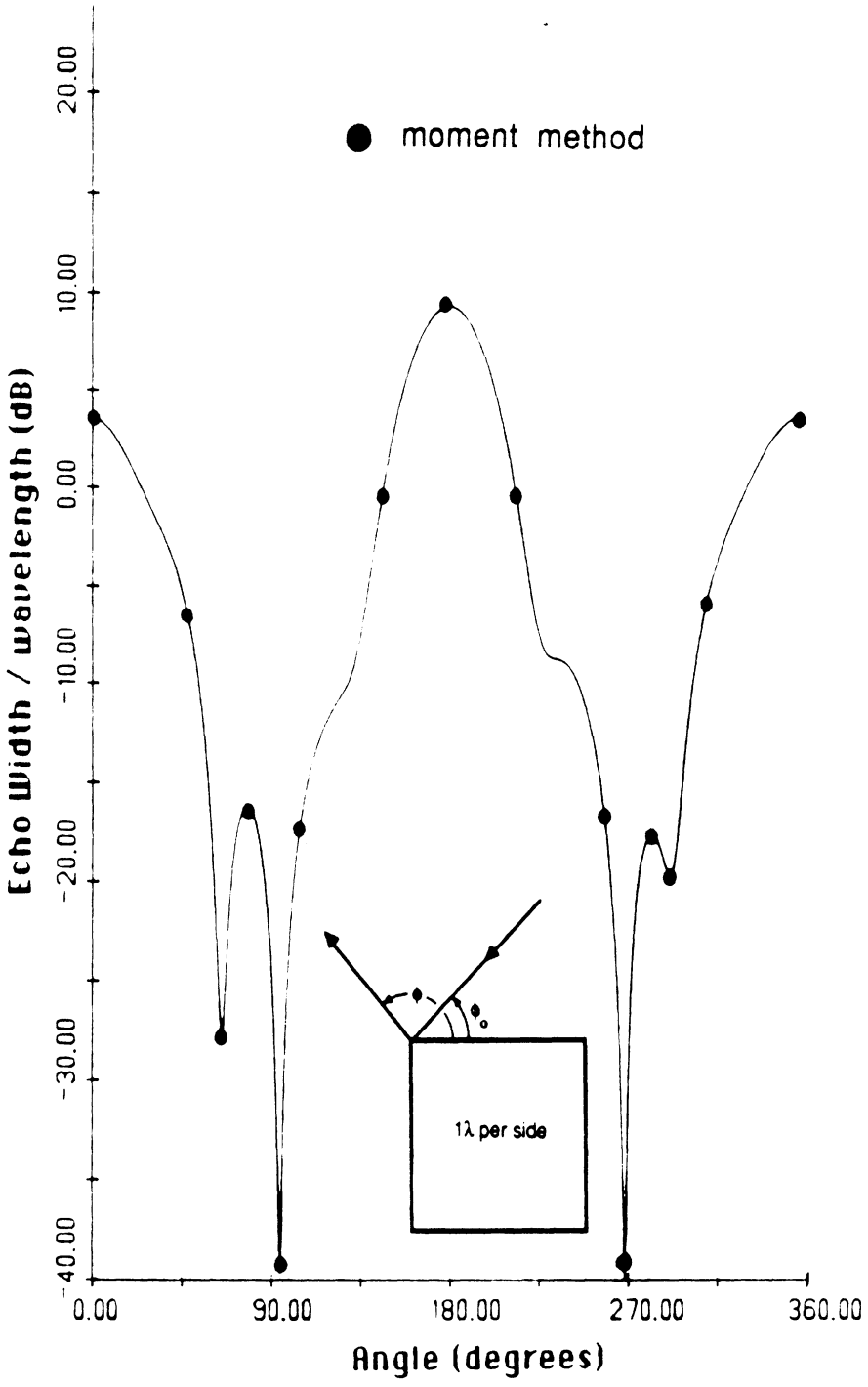

Figure 7.12 — Comparison of bistatic pattern from an equilateral square cylinder (E-polarization) with moment method results. Primary, double, and triple diffraction mechanisms.

1λ in length per side on the cylinder and $\eta = 4$.

The impedances on all faces are equal and the angle of incidence $\phi_0 = 1^\circ$

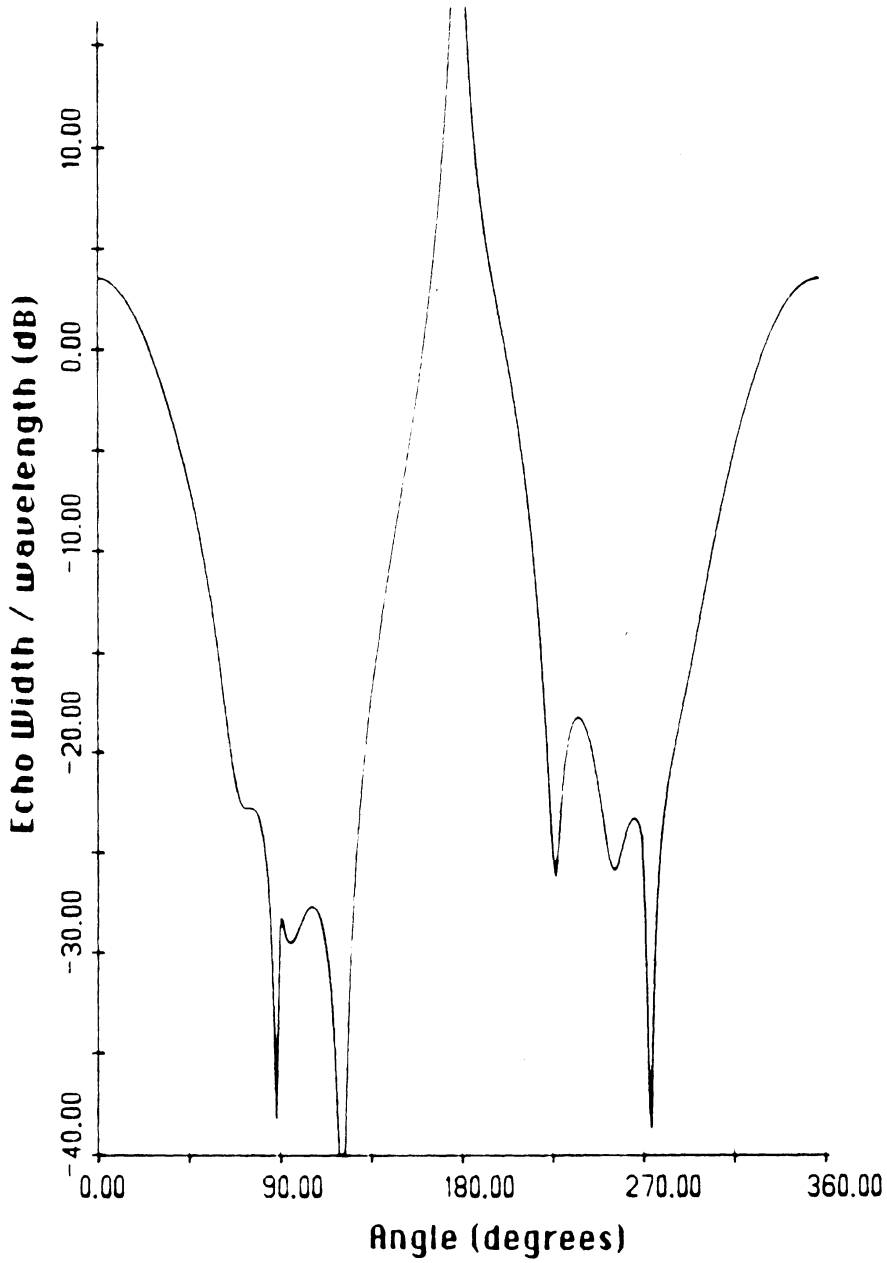

Figure 7.13 — Bistatic pattern from an equilateral square cylinder. Primary diffraction mechanism.

1λ in length per side on the cylinder and $\eta = 4$. The impedances on all faces are equal. E-polarization and the angle of incidence $\phi_0 = 1^\circ$

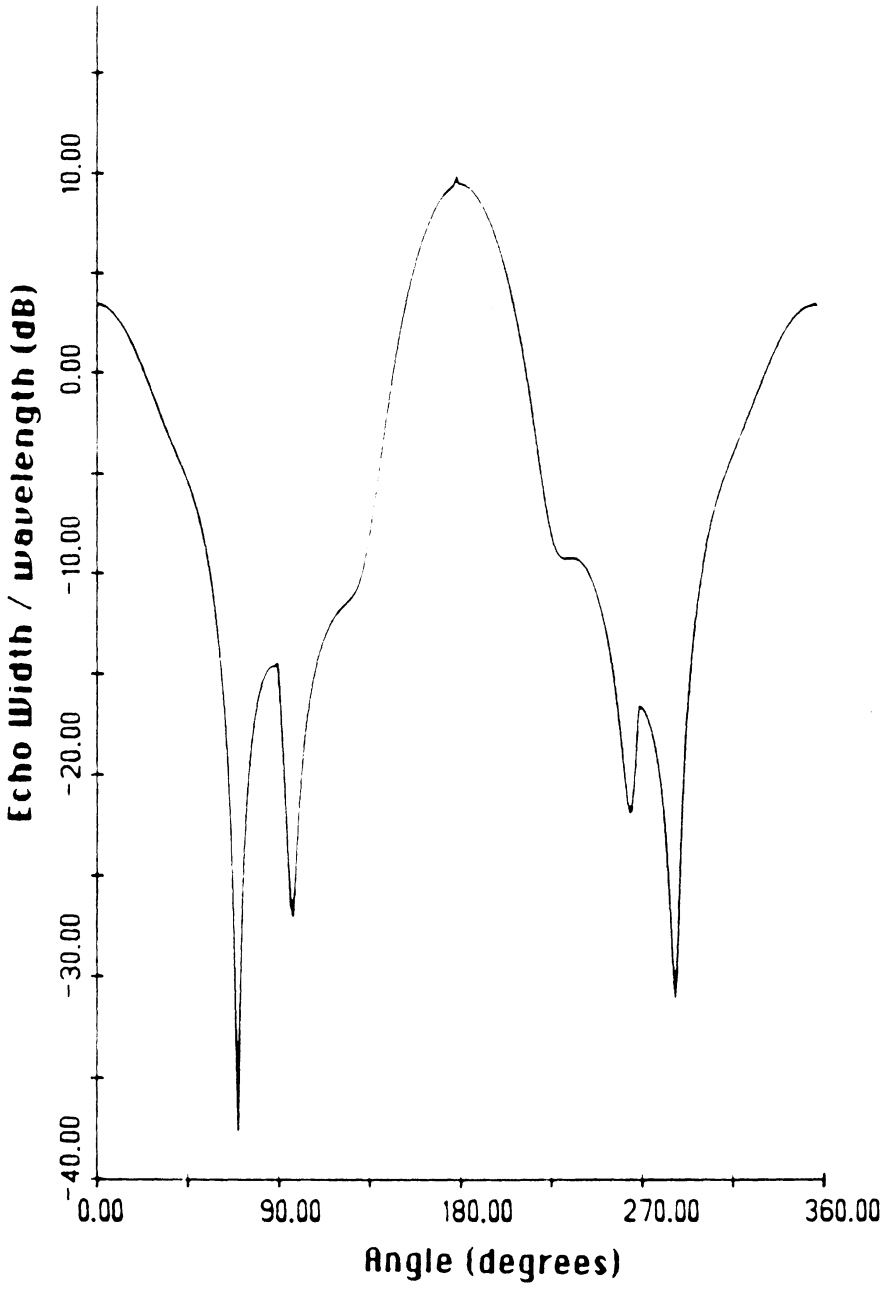

Figure 7.14 — Bistatic pattern from an equilateral square cylinder. Primary and double diffraction mechanisms.

1λ in length per side, $\eta = 4$. The impedances on all faces are equal.

E-polarization and the angle of incidence $\phi_0 = 1^o$

For a strip there exist four double diffraction mechanisms and eight triple mechanisms as shown in figures 4.2 and 4.4 . Fortunately, we need to only solve for the contribution of two double diffraction and four triple diffraction mechanisms. The contributions of the other mechanisms can then be obtained via an appropriate transformation of the geometrical variables.

Double Diffraction Mechanism From an Impedance Strip

Let us first consider the diffraction coefficients corresponding to the double diffraction mechanisms from Q_1 to Q_2. As discussed above, the coefficients associated with the mechanisms from Q_2 to Q_1 can be subsequently found by an appropriate variable transformation. The contribution of the double diffraction mechanism for the top surface is given by (6.3), and is still applicable for the strip provided we set $n = m = 2$. However, in the case of the impedance strip, the field due to the double diffraction mechanism associated with the bottom surface must also be accounted for. The procedure in deriving this doubly diffracted field via the ESRM is very similar to that employed in association with the top surface. Some care, though, must be exercised in the definition of the local angles corresponding to the spectral plane waves. Particularly, if we use the bottom ("n") face of the strip as our reference, then the spectral waves in the integral of (5.3) must be interpreted as forming an angle of α with respect to the bottom face at Q_1. Consequently, they will be forming an angle of -α with the bottom strip face at Q_2. Accordingly, we find that

$$
\begin{aligned}
u_{21}^{d}(\phi_2,\phi_o) = & \frac{-j}{16\pi k}\frac{e^{-jkw}}{\sqrt{w}}\frac{e^{-jk\rho}}{\sqrt{\rho}}\frac{[\Psi(0)]^2}{\Psi(\pi-\phi_o)\Psi(\pi-\phi_2)} \\
& \cdot a_1 a_2 a_3^{'}[A^{'}\{1-F_{KP}(kwa_1)\}+B^{'}\{1-F_{KP}(kwa_2)\}+C^{'}\{1-F_{KP}(kwa_3^{'})\}] \\
& \cdot\left\{\frac{1}{1+\sin(\frac{\phi_o}{2})}-\frac{1}{1-\sin(\frac{\phi_o}{2})}+\frac{\sin(\frac{\phi_o}{2})C_{2n}(0)}{\cos(\frac{\phi_o}{2})}\right\} \\
& \cdot\left\{\frac{1}{1-\sin(\frac{\phi_2}{2})}-\frac{1}{1+\sin(\frac{\phi_2}{2})}-\frac{\sin(\frac{\phi_2}{2})C_{2m}(0)}{\cos(\frac{\phi_2}{2})}\right\}\frac{e^{-jkr}}{2}
\end{aligned}
\tag{7.6}
$$

where

$$
C_2(\alpha,\theta^+,\theta^-,n)-1=\sin\frac{\alpha}{n}C_{2n}(\alpha), \tag{7.7}
$$

$$C_{2n}(\alpha) = -.25\left\{ \frac{\sin(\frac{\theta^+}{n}) - \sin(\frac{\theta^-}{n}) - 2\sin(\frac{\pi}{n})\cos(\frac{\alpha-2\pi}{n}) + \sin(\frac{\pi-\theta^+}{n}) + \sin(\frac{\theta^- - \pi}{n})}{\sin(\frac{\alpha-\pi-\theta^+}{2n})\sin(\frac{\alpha+\theta^+-2\pi}{2n})\cos(\frac{\alpha-\pi-\theta^-}{2n})\cos(\frac{\alpha-2\pi+\theta^-}{2n})} \right\}, \tag{7.8}$$

$$a_3' = 2\sin^2(\frac{\theta^-}{2}), \tag{7.9}$$

and

$$A' = \frac{-1}{(a_2 - a_1)(a_3' - a_1)} \tag{7.10}$$

$$B' = \frac{-1}{(a_1 - a_2)(a_3' - a_2)} \tag{7.11}$$

$$C' = \frac{-1}{(a_1 - a_3')(a_2 - a_3')} \tag{7.12}$$

Once again, r is equal to $-w\cos\phi$, and a factor of one-half is included to account for grazing effects.

All together there are four double diffraction mechanisms for the strip and the coefficients presented above are for the incident wave impinging upon Q_1 first. If we were concerned with diffraction from Q_2 to Q_1 then we would make the following transformations in (6.3) and (7.6) : $r \rightarrow -w\cos\phi_o$, $\phi_o \rightarrow \pi - \phi_o$ and $\phi_2 \rightarrow \pi - \phi_2$.

Triple Diffraction Mechanism from an Impedance Strip

The eight triple diffraction mechanisms are paired in groups of two as shown in figure 4.4. Each pair has the same formulation with differing references and angle specifications. The contribution of the triple diffraction mechanisms shown in figure 4.4(a) is given by (6.13). Normally we would just list the results for the next three sets of mechanisms if the derivations were the same as those shown in figure 4.4(a). Unfortunately, this is not the case at hand. Particularly, we must consider the fact that the diffracted field wraps around the strip for the mechanisms in figure 4.4(c) and (d). Thus, for the sake of completeness the diffracted fields due to the rest of the mechanisms will be derived next.

Starting with the mechanisms in figure 4.4(b), the integral for the corresponding triply diffracted field is

$$u^d_{121}(\phi,\phi_o) = \frac{j}{4\pi}\int_{S(0)} e^{-jkw\cos\alpha}\sin(\frac{\phi}{2})u^d_{21}(2\pi+\alpha,\phi_o) \cdot \left[\frac{\Psi(\alpha)}{\sin(\frac{\alpha}{2}) - \cos(\frac{\phi}{2})} + \frac{\Psi(-2\pi+\alpha)}{\sin(\frac{\alpha}{2}) + \cos(\frac{\phi}{2})}\right] d\alpha \tag{7.13}$$

where u_{21}^d is defined in (7.6). Equation (7.13) can be again interpreted as an infinite sum of spectral plane waves forming an angle α with the bottom face at Q_1 . The angles in u_{21}^d are, of course, defined with respect to the top surface and to be consistent the spectral waves make an angle of $-\alpha$ with the bottom face at Q_2. Inserting (7.6) into (7.13) gives

$$\begin{aligned} u_{121}^d(\phi,\phi_o) =& \Delta \int_{S(0)} e^{-jkw\cos\alpha} \sin(\frac{\alpha}{2}) \sin(\frac{\alpha}{2}) \frac{\Psi(\alpha)}{\Psi(-\pi-\alpha)} \\ & \cdot \left\{ \frac{2}{\cos^2(\frac{\alpha}{2})} + \frac{C_{2m}(0)}{\cos(\frac{\alpha}{2})} \right\} \\ & \cdot \left\{ \frac{1}{\sin(\frac{\phi}{2}) - \cos(\frac{\alpha}{2})} + \frac{1}{\sin(\frac{\phi}{2}) + \cos(\frac{\alpha}{2})} + \frac{\sin(\frac{\phi}{2}) C_{2n}(\alpha)}{\sin(\frac{\alpha}{2}) + \cos(\frac{\phi}{2})} \right\} \\ & \cdot a_2 [A^{'} \{1 - F_{KP}(kwa_1)\} + B^{'} \{1 - F_{KP}(kwa_2)\} + C^{'} \{1 - F_{KP}(kwa_3^{'})\}] d\alpha \end{aligned} \tag{7.14}$$

where

$$\begin{aligned} \Delta =& \frac{e^{-jkw} e^{-jk\rho}}{64\pi^2 k \sqrt{w\rho}} \frac{\Psi(0)\Psi(2\pi)}{\Psi(\pi-\phi_o)\Psi(\pi-\phi)} a_1 a_3^{'} \\ & \cdot \left\{ \frac{1}{1+\sin(\frac{\phi_o}{2})} - \frac{1}{1-\sin(\frac{\phi_o}{2})} + \frac{\sin(\frac{\phi_o}{2}) C_{2n}(0)}{\cos(\frac{\phi_o}{2})} \right\} \end{aligned} \tag{7.15}$$

Finally, by using the modified Pauli-Clemmow approach, (7.14) yields

$$\begin{aligned} u_{121}^d(\phi,\phi_o) =& \frac{\sqrt{2} e^{-j2kw} e^{j\frac{\pi}{4}}}{64(k\pi)^{\frac{3}{2}} w} \frac{e^{-jk\rho}}{\sqrt{\rho}} \frac{[\Psi(0)]^2 \Psi(2\pi)}{\Psi(\pi-\phi_o)\Psi(\pi-\phi)\Psi(-\pi)} \\ & \cdot \frac{a_1 a_3^{'2} a_4}{a_3^{'} - a_4} [A^{'} \{1 - F_{KP}(kwa_1)\} + B^{'} \{1 - F_{KP}(2kw)\} + C^{'} \{1 - F_{KP}(kwa_3^{'})\}] \\ & \cdot [F_{KP}(kwa_3^{'}) - F_{KP}(kwa_4)] \cdot \frac{1}{4} e^{-jkr} \\ & \cdot \left\{ \frac{1}{1+\sin(\frac{\phi_o}{2})} - \frac{1}{1-\sin(\frac{\phi_o}{2})} + \frac{\sin(\frac{\phi_o}{2}) C_{2n}(0)}{\cos(\frac{\phi_o}{2})} \right\} \\ & \cdot \left\{ \frac{1}{1+\sin(\frac{\phi}{2})} - \frac{1}{1-\sin(\frac{\phi}{2})} + \frac{\sin(\frac{\phi}{2}) C_{2n}(0)}{\cos(\frac{\phi}{2})} \right\} \\ & \cdot \{2 + C_{2m}(0)\} \end{aligned} \tag{7.16}$$

where $r = 0$ if the diffraction occurs from Q_1 and $r = -w[\cos\phi + \cos\phi_o]$ if the diffraction occurs from Q_2.

Continuing our derivation for the contribution of the mechanisms in figure 4.4(c). Let us first consider the mechanism which initially diffracts along the top face of the strip before wrapping around the bottom face. Using reciprocity, the triple diffraction integral for this case will consist of spectral plane waves diffracting at Q_1 at an angle α. Thus, they will be forming an angle -α with respect to the bottom face at Q_2. As a result the triple diffraction integral for this case is

$$u^d_{121}(\phi,\phi_o) = \frac{j}{4\pi}\int_{S(0)} e^{-jkw\cos\alpha}\sin\frac{\phi}{2}\,u^d_{21}(2\pi+\alpha,\phi_o) \cdot\left[\frac{\Psi(\alpha)}{\sin(\frac{\alpha}{2})-\cos(\frac{\phi}{2})}+\frac{\Psi(-2\pi+\alpha)}{\sin(\frac{\alpha}{2})+\cos(\frac{\phi}{2})}\right]d\alpha. \tag{7.17}$$

where u^d_{21} is the doubly diffracted field given in (6.3) with $\rho = w$. Inserting (6.3) and (5.39)-(5.42) in (7.17) gives

$$\begin{aligned} u^d_{121}(\phi,\phi_o) =& \Delta\int_{S(0)} e^{-jkw\cos\alpha}\sin(\frac{\alpha}{2})\sin(\frac{\alpha}{2})\frac{\Psi(\alpha)}{\Psi(-\pi-\alpha)}\left\{\frac{2}{\cos^2(\frac{\alpha}{2})}-\frac{C_{om}(0)}{\cos(\frac{\alpha}{2})}\right\} \\ &\cdot\left\{\frac{1}{\sin(\frac{\phi}{2})-\cos(\frac{\alpha}{2})}+\frac{1}{\sin(\frac{\phi}{2})+\cos(\frac{\alpha}{2})}+\frac{\sin(\frac{\phi}{2})C_{2n}(\alpha)}{\sin(\frac{\alpha}{n})+\cos(\frac{\phi}{2})}\right\} \\ &\cdot a_2[A\{1-F_{KP}(kwa_1)\}+B\{1-F_{KP}(kwa_2)\}+C\{1-F_{KP}(kwa_3)\}]d\alpha \end{aligned} \tag{7.18}$$

where

$$\begin{aligned} \Delta =& \frac{e^{-jkw}e^{-jk\rho}}{64\pi^2 k\sqrt{w\rho}}\frac{[\Psi(2\pi)]^2}{\Psi(\pi-\phi_o)\Psi(\pi-\phi)}a_1a_3 \\ &\cdot\left\{\frac{1}{1-\sin(\frac{\phi_o}{2})}-\frac{1}{1+\sin(\frac{\phi_o}{2})}+\frac{\sin(\frac{\phi_o}{2})C_{on}(0)}{\cos(\frac{\phi_o}{2})}\right\} \end{aligned} \tag{7.19}$$

and

$$a_3 = \sin^2(\frac{\theta^+}{2}) \tag{7.20}$$

A subsequent modified Pauli-Clemmow evaluation of (7.18) yields

$$
\begin{aligned}
u_{121}^{d}(\phi,\phi_o) =& \frac{j\sqrt{2}e^{-j2kw}e^{j\frac{3\pi}{4}}}{64(k\pi)^{\frac{3}{2}}w}\frac{e^{-jk\rho}}{\sqrt{\rho}}\frac{\Psi(0)[\Psi(2\pi)]^2}{\Psi(\pi-\phi_o)\Psi(\pi-\phi)\Psi(-\pi)} \\
&\cdot \frac{a_1 a_3 a_3' a_4}{a_3'-a_4}[A\{1-F_{KP}(kwa_1)\}+B\{1-F_{KP}(2kw)\}+C\{1-F_{KP}(kwa_3)\}] \\
&\cdot [F_{KP}(kwa_3')-F_{KP}(kwa_4)]\cdot\frac{1}{4}e^{-jkr} \\
&\cdot \left\{\frac{1}{1-\sin(\frac{\phi_o}{2})}-\frac{1}{1+\sin(\frac{\phi_o}{2})}+\frac{\sin(\frac{\phi_o}{2})C_{on}(0)}{\cos(\frac{\phi_o}{2})}\right\} \\
&\cdot \left\{\frac{1}{1+\sin(\frac{\phi}{2})}-\frac{1}{1-\sin(\frac{\phi}{2})}+\frac{\sin(\frac{\phi}{2})C_{2n}(0)}{\cos(\frac{\phi}{2})}\right\} \\
&\cdot \{2-C_{om}(0)\}.
\end{aligned}
\tag{7.21}
$$

where $r=0$ if the final diffraction occurs at Q_1 as developed above and $r=-w[\cos\phi+\cos\phi_o]$ if the final diffraction is at Q_2.

Finally, the last set of triple diffraction mechanisms to be considered is shown in figure 4.4(d). This situation is, of course, very similar to the pair of mechanisms in figure 4.4(c) whose contribution is given by (7.21). Let us first consider the mechanism which initially involves diffraction along the bottom surface and subsequently over the top surface. In this case the triple diffraction integral will consist of spectral plane waves diffracting from Q_1 at an angle of -α with the top surface if reciprocity is involved. Thus, they will be forming an angle of α with respect to the top face at Q_2. As a result the triple diffraction integral will be

$$
\begin{aligned}
u_{121}^{d}(\phi,\phi_o) =& \Delta\int_{S(0)} e^{-jkw\cos\alpha}\sin(\frac{\alpha}{2})\sin(\frac{\alpha}{2})\frac{\Psi(\alpha+2\pi)}{\Psi(\pi-\alpha)} \\
&\cdot \left\{\frac{2}{\cos^2(\frac{\alpha}{2})}-\frac{C_{2m}(0)}{\cos(\frac{\alpha}{2})}\right\} \\
&\cdot \left\{\frac{1}{-\sin(\frac{\phi}{2})-\cos(\frac{\alpha}{2})}-\frac{1}{\sin(\frac{\phi}{2})-\cos(\frac{\alpha}{2})}-\frac{\sin(\frac{\phi}{2})C_{on}(\alpha)}{\sin(\frac{\alpha}{2})-\cos(\frac{\phi}{2})}\right\} \\
&\cdot a_2[A'\{1-F_{KP}(kwa_1)\}+B'\{1-F_{KP}(kwa_2)\}+C'\{1-F_{KP}(kwa_3')\}]d\alpha
\end{aligned}
\tag{7.22}
$$

where

$$\Delta = \frac{e^{-jkw}e^{-jk\rho}}{64\pi^2 k\sqrt{w\rho}} \frac{[\Psi(0)]^2}{\Psi(\pi-\phi_o)\Psi(\pi-\phi)} a_1 a_3' \cdot \left\{ \frac{1}{1+\sin(\frac{\phi_o}{2})} - \frac{1}{1-\sin(\frac{\phi_o}{2})} + \frac{\sin(\frac{\phi_o}{2})C_{2n}(0)}{\cos(\frac{\phi_o}{2})} \right\} \tag{7.23}$$

and we have employed the doubly diffracted field u_{21}^d given in (7.6). Evaluating (7.22) via the modified Pauli-Clemmow approach gives

$$\begin{aligned} u_{121}^d(\phi,\phi_o) = & \frac{j\sqrt{2}e^{-j2kw}e^{j\frac{3\pi}{4}}}{64(k\pi)^{\frac{3}{2}}w} \frac{e^{-jk\rho}}{\sqrt{\rho}} \frac{[\Psi(0)]^2\Psi(2\pi)}{\Psi(\pi-\phi_o)\Psi(\pi-\phi)\Psi(\pi)} \\ & \cdot \frac{a_1 a_3 a_3' a_4}{a_3' - a_4} [A'\{1-F_{KP}(kwa_1)\} + B'\{1-F_{KP}(kwa_2)\} + C'\{1-F_{KP}(kwa_3')\}] \\ & \cdot [F_{KP}(kwa_3') - F_{KP}(kwa_4)] \cdot \frac{1}{4}e^{-jkr} \\ & \cdot \left\{ \frac{1}{1+\sin(\frac{\phi_o}{2})} - \frac{1}{1-\sin(\frac{\phi_o}{2})} + \frac{\sin(\frac{\phi_o}{2})C_{2n}(0)}{\cos(\frac{\phi_o}{2})} \right\} \\ & \cdot \left\{ \frac{1}{1-\sin(\frac{\phi}{2})} - \frac{1}{1+\sin(\frac{\phi}{2})} + \frac{\sin(\frac{\phi}{2})C_{on}(0)}{\cos(\frac{\phi}{2})} \right\} \\ & \cdot \{2 - C_{2m}(0)\} \end{aligned} \tag{7.24}$$

for the mechanisms in figure 4.4(d) where $r = 0$ if the final diffraction occurs at Q_1 and $r = -w[\cos\phi + \cos\phi_o]$ if the final diffraction is at Q_2. The transformations listed in the double diffraction for a strip apply in this situation to recover the components whose incident field is at Q_2. They are: $\phi_o \rightarrow \pi - \phi_o$ and $\phi \rightarrow \pi - \phi$.

Comments On The Impedance Strip

The diffracted fields given above for the impedance strip are identical to those derived by employing the half plane diffraction integral given by Senior in chapter IV. The last has, of course, been verified to agree with moment method scattering data for strip widths down to $\frac{\lambda}{8}$ in the case of backscattering. Figures 7.15 and 7.16 present the backscattering from an impedance strip similar to that run in figures 4.20 and 4.21, respectively. The results are identical.

The high frequency results generated in this section for the impedance strip has the added advantage of allowing non-equal impedances on the top and bottom sides of the strip.

This is demonstrated by making the bottom of the strip in the previous two cases perfectly conducting, see figures 7.17 and 7.18. In both, cases the backscatter is greater than that generated by a strip having equal impedances on both sides. This is particularly true in the case of figure 7.17 where the surface wave pole is closer to the saddle point and as a result it will have a profound effect near edge-on incidences (up to $\sim 60^o$).

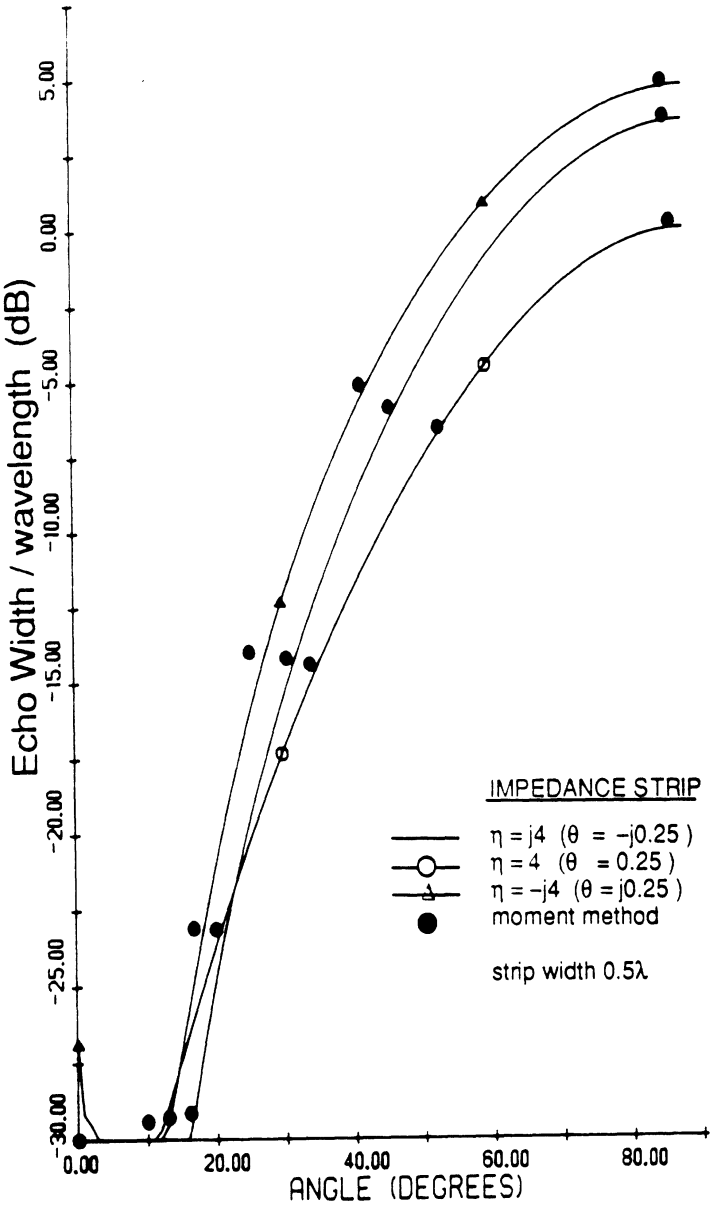

Figure 7.15 — Backscatter from an impedance strip using the double wedge formulation. Equal impedances on both sides $\eta = j4$. 4. and $-j4$.

Strip width is 0.5λ. E-polarization

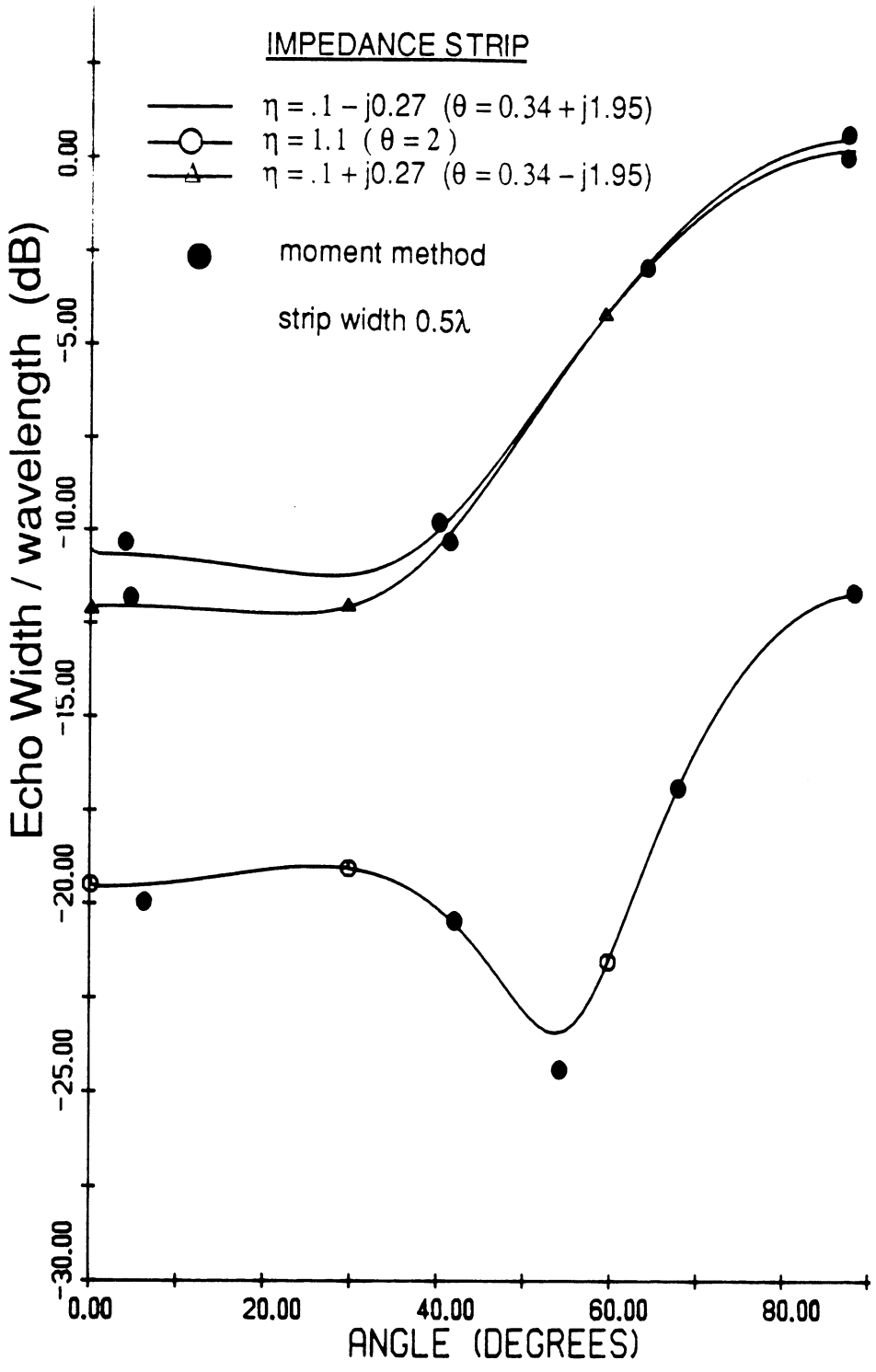

Figure 7.16 — Backscatter from an impedance strip using the double wedge formulation. Equal impedances on both sides $\eta = 0.1 - j0.27$, 1.1, and $0.1 - j0.27$.

Strip width is 0.5λ, E-polarization

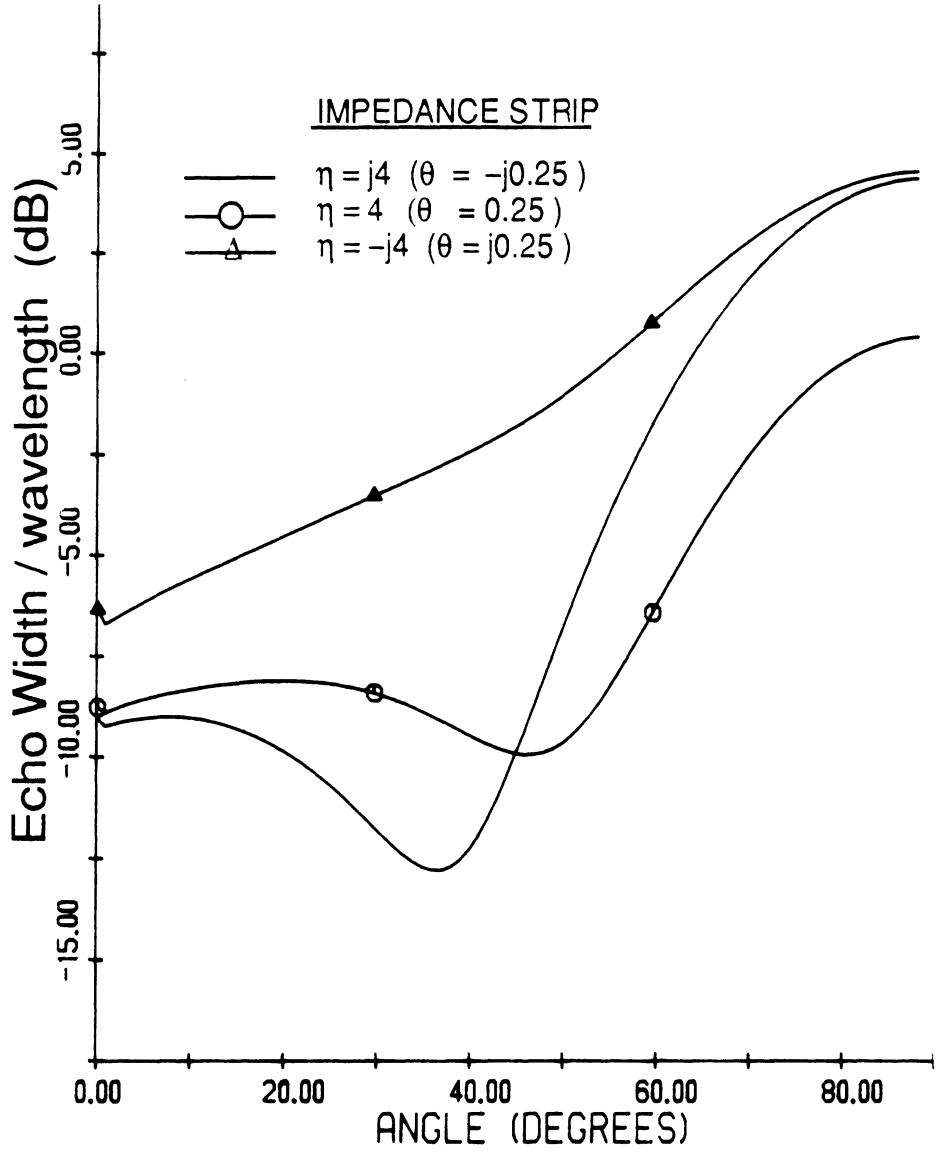

Figure 7.17 — Backscatter from an impedance strip using the double wedge formulation. Top face impedance is $\eta = j4$. 4. and $-j4$. The bottom is perfectly conducting.

Strip width is 0.5λ. E-polarization

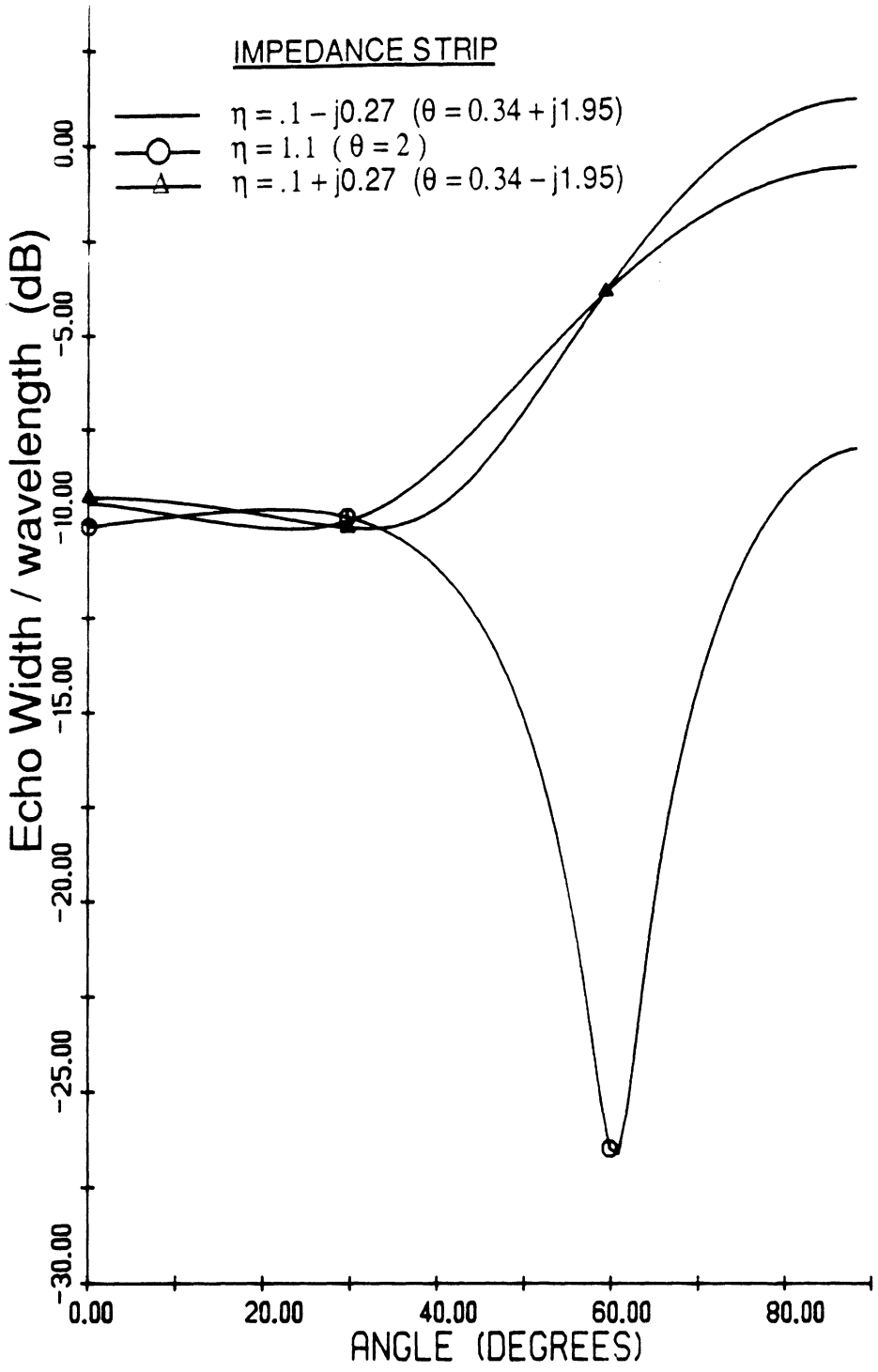

Figure 7.18 — Backscatter from an impedance strip using the double wedge formulation. Top face impedance is $\eta = 0.1 - j0.27$, 1.1, and $0.1 - j0.27$. The bottom is perfectly conducting.

Strip width is 0.5λ, E-polarization

CHAPTER VIII

CONCLUSION AND RECOMMENDATIONS

Chapters II and V of this dissertation presented uniform diffraction coefficients for the impedance half plane and wedge in which the surface wave contributions were rigorously included. Due to the nature of the integral equation we also obtained the uniform diffraction coefficients for resistive and conductive half planes.

In order to study the diffraction by multi-edge structures the Extended Spectral Ray Method (ESRM) was employed. A key feature in the application of the ESRM is the geometrical interpretation of the formulated spectral waves. This provided a physical understanding of the multi-edge diffraction phenomena even when non ray-optical fields are involved. Using the ESRM, second and triple order diffraction coefficients were derived for the resistive, conductive and impedance strips (see chapter IV). The analytic results matched data obtained via moment method codes. Unlike previous solutions ours was valid for any angle of incidence and observation, while accounting for all surface wave contributions in a uniform manner.

Another application of the ESRM was in the case of double wedge structures as presented in chapters VI and VII. Before proceeding with the analysis, highly accurate approximations for special functions had to be formulated. Also key identities were introduced in order to rewrite the integral equation in a form amenable to asymptotic evaluation via the modified Pauli-Clemmow steepest descent approach. The results of this formulation for isolated double wedge structures such as the thick impedance half plane and impedance insert agreed with those generated with alternate procedures such as the Angular Spectrum

Method - Generalized Scattering Matrix Formulation and moment method data, respectively. Likewise, the comparison between the analytic solution for convex polygons and moment method data was excellent.

Despite the success of the presented analysis , limitations with our solutions naturally exist. For the case of resistive (conductive and impedance) strips the width of the strip may be as small as $\frac{\lambda}{8}$ for backscatter cases and $\frac{\lambda}{2}$ for forward scattering. In the case of the isolated double wedge structure two variables determine the validity, the size of the common wedge face and the outer as well as common face impedances. When surface wave interactions are strong, higher order ray mechanisms must be included beyond the third. As shown in chapter VI the extension of our solution beyond the triple diffraction mechanism is easy to implement analytically using the ESRM although the result had a large number of terms associated with it. With the use of computers this is not a major problem to overcome. The same limitations for the isolated double wedge apply to the convex polygonal cylinder. However, when one considers the latter structures, the size of each cylinder face as well as the number of faces have to be considered. As the size of the faces decrease or the number of sides increase one must be aware that higher order ray mechanisms must be included in the solution.

A natural extension of the work presented is to investigate the scattering from multi-edge structures when the plane wave is not normal to the structure (skew incidence). Also one may consider development of diffraction coefficients for multi-edge curved structures in which the spatial rate of change is slowly varying. A final recommendation is to use the coefficients presented to study transient effects from material structures composed of wedges and half planes. Variation of object length corresponds to change of frequency since the echowidth is normalized to the wavelength. Fourier transformation of this data will yield the time domain response of the structure.

APPENDICES

APPENDIX A

IMPEDANCE BOUNDARY CONDITION

Impedance boundary conditions cannot be derived only postulated [37.38]. They enable us to solve a two media problem while solving explicitly for the fields only in one. This is accomplished by relating the tangential fields along the surface which takes into account the effective material composition of the second media. The impedance boundary condition is credited to the work of Leontovich and is the common factor in the integral formulations utilized in this dissertation. Therefore, it is of interest to know what conditions are assumed in order to postulate this boundary condition. Senior [38,39] has reviewed and expounded upon the use and limitations of this principle. Mathematically stated the impedance boundary condition is

$$\overline{E} - (\hat{n} \cdot \overline{E})\hat{n} = \eta Z \hat{n} \times \overline{H} \tag{A.1}$$

where $\hat{n}$ is the normal to the surface, η is the surface impedance, Z is the free space impedance and $\overline{E}$ and $\overline{H}$ are the total electric and magnetic fields respectively. Senior [39] has shown that a dual relationship exists for (A.1) where $Z\overline{H} \rightarrow -\overline{E}/Z$, $\overline{E} \rightarrow \overline{H}$ and $\eta \rightarrow \frac{1}{\eta}$ giving

$$\overline{H} - (\hat{n} \cdot \overline{H})\hat{n} = -\frac{1}{\eta Z}\hat{n} \times \overline{E} \tag{A.2}$$

The main assumptions implied in the postulation of the impedance boundary condition are that the material medium has a high index of refraction , it is infinite to the extent neither edge effects nor any internal reflections are observed, the interface has a slow spatial variation and the impedance is neither zero nor infinity. These are the main constraints which the solutions in this dissertation are based upon.

In the case of an infinitely thin impedance half plane it can be shown [4] that both the electric and magnetic tangential field components are discontinuous by an amount equivalent to the electric and magnetic current, respectively. For the special case in which the tangential electric fields are continuous but not the magnetic we have the boundary condition for a "resistive sheet"

$$\hat{n} \times \overline{E}^{\pm} = 0 \tag{A.3}$$

$$\hat{n} \times (\hat{n} \times \overline{E}) = -R\overline{K}_E \tag{A.4}$$

where $\overline{E}^{\pm}$ and $\overline{H}^{\pm}$ are the discontinuity of the tangential electric and magnetic fields respectively, $\overline{K}_E = \hat{n} \times \overline{H}^{\pm}$ is the electric current on the sheet and R is the resistivity which is defined as

$$R = \frac{\eta Z}{2} \tag{A.5}$$

We can parallel this scenario for the case of a "conductive sheet" when the tangential magnetic fields are continuous but not the electric by the amount proportional to the magnetic current sheet ($\overline{K}_M = -\hat{n} \times \overline{E}^{\pm}$) yielding

$$\hat{n} \times \overline{H}^{\pm} = 0 \tag{A.6}$$

$$\hat{n} \times (\hat{n} \times \overline{H}) = -R^{*}\overline{K}_M \tag{A.7}$$

where

$$R^{*} = \frac{1}{2\eta Z}. \tag{A.8}$$

These relationships can be derived from A.3 and A.4 by using duality. The impedance half plane may be considered as a superposition of electric and conductive sheets which obey the opaque condition $4RR^{*} = 1$ [22].

For an excellent discussion of the impedance boundary condition one is referred to the work of LaHaie [40] which includes many references for those interested in even more detail.

APPENDIX B

UNIFORM ASYMPTOTIC EVALUATION OF INTEGRALS

Often in electromagnetic scattering or diffraction problems the integral of the form

$$I(\phi) = \int_C g(\alpha), \phi) e^{\kappa f(\alpha,\phi)} d\alpha = \int_c \frac{p(\alpha,\phi)}{q(\alpha,\phi)} e^{\kappa f(\alpha,\phi)} d\alpha. \qquad (B.1)$$

is encountered at the final steps of the analysis. [1] The evaluation of this integral via the steepest descent method for large real κ involves the deformation of C to a steepest decent path (SDP) through the saddle point(s) defined by $f'(\alpha_s, \phi) = 0$. In so doing the evaluation of (B.1) is decomposed to contributions obtained from the SDP integral(s) and those associated with the residues of all poles (real or complex) that were captured during the contour deformation process (assuming no branch cuts exist).

When evaluating the SDP integrals(s), one must carefully consider the presence of any poles near the SDP such that $I(\phi)$ remains bounded and continuous when the pole crosses the SDP as ϕ is varied (the variable ϕ here represents the pattern angle). Such evaluations are usually referred to as uniform and have been the subject of several investigations [31,41,42]. However, none of the previous formulations are applicable to situations involving several complex integrand poles which may cross the SDP anywhere in the complex plane. Therefore, the purpose of this appendix is to introduce a technique which can be used for obtaining uniform evaluations of integrals involving complex integrands which may contain several distinct singularities in the complex plane. With the appropriate definitions [42] may be shown to be equivalent to the results of this appendix.

The procedure involves the regularization of the integrand over the SDP by the subtraction and addition of certain auxiliary integrals (one for each singularity) whose integrands

[1] Many portions of this dissertation have been submitted for publication in a variety of journals and are currently under review. This appendix is the only section whose main content has appeared in the literature [9].

satisfy a condition so that the desired uniformity is achieved. The resulting integrals with or without singularities can then be evaluated asymptotically. This procedure is a generalization of a method applied by Clemmow[7] and Senior [8] to integrals with specific $f(\alpha,\phi)$ when considering a single pole.

Formulation

In proceeding with the uniform evaluation of (B.1) we assume that the integral exists as $\kappa \to \infty$. For the sake of simplicity, this section will also be restricted to the case that $q(\alpha,\phi)$ is associated with a single zero at $\alpha = \alpha_p$ and the SDP crosses a single first-order saddle point at $\alpha = \alpha_s$. Generalizations to several integrand poles and saddle points are given in the next section.

On the basis of the above assumptions, (B.1) can be written as

$$I(\phi) = 2\pi j R_p(\phi) + A_p(\phi)\int_{C_{SDP}} G_p(\alpha,\phi)e^{\kappa f(\alpha,\phi)}\,d\alpha + \int_{C_{SDP}} K(\alpha,\phi)e^{\kappa f(\alpha,\phi)}\,d\alpha \quad (B.2)$$

with

$$K(\alpha,\phi) = g(\alpha,\phi) - A_p(\phi)G_p(\alpha,\phi) \quad (B.3)$$

where

$$R_p(\phi) = \begin{cases} p(\alpha_p,\phi)e^{\kappa f(\alpha_p,\phi)}/q'(\alpha_p,\phi), & \text{pole enclosed by } C - C_{SDP} \\ 0, & \text{otherwise} \end{cases} \quad (B.4)$$

is the residue of the enclosed pole and $A_p(\phi)G_p(\alpha,\phi)$ is an unknown product of functions which has been added and subtracted to $g(\alpha,\phi)$. Note also that $q'(\alpha_p,\phi) = \frac{dq(\alpha,\phi)}{d\alpha}\big]_{\alpha=\alpha_p}$.

If we, however, require

$$G_p(\alpha,\phi) = \frac{1}{q_p(\alpha,\phi)} \quad (B.5)$$

to have a pole at $\alpha = \alpha_p$ (there is no restriction for additional poles provided they are not close to the SDP) and choose

$$A_p(\phi) = \lim_{\alpha\to\alpha_p}\left[\frac{g(\alpha,\phi)}{G_p(\alpha,\phi)}\right] = p(\alpha_p,\phi)\frac{q_p'(\alpha_p,\phi)}{q'(\alpha_p,\phi)} \quad (B.6)$$

then $K(\alpha,\phi)$ becomes free of singularities and thus the asymptotic evaluation of the pertinent (second) integral in (B.2) is known to be continuous and can be found in [43] up to

$O(\frac{1}{\kappa^3})$. Our task has then reduced to finding an appropriate $G_p(\alpha,\phi)$ which account for the discontinuity of $R_p(\phi)$.

Since $G_p(\alpha,\phi)$ has a single pole near the SDP, we have that for large κ [31,41]

$$I(\phi) = 2\pi j R_p(\phi) - \sqrt{\frac{-2\pi}{\kappa f''(\alpha_s,\phi)}}\, e^{\kappa f(\alpha_s,\phi)} \left[A_p(\phi) G_p(\alpha_s,\phi) F_{KP}(\mp\kappa b_p^2) - K(\alpha_s,\phi) \right] + O(\frac{1}{\kappa}) \tag{B.7}$$

with the upper sign for $-\frac{3\pi}{4} < \arg(b_p) < \frac{\pi}{4}$ and lower sign for $\frac{\pi}{4} < \arg(b_p) < \frac{5\pi}{4}$, where

$$b_p = \sqrt{2\left[f(\alpha_s,\phi) - f(\alpha_p,\phi)\right]} \tag{B.8}$$

The function $F_{KP}(\mp z^2)$ is given by

$$F_{KP}(\mp z^2) = \mp 2jze^{jz^2} \int_{\mp z}^{\infty} e^{-jt^2}\, dt \tag{B.9}$$

and thus satisfy the identity

$$F_{KP}(-z^2) = -2jz\sqrt{\pi}\, e^{-j\frac{\pi}{4}}\, e^{-jz^2} + F_{KP}(z^2) \tag{B.10}$$

Furthermore, the transition points associated with b_p correspond to the crossing of C_{SDP} by the pole (the particular order of correspondence may vary).

By employing (B.4) and (B.10) in (B.7), it is found that $I(\phi)$ as given in (B.7) is continuous (uniform) only if

$$\frac{q_p'(\alpha_p,\phi)}{q_p(\alpha_s,\phi)} = e^{-j(\phi_s-\frac{\pi}{4})} \sqrt{\frac{f''(\alpha_s,\phi)}{2}}\, \frac{1}{b_p} \tag{B.11}$$

where ϕ_s is the angle formed by the real axis of the $\alpha-$plane and the direction of the C_{SDP} at the saddle point [43]. For example, if $f(\alpha,\phi) = -j\cos(\phi-\alpha)$ then $\alpha_s = \phi$, $\phi_s = \frac{\pi}{4}$, $b_p = \sqrt{2}\cos[(\phi-\alpha_p-\pi)/2]$, and an appropriate choice for $G_p(\alpha,\phi)$ is $G_p(\alpha,\phi) = G_p(\alpha) = \sec[(\alpha-\alpha_p-\pi)/2]$. Therefore, for this example the integration of the singular integrand as given in (B.7) is exact and the accuracy of $I(\phi)$ is only limited by the asymptotic expansion of the integral associated with $K(\alpha,\phi)$.

When α_p is far from the SDP, then $F_{KP}(z) \sim 1$ with $-\frac{3\pi}{4} < \arg(z) < \frac{\pi}{4}$, and (B.7) reduces to the usual nonuniform asymptotic form. To avoid any complication with any other poles of $G_p(\alpha,\phi)$, one should always return to this nonuniform form especially when dealing with multiple saddle points as discussed in the next section.

Generalization To Multi-pole and Saddle Points

When the integrand of (B.1) contains N distinct poles, α_p, which may cross or be near the SDP, the formulation given above can be generalized to give

$$I(\phi) = 2\pi j \sum_{p=1}^{N} R_p(\phi) - \sqrt{\frac{-2\pi}{\kappa f''(\alpha_s,\phi)}}\, e^{\kappa f(\alpha_s,\phi)} K_A(\alpha_s,\phi) - \sum_{p=1}^{N} A_p(\phi) G_p(\alpha_s,\phi) F_{KP}(=\kappa b_p^2) + O(\frac{1}{\kappa}) \tag{B.12}$$

where

$$K_A(\alpha,\phi) = g(\alpha,\phi) - \sum_{p=1}^{N} A_p(\phi) G_p(\alpha,\phi) \tag{B.13}$$

and $R_p(\phi)$ with $A_p(\phi)$ are defined in (B.4) and (B.6), respectively. In addition, each of the functions $G_p(\alpha,\phi)$ must have a pole at $\alpha = \alpha_p$ and be chosen to satisfy (B.11).

The above uniform evaluation of integrals can be also generalized to cases where C_{SDP} may be associated with more than one saddle point. This is accomplished by simply treating each saddle point individually and only in conjunction with those poles which may cross or be near the SDP.

APPENDIX C

DOUBLE DIFFRACTION CALCULATION

The integral representation of the diffracted field from the first to the second edge of the resistive strip is given by

$$u_1^d = \frac{-j}{2\pi} \int_{S(0)} \frac{\sin\frac{\alpha}{2}}{\cos\alpha + \cos\phi_o} K_{+c}(\alpha) K_+(\phi_o) e^{-jk\rho\cos(\alpha)}\, d\alpha \qquad (C.1)$$

where

w width of the strip($/\lambda$)

$K_+(\pm\alpha)$ split function

$$K_{+c}(\pm\alpha) = \frac{K_+(\pm\alpha)}{\sin(\frac{\pm\alpha}{2})}$$

$$K_{+u}(\alpha) = \left\{1 + \sqrt{2}\cos[(\frac{3\pi}{2} - \alpha - \theta)/2]\right\} K_+(\alpha)$$

ϕ_o incident angle at edge 1

ϕ_2 launching angle at edge 2

Equation (C.1) can be considered as an integral sum of inhomogeneous plane waves incident upon the second edge at an angle of -α. The negative sign prevents the occurrence of a double surface wave pole in the later calculations. The far zone diffracted field from the second edge due a plane wave incidence at $-\alpha$ is

$$u_2^d = \frac{-j}{2\pi}\sqrt{\frac{2\pi}{k\rho}} e^{j\frac{\pi}{4}} e^{-jk\rho} \frac{\sin(-\alpha/2)}{\cos\alpha + \cos\phi_2} K_{+c}(-\alpha) K_+(\phi_2) \qquad (C.2)$$

where ϕ_2 is the angle of incidence and $-\alpha$ is the angle of diffraction. By invoking reciprocity along with the above interpretation of (C.1), we can express the doubly diffracted field as

$$u_{21}^d = -\frac{\sqrt{2\pi}}{4\pi^2} \frac{e^{j\pi/4} e^{-jk\rho}}{\sqrt{k\rho}} \int_{S(\phi)} \frac{-\sin^2(\frac{\alpha}{2}) K_{+c}(\alpha) K_{+c}(-\alpha)}{[\cos\alpha + \cos\phi_o][\cos\alpha + \cos\phi_2]} \cdot K_+(\phi_o) K_+(\phi_2) e^{-jkw\cos(\alpha-\phi)}\, d\alpha \qquad (C.3)$$

or,

$$u_{21}^{d} = \frac{\sqrt{2\pi}}{64\pi^2} \frac{K_+(\phi_o)K_+(\phi_2)}{\cos\frac{\phi_o}{2}\cos\frac{\phi_2}{2}} \frac{e^{j\frac{\pi}{4}}e^{-jk\rho}}{\sqrt{k\rho}}$$
$$\cdot \int_{S(\phi)} \left\{ \left[\sec\left(\frac{\alpha+\phi_o}{2}\right) + \sec\left(\frac{\alpha-\phi_o}{2}\right) \right] \left[\sec\left(\frac{\alpha+\phi_2}{2}\right) + \sec\left(\frac{\alpha-\phi_2}{2}\right) \right] \right\} \tag{C.4}$$
$$\cdot \sin^2\left(\frac{\alpha}{2}\right) \frac{K_{+c}(\alpha)K_{+c}(-\alpha)}{\cos^2\frac{\alpha}{2}} e^{-jkw\cos(\alpha-\phi)}\, d\alpha$$

where the poles of (C.4) are

$$\text{g.o.} : \alpha_{p1} = \pi \pm \phi_o \tag{C.5}$$

$$\alpha_{p2} = \pi \pm \phi_2 \tag{C.6}$$

$$\text{s.w.} : \alpha_{p3} = -\theta \tag{C.7}$$

Expanding the trigonometric terms in (C.4), u_{21}^{d} becomes

$$u_{21}^{d} = \frac{\sqrt{2\pi}}{64\pi^2} \frac{K_+(\phi_o)K_+(\phi_2)}{\cos\frac{\phi_o}{2}\cos\frac{\phi_2}{2}} \frac{e^{j\frac{\pi}{4}}e^{-jk\rho}}{\sqrt{k\rho}} \int_{S(0)} \frac{1}{\cos^2\frac{\alpha}{2}}$$
$$\cdot \left[\sec\left(\frac{\alpha+\phi_o}{2}\right)\sec\left(\frac{\alpha+\phi_2}{2}\right) K_{+c}(\alpha)K_{+c}(-\alpha)\sin^2\frac{\alpha}{2} \right.$$
$$+ \sec\left(\frac{\alpha+\phi_o}{2}\right)\sec\left(\frac{\alpha-\phi_2}{2}\right) K_{+c}(\alpha)K_{+c}(-\alpha)\sin^2\frac{\alpha}{2}$$
$$+ \sec\left(\frac{\alpha-\phi_o}{2}\right)\sec\left(\frac{\alpha+\phi_2}{2}\right) K_{+c}(\alpha)K_{+c}(-\alpha)\sin^2\frac{\alpha}{2} \tag{C.8}$$
$$\left. + \sec\left(\frac{\alpha-\phi_o}{2}\right)\sec\left(\frac{\alpha-\phi_2}{2}\right) K_{+c}(\alpha)K_{+c}(-\alpha)\sin^2\frac{\alpha}{2} \right]$$
$$\cdot e^{-jkw\cos(\alpha)}\, d\alpha$$

consisting of four terms each producing the same result when evaluated via the modified Pauli-Clemmow steepest descents approach. Therefore, it is only necessary to perform this evaluation for one of them and multiply the result by four. The details of the modified Pauli-Clemmow approach used to evaluate the integral asymptotically are given below.

The steepest descent path is mapped to the real axis via the transformation $f(\alpha) = f(\alpha_s) - \mu^2$, where α_s is the saddle point. From this relationship we obtain the relations

$$f(\alpha) = -j\cos(\alpha) \tag{C.9}$$

$$\sin\frac{\alpha}{2} = \sqrt{\frac{j}{2}}\mu \tag{C.10}$$

$$\frac{d\alpha}{d\mu} = \frac{\sqrt{2j}}{\sqrt{1-\frac{j}{2}\mu^2}} \tag{C.11}$$

$$e^{-jk\rho\cos(\alpha)} = e^{-jk\rho}e^{-k\rho\mu^2} \tag{C.12}$$

Mapping one of the integral terms in (C.8) unto the real axis we have

$$I(kw) = e^{kwf(\alpha_s)}\int_{-\infty}^{\infty} F(\alpha)\frac{d\alpha}{d\mu}e^{-kw\mu^2}\,d\mu \tag{C.13}$$

where

$$F(\alpha) = G\frac{\sin^2\frac{\alpha}{2}K_{+c}(\alpha)K_{+c}(-\alpha)}{\cos^2\frac{\alpha}{2}}\sec\left(\frac{\alpha+\phi_o}{2}\right)\sec\left(\frac{\alpha+\phi_2}{2}\right) \tag{C.14}$$

and

$$G = \frac{\sqrt{2\pi}}{64\pi^2}\frac{K_+(\phi_o)K_+(\phi_2)}{\cos\frac{\phi_o}{2}\cos\frac{\phi_2}{2}}\frac{e^{j\frac{\pi}{4}}e^{-jk\rho}}{\sqrt{k\rho}} \tag{C.15}$$

Noting that α_{pi} are the poles of F(α)

$$\begin{aligned} f(\alpha)-f(\alpha_{p1}) &= f(\alpha_s)-\mu^2-f(\alpha_{p1}) \\ &= -j(1+\cos\phi_o)-\mu^2 \\ &= -(\mu^2+ja_1) \qquad a_1 = 2\cos^2\frac{\phi_o}{2} \end{aligned} \tag{C.16}$$

$$\begin{aligned} f(\alpha)-f(\alpha_{p2}) &= f(\alpha_s)-\mu^2-f(\alpha_{p2}) \\ &= -j(1+\cos\phi_2)-\mu^2 \\ &= -(\mu^2+ja_2) \qquad a_2 = 2\cos^2\frac{\phi_2}{2} \end{aligned} \tag{C.17}$$

$$\begin{aligned} f(\alpha)-f(\alpha_{p3}) &= f(\alpha_s)-\mu^2-f(\alpha_{p3}) \\ &= -j(1-\cos\theta)-\mu^2 \\ &= -(\mu^2+ja_3) \qquad a_3 = 2\sin^2\frac{\theta}{2} \end{aligned} \tag{C.18}$$

I(kw) can be written as

$$I(kw) = e^{-jkw}\int_{-\infty}^{\infty}\frac{F_o(\mu)e^{-kw\mu^2}}{(\mu^2+ja_1)(\mu^2+ja_2)(\mu^2+ja_3)}\,d\mu \tag{C.19}$$

where

$$F_o(\mu) = -F(\alpha)\frac{d\alpha}{d\mu}(\mu^2+ja_1)(\mu^2+ja_2)(\mu^2+ja_3) \tag{C.20}$$

is a regular function. Thus it can be represented by a Maclaurin series expansion

$$F_o(\mu) = \sum_{m=0}^{\infty} A_m \mu^m. \tag{C.21}$$

substituting in (C.19) yields

$$I(kw) = e^{-jkw} \sum_{m=0}^{\infty} A_m \int_{-\infty}^{\infty} \frac{\mu^m e^{-kw\mu^2}}{(\mu^2 + ja_1)(\mu^2 + ja_2)(\mu^2 + ja_3)} d\mu \tag{C.22}$$

Clearly the integral in (C.22) vanishes for odd m and we further note the A_o=0. Thus, the first non-vanishing term of the Maclaurin series expansion corresponds to m=2. To evaluate the integral in (C.22) for m=2, we first employ the partial fraction expansion

$$\frac{1}{(\mu^2 + ja_1)(\mu^2 + ja_2)(\mu^2 + ja_3)} = \frac{A}{(\mu^2 + ja_1)} + \frac{B}{(\mu^2 + ja_2)} + \frac{C}{(\mu^2 + ja_3)} \tag{C.23}$$

where

$$A = \frac{1}{(-ja_1 + ja_2)(-ja_1 + ja_3)} = \frac{-1}{(a_2 - a_1)(a_3 - a_1)} \tag{C.24}$$

$$B = \frac{1}{(-ja_2 + ja_1)(-ja_2 + ja_3)} = \frac{-1}{(a_1 - a_2)(a_3 - a_2)} \tag{C.25}$$

$$C = \frac{1}{(-ja_3 + ja_1)(-ja_3 + ja_2)} = \frac{-1}{(a_1 - a_3)(a_2 - a_3)} \tag{C.26}$$

In addition, noting that

$$\int_{-\infty}^{\infty} \frac{e^{-kw\mu^2}}{\mu^2 + ja} d\mu = \sqrt{\frac{\pi}{kw}} \frac{F_{KP}(kwa)}{ja} \tag{C.27}$$

$$\int_{-\infty}^{\infty} \frac{\mu^2 e^{-kw\mu^2}}{\mu^2 + ja} d\mu = \sqrt{\frac{\pi}{kw}} \{1 - F_{KP}(kwa)\} \tag{C.28}$$

it is found that

$$\begin{aligned} u_{21}^d = &- e^{-jkw} A_2 \sqrt{\frac{\pi}{kw}} \\ &\cdot [A\{1 - F_{KP}(kwa_1)\} + B\{1 - F_{KP}(kwa_2)\} + C\{1 - F_{KP}(kwa_3)\}] \end{aligned} \tag{C.29}$$

where

$$A_2 = \frac{1}{2} F_o''(\mu)|_{\mu=0} = \frac{1}{2} \frac{\partial^2 F_{o_1}(\alpha)}{\partial \alpha^2} \left(\frac{d\alpha}{d\mu}\right)^3. \tag{C.30}$$

Since

$$F_{o_1}(\alpha) = F(\alpha)(f(\alpha) - f(\alpha_{p1}))(f(\alpha) - f(\alpha_{p2}))(f(\alpha) - f(\alpha_{p3})) \tag{C.31}$$

$$\begin{aligned} &= -G \sin^2 \frac{\alpha}{2} \sec\left(\frac{\alpha - \phi_o}{2}\right) \sec\left(\frac{\alpha - \phi_2}{2}\right) \frac{K_{+c}(\alpha) K_{+c}(-\alpha)}{\cos^2 \frac{\alpha}{2}} \\ &\cdot (j \cos \phi_o + j \cos \alpha)(j \cos \phi_2 + j \cos \alpha)(-j \cos \theta + j \cos \alpha) \end{aligned} \tag{C.32}$$

we find that (note that μ=0 maps to $\alpha = \alpha_s = 0$)

$$F_{o_1}(\alpha_s) = jG\frac{\alpha^2}{4}\sec\frac{\phi_o}{2}\sec\frac{\phi_2}{2}K_{+c}^2(\alpha=0)(2\cos^2\frac{\phi_o}{2})(2\cos^2\frac{\phi_2}{2})(2\sin^2\frac{\theta}{2}) \quad (C.33)$$

$$= jG2\alpha^2\cos\frac{\phi_o}{2}\cos\frac{\phi_2}{2}K_{+c}^2(\alpha=0)\sin^2\frac{\theta}{2} \quad (C.34)$$

$$F'_{o_1}(\alpha_s) = j4G\alpha\cos\frac{\phi_o}{2}\cos\frac{\phi_2}{2}K_{+c}^2(\alpha=0)\sin^2\frac{\theta}{2} \quad (C.35)$$

$$\frac{\partial^2 F_{o_1}(\alpha_s)}{\partial\alpha^2} = j4G\cos\frac{\phi_o}{2}\cos\frac{\phi_2}{2}K_{+c}^2(\alpha=0)\sin^2\frac{\theta}{2} \quad (C.36)$$

$$\frac{\partial^2 F_{o_1}(\alpha_s)}{\partial\alpha^2} = j2G\cos\frac{\phi_o}{2}\cos\frac{\phi_2}{2}K_{+c}^2(\alpha=0)a_3 \quad (C.37)$$

$$\frac{d\alpha}{d\mu}|_{\mu=0} = \sqrt{2j} \quad (C.38)$$

$$\left(\frac{d\alpha}{d\mu}\right)^3|_{\mu=0} = 2^{\frac{3}{2}}e^{j\frac{3\pi}{4}} \quad (C.39)$$

Using (C.31) to (C.39) gives

$$A_2 = G\frac{1}{2}[j2\cos\frac{\phi_o}{2}\cos\frac{\phi_2}{2}K_{+c}^2(\alpha=0)a_3]2^{\frac{3}{2}}e^{j\frac{3\pi}{4}} \quad (C.40)$$

Substituting this in (C.29) and multiplying by 4 yields the doubly diffracted field

$$u_{21}^d = +j\frac{K_+(\phi_o)K_+(\phi_2)}{8\pi^{\frac{3}{2}}}K_{+c}^2(\alpha=0)a_3\frac{e^{-jkw}e^{-jk\rho}}{\sqrt{k\rho}}\sqrt{\frac{\pi}{kw}}$$
$$\cdot[A\{1-F_{KP}(kwa_1)\}+B\{1-F_{KP}(kwa_2)\}+C\{1-F_{KP}(kwa_3)\}] \quad (C.41)$$

A factor of one-half has been incluided to account for the grazing incidence of the singly diffracted wave upon the second edge.

APPENDIX D

TRIPLE DIFFRACTION CALCULATION

The approach for deriving the third order diffracted field uses the Extended Spectral Ray Method which was utilized in the derivation of the double diffraction coefficient. The double diffraction coefficient (see Appendix C) is

$$u_{21}^{d}(\phi_2,\phi_o) = +j\frac{K_+(\phi_o)K_+(\phi_2)}{4\pi^{\frac{3}{2}}}K_{+c}^{2}(\alpha=0)a_3\frac{e^{-jkw}e^{-jk\rho}}{\sqrt{k\rho}}\sqrt{\frac{\pi}{kw}} \cdot [A\{1-F_{KP}(kwa_1)\}+B\{1-F_{KP}(kwa_2)\}+C\{1-F_{KP}(kwa_3)\}] \tag{D.1}$$

where

w width of the strip($/\lambda$)

$K_+(\pm\alpha)$ split function

$$K_{+c}(\pm\alpha) = \frac{K_+(\pm\alpha)}{\sin(\frac{\pm\alpha}{2})}$$

$$K_{+u}(\alpha) = \left\{1+\sqrt{2}\cos[(\frac{3\pi}{2}-\alpha-\theta)/2]\right\}K_+(\alpha)$$

ϕ_o incident angle at edge 1

ϕ_2 launching angle at edge 2

$$A = \frac{-1}{(a_2-a_1)(a_3-a_1)}$$

$$B = \frac{-1}{(a_1-a_2)(a_3-a_2)}$$

$$C = \frac{-1}{(a_1-a_3)(a_2-a_3)}$$

and

$$a_1 = 2\cos^2\frac{\phi_o}{2} \tag{D.2}$$

$$a_2 = 2\cos^2\frac{\phi_2}{2} \tag{D.3}$$

$$a_3 = 2\sin^2\frac{\theta}{2} \tag{D.4}$$

The triply diffracted field may then be represented

$$u_{121}^d = \frac{-j}{2\pi}\int_{S(0)} \frac{\sin\frac{\alpha}{2}}{\cos\alpha+\cos\phi} u_{21}^d(-\alpha,\phi_o)K_{+c}(\alpha)K_+(-k\cos\phi)e^{-jk\rho\cos(\alpha)}\,d\alpha. \tag{D.5}$$

This integral can be interpreted as a sum of inhomogeneous plane waves diffracting from the second edge and incident upon the first at a complex angle of $-\alpha$. The negative sign is used to prevent the occurrence of a double surface wave pole later in the calculations. Using the identity

$$\frac{1}{\cos\alpha+\cos\phi_o} = \frac{1}{4\cos\frac{\alpha}{2}\cos\frac{\phi_o}{2}}\left[\sec\left(\frac{\alpha+\phi_o}{2}\right)+\sec\left(\frac{\alpha-\phi_o}{2}\right)\right] \tag{D.6}$$

in (D.5), we obtain

$$\begin{aligned} u_{121}^d =& \frac{1}{2\pi}\int_{S(0)}\left\{\frac{\sin\frac{\alpha}{2}}{4\cos\frac{\alpha}{2}\cos\frac{\phi}{2}}\left[\sec\left(\frac{\alpha+\phi_o}{2}\right)+\sec\left(\frac{\alpha-\phi_o}{2}\right)\right]K_{+c}(\alpha)K_+(\phi)\right. \\ &\cdot K_+(\phi_o)K_+(-\alpha)K_{+c}^2(\alpha=0)a_3\frac{e^{-j2kw-jk\rho\cos(\alpha)}}{4\pi kw} \\ &\cdot\left[\frac{1}{(a_2-a_1)(a_3-a_1)}\{1-F_{KP}(kwa_1)\}+\frac{1}{(a_1-a_2)(a_3-a_2)}\{1-F_{KP}(kwa_2)\}\right. \\ &\left.\left.+\frac{1}{(a_1-a_3)(a_2-a_3)}\{1-F_{KP}(kwa_3)\}\right]\right\}d\alpha. \end{aligned} \tag{D.7}$$

which can be evaluated via the modified Pauli-Clemmow steepest descents method.

The steepest descent path is mapped to the real axis via the transformation $f(\alpha) = f(\alpha_s) - \mu^2$, where α_s is the saddle point. From this relationship we obtain relations similar to those given in Appendix C (C.9)-(C.12). The triply diffracted term in (D.7) can then be written as

$$u_{121}^d = e^{kwf(\alpha_s)}\int_{-\infty}^{\infty} F(\alpha)\frac{d\alpha}{d\mu}e^{-kw\mu^2}\,d\mu \tag{D.8}$$

Noting that α_{pi} are the poles of F(α)

$$\begin{aligned} f(\alpha)-f(\alpha_{p3}) &= f(\alpha_s)-\mu^2-f(\alpha_{p3}) \\ &= -j(1-\cos\theta)-\mu^2 \\ &= -(\mu^2+ja_3) \qquad a_3 = 2\sin^2\frac{\theta}{2} \end{aligned} \tag{D.9}$$

$$\begin{aligned} f(\alpha)-f(\alpha_{p4}) &= f(\alpha_s)-\mu^2-f(\alpha_{p4}) \\ &= -j(1+\cos\phi)-\mu^2 \\ &= -(\mu^2+ja_4) \qquad a_4 = 2\cos^2\frac{\phi}{2} \end{aligned} \tag{D.10}$$

u^d_{121} can be expressed as

$$u^d_{121} = e^{-jkw} \int_{-\infty}^{\infty} \frac{F_o(\mu) e^{-kw\mu^2}}{(\mu^2 + j a_3)(\mu^2 + j a_4)} d\mu \tag{D.11}$$

where

$$F_o(\mu) = F(\alpha) \frac{d\alpha}{d\mu} (\mu^2 + j a_3)(\mu^2 + j a_4) \tag{D.12}$$

is a regular function. Thus it can be represented by a Maclaurin series expansion

$$F_o(\mu) = \sum_{m=0}^{\infty} A_m \mu^m. \tag{D.13}$$

which when substituted in (D.11) yields

$$u^d_{121} = e^{-jkw} \sum_{m=0}^{\infty} A_m \int_{-\infty}^{\infty} \frac{\mu^m e^{-kw\mu^2}}{(\mu^2 + j a_3)(\mu^2 + j a_4)} d\mu \tag{D.14}$$

Clearly the integral in (D.14) vanishes for odd m and we further note the A_o=0. Thus, the first non-vanishing term of the Maclaurin series expansion corresponds to m=2. To evaluate the integral in (D.14) for m=2, we first employ a partial fraction expansion. In addition, noting that

$$\int_{-\infty}^{\infty} \frac{e^{-kw\mu^2}}{\mu^2 + j a} d\mu = \sqrt{\frac{\pi}{kw}} \frac{F_{KP}(kwa)}{j a} \tag{D.15}$$

$$\int_{-\infty}^{\infty} \frac{\mu^2 e^{-kw\mu^2}}{\mu^2 + j a} d\mu = \sqrt{\frac{\pi}{kw}} \{1 - F_{KP}(kwa)\} \tag{D.16}$$

it is found that

$$u^d_{121} = e^{kwf(\alpha_s)} A_2 \int_{-\infty}^{\infty} \frac{\mu^2 e^{-k\mu^2} d\mu}{(\mu^2 + j a_4)(\mu^2 + j a_3)} \tag{D.17}$$

$$= e^{-jkw} A_2 \frac{1}{j(a_3 - a_4)} \int_{-\infty}^{\infty} \frac{\mu^2 e^{-k\mu^2} d\mu}{(\mu^2 + j a_4)} - \int_{-\infty}^{\infty} \frac{\mu^2 e^{-k\mu^2} d\mu}{(\mu^2 + j a_3)} \tag{D.18}$$

$$= e^{-jkw} A_2 \frac{1}{j(a_3 - a_4)} \left[\sqrt{\frac{\pi}{kw}} \{1 - F_{KP}(kwa_4)\} - \sqrt{\frac{\pi}{kw}} \{1 - F_{KP}(kwa_3)\} \right] \tag{D.19}$$

$$= e^{-jkw} A_2 \frac{1}{j(a_3 - a_4)} \sqrt{\frac{\pi}{kw}} \{F_{KP}(kwa_3) - F_{KP}(kwa_4)\} \tag{D.20}$$

where

$$A_2 = \frac{1}{2} F''_o(\mu)|_{\mu=0} = \frac{1}{2} \frac{\partial^2 F_{o_1}(\alpha)}{\partial \alpha^2} \left(\frac{d\alpha}{d\mu} \right)^3. \tag{D.21}$$

Since

$$F_{o_1}(\alpha) \approx \frac{-\alpha^2 K_{+c}^4(\alpha=0)2\cos^2\frac{\phi}{2}a_3^2}{4\cdot 16\pi^2 k\sqrt{w}\cos^2\frac{\phi}{2}} K_+(\phi_o)K_+(\phi)e^{-jkw}$$
$$\cdot\left[\frac{1}{(2-a_1)(a_3-a_1)}\{1-F_{KP}(kwa_1)\} + \frac{1}{(a_1-2)(a_3-2)}\{1-F_{KP}(kwa_2)\}\right.$$
$$\left. + \frac{1}{(a_1-a_3)(2-a_3)}\{1-F_{KP}(kwa_3)\}\right] \qquad (D.22)$$

$$F''_{o_1}(\alpha) \approx \frac{-K_{+c}^4(\alpha=0)a_3^2}{16\pi^2 k\sqrt{w}} K_+(\phi_o)K_+(\phi)e^{-jkw}$$
$$\cdot\left[\frac{1}{(2-a_1)(a_3-a_1)}\{1-F_{KP}(kwa_1)\}\right.$$
$$+\frac{1}{(a_1-2)(a_3-2)}\{1-F_{KP}(kw2)\}$$
$$\left.+\frac{1}{(a_1-a_3)(2-a_3)}\{1-F_{KP}(kwa_3)\}\right]. \qquad (D.23)$$

Also

$$\frac{d\alpha}{d\mu}|_{\mu=0} = \sqrt{2j} \qquad (D.24)$$

$$\left(\frac{d\alpha}{d\mu}\right)^3|_{\mu=0} = 2^{\frac{3}{2}}e^{j\frac{3\pi}{4}} \qquad (D.25)$$

Using (D.21) to (D.25) to solve for A_2 and substituting the result into (D.20) gives

$$u_{121}^d = \sqrt{2}e^{j3\pi/4}e^{-jkw}\left(\frac{-K_{+c}^4(\alpha=0)a_3^2}{16\pi^2 k\sqrt{w}} K_+(\phi_o)K_+(\phi)e^{-jkw}\right.$$
$$\cdot\left[\frac{1}{(2-a_1)(a_3-a_1)}\{1-F_{KP}(kwa_1)\}\right.$$
$$\left.\left.+\frac{1}{(a_1-2)(a_3-2)}\{1-F_{KP}(kwa_2)\}+\frac{1}{(a_1-a_3)(2-a_3)}\{1-F_{KP}(kwa_3)\}\right]\right)$$
$$\cdot\frac{1}{j(a_3-a_4)}\sqrt{\frac{\pi}{kw}}\left\{F_{KP}(kwa_3)-F_{KP}(kwa_4)\right\}\frac{e^{-jk\rho}}{\sqrt{\rho}}$$
$$(D.26)$$

Rewriting (D.26)

$$
\begin{aligned}
u_{121}^{d} = & j\frac{\sqrt{2}}{16(kw)^{\frac{3}{2}}w}e^{j3\pi/4}e^{-j2kw}K_{+c}^{4}(\alpha=0)a_3^2K_+(\phi_o)K_+(\phi) \\
& \cdot\left[\frac{1}{(2-a_1)(a_3-a_1)}\{1-F_{KP}(kwa_1)\}+\frac{1}{(a_1-2)(a_3-2)}\{1-F_{KP}(kw2)\}\right. \\
& \left.+\frac{1}{(a_1-a_3)(2-a_3)}\{1-F_{KP}(kwa_3)\}\right] \\
& \cdot\frac{1}{(a_3-a_4)}\{F_{KP}(kwa_3)-F_{KP}(kwa_4)\}\frac{e^{-jk\rho}}{\sqrt{\rho}}
\end{aligned}
\qquad (D.27)
$$

Equation (D.27) is the complete triply diffracted field. It contains the factors of 4 for four mechanisms per edge times one-fourth to account for two cases of grazing incidence upon the edges (note that (D.1) was multiplied by a factor of two to prevent any double counting of grazing incidence effects).

BIBLIOGRAPHY

BIBLIOGRAPHY

[1] Maliuzhinets, G. D. , "Excitation, Reflection And Emission Of Surface Waves From A Wedge With Given Face Impedances," *Sov. Phys. Dokl.*, Engl. Transl., 3, pp. 752-755, 1958.

[2] Volakis, J. L. and T.B.A. Senior , "Simple Expressions For A Function Occurring In Diffraction Theory," *IEEE Trans. Antennas Propag.*,AP-33, pp. 678-680, 1985.

[3] Senior, T.B.A. , "Diffraction By A Semi-Infinite Metallic Sheet," *Proc. Roy. Soc.* (London), A 213(1115), pp. 436-458, 1952.

[4] Senior, T.B.A. , "Half Plane Edge Diffraction," *Radio Sci.*,10(6), pp. 645-650, 1975.

[5] Bucci, O.M. and G. Franceschetti , " Electromagnetic Scattering By A Half-Plane With Two Face Impedances," *Radio Sci.*,11(1), pp. 49-59, 1976.

[6] Anderson, I. , "Plane Wave Diffraction By A Thin Dielectric Half-Plane," *IEEE Trans. Antennas Propag.*, AP-27, pp. 584-589, 1979.

[7] Clemmow, P.C. , The Plane Wave Spectrum Representation of Electromagnetic Fields, Pergamon, New York, 1966.

[8] Senior, T.B.A. , "The Current Induced In A Resistive Half Plane," *Radio Sci.*, 16(6), pp. 1248-1254, 1981.

[9] Volakis, J. L. and M. I. Herman , "A Uniform Asymptotic Evaluation Of Integrals," *Proc. IEEE*, 74(7), pp. 1043-1044, 1986.

[10] Bowman, J.J. , "High-Frequency Backscattering From An Absorbing Infinite Strip With Arbitrary Face Impedances," *Can. J. Phys.*, 45(7), pp. 2409-2430, 1967.

[11] Senior, T.B.A. , "Backscattering From Resistive Sheets," *IEEE Trans. Antennas Propag.*, AP-27, pp. 808-813, 1979.

[12] Senior, T.B.A. , "Scattering By Resistive Strips," *Radio Sci.*,14(5), pp. 911-924, 1979.

[13] Tiberio, R. and R.G. Kouyoumjian , "A Uniform GTD Solution For The Diffraction By Strips At Grazing Incidence," *Radio Sci.*, 14(6), pp. 933-941, 1979.

[14] Kouyoumjian, R.G. , The geometrical theory of diffraction and its applications , in Numerical and Asymptotic Techniques in Electromagnetics, R. Mittra, Ed, New York, Springer-Verlag, 1975.

[15] Buyukdura, O.M., Radiation From Sources and Scatterers Near The Edge Of A Perfectly Conducting Wedge, Ph.D. dissertation, The Ohio State University, 1984.

[16] Fialkovskiy, A.T. , "Diffraction Of Planar Electromagnetic Waves By A Slot And A Strip," *Radio Eng. Electron.*, 11, pp. 150-157, 1966.

[17] Tiberio, R. and R.G. Kouyoumjian , "Calculation Of High-Frequency Diffraction By Two Nearby Edges Illuminated At Grazing Incidence," *IEEE Trans. Antennas Propag.*, AP-32, pp. 1186-1196, 1984.

[18] Kouyoumjian, R.G., and P.H. Pathak , "A Uniform Geometrical Theory Of Diffraction For An Edge In A Perfectly Conducting Surface," *Proc. IEEE*, 62(11), pp. 1448-1461, 1974.

[19] Rahmat-Samii, Y. and R. Mittra , "A Spectral Domain Interpretation Of High-Frequency Diffraction Phenomena," *IEEE Trans. Antennas Propag.*, AP-25, pp. 676-687, 1977.

[20] Rahmat-Samii, Y. and R. Mittra , "On The Investigation Of Diffraction Fields At The Shadow Boundaries Of Staggered Parallel Plates - A Spectral Domain Approach," *Radio Sci.*, 12(5), pp. 659-670, 1977.

[21] Rahmat-Samii, Y. and R. Mittra , "Spectral Analysis Of High-Frequency Diffraction Of An Arbitrary Incident Field By A Half-Plane - Comparison With Four Asymptotic Techniques," *Radio Sci.*, 13(1), pp. 31-48, 1978.

[22] Senior, T.B.A. , "Combined Resistive and Conductive Sheets," *IEEE Trans. Antennas Propag.*, AP-33, pp. 577-579, 1985.

[23] Liepa, V., E.F. Knott and T.B.A. Senior , "Scattering From Two-Dimensional Bodies with Absorber Sheets," Technical Report AFAL-TR-77-119, 1974.

[24] Tiberio, R., G. Pelosi and G. Manara ,"A Uniform GTD Formulation For The Diffraction By A Wedge With Impedance Faces," *IEEE Trans. Antennas Propag.*, AP-33, pp. 867-873, 1985.

[25] Herman M.I., J.L. Volakis and T.B.A. Senior, "Analytic Expressions For A Function Occurring In Diffraction Theory," submitted to *IEEE Trans. Antennas Propag.*, 1987.

[26] Tiberio, R., G. Manara, G. Pelosi and R. G. Kouyoumjian , "High-Frequency Diffraction By A Double Wedge," 1985 IEEE AP-S Symposium Digest, pp. 443-446, 1985.

[27] Volakis, J. L. and M. A. Ricoy , "Diffraction By A Thick Perfectly Conducting Half Plane," *IEEE Trans. Antennas Propag.*, 1987.

[28] Volakis, J. L. , "Scattering By A Thick Impedance Half Plane," *Radio Sci.*, in press, 1987.

[29] Pathak, P.H. and R.G. Kouyoumjian , The Dyadic Diffraction Coefficient For A Perfectly Conducting Wedge, Sci. Rep. 5, ElectroScience Lab., Dep. of Electr. Eng., Ohio State Univ., Columbus, Ohio, 1970.

[30] Wang, N. , "Self-Consistent GTD Formulation For Conducting Cylinders With Arbitrary Convex Cross Section," *IEEE Trans. Antennas Propag.*, AP-24, pp. 463-468, 1976.

[31] Clemmow, P.C., "A Method For The Exact Solution Of A Class Of Two-Dimensional Diffraction Problems," *Proc. Roy. Soc.* (London), 205(A), pp. 286-308, 1951.

[32] Richmond, J.H. , "Scattering By Thin Dielectric Strips," *IEEE Trans. Antennas Propag.*, AP-33, pp. 64-68, 1985.

[33] Rudduck, R.C. , "Application Of Wedge Diffraction and Wave Interaction Methods To Antenna Theory," OSU short course notes for GTD and Numerical Techniques, vol. 1, September 1975.

[34] Zavadskii, V. and M. Sakharova, "Application Of The Special Function In Problems Of Wave Diffraction In Wedge-Shaped Regions," *Sov. Phys. Acoustics*, Vol. 13, pp. 48-54, 1967.

[35] Tiberio, R., and G. Pelosi , "High Frequency Scattering From The Edges Of Impedance Discontinuities On A Fat Plane," *IEEE Trans. Antennas Propag.*, AP-31, pp. 590-596, 1983.

[36] Tiberio, R., F. Bessi, G. Manara and G. Pelosi, "Scattering By A Strip With Two Face Impedances At Edge-On Incidence," *Radio Sci*, 17(5), pp. 1199-1210, 1982.

[37] Tai, C.-T., lecture notes at The University of Michigan, Electromagnetic Fields (ECE 525), 1982

[38] Senior, T.B.A., "Impedance Boundary Conditions For Imperfectly Conducting Surfaces," *Appl. Sci. Res.*, Sec. B, vol. 8, pp. 418-436, 1960.

[39] Senior, T.B.A., "A Note On Impedance Boundary Conditions," *Can. J. Phys.*, vol. 40, pp. 663-665, 1962.

[40] LaHaie, I.J., "Function-Theoretic Techniques For The Electromagnetic Scattering By A Resistive Wedge," University of Michigan Technical Report 015224-2-T, pp. 8-21, 1981.

[41] Felson, L.B. and N. Marcuvitz, Radiation and Scattering Of Waves, Englewood Cliffs, NJ: Prentice-Hall, 1973.

[42] Gennarelli, C. and L. Palumbo, " A Uniform Asymptotic Expansion of Typical Diffraction Integrals With Many Coalescing Simple Pole Singularities and A First-Order Saddle Point," *IEEE Trans. Antennas Propag.*, AP-32, pp. 1122-1124, 1984.

[43] Schafer, R.H. and R.G. Kouyoumjian, "Higher Order Terms In The Saddle Point Approximation," *Proc. IEEE*, vol. 55, pp. 1496-1497, 1967.